The spatiotemporal dynamics of autophagy during *Mycobacterium tuberculosis* infection of human induced pluripotent stem cell derived macrophages

Elliott Michael Bernard

Thesis submitted to University College London

for the Degree of Doctor of Philosophy

December 2020

Declaration

I, Elliott Bernard, confirm that the work submitted in this thesis is my own. Where information has been derived from other sources, I can confirm that this has been indicated in the thesis.

Acknowledgments

Firstly I'd like to thank Max for the opportunity to work in his lab on a challenging but rewarding project that has enabled me develop as both a scientist and a person. The project would not have been possible without the continued encouragement, support and guidance of the entire lab. Tony Fearns, Chris Peddie and Matt Russell were invaluable for the acquisition and analysis of electron microscopy data presented here. Laure Botella generated the CpsA mutant and complemented strains of Mtb. The iPS team – Claudio, Pierre, Beren and Enrica – have been fundamental in maintaining the macrophage factories and facilitating the scale up of production; without them it would not have been possible to take the macrophage production to the next level. I wish them all the best of luck with their projects using iPSDM. Enrica, especially was instrumental in the design and generation of the Atg7 and Atg14 KO lines. Finally, a big thank you to Rachel Lai for her help in the preparation of RNA-seq libraries and data analysis.

The staff and facilities at The Crick have been second-to-none in supporting me in my PhD and enabling many of the experiments here. The Science Technology Platforms, especially Flow Cytometry, Electron Microscopy, Advanced Sequencing, and Advanced Light Microscopy were all very helpful. A special mention to Lyn Healy of the Human Embryonic Stem Cell Unit, and her team, as well as Rabia Khan of the Frickel lab who helped to establish the iPSDM system.

Outside the lab, the support of my family and friends has been unwavering. I am very grateful to my parents, Richard and Julie, my sister, Jasmine, and my grandparents who have been there every step of the way. My friends, from school, university and St John Ambulance provided much needed breaks from thinking about my project to unwind, relax and come back refreshed and ready to go.

Abstract

The interaction of macrophages with the intracellular pathogen *Mycobacterium tuberculosis* (Mtb) is critical in determining disease outcomes. Presently, we lack human macrophage models that are genetically tractable, karyotypically normal, and available in large cell numbers. Thus, new human macrophage models are required to facilitate the study of host-pathogen interactions, especially where genetic manipulation is required.

In this thesis I set up and characterise a stem cell derived model of human macrophages (iPSDM). iPSDM recapitulate many known interactions between Mtb and human macrophages. An RNA-seq comparison of the transcriptional response to infection between Mtb WT and the attenuated strain Mtb ΔRD1, which lacks the ESX-1 secretion system, revealed commonalities with previous studies along with a novel, RD1 dependent response at 48 h post infection.

In macrophages, the autophagy pathway plays diverse roles in infection with intracellular pathogens, including capturing cytosol invading pathogens and targeting them for lysosomal killing. The role of the autophagy pathway during Mtb infection is still unclear. Live cell imaging in iPSDM revealed, following membrane damage by Mtb, the induction of LC3 positive tubulovesicular structures, which fail to capture the bacteria. Correlative 3D focussed ion beam scanning electron microscopy showed the bacteria in the macrophage cytosol following successful dissociation from autophagic structures. Genetic disruption of the autophagy pathway through the knockout of Atg7 failed to alter intracellular Mtb replication or rescue replication of the attenuated mutants Mtb ΔRD1 and Mtb ΔCpsA, which has previously been shown to be more susceptible to restriction by non-canonical autophagy. On the other hand, knockout of Atg14 resulted in enhanced Mtb replication, likely through an autophagy-independent mechanism.

This work validates iPSDM to study hitherto unexplored aspects of human macrophage-Mtb interactions. Moreover, these data revealed novel autophagy dynamics in space and time and evasion mechanisms employed by Mtb to subvert this host defence pathway.

Impact Statement

With antibiotic resistance continuing to impact health globally and previously treatable infections now claiming more lives, it is increasingly important to investigate novel therapeutic routes. One much touted route is through the use of host-directed therapies; that is enhancing the body's natural defence mechanisms against infection to promote bacterial killing and restoration of health. This applies to many infections, including for people suffering with tuberculosis (TB), especially those infected with multi- or extensively-drug resistant strains.

The autophagy pathway, a cellular recycling process whereby cellular contents are targeted for lysosomal degradation, is capable of capturing many bacteria, including *Mycobacterium tuberculosis*, in order to restrict their replication. Autophagy induction has been the subject of drug development as a potential host-directed therapy for TB patients, as well as in many other diseases. To fully understand the potential for these therapies, it is important to understand the role of the autophagy pathway during infection in relevant human models.

The work presented here demonstrates how studying fundamental biology of the virulent pathogen in its natural host can yield unexpected insights into subversion of host defence pathways by pathogens. Without fully understanding the basic biology behind the success of Mtb as an intracellular human pathogen we risk wasting time, resources and money pursuing treatments that will not work because the data supporting them is based on incorrect models.

More widely, Mtb is just one of many pathogenic bacteria capable of infecting and replicating within macrophages. The current limitations of human macrophage models, along with an over-reliance on mouse models that may poorly reflect the interaction between pathogen and human host, mean many fundamental questions remain unanswered. Thus, the development and further characterisation of human induced pluripotent stem cell derived macrophages, as well as protocols for plasmid DNA transfection will enable research into a wide range of pathogens.

Additionally, tools generated within this thesis will provide a useful resource for researchers working in diverse fields. Both canonical and non-canonical autophagy have been implicated in protecting against diverse diseases including cancer and neurodegeneration. The ability to differentiate the autophagy knockout induced pluripotent stem cell lines created here into multiple disease relevant cell types will enable their use to understand the role of these processes in during disease development and progression.

Contents

Table of Figures

List of Tables

Abbreviations

1-TbAd	1-tuberculosinyladenosine
ADC	Albumin dextrose catalase
ALR	Autophagic lysosome reformation
AMPK	AMP dependent kinase
Atg	Autophagy gene
BafA1	Bafilomycin A1
BAL	Bronchoalveolar lavage
BMDM	Bone marrow derived macrophage
BMP4	Bone morphogenic protein 4
bp	Base pairs
CCL	C-C motif chemokine ligand
CCR	C-C motif chemokine receptor
CD	Cluster of differentiation
CFP-10	Culture filtrate protein 10 kDa/EsxB
CFTR	Cystic fibrosis transmembrane receptor
CFU	Colony forming units
cGAMP	Cyclic GMP-AMP
cGAS	Cyclic GMP-AMP synthase
CLEM	Correlative light and electron microscopy
CXCL	C-X-C motif containing ligand
DAG	Diacylglycerol
DEG	Differentially expressed gene
DRAM	DNA damage responsive autophagy modulator
EB	Embryonic body
EE	Early endosome
EEA1	Early endosome antigen 1
EM	Electron microscopy
EPG5	Ectopic P granules protein 5
ESAT-6	Early secreted antigenic target 6 kDa/EsxA
ESCRT	Endosomal sorting complex required for transport

FACS	Fluorescence activated cell sorting
FIB SEM	Focused ion beam scanning electron microscopy
FRET	Forster resonance energy transfer
FYCO1	FYVE and coiled-coil domain containing protein 1
GA	Glutaraldehyde
GABARAP	γ-amino butyric acid receptor associated protein
Gal	Galectin
GAS	Group A *Streptococcus*
GBP	Guanylate binding protein
gDNA	Genomic DNA
GILT	Gamma interferon inducible lysosomal thiol reductase
GIM	GABARAP interacting motif
GM-CSF	Granulocyte macrophage colony stimulating factor
hLEC	Human lymphatic endothelial cell
hMDM	Human monocyte derived macrophage
HOPS	Homotypic fusion and protein sorting
HSC	Haematopoietic stem cell
IDO	Indoleamine-2,3-dioxygenase
IFN	Interferon
IL	Interleukin
IL-1Ra	Interleukin 1 receptor antagonist
iNOS	Inducible nitric oxide synthase
iPSC	Induced pluripotent stem cell
iPSDM	Induced pluripotent stem cell derived macrophage
IRF	Interferon regulatory factor
IRG	Immunity-related GTPase
KO	Knockout
LAMP	Lysosome associated membrane protein
LANDO	LC3 associated endocytosis
LAP	LC3 associated phagocytosis
LC3	Microtubule associated protein light chain 3

LC3-TVS	LC3 tubulovesicular structure
LCP	LytR-CpsA-Psr domain containing protein
LE	Late endosome
LIR	LC3 interacting region
LLO	Listeriolysin O
LLOMe	L-leucyl-L-leucyl methyl ester
LPS	Lipopolysaccharide
LRRK2	Leucine repeat rich kinase 2
LTR	Lysotracker
LUBAC	Linear ubiquitin assembly complex
Lys	Lysosome
M-6-PR	Mannose-6-phosphate receptor
ManLAM	Mannose-capped lipoarabinomannan
MCP-1	Monocyte chemotactic protein-1
M-CSF	Macrophage colony stimulating factor
MFI	Mean fluorescence intensity
MHC	Major histocompatibility complex
MIP-1	Macrophage inflammatory protein-1
Mtb	*Mycobacterium tuberculosis*
mTORC	Mechanistic target of rapamycin
MVP	Major vault protein
NBR1	Next to BRCA1 gene
Ndk	Nucleotide diphosphate kinase
NDP52	Nuclear dot protein 52
NEMO	NF-κB essential modulator
NF-κB	Nuclear factor κB
NLR	NOD like receptor
NLRP3	NOD- LRR- pyrin containing protein 3
NO	Nitric oxide
NOD	Nucleotide oligomerisation domain
PAM	Protospacer adjacent motif

PAP	Pulmonary alveolar proteinosis
PBMC	Peripheral blood mononuclear cells
PDIM	Phthiocerol dimycocerosates
PFA	Paraformaldehyde
PGL	Phenolic glycolipid
PI3,5,P_2	Phosphatidylinositol-3,5-bisphosphate
PI3K	Phosphatidylinositiol-3-kinase
PI3P	Phosphatidylinositiol-3-phosphate
PKC	Protein kinase C
PknG	Protein kinase G
PLEKHM1	Pleckstrin homology domain containing family M protein 1
PMA	Phorbol 12-myristate 13-acetate
PRR	Pattern recognition receptor
PtpA	Protein tyrosine phosphatase A
RD1	Region of difference 1
RILP	Rab7 interacting lysosomal protein
ROCKi	Rho kinase inhibitor Y27632
ROS	Reactive oxygen species
SapM	Secreted acid phosphatase M
SCF	Stem cell factor
SCV	Salmonella containing vacuole
SEM	Scanning electron microscopy
SLAPs	Spacious *Listeria* containing phagosomes
SNAP	Synaptosomal associated protein
SNARE	Soluble N-ethylmaleimide-sensitive factor attachment protein receptor
SNX-BAR	Sorting nexin and BAR domain containing
STING	Stimulator of interferon genes
STX	Syntaxin
T3SS	Type 3 secretion system
T7SS	Type 7 secretion system

TAX1BP1	TAX1 binding protein 1
TB	Tuberculosis
TBK1	TANK binding kinase 1
TEM	Transmission electron microscopy
TFEB	Transcription factor EB
TLC	Thin layer chromatography
TLR	Toll like receptor
TNF	Tumour necrosis factor
TRIM	Tripartite motif domain containing protein
ULK1	Unc51-like autophagy modulating kinase 1
UVRAG	UV radiation resistance associated gene
VAMP	Vesicle associated membrane protein
v-ATPase	Vacuolar type H+ ATPase
VEGF	Vascular endothelial growth factor
WIPI2b	WD40 repeat domain phosphoinositide interacting protein 2b

1. Introduction

1.1 Mycobacterium tuberculosis interactions with macrophages

Mycobacterium tuberculosis infection is complex and difficult to treat

The bacterium *Mycobacterium tuberculosis* (Mtb) is the etiological agent of tuberculosis (TB) in humans and causes the death of more people worldwide than any other single infectious agent. In 2019, TB killed an estimated 1.4 million people and caused disease in a further 10 million people. Moreover, there is believed to be a large, latently infected pool of individuals who can develop and spread TB in later life. Finally, antibiotic resistant strains are an ever-increasing problem and are associated with very high mortality rates (World Health Organisation, 2020).

Infected individuals with active TB expel aerosols containing Mtb through coughs and sneezes, which are inhaled by those around them and the bacteria are distributed throughout the upper and lower airways. In the upper airways, Mtb can cause disease in the oropharynx and cervical lymph nodes whilst epithelial cells appear to be largely protected from infection by mucus. In the lower airways various cell types become infected including myeloid cells such as alveolar macrophages, neutrophils and dendritic cells and non-myeloid cells such as Type II alveolar epithelial cells (Randall et al., 2015; Ganbat et al., 2016; Lerner et al., 2015). Alveolar macrophages are the first cells to become infected in mice (Cohen et al., 2018), whereas in patient sputum neutrophils are the predominantly infected myeloid cell (Eum et al., 2010). As well as causing disease in the lungs – pulmonary TB – Mtb can also cause disseminated disease in almost any organ of the body, for example the lymph nodes. A hallmark of human TB in the lung is the formation of granulomas; highly ordered structures of mostly immune cells that should restrict bacterial growth and dissemination, but necrosis and granuloma failure can release bacteria into the airway for transmission (Russell et al., 2009; Kaplan et al., 2003). Granuloma formation and active disease are only seen in approximately 10% of infected individuals; the remaining 90% either clear the infection completely or develop a latent infection. Latently infected individuals can experience active disease later in life, often due to immunosuppression (Flynn and Chan, 2001b). Overall, the

heterogeneous distribution of Mtb in different organs, cell types and structures such as granulomas, makes the understanding of TB pathogenesis very difficult and poses challenges for antibiotic therapy.

The roles of macrophages in Mtb infection

Macrophages are one of several professional phagocytic cells of the immune system (Silva and Correia-Neves, 2012). They play essential roles in homeostasis, tissue development, wound repair, inflammation, and innate immune defence (Lugo-Villarino et al., 2019).

Macrophages are arguably the most important cell type during Mtb infection. Alveolar macrophages provide a first line of defence against inhaled pathogens, such as Mtb, that reach the alveoli. Depletion of alveolar macrophages in mice leads to reduced bacterial burden and improved survival following Mtb infection, therefore implicating them as being critical for establishing infection (Leemans et al., 2001), likely due to supporting intracellular Mtb replication (Pisu et al., 2020). Additionally, infected alveolar macrophages migrate into the lung interstitium and this precedes dissemination to other immune cells, which migrate to disseminate disease in mice (Cohen et al., 2018). In the zebrafish and *M. marinum* model, macrophages also contribute to the dissemination of bacteria and their transport across epithelial and endothelial barriers (Clay et al., 2007).

Following Mtb infection, the release of chemokines drives the recruitment of circulating monocytes to the lung where they can transmigrate into the interstitium and differentiate into macrophages. The mycobacterial lipid phenolic glycolipid (PGL) activates the production and secretion of C-C motif chemokine ligand 2 (CCL2) from alveolar macrophages to recruit monocytes that are permissive to bacterial replication and dissemination (Cambier et al., 2017). The secretion of other monocyte and macrophage chemotactic proteins is upregulated following Mtb infection, including monocyte chemoattractant protein-1 (MCP-1) and macrophage inflammatory protein-1α (MIP-1α), however this is an underexplored area of research during Mtb infection and further studies are warranted (Sadek et al., 1998; Lin et al., 1998; Flynn and Chan, 2001a).

In mice, alveolar and recruited macrophages respond differently to Mtb infection. Alveolar macrophages become M2 polarised, showing increased fatty acid oxidation and decreased pro-inflammatory cytokine levels, whereas interstitial macrophages are M1 polarised, showing increased glycolytic activity and enhanced pro-inflammatory cytokine secretion (Pisu et al., 2020). Furthermore, murine alveolar macrophages are more permissive for Mtb replication compared with the interstitial macrophages (Pisu et al., 2020). This is different from a study in zebrafish using *M. marinum* where the recruited macrophages were more permissive (Cambier et al., 2017).

Cytokine secretion by macrophages to establish a pro-inflammatory environment is essential for control of Mtb in mice. Tumour necrosis factor-α (TNF-α) is one of the major cytokines released and is essential for effective control of infection (Clay et al., 2008; Iliopoulos et al., 2006; Flynn et al., 1995). Both interleukin (IL)-1α and β are secreted by macrophages in response to Mtb infection and mice deficient in the receptor for these cytokines are highly susceptible to Mtb infection (Cooper et al., 2011; Sugawara et al., 2001). Whilst IL-6 plays a role in controlling Mtb during the innate phase of infection, IL-6 deficiency does not have an impact in mice following onset of the adaptive immune response (Flynn and Chan, 2001a). However, not all macrophage-derived cytokines play a protective role, for example high levels of IL-10 and Type I interferon (IFN) (IFN-α and -β) are, in certain contexts, detrimental to infection outcomes (Cooper et al., 2011; Moreira-Teixeira et al., 2018).

As well as providing a signal for the recruitment of monocytes and macrophages, the release of chemokines attracts other cell types including neutrophils, dendritic cells, and T cells. Whilst high levels of neutrophils are detrimental for the host (Lowe et al., 2012), dendritic cell (Tian et al., 2005) and T cell recruitment (Orme et al., 1993) is essential for successful immune defence (O'Garra et al., 2013). Once infected with Mtb, dendritic cells migrate to lung-draining lymph nodes where they prime naïve T cells towards a Th1 response (O'Garra et al., 2013), for which macrophage and dendritic cell derived IL-12 is important (Flynn and Chan, 2001a). These activated T cells then to migrate to the lung, where they secrete large amounts if IFN-γ, a key

cytokine in the protective immune response to Mtb (**Figure 1.1.1**). IFN-γ is a potent activator of macrophages (Nathan et al., 1983) and individuals with polymorphisms in the receptor are highly susceptible to mycobacterial infections (Bustamante et al., 2014). Stimulation of mouse macrophages with IFN-γ restricts Mtb replication (Flesch and Kaufmann, 1987), although there are conflicting reports regarding the effect of IFN-γ on Mtb replication in human macrophages (Douvas et al., 1985; Lerner et al., 2017; Flynn and Chan, 2001a). Regardless, studies generally agree that any anti-mycobacterial response induced by IFN-γ is lower in human macrophages compared with mice (Rook et al., 1986). The protective role of IFN-γ mediated macrophage activation is likely through increasing phagosome maturation, inducing autophagy (Gutierrez et al., 2004a), induction of nitric oxide (NO) production (Ehrt et al., 2001), and combining with TNF-α and Vitamin D to increase the production of reactive nitrogen intermediates (Rockett et al., 1998; Bonecini-Almeida et al., 1998).

Macrophages also play a key role in maintaining the adaptive immune response. Macrophages are antigen presenting cells and therefore display derivatives of bacterial components at the plasma membrane though major histocompatibility complex (MHC) class I and II. Following migration to the lung, primed T cells interact with these displayed antigens to stimulate release of IFN-γ (Flynn and Chan, 2001a) (**Figure 1.1.1**). Without the successful induction of adaptive immunity, TB cannot be controlled (Lazarevic et al., 2005).

Finally, macrophages are essential for the initiation of granuloma formation (Davis and Ramakrishnan, 2009). As the granuloma forms and evolves several macrophage subtypes, including multinucleated giant cells (Helming and Gordon, 2008), epithelioid and foamy macrophages (Russell et al., 2009), and pro- and anti-inflammatory macrophages (Mattila et al., 2013), are required for its maintenance (**Figure 1.1.1**). Whilst only a small proportion of granuloma macrophages are thought to be infected with Mtb bacilli (Flynn et al., 2011), macrophages at the surface of granulomas contain Mtb (Kaplan et al., 2003). Additionally, during the

innate phase of infection in zebrafish, infected macrophages migrate out from one granuloma, to seed secondary granulomas (Davis and Ramakrishnan, 2009).

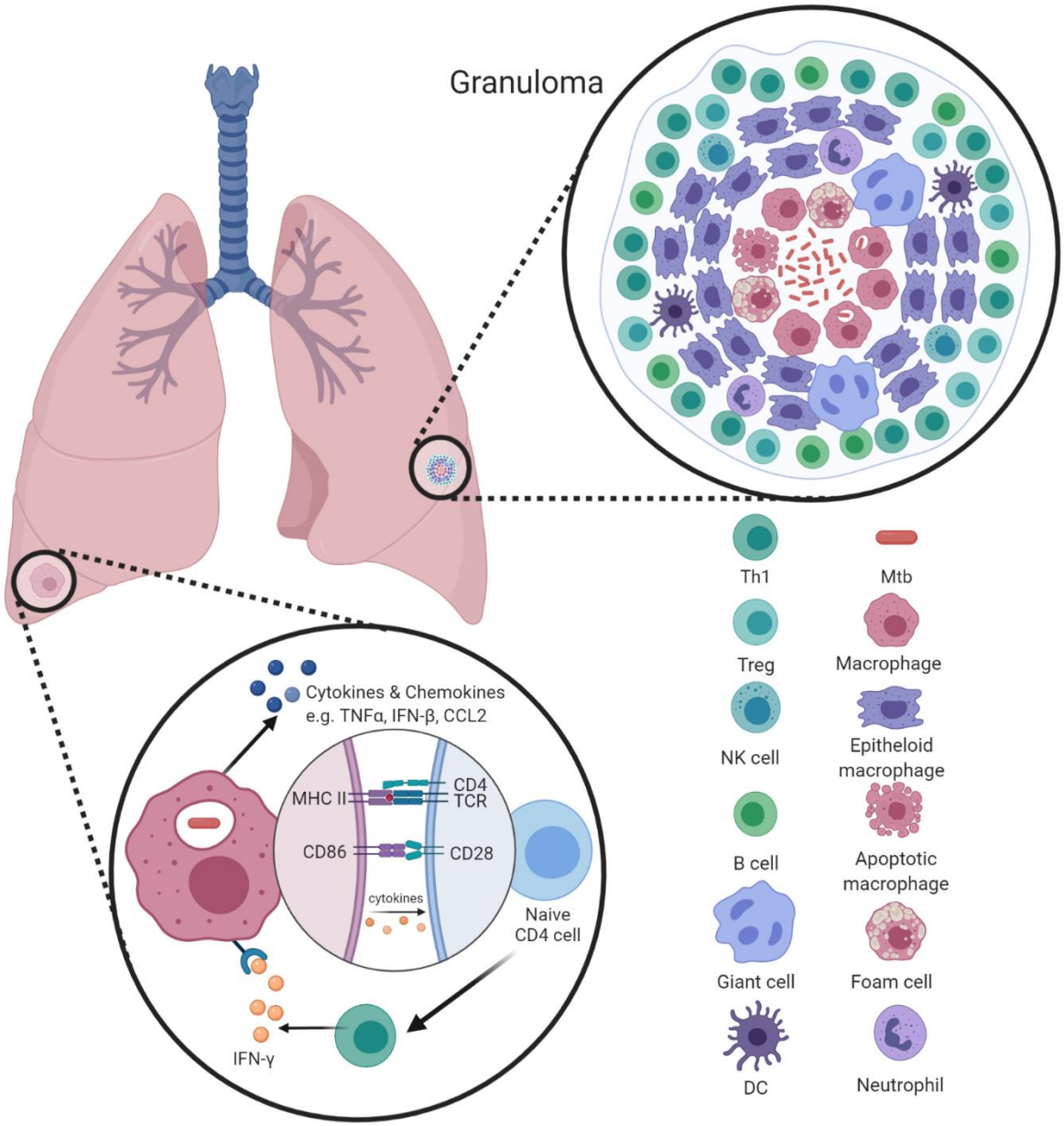

Figure 1.1.1 Macrophages are crucial for immune responses in TB. Macrophages play many roles during Mtb infection. Following phagocytosis of Mtb macrophages secrete a range of cytokines and chemokines to create an inflammatory immune response and recruit additional immune cells to the site of infection. Additionally, during adaptive immunity macrophages activate naïve T cells to secrete IFN-γ, which then activates antibacterial programs in the macrophages. Moreover,

macrophages seed, and are a key cell type in, granuloma formation and maintenance. TCR: T cell receptor, Treg: regulatory T cell, DC: dendritic cell, NK: Natural killer. Created with BioRender.com

The origins of macrophages

The single term ‘macrophage’ belies the complex heterogeneity found with this cell type. Specialised macrophages are found within tissues, with each adapting to its specific niche through interactions with the cellular components of the tissue and other cues from the microenvironment (T’Jonck et al., 2018). In mice, tissue resident alveolar macrophages are derived from yolk sac macrophages or foetal monocytes a few days after birth (van de Laar et al., 2016) and form a self-renewing pool of macrophages in the lung (Guilliams et al., 2013). Whether this also applies to humans remains uncertain (Ginhoux and Guilliams, 2016). It is also possible for adult monocytes to differentiate into tissue specific macrophages, such as Kupffer cells in the liver, following destruction of the pre-existing tissue resident cells (Bonnardel et al., 2019). A similar situation occurs in the lung where adult monocytes repopulate the alveolar niche when the resident macrophages are depleted, for example during influenza or gammaherpesvirus infection (Misharin et al., 2017; Machiels et al., 2017). At resting state, the ontogeny of tissue macrophages does not appear to play much of a role in function, likely due to thorough imprinting of function by the niche (Bonnardel and Guilliams, 2018). However, following inflammation it is possible that the different macrophages react heterogeneously based on, for example, epigenetic differences and during the recovery phase the recruited macrophages are transcriptionally distinct from tissue resident cells (Bonnardel and Guilliams, 2018).

Macrophages can also differentiate from monocytes circulating in the blood in response to wounds, infection, inflammation, and tissue damage, the mechanisms of which have been elucidated mostly using mouse systems. The monocytes are derived from haematopoietic stem cells found within the bone marrow (van Furth and Cohn, 1968; Hettinger et al., 2013). Under resting conditions monocytes are mostly retained within the bone marrow, although some circulate in the blood stream or patrol the lining of vessels sensing injury or infection that requires mobilisation of a defence response. Following inflammation or infection local secretion of chemokines, especially CCL2 and CCL7, triggers the rapid recruitment of these

monocytes (Shi and Pamer, 2011). CCL2 production by bone marrow stromal cells triggers the release of monocytes from the bone marrow and CCL2 also triggers transmigration of monocytes across the blood vessel endothelium. C-C chemokine motif receptor 2 (CCR2) knockout mice, which cannot respond to CCL2 or 7, are more susceptible to bacterial, parasitic and fungal infections, demonstrating the importance of these recruited macrophages in resolving infection and repairing the damaged tissue (Shi and Pamer, 2011).

Further complexity is added as macrophages can be activated by various stimuli and these will polarise the macrophage response. *In vitro* studies of mouse macrophages have shown that stimulation with IFN-γ and lipopolysaccharide (LPS) leads to a classically activated, or M1 phenotype, whereas activation with IL-13 and IL-4 leads to alternatively activated, M2 polarisation. Whilst M1 macrophages are pro-inflammatory, M2 have a more regulatory and anti-inflammatory role in the immune response (Atri et al., 2018). *In vivo*, the M1 phenotype is associated with intracellular pathogens and inflammatory cytokines such as TNF–α, whereas M2 polarisation in implicated in wounding, parasite infection and anti-inflammatory cytokines such as IL-10 (Atri et al., 2018). This nomenclature is widely used in mouse immunology with clear markers for each subset, however how well it is reflected in human systems remains unclear. Studies have shown M1 and M2 like responses in human macrophages (Tarique et al., 2015). Altogether, it is clear these states represent two ends of a broad spectrum and macrophages are very plastic and can repolarise in response to changes in stimuli and environment (Atri et al., 2018; Xu et al., 2013).

Human monocytes can differentiate into macrophages in response to either macrophage colony stimulating factor (M-CSF) or granulocyte macrophage colony stimulating factor (GM-CSF). GM-CSF stimulation is linked with M1 and M-CSF to M2 polarisation. GM-CSF is essential for alveolar macrophage differentiation and maintenance throughout life (Draijer et al., 2019). M-CSF is also important for proper alveolar macrophage development with mice lacking functional M-CSF having low numbers shortly after birth, but this is recovered by 4 months of age (Shibata et al., 2001). A direct comparison between M-CSF and GM-CSF differentiated human

macrophages infected with Mtb showed no significant differences in terms of bacterial replication or subcellular localisation (Lerner et al., 2017). When comparing gene expression in human and mouse macrophages after M-CSF or GM-CSF differentiation, there was minimal overlap between the species (Lacey et al., 2012). Moreover, the gene expression landscape is largely similar between resting M-CSF and GM-CSF differentiated human macrophages but the relatively small proportion of differentially expressed genes likely convey functional differences in, for example, the immune response (Lacey et al., 2012).

Overall several key questions surrounding the origins of human macrophages remain. As highlighted above, much of the work on distinct macrophage populations, e.g. tissue resident vs recruited, has been conducted using the mouse model system, thus it will be important to validate how this relates to humans. The influence of environment on these macrophage populations is also important, for example, mice are housed in very clean, pathogen free environments whereas humans are continuously exposed to stimuli such as pathogens and pollutants, how this affects macrophage activation and recruitment remains to be determined. Moreover, the stimuli used to deplete tissue resident macrophages and study the repopulation of the niche are very strong and often totally deplete the resident macrophage pool (Bonnardel et al., 2019), thus the ability of recruited macrophages to repopulate the niche under less harsh, more physiological conditions remains to be determined.

Phagocytosis and phagosome maturation

The innate immune function of macrophages relies on their ability to phagocytose pathogens and target them for lysosome-mediated killing by phagosome maturation.

Phagocytosis commences following recognition of a pathogen by receptors at the plasma membrane; many cells are capable of phagocytosis but professional phagocytes – macrophages, dendritic cells and neutrophils – are the most proficient (Rabinovitch, 1995). Various receptors participate in triggering phagocytosis including pattern recognition receptors (PRR) and opsonic receptors such as FcγR (Flannagan et al., 2012). Following ligation of these receptors, the actin cytoskeleton is rearranged to produce plasma membrane protrusions that internalise the

pathogen into a phagosome. In the context of Mtb many PRRs are required for efficient internalisation including toll like receptors (TLR), C-type lectins, scavenger receptors, cluster of differentiation (CD) 14, and nucleotide oligomerisation domain (NOD) like receptors (NLR), which recognise components of the Mtb cell wall (Killick et al., 2013).

Following phagocytosis, the resulting phagosome containing the internalised cargo undergoes a process of maturation; a series of regulated sequential fusion events with early and late endosomes, into a phagolysosome (Flannagan et al., 2012) (**Figure 1.1.2**). Phagosomes initially have a neutral pH of 7 and as they mature the pH drops to approximately 4.5 and the membrane and luminal composition changes (Flannagan et al., 2012). Early phagosomes have membranes containing high levels of phosphatidylinositol-3-phosphate (PI3P) and Rab5, whereas late phagosomes are enriched for Rab7 and phosphatidylinositol-3,5-bisphosphate ($PI3,5P_2$). It is these differences in membrane composition that allow the regulation of the directionality of maturation. Rab5 and PI3P recruit effectors such as early endosome antigen 1 (EEA1), which is important for tethering and fusion with endosomes, whereas Rab7 recruits Rab-interacting lysosomal protein (RILP), which is required for lysosome fusion (Flannagan et al., 2012). Ultimately, phagocytosed cargo is delivered to the phagolysosome, an acidic organelle loaded with degradative proteases, lipases and hydrolases aimed to degrade their content. In this context, the vacuolar type H^+ ATPase (v-ATPase) plays an essential role in phagosomal acidification and the decreased pH is required for the activity of some proteolytic and other degradative enzymes.

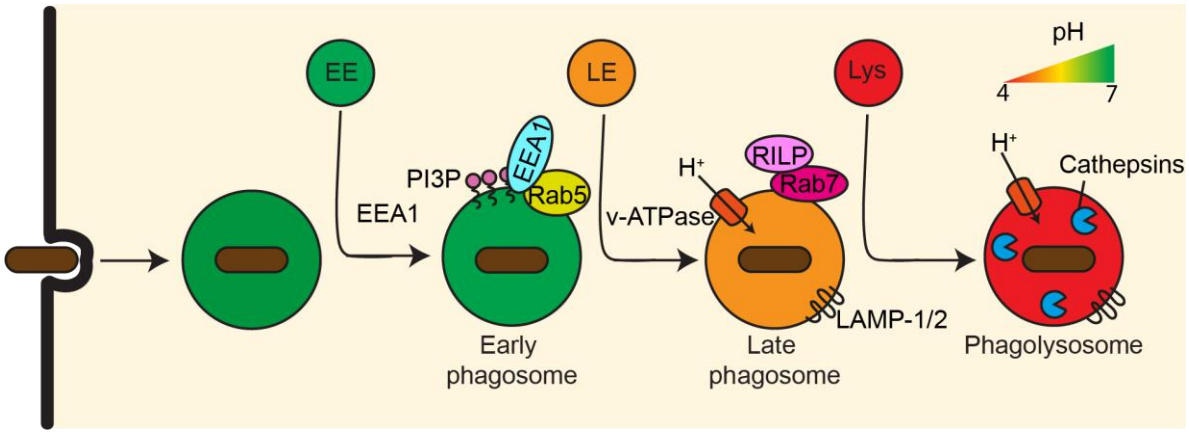

Figure 1.1.2 Phagosome maturation. Phagosomes undergo sequential fusion with vesicles of the endocytic network leading to changes in the membrane and luminal contents, as well as pH. Ultimately, the formation of the phagolysosome creates a degradative environment capable of restricting pathogen replication through a low pH and the presence of degradative enzymes such as cathepsins. EE – early endosome; LE – late endosome; Lys – lysosome.

Manipulation of phagosome maturation by intracellular pathogens

Successful intracellular pathogens have all adapted to survive through either subverting phagosome maturation or resisting the normally toxic environment of the phagolysosome. Some bacteria, such as *Listeria monocytogenes* and *Shigella flexneri*, have adapted to successfully invade the cytosol of the infected cell thus evading the phagolysosome; for these bacteria cytosolic access is essential for their replication and cell-to-cell spread. For *L. monocytogenes* the secretion of the pore forming toxin listeriolysin O (LLO) leads to the rupture of the phagosomal membrane (Gaillard et al., 1987); indeed *Bacillus subtilis* expressing LLO is able to translocate into the cytosol of infected cells and undergo enhanced replication (Bielecki et al., 1990). The *S. flexneri* Type III secretion system (T3SS) substrate proteins IpaB and IpaC, which can insert into host membranes, induce vacuolar rupture (High et al., 1992; Blocker et al., 1999). Whilst *Salmonella typhimurium* bacteria are capable of successfully replicating inside the vacuole, a subset of the bacteria damage the vacuolar membrane through the action of a T3SS and undergo hyper replication in the cytosol of epithelial cells (Knodler et al., 2010).

The parasite *Leishmania donovani* inhibits fusion events with late endosomes and lysosomes through the action of cell surface lipophosphoglycan to prevent the

acidification of the phagosome (Scianimanico et al., 1999). This mechanism is also used by *Brucella abortus*, which uses bvr-R and bvr-S to inhibit phagosome maturation and forms a compartment with autophagic and ER like morphology (Pizarro-Cerdá et al., 1998; Sola-Landa et al., 1998). *Legionella pneumophila* reside in a non-acidified phagosome that is devoid of markers of phagosome maturation, such as Rab7 and lysosome associated membrane protein (LAMP)-2, which is achieved through the action of the Type IV secretion system proteins dotA and Icm (Horwitz and Maxfield, 1984; Roy et al., 1998). It has been proposed that dotA/Icm is important for maintaining phagosome integrity, however proving this using solely electron microscopy is difficult (Molmeret et al., 2007). As previously mentioned, *S. typhimurium* can replicate in vacuoles, which interact with components of the early and late endocytic network. It is known that *S. typhimurium* acquires late endocytic markers such as Rab7 and the v-ATPase. However, the *Salmonella* containing vacuole does not acquire the cation-independent mannose-6-phosphate receptor (M-6-PR) and many of the proteases that require M-6-PR for their trafficking, thus maturation is not completed and the vacuole is non-degradative (Méresse et al., 1999; Steele-Mortimer et al., 1999; Mcgourty et al., 2012).

Manipulation of intracellular trafficking by Mtb

As an intracellular pathogen, Mtb is no exception and extensive studies have shown that mycobacteria are able to subvert the phagosome maturation pathway to facilitate survival and replication. Early electron microscopy observations of mycobacteria in macrophages revealed that whilst some phagosomes have phagolysosomal morphology (Armstrong and D'Arcy Hart, 1975), many bacilli are found in non-acidified compartments that lack markers of phagolysosomes (Crowle et al., 1991; Clemens and Horwitz, 1995). Decades of work, primarily using the attenuated strain *M. bovis* BCG, have subsequently shown the exclusion of Rab5 and Rab7 effectors from the mycobacterial phagosome is responsible for arresting phagosome maturation. EEA1 is an important Rab5 effector for tethering and fusion of early endosomes. The secreted acid phosphatase (SapM) hydrolyses PI3P in the early *M. bovis* BCG containing phagosome membrane (Vergne et al., 2005), nuclear diphosphate kinase (Ndk) inactivates Rab5 (Sun et al., 2010), and the cell wall lipid

mannose-capped lipoarabinomannan (ManLAM) inhibits Ca^{2+} dependent signalling events (Fratti et al., 2001, 2003; Vergne et al., 2003), all leading to EEA1 exclusion (**Figure 1.1.3**). In addition Ndk inactivates Rab7 to prevent the recruitment of RILP, an important mediator of late phagosome-lysosome fusion (Sun et al., 2007, 2010). Protein kinase G (PknG) also contributes to the survival of *M. bovis* BCG within macrophages by blocking phagosome maturation, however the mechanism for this remains unknown (Walburger et al., 2004; Scherr et al., 2009). The v-ATPase is excluded from the mycobacterial phagosome (Sturgill-Koszycki et al., 1994), likely as a result of the mechanisms described above, plus the action of protein tyrosine phosphatase A (PtpA) (Wong et al., 2011; Bach et al., 2008). Thus, the mycobacterium containing phagosome is a highly modified and unusual compartment largely devoid of its normal components and function.

Whilst it was initially shown that *M. bovis* BCG phagosomes fail to undergo the Rab5 to Rab7 conversion associated with phagosome maturation (Via et al., 1997), live cell imaging of Mtb in mouse macrophages revealed that this conversion does indeed take place (Schnettger et al., 2017). This suggests that at least some Mtb containing phagosomes undergo phagosome maturation. For Mtb that are exposed to an acidic lysosomal environment, they are eventually able to detoxify it; for example by shedding the lipid 1-tuberculosinyladenosine (1-TbAd) to neutralise the pH (Buter et al., 2019). Additionally, the serine protease MarP enables Mtb and *M. marinum* to survive within acidic environments; likely through modifying the bacterial cell wall to preserve intrabacterial pH (Levitte et al., 2016; Vandal et al., 2008; Small et al., 2013; Botella et al., 2017) (**Figure 1.1.3**).

The majority of the early work deciphering the manipulation of phagosome maturation by mycobacteria used the attenuated model *M. bovis* BCG, which, whilst being closely related to Mtb, lacks key virulence factors (Pym et al., 2002; Brodin et al., 2006). Moreover, many of these studies used mouse macrophage models of infection, which fail to reflect some aspects of Mtb infection that are observed in human cells (Bussi and Gutierrez, 2019). Thus, to what extent these mechanisms are important during Mtb infection of human macrophages remains partially

unresolved. Additionally, as highlighted in (Schnettger et al., 2017), the use of live cell imaging-based dynamic studies can reveal details of relatively transient, but important trafficking events during Mtb infection. Most studies to date have used fixed cell fluorescence and electron microscopy-based techniques to understand the phagosome maturation pathway in mycobacteria infected macrophages. Overall, it is important to test these findings in human macrophage models infected with Mtb and use live imaging to understand the temporal dynamics of the process.

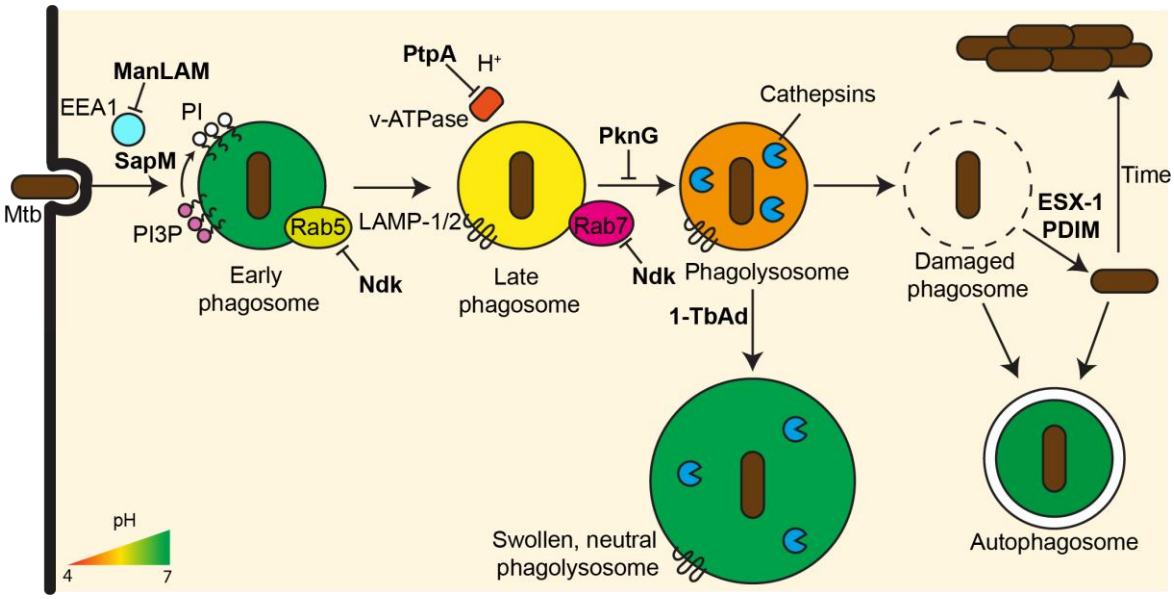

Figure 1.1.3 Phagosome maturation manipulation by Mtb. Mtb secretes several proteins and lipids (bold text) that are able to manipulate phagosome maturation to prevent trafficking of the bacteria to a phagolysosome. Almost all stages of maturation are affected including endosomal fusion, luminal acidification and membrane integrity.

Accessing the cytosol

For many intracellular pathogens, the best way to avoid being targeted to the lysosome is likely to escape from the phagosome into the cytosol, as is seen with *Listeria* and *Shigella*. Although there are sensors that detect and aim to prevent cytosolic access by pathogens (Thurston et al., 2012) (see below), or to induce cell death following cytosolic pathogen detection (Wandel et al., 2020; Santos et al., 2020; Fisch et al., 2020), the cytosol can provide a spacious and potentially nutrient rich niche for replication (Case et al., 2016). Mtb was initially observed in the cytosol of macrophages decades ago (Leake et al., 1984; McDonough et al., 1993), however

this finding was largely ignored until 2007 when it was shown by transmission electron microscopy (TEM) in human dendritic cells that a proportion of Mtb is cytosolic (van der Wel et al., 2007). Hereafter a number of reports showed Mtb in the cytosol of various cell types including human macrophages (Simeone et al., 2012; Lerner et al., 2017) and lymphatic endothelial cells (Lerner et al., 2016). In human macrophages, cytosolic access occurs relatively early during infection, with approximately 20% of bacteria in the cytosol after 2 h with the numbers of cytosolic bacilli increasing to 50% over 48 h of infection (Lerner et al., 2017). In cultured human lymphatic endothelial cells (hLEC) up to 75% of Mtb is in the cytosol by 48 h after infection (Lerner et al., 2016). In dendritic cells, a small number of cytosolic bacteria are also detected by 2 h post infection and this number increases as the infection progresses over several days (van der Wel et al., 2007). Using a Förster resonance energy transfer (FRET) based assay, Simeone et al. demonstrated that Mtb can access the cytosol of THP-1 cells as early as 2 h post infection, and the FRET signal increases over time, suggesting increasing cytosolic access as the infection progresses (Simeone et al., 2012).

Some of the mycobacterial factors that contribute to phagosome rupture and cytosolic access have been described (Queval et al., 2017). The ESX-1 Type VII secretion system (T7SS), especially the substrates early secreted antigen target 6 kDa (ESAT-6 or EsxA) and culture filtrate protein 10 kDa (CFP-10 or EsxB), is important for cytosolic localisation in several human cell models (van der Wel et al., 2007; Simeone et al., 2012; Lerner et al., 2017, 2016). The mechanism of ESX-1 dependent phagosomal rupture remains poorly understood, however contact of ESX-1 with the plasma membrane appears to cause large perturbations in the membrane rather than pores, as was previously reported (Conrad et al., 2017). The cell wall lipid phthiocerol dimycocerosates (PDIM) facilitates this cytosolic translocation (Augenstreich et al., 2017; Lerner et al., 2018; Quigley et al., 2017; Barczak et al., 2017; Osman et al., 2020), potentially through insertion into the phagosomal membrane and increasing the activity of EsxA (Augenstreich et al., 2019, 2020).

The ESX-1 secretion system is the most intensively studied of the five T7SS encoded by the Mtb genome. Mycobacteria capable of causing disease in immunocompetent people encode ESX-1 and its deletion from *M. bovis* is responsible for the attenuation of the vaccine strain *M. bovis* BCG (Pym et al., 2002; Majlessi et al., 2005; Brodin et al., 2006). The majority of the components of ESX-1 are encoded by the region of difference 1 (RD1) of the Mtb genome and deletion of this region inactivates the secretion system. The deletion of the RD1 region from Mtb mimics *M. bovis* BCG and Mtb lacking RD1 is unable to replicate efficiently or elicit cell death in THP-1 macrophages or peripheral blood mononuclear cells (PBMC), as well as showing severe attenuation in the mouse model of TB (Lewis et al., 2003). *M. marinum* lacking RD1 is unable to induce macrophage aggregation that precedes granuloma formation in Zebrafish (Volkman et al., 2004). The expression of key ESX-1 genes is controlled by the stress responsive transcription factor WhiB6 (Chen et al., 2016) and PhoPR two component system (Kumar et al., 2016; Frigui et al., 2008). Interestingly, ESAT-6 secretion is higher in clinical isolates of Mtb than in the lab adapted strain H37Rv (Solans et al., 2014). Whilst structures of the ESX-3 T7SS have recently been published, a full understanding of their secretion mechanism remains elusive, especially regarding how secreted proteins cross the periplasm and outer cell wall (Famelis et al., 2019; Poweleit et al., 2019).

The complex lipids PDIMs are also required for virulence, with all pathogenic mycobacteria and clinical isolates of Mtb expressing PDIMs (Onwueme et al., 2005; Goren et al., 1974). Mtb strains lacking PDIMs are attenuated in mice as they are more efficiently cleared by the innate immune response (Cox et al., 1999; Day et al., 2014). PDIMs also shield pathogen associated molecular patterns (PAMPs) to restrict the microbicidal activation of macrophages (Cambier et al., 2014).

The importance of cytosolic access during Mtb infection is not well understood. Mtb is able to replicate in membrane bound compartments (Lerner et al., 2016) and is able to cause disease in mice *in vivo*, where cytosolic access is yet to be shown. However, smuggling Mtb lacking the RD1 region or unable to synthesise PDIMs into the cytosol increases their replication and allows virulence-associated cording

(Lerner et al., 2020); suggesting that successful localisation to the cytosol may increase virulence. Moreover, whilst several virulent strains of mycobacteria have been shown to access the cytosol, non-pathogenic strains and mutants do not (Houben et al., 2012). Additionally, given the essential roles for both ESX-1 and PDIM in cytosolic access and virulence, a link between the two is highly likely. Further, complementation of *M. bovis* BCG restored cytosolic localisation of the bacteria and virulence in mice (Houben et al., 2012; Brodin et al., 2006; Pym et al., 2002).

It is also important to distinguish the difference between cytosolic access and being free in the cytosol. Whilst assays such as the FRET approach in (Simeone et al., 2012) can show a loss of phagosome membrane integrity, facilitating contact between the β-lactamase and substrate, it cannot determine if the bacteria has fully accessed the cytosol and has no host membranes around it. Electron microscopy (EM) based approaches, such as those used by (van der Wel et al., 2007; Lerner et al., 2017), can, however, demonstrate bacteria free in the cytosol. One important caveat to the 2D EM approach is that it cannot be determined if host membranes partially cover the bacteria in areas not imaged.

Several consequences of phagosome damage and cytosolic access by Mtb are known. Initially, damage to the phagosome membrane triggers targeting to autophagy (Watson et al., 2012), which can also be subverted by Mtb in an ESX-1 dependent manner (Romagnoli et al., 2012), discussed in detail later. In THP-1 cells phagosome damage is rapidly followed by plasma membrane damage, NOD- LRR- and Pyrin-domain containing protein 3 (NLRP3) inflammasome activation and pyroptotic cell death (Beckwith et al., 2020). Primary human macrophages and THP-1 cells can survive for several days following Mtb infection before undergoing necrotic cell death, in an RD1 dependent manner, with Mtb replicating in the necrotic corpses (Lerner et al., 2017; Simeone et al., 2012). Human dendritic cells undergo increased apoptotic cell death when infected with Mtb WT but not *M. bovis* BCG or Mtb RD1 mutants (van der Wel et al., 2007). Regardless of the mode, cytosolic

access eventually triggers cell death and lysis facilitating cell-to-cell spread of Mtb (Beckwith et al., 2020).

1.2 Intracellular membrane damage and repair

Causes of intracellular membrane damage

Damage to intracellular membranes occurs due to various insults including pathogen infection, osmotic stress, and crystal formation. As well as being pathological, membrane damage can be important for normal biological processes, for example selective damage to lysosomes plays a role in chromosome segregation during mitosis (Hämälistö et al., 2020). Regardless of the cause of the membrane damage cells need to be able to either repair it or degrade the damaged organelle. Failure to do so can be cytotoxic and this may play a role in many human diseases, including Parkinson's disease (Repnik et al., 2017; Herbst et al., 2020; Papadopoulos et al., 2020).

As with Mtb, many other intracellular pathogens damage their limiting host membrane in order to access the cytosol. For most of these, a role for both bacterial and host proteins and processes has been described. Listeria uses LLO in concert with bacterial phospholipases (Smith et al., 1995). The action of LLO is potentiated by host proteins including the cystic fibrosis transmembrane conductance regulator (CFTR) and γ-interferon inducible lysosomal thiol reductase (GILT) (Radtke et al., 2011; Singh et al., 2008). The *Salmonella* T3SS, SPI-1, has been implicated in damaging the membrane of the *Salmonella* containing vacuole (SCV) (Knodler et al., 2010; Malik-Kale et al., 2012; Roy et al., 2004). This process is aided by the dynamic expansion and shrinkage of the SCV through fusion with macropinosomes and tubule-based membrane removal (Stévenin et al., 2019). Infection associated macropinosomes also increase IpaB and IpaC triggered rupture of the *Shigella* vacuole, through a contact dependent mechanism (Weiner et al., 2016; Mellouk et al., 2014).

The formation of pores is a common mechanism deployed by many pathogen effectors in order to induce membrane damage. Some gram positive bacteria encode proteins belonging to the cholesterol-dependent cytolysin family, for example *Listeria*

derived LLO and streptolysin-O produced by Group A *Streptococcus* (GAS), which form pores in membranes to facilitate cytosolic access (Schnupf and Portnoy, 2007; Nakagawa et al., 2004; Feil et al., 2014).

Recognition of membrane damage by galectins

Given that endomembrane damage can cause significant cellular damage and be cytotoxic (Papadopoulos et al., 2020), it is important that cells are able to detect perturbations in membrane integrity. Following endomembrane damage select members of a family of cytosolic lectins, called galectins (Gal), recognise luminal sugar moieties exposed to the cytosol (Thurston et al., 2012; Paz et al., 2010). From the galectin family, Gal3, Gal8 and Gal9 have had their functions best characterised (**Figure 1.2.1**). Gal3 regulates the recruitment of the endosomal sorting complex required for transport (ESCRT) machinery to coordinate repair of small damage (Jia et al., 2020b). Gal9 activates AMP dependent kinase (AMPK) to promote autophagosome biogenesis (Jia et al., 2018, 2020a). Gal8 controls autophagy through inhibiting mechanistic target of rapamycin complex 1 (mTORC1) (Jia et al., 2018) and recruitment of the initiation machinery (Thurston et al., 2012; Ravenhill et al., 2019). Following recognition of membrane damage Gal8 recruits the adaptor protein nuclear dot protein 52 (NDP52) (Thurston et al., 2012), which facilitates recruitment of the Unc-51 like autophagy activating kinase 1 (ULK1) complex directly to the bacteria to initiate selective autophagy, known as xenophagy (Ravenhill et al., 2019). A similar pathway operates during mitophagy, where damaged and dysfunctional mitochondria are targeted for degradation (Vargas et al., 2019; Turco et al., 2019).

The recognition of extensive membrane damage by galectins is preceded by flipping of sphingomyelin from the inner to the outer leaflet of endomembranes and the presence of small, 100-200 nm pores (Ellison et al., 2020). Molecular dynamics simulations have shown that lipids likely move between bilayers through a flip-flop mechanism during various pore-forming processes (Marrink et al., 2009). As transbilayer movement of lipids can be an energetically costly process, it is often assisted by lipid flippases, floppases and scramblases (Hankins et al., 2015).

Whether such events are required to transfer sphingomyelin, or if it undergoes flip-flop due to small pores is unknown. Moreover, alterations in membrane lipid content, especially cholesterol, are linked to alterations in membrane stability, damage susceptibility and pore forming toxin activity (Rojko and Anderluh, 2015; Raffy and Teissié, 1999). For example, clusters of sphingomyelin are associated with the insertion of the pore forming toxins lysenin, which is now used as a probe for sphingomyelin (Yamaji et al., 1998; Ellison et al., 2020). If, and how, sphingomyelin flipping prior to or during membrane damage is detected by cells, and the cellular response to this flipping currently requires further study.

Repair of damaged intracellular membranes

Following successful recognition of membrane damage cells are thought to initially attempt repair of the damage, so long as it is limited and small (Skowyra et al., 2018). If the damage extends, or if repair fails then the autophagy machinery – introduced in detail below – will degrade the damaged organelle (Gutierrez and Carlton, 2018; Radulovic et al., 2018; Herbst et al., 2020).

The ESCRT-III machinery recognises a reverse membrane topology and brings about scission during multivesicular body formation (Babst et al., 2002a; b; Katzmann et al., 2001). The ESCRT machinery has subsequently been shown to have diverse roles in cells where similar membrane topologies are observed such as cell division and nuclear envelope reformation (Carlton and Martin-serrano, 2007; Olmos et al., 2015). Additionally, the ESCRT machinery participates in the repair of damaged endolysosomal membranes (Skowyra et al., 2018; Radulovic et al., 2018). It is believed that the ESCRT machinery will repair small damage to endolysosomes, in the order of less than 100 nm in diameter, as was shown for ESCRT-mediated plasma membrane repair (Jimenez et al., 2014). The exact mechanism of how repair is achieved is unknown. Putative hypotheses include pinching off of small vesicles to seal the two ends of the membrane, or forming spiral disks occluding the hole to allow membrane to flow over and seal the sap (Gutierrez and Carlton, 2018). One question that is still not answered is what triggers the recruitment of the ESCRT machinery. Calcium has been proposed (Scheffer et al., 2014; Skowyra et al., 2018)

however this was not recapitulated by (Radulovic et al., 2018). Ca^{2+} dependent, leucine rich repeat kinase 2 (LRRK2) mediated phosphorylation of Rab8 also plays a role, although the mechanistic link between Rab8 and ESCRT recruitment is still unknown (Herbst et al., 2020).

In addition to repairing endolysosomal damage, some components of the ESCRT machinery are also recruited to mycobacterial phagosomes (López-Jiménez et al., 2018; Mittal et al., 2018). Interestingly, the recruitment of ESCRT-III is enhanced by, but not dependent on, the ESX-1 T7SS (Mittal et al., 2018), suggesting that whilst the ESX-1 machinery is required for large enough damage to facilitate phagosome escape, smaller damage may occur without it. Alternatively, the ESCRT machinery could have a different function in non-damage related activities on Mtb ΔRD1 phagosomes. The correct functioning of the ESCRT machinery is disrupted in Mtb infected macrophages. Through the secretion of EsxG and EsxH by the ESX-3 T7SS Mtb blocks the action of the ESCRT machinery in repairing membranes damaged by Mtb or L-leucyl-L-leucyl methyl ester (LLOMe), a compound that damages lysosomal membranes (Mittal et al., 2018). EsxH interacts with Hrs, a component of the ESCRT-0 machinery responsible for cargo recognition during endosomal sorting, to disrupt phagosome maturation (Mehra et al., 2013). This interaction between EsxH and Hrs is not required for inhibiting ESCRT-III mediated endomembrane repair, thus the precise mechanism of EsxGH mediated inhibition of ESCRT-III action is unknown (Mittal et al., 2018). Although no direct link has been made, it is tempting to speculate there is a link between the EsxH mediated inhibition of antigen presentation and T cell activation and its ability to block phagosome maturation and endomembrane repair (Portal-Celhay et al., 2016).

When endosomal and phagosomal membranes have been more extensively damaged and the ESCRT machinery is unable to close the gap autophagosomes may contribute to repair; as reported with damaged *Salmonella* containing endosomes (Kreibich et al., 2015). During macrophage infection with the fungal pathogen *Candida albicans* continued influx of lysosomal membranes facilitates maintenance of phagosome membrane integrity as the pathogen replicates

(Westman et al., 2020). Disruption of lysosomal membrane influx leads to increased membrane damage, enhanced inflammasome activation and increased cell death. It has been postulated that the lysosomal protein Synaptotagmin VII, which plays a role in plasma membrane repair through lysosomal fusion (Reddy et al., 2001), aids in repairing or recapturing *Yersinia pseudotuberculosis*, and possibly *Salmonella*, following phagosome permeabilisation through increased lysosomal fusion (Roy et al., 2004).

Removal of damaged membranes

Terminally damaged organelles, such as lysosomes, are removed and degraded by the autophagy machinery (Maejima et al., 2013; Settembre et al., 2011). Signals for removal include Gal8 recruitment (Thurston et al., 2012) and polyubiquitination (Maejima et al., 2013; Koerver et al., 2019). Polyubiquitin chains, particularly K63 linked, decorate terminally damaged lysosomes. This ubiquitination requires the E2 UBE2QL1 but the implicated E3 enzymes have yet to be identified (Koerver et al., 2019). The removal of damaged lysosomes by the autophagy pathway is important for the restoration of the cellular pool of acidified lysosomes as the previously damaged lysosomes re-acidify (Maejima et al., 2013).

Lysosomal damage also leads to replacement of lysosomes in order to restore lysosomal function. This requires translocation of the transcription factor EB (TFEB) to the nucleus and membrane protein recycling (Eriksson et al., 2020). TFEB regulates the transcription of lysosomal biogenesis genes, as well as genes for proteins that regulate the autophagy pathway (Napolitano and Ballabio, 2016). The lysosome resident, energy sensing kinase mTORC1 inhibits TFEB activity through phosphorylation (Settembre et al., 2012; Roczniak-Ferguson et al., 2012) so the inactivation of mTORC1 by Gal8 upon recognition of damage leads to the lysosome replacement program (Jia et al., 2018).

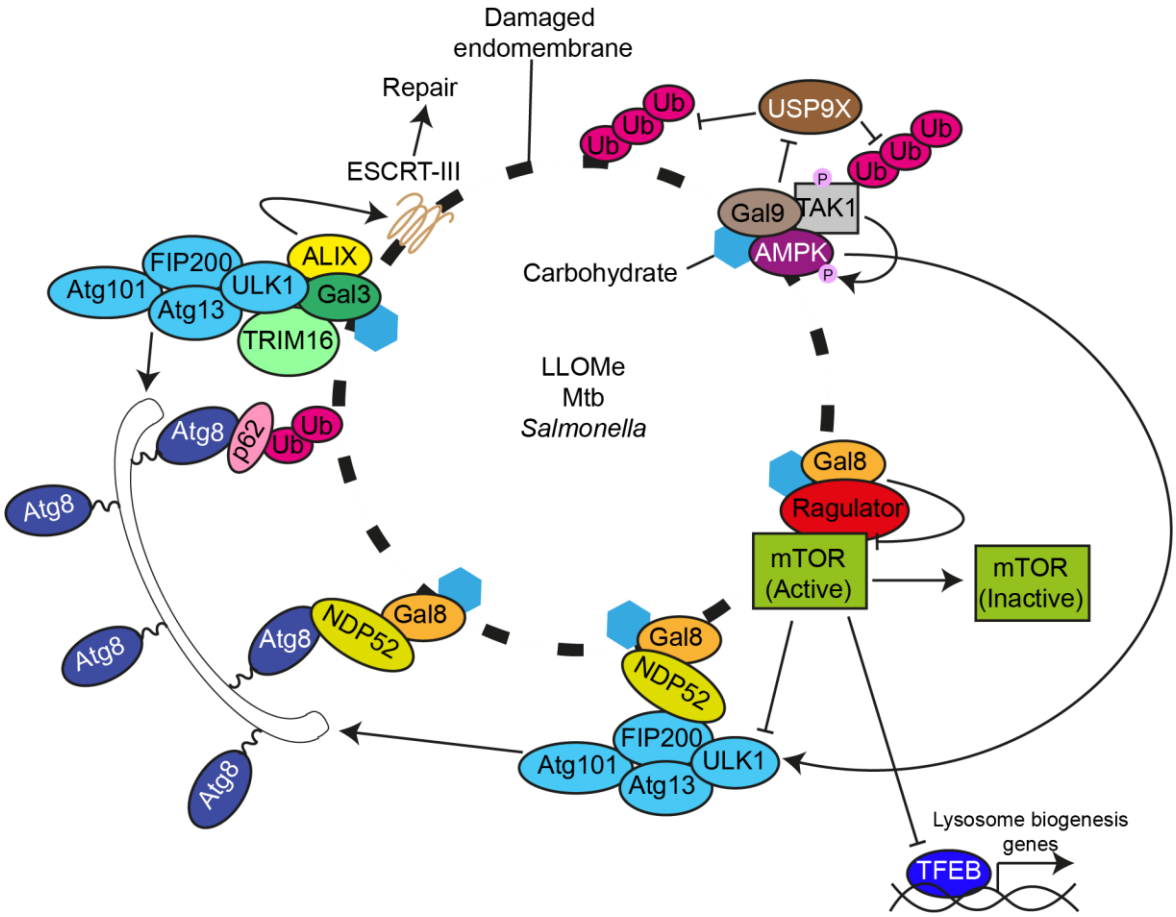

Figure 1.2.1 Recognition and resolution of endomembrane damage. Damage to membranes of the endosomal and phagosomal systems can be induced by chemicals, crystals and intracellular pathogens. Galectins and polyubiquitin serve as recognition signals for damaged endomembranes. Through the recruitment of additional proteins, galectins can coordinate the repair of damage by ESCRTs, removal of irreparable damage by autophagy and replacement of lysosomes through TFEB regulated transcription. Membrane protein ubiquitination further enhances autophagic clearance of damaged organelles through an interaction with autophagy receptors, such as p62. Overall, this system achieves endomembrane homeostasis to prevent cytotoxicity from the leaking of luminal contents into the cytosol.

1.3 Autophagy and immune defence

Autophagosome biogenesis, maturation and degradation

Macroautophagy, hereafter referred to as autophagy, is the process by which cells enwrap regions of cytoplasm in a double membraned organelle – the autophagosome – for targeting to the lysosome for degradation (Eskelinen and Saftig, 2009). Initially discovered in yeast as a starvation response, autophagy is

highly conserved across eukaryotes with diverse functions (Yang and Klionsky, 2009). Autophagosome biogenesis in response to starvation is tightly regulated by the two energy-sensing kinases – mTOR and AMPK. Autophagy begins with the formation of a membrane structure called the phagophore from the endoplasmic reticulum (ER) followed by rapid expansion of this membrane to form an autophagosome, which closes to isolate the luminal contents from the rest of the cytoplasm (**Figure 1.3.1**). During cellular energy depletion, which causes mTORC1 inactivation and AMPK activation, the ULK1 complex localises to the ER and phosphorylation changes lead to the initiation of autophagosome biogenesis (Kim et al., 2011b). ULK1 activates the lipid kinase activity of phosphatidylinositol-3-kinase (PI3K) catalytic subunit type 3 (Vps34) to generate PI3P at defined sites on the ER, termed the omegasome (Russell et al., 2013; Park et al., 2016; Axe et al., 2008). WD40 repeat domain phosphoinositide interacting protein 2b (WIPI2b) binds to PI3P to recruit the Atg5-12-16L1 complex (Dooley et al., 2014), which proceeds to conjugate Atg8 family proteins (LC3s, GABARAPs) to phosphatidylethanolamine lipids in the forming phagophore (Fujita et al., 2008; Sou et al., 2006). The recruitment of Atg8 proteins is essential for elongation and closure of the phagophore as well as cargo recruitment (Slobodkin and Elazar, 2013). Once the forming autophagosome has two ends that are close together, a fusion event, mediated by the ESCRT machinery and Atg8, leads to completion of the autophagosome (Takahashi et al., 2018; Zhou et al., 2019; Zhen et al., 2020; Nakatogawa et al., 2007). A Rab5 dependent interaction of Atg17 with the ESCRT-III component Snf7 is implicated in the recruitment of ESCRTs to the phagophore (Zhou et al., 2019) and depletion of ESCRT-III components leads to increased numbers of open phagophores, as observed by electron microscopy (Takahashi et al., 2018), and a failure to engulf mitochondria in closed autophagosomes (Zhen et al., 2020).

Following closure, autophagosomes dissociate from the ER and mature in a similar way to endosome maturation in the endocytic pathway (Tooze et al., 2014; Lamb et al., 2013). Following lysosomal fusion to form autophagolysosomes, the luminal contents and inner membrane are degraded (Zhao and Zhang, 2019). Initially, fusion

events of autophagosomes with early and late endosomes leads to the formation of the amphisome – an Atg8 positive structure with a single membrane and autophagosomal and endosomal material in the lumen. The molecular machinery governing these fusion remains poorly understood (Zhao and Zhang, 2019). Finally, the amphisome fuses with lysosomes to generate a hydrolytic and acidic environment in order to degrade the luminal contents. The fusion of amphisomes with lysosomes is regulated by two soluble n-ethylmaleimide-sensitive factor attachment protein receptor (SNARE) complexes consisting of syntaxin (STX)17-synaptosomal associated protein (SNAP)29-vesicle associated membrane protein (VAMP)8 (Itakura et al., 2012) and YKT6-SNAP26-STX7 (Matsui et al., 2018). STX17 is targeted to autophagosomes by immunity-related GTPase (IRG)-M (Kumar et al., 2018) and collapse of the inner autophagosome membrane leads to dissociation of STX17, independently of acidification (Tsuboyama et al., 2016). The small GTPase Rab7 plays a crucial role in autophagosome-lysosome fusion (Gutierrez et al., 2004b) through the targeting of various tethers, including ectopic P granules protein 5 (EPG5) (Wang et al., 2016), the homotypic fusion and protein sorting (HOPS) complex (Hegedus et al., 2016; Gao et al., 2018), and pleckstrin homology domain containing family member 1 (PLEKHM1) (McEwan et al., 2015; Tabata et al., 2010; Nguyen et al., 2016), to lysosomes. These tethers work to stabilise the SNARE complexes and promote fusion. Other tethers including Atg14 (Diao et al., 2015) and GRASP55 (Zhang et al., 2018) have been implicated in enhancing the activity of autophagosomal SNARE complexes.

Of the Atg8 family proteins, of which there are six in humans: LC3A/B/C, GABARAP, GABARAPL1, and GABARAPL2 (Shpilka et al., 2011), LC3 is the most commonly studied and is frequently used as a specific marker for autophagic compartments. LC3 localisation to autophagosomes is dependent on form II formation, i.e. the lipidation onto lipids, primarily phosphatidylethanolamine, in the phagophore/autophagosome membrane (Kabeya et al., 2004, 2000) and both LC3s and GABARAPs are essential for autophagy (Weidberg et al., 2010). Prior to lipidation, Atg8s must be activated through a C-terminal cleavage event mediated by Atg4 (Agrotis et al., 2019) and then loaded onto the E1- and E2-like enzymes,

Atg7 and Atg3 respectively, prior to lipid conjugation by the Atg5-12-16L1 E3-like complex. Proteins containing either an LC3 interacting region (LIR) or GABARAP interaction motif (GIM) (Rogov et al., 2017) can bind to members of their respective Atg8 family in order to be recruited to the autophagosome. Through this recruitment of proteins Atg8s are important for cargo recruitment, membrane elongation, and autophagosome trafficking (Olsvik et al., 2015). Whilst a large degree of sequence and structural homology exists among Atg8s, key differences provide specificity for receptor and adaptor recruitment. For example the cargo receptor NDP52 specifically binds to LC3C (von Muhlinen et al., 2012) and the trafficking protein FYVE and coiled-coil domain containing protein 1 (FYCO1) preferentially binds LC3A/B (Olsvik et al., 2015). GABARAPs are particularly important in autophagosome maturation, likely due to the presence of a GIM in PLEKHM1 (Weidberg et al., 2010; Rogov et al., 2017).

Monitoring LC3B processing is frequently used to monitor autophagosome formation and degradation, known as flux, due to a wide range of tools available including fluorescent protein constructs and validated antibodies. By Western blot, LC3 conjugated to lipids (LC3-II) – thus incorporated into autophagic membranes – runs at 15 kDa whereas the Atg4 processed, unconjugated, cytosolic form (LC3-I) runs at 18 kDa. By measuring changes in the ratio of these two forms or levels of LC3-II, one can identify changes in levels of autophagosomes. By inhibiting lysosomal function, e.g. by inhibiting the v-ATPase with Bafilomycin A1 (BafA1), and thus blocking autophagosome degradation it is possible to determine if changes in LC3 processing are due to changes in biogenesis or degradation (Klionsky et al., 2016). Additionally, the conjugated form will produce puncta by fluorescence microscopy so counts of LC3B puncta show how autophagosome numbers change in response to stimuli.

The source of the autophagosomal membrane is one of the most controversial questions in the field. The ER is a well-defined and broadly accepted platform for autophagosome biogenesis (Hayashi-Nishino et al., 2010; Biazik et al., 2015), with ER-mitochondria contact sites being the specific subdomain where this occurs

(Hamasaki et al., 2013). The expansion of the phagophore requires an influx of membrane and lipids from various sources including mitochondria, the Golgi apparatus, recycling endosomes, and the ER (Yamamoto et al., 2012; Valverde et al., 2019; Osawa et al., 2019; Maeda et al., 2019; Hamasaki et al., 2013; De Tito et al., 2020). Moreover, lipid influx from the ER is mediated by Atg2 and these lipids are directly incorporated into the autophagosomal membrane (Valverde et al., 2019; Tang et al., 2019; Osawa et al., 2019; Maeda et al., 2019).

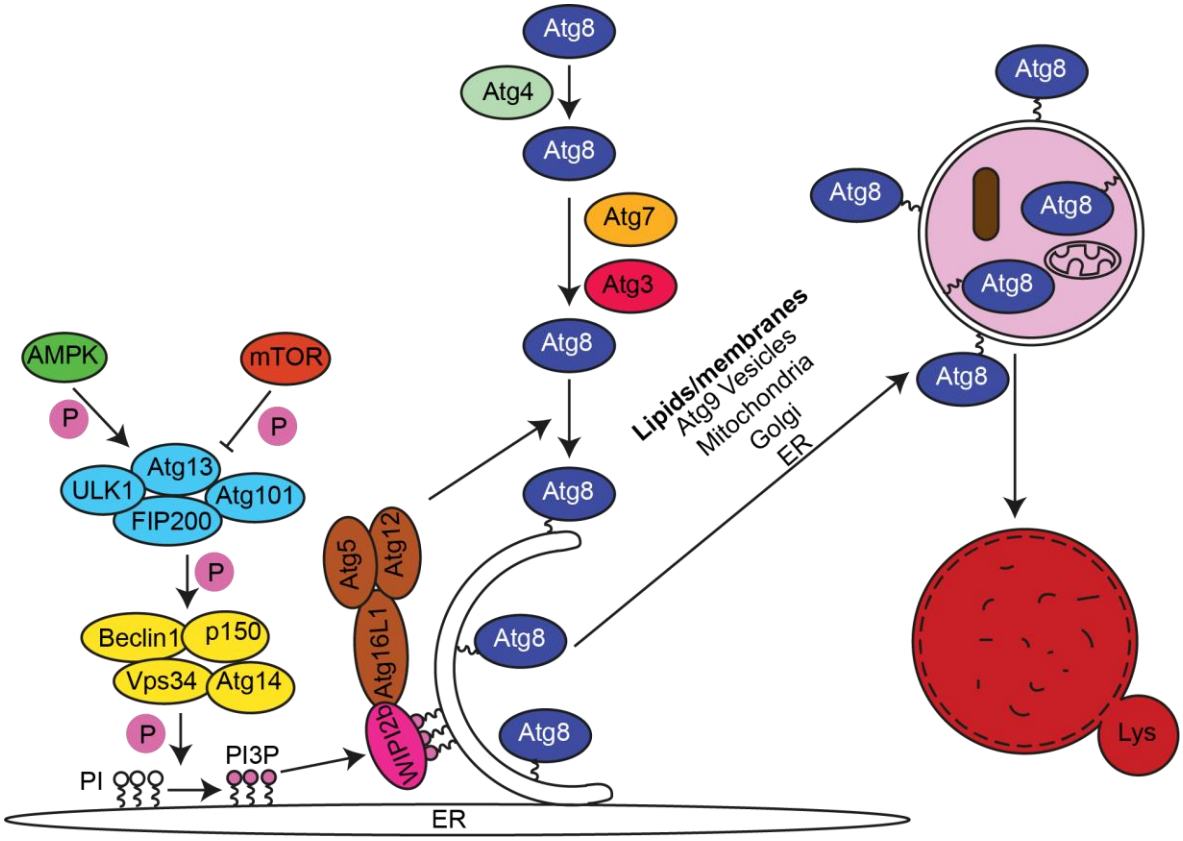

Figure 1.3.1 Autophagosome biogenesis. Autophagosome biogenesis is controlled by the two energy sensing kinases mTOR and AMPK. Activation of autophagosome biogenesis is triggered through the activity of a protein and lipid kinase complex to generate PI3P enriched microdomains of the ER. PI3P facilitates the recruitment of WIPI proteins, which recruit the Atg5-12-16L1 E3 like complex to lipidate Atg8 family proteins onto the phagophore. An influx of lipids and membranes from various sources facilitates the elongation of the phagophore to the fully formed autophagosome. After formation, autophagosomes eventually fuse with lysosomes to degrade the inner membrane and luminal contents.

Non-canonical autophagy

Over the past decade, research has uncovered alternative pathways that co-opt components of the autophagy machinery to conjugate Atg8 family proteins, especially LC3, onto single membranes. This single membrane autophagy is broadly known as non-canonical autophagy. Initially discovered as a response following neutralisation and swelling of endolysosomal compartments by compounds such as monensin and chloroquine, it is now known to also play a role during entosis, the engulfment of living cells (Florey et al., 2011, 2015). Moreover, a form of non-canonical autophagy, known as LC3-associated phagocytosis (LAP), has also been shown to play a role in immune defence (see below) (Martinez et al., 2011). Finally, in microglia LC3-associated endocytosis (LANDO) has been implicated in clearance of Aβ to prevent neurodegeneration (Heckmann et al., 2019).

Autophagy and pathogen immunity

Targeting of bacteria to autophagy mediated clearance, known as xenophagy, has been implicated in defending multiple cell types against multiple pathogens (Gutierrez et al., 2004a; Randow and Münz, 2012; Nakagawa et al., 2004; Birmingham et al., 2006). Xenophagy refers to the recognition of bacteria, usually as they translocate into the cytosol, and their capture by newly formed autophagosomes (**Figure 1.3.2**), as is discussed in detail below. Defects in xenophagy are frequently, but not always, associated with increased pathogen replication and poorer outcomes of infection both *in vitro* and *in vivo*.

The non-canonical autophagy pathway of LAP leads to the direct conjugation of LC3 to the phagosomal membrane with the resulting structure referred to as a LAPosome (Martinez et al., 2011, 2015; Sanjuan et al., 2007) (**Figure 1.3.2**). LAP is independent of the ULK1 complex and does not require Atg14 but instead uses UV radiation resistance-associated gene (UVRAG) and Rubicon as subunits of the Vps34 complex (Martinez et al., 2015). In the context of canonical autophagy, Rubicon is a negative regulator (Matsunaga et al., 2009). The non-canonical autophagy pathways require the lipidation machinery of Atg4, Atg7, Atg3 and Atg5-12-16L1. LAP is triggered following ligation of pathogen recognition receptors such as TLRs (Sanjuan

et al., 2007), Dectin1/2 (Ma et al., 2012) or antibody receptors like FcγR2a. This initiates signalling pathways involving Syk (Tam et al., 2014) and diacylglycerol (DAG) mediated recruitment of protein kinase C (PKC) isoform δ (Shahnazari et al., 2010) to assemble active NADPH oxidase on the nascent phagosome (Huang et al., 2009) and this triggers LAP through the generation of reactive oxygen species (ROS). The Rubicon containing PI3K complex generates PI3P to recruit the $p40^{phox}$ subunit of NAPH oxidase and Rubicon itself stabilises the $p22^{phox}$ subunit (Martinez et al., 2015; Yang et al., 2012; Bagaitkar et al., 2017; Nunes et al., 2013). In addition to conjugation to phosphatidylethanolamine, LC3 is also conjugated to phosphatidylserine during non-canonical autophagy (Durgan et al., 2020).

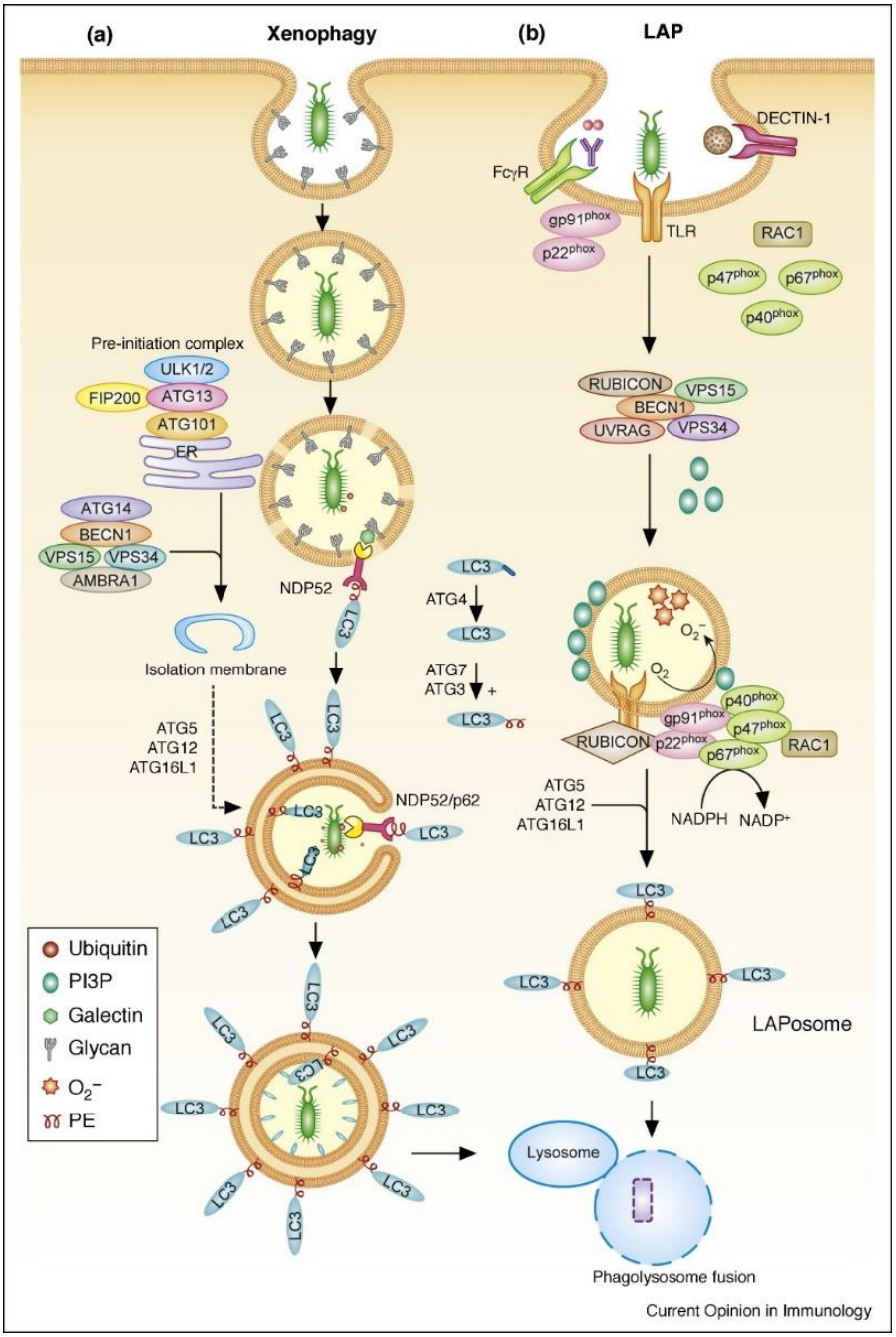

Figure 1.3.2 Mechanisms of canonical vs non-canonical autophagy in pathogen infection. Following phagocytosis pathogens can be targeted to LC3 positive compartments by a canonical pathway, xenophagy (a), or non-canonical autophagy, LAP (b). Whilst xenophagy requires all components of the autophagosome biogenesis machinery and the de novo formation of an autophagosome, LAP conjugates LC3 directly onto the newly formed phagosomal membrane. Both pathways deliver their contents to lysosomes for degradation. Reproduced from (Upadhyay and Philips, 2019), copyright 2019 with permission of Elsevier.

Another mechanism by which bacteria could be targeted to autophagic compartments is through the fusion of the phagosome directly with an autophagosome (**Figure 1.3.3**). Whilst evidence for this is currently lacking, it is feasible that phagosomes could fuse with autophagosomes, as is seen with autophagosome-endosome fusion during amphisome generation (Zhao and Zhang, 2019), if they have the required tethering and fusion machinery.

Initiation of xenophagy

Commonly, the autophagy machinery targets bacteria as they translocate to the cytosol through two predominant mechanisms: recognition of the membrane damage event (Thurston et al., 2012) or ubiquitination of pathogens and/or host proteins (Perrin et al., 2004; Zheng et al., 2009) (**Figure 1.3.3**). As described earlier, endomembrane damage leads to the recruitment of galectins (Thurston et al., 2012). In the context of xenophagy, Gal8 is required for successful autophagic targeting through the recruitment of NDP52, ULK1, TANK binding kinase 1 (TBK1) and Tax-1 binding protein 1 (TAX1BP1) (Thurston et al., 2012; von Muhlinen et al., 2012; Thurston et al., 2016; Ravenhill et al., 2019; Bell et al., 2020). Gal3 recruits the ubiquitin ligase tripartitie motif containing protein (TRIM) 16 in the context of Mtb infection and defects in this pathway reduce ubiquitination and lysosomal targeting of Mtb (Chauhan et al., 2016). During infection with *L. pneumophila*, Gal3 recruits guanylate binding proteins (GBP), although this is not associated with autophagy, further supporting the concept of galectins having multiple autophagy dependent and independent functions during infection (Feeley et al., 2017).

In general, ubiquitination follows the galectin-mediated recognition of membrane damage (Chauhan et al., 2016; Noad et al., 2017). Ligation of polyubiquitin to bacteria and/or damaged membranes serves as a platform for enhancing autophagic targeting (Perrin et al., 2004; Zheng et al., 2009). Ubiquitin is able to recruit cargo receptors such as p62, NDP52, TAX1BP1, Optineurin, and next to BRCA1 gene (NBR1), which also contain LIRs (Wild et al., 2011; Tumbarello et al., 2015; Zheng et al., 2009; Thurston et al., 2009; Franco et al., 2016). LIRs enable the targeting of ubiquitinated substrates to autophagosomes by binding to LC3 on the luminal

surface of the forming autophagosome. It is likely that cargo receptors provide a scaffolding role to shape the growing autophagosome and anchor it to the bacteria. Additionally, Atg16L1 is able to bind ubiquitin directly, through its C-terminal WD40 domain, to initiate xenophagy (Fujita et al., 2013).

The substrates for ubiquitination are poorly characterised but are likely a combination of both bacterial and host proteins (Fiskin et al., 2016; Chai et al., 2019). Further argument for ubiquitination of the bacterial surface comes from *in vitro* experiments performed with GAS where NO induced S-guanylation of surface proteins increases K63 polyubiquitin and autophagic targeting (Ito et al., 2013). Ubiquitination of host proteins also occurs; however, whether this impacts xenophagy is unclear. Ubiquitination of host proteins is important for autophagy mediated clearance of membrane remnants from phagosomal rupture by *Shigella* to limit early inflammasome activation (Dupont et al., 2009).

It is generally accepted that the successful re-localisation of bacteria from a membrane bound compartment into the cytosol is detrimental for the cell. Cytosolic bacteria are not exposed to the bactericidal environment of the phagolysosome, have greater space for replication and potentially increased nutrient availability; all of which will favour bacterial survival (Case et al., 2016). In the context of *Salmonella*, successful access to the cytosol is associated with hyper-replication (Brumell et al., 2002). Additionally, successful escape into the cytosol allows actin-mediated cell-to-cell spread of certain pathogens such as *Listeria* and *Shigella* (Bernardini et al., 1989; Tilney and Portnoy, 1989). Ultimately, uncontrolled pathogen replication in the cytosol will lead to cell death (Fredlund and Enninga, 2014). Thus, having temporally regulated responses likely provides fail-safes to prevent bacterial replication, cell-to-cell spread and cell death.

There are multiple ubiquitin binding cargo receptors that lead to autophagic targeting, likely to provide multiple layers of regulation. It is possible that this is simply a mechanism for redundancy in the system, indeed deletion of any single cargo receptor only has a small effect on pathogen autophagic targeting (Thurston et al., 2009; Zheng et al., 2009). Combined knockdown of NDP52 and Optineurin doesn't

have an additive effect on increasing *Salmonella* burden in HeLa cells, suggesting some redundancy (Wild et al., 2011). Autophagy receptor expression is also restricted in tissues, for example TAX1BP1 is only detected in human brain and kidney, although cell type specific expression was not analysed in this work (Sarraf et al., 2020). NDP52 is an autophagy adaptor that contains a LIR motif with specificity for LC3C binding and is particularly important for xenophagy (von Muhlinen et al., 2012). Additionally, polyubiquitin chains formed through different lysine residues in ubiquitin are associated with bacteria and these alternative linkages have different downstream consequences (Huett et al., 2012; Noad et al., 2017; Polajnar et al., 2017). Linear ubiquitin, synthesised by the E3 ligase linear ubiquitin assembly complex (LUBAC) on the surface of *Salmonella*, specifically recruits Optineurin for xenophagy as well as NF-κB essential modulator (NEMO) to induce NF-κB signalling (Noad et al., 2017). In Mtb infection the E3 ubiquitin ligase Parkin catalyses the formation of K63 and SMURF1 K48 polyubiquitin (Franco et al., 2016; Manzanillo et al., 2013). Knockdown of SMURF1 decreased NBR1 but not p62 recruitment, implicating K48 linked polyubiquitin in NBR1 but not p62 recruitment (Franco et al., 2016). In addition to recruiting the autophagy machinery, K48 linked polyubiquitin recruits the proteasome to bacteria (Perrin et al., 2004; Franco et al., 2016). Specific recognition of different signals is also implied by the localisation of Optineurin, NDP52 and p62 to different microdomains around *Salmonella* (Cemma et al., 2011; Wild et al., 2011).

Atg16L1 is important for the process of xenophagy as cells carrying the T300A mutation, which increases caspase mediated cleavage and is associated with Crohn's disease (Murthy et al., 2014), show increased replication of *S. flexneri* (Lassen et al., 2014). This phenotype can be explained as the result of a direct interaction between Atg16L1 and the v-ATPase to initiate xenophagy (Xu et al., 2019) and NOD1 and NOD2 dependent recruitment Atg16L1 to sites of bacterial entry (Travassos et al., 2010) thus implicating Atg16L1, and the Atg5-12-16L1 complex, as key for efficient xenophagy.

Following phagocytosis and membrane rupture, cytosolic *Shigella* polymerise actin for intracellular motility and to facilitate cell-to-cell spread. At these sites of actin polymerisation, Septins form rings which assemble into cages to restrict *Shigella* prior to formation of the actin tail. Interestingly, these Septin cages colocalised with ubiquitin, p62 and LC3B suggesting a link with xenophagy (Mostowy et al., 2010). Disrupting Septin cage formation by siRNA decreased autophagic targeting of *Shigella* and depleting key autophagy proteins disrupted Septin cage formation, suggesting an intricate link between these processes (Mostowy et al., 2010).

Activation of one of the critical kinases controlling autophagy, AMPK, during Mtb infection or as a result of *Salmonella* outer membrane vesicles enhances the xenophagy response (Losier et al., 2019; Yang et al., 2014). Chemical activation of AMPK in Mtb infected murine bone marrow derived macrophages (BMDM) blocks Mtb induced mTOR phosphorylation to promote autophagosome biogenesis and increases targeting of Mtb to LC3 positive compartments (Yang et al., 2014). *Salmonella* outer membrane vesicles prime uninfected cells by phosphorylation events so the cells are ready to defend themselves following infection, without affecting basal autophagy (Losier et al., 2019).

An essential kinase for efficient xenophagy is TBK1, with multiple downstream targets being implicated. TBK1 was initially described for its role in induction of Type I IFN in anti-viral immune responses. TBC1D9 is recruited to GAS through ubiquitin and Ca^{2+} binding to promote TBK1 activation for xenophagy mediated clearance of GAS (Nozawa et al., 2020). Rab35 mediated recruitment of NDP52 facilitates the recruitment of TBK1 to *Salmonella* (Thurston et al., 2009; Minowa-Nozawa et al., 2017). In Mtb infection TBK1 is activated by stimulator of interferon genes (STING) following cytosolic DNA sensing and elimination of *M. bovis* BCG by xenophagy requires both Rab8B and TBK1 (Pilli et al., 2012; Watson et al., 2015). In the context of xenophagy, TBK1 phosphorylates multiple cargo receptors, including Optineurin and p62, to enhance their ubiquitin and LC3 binding (Richter et al., 2016; Wild et al., 2011; Pilli et al., 2012). As well as controlling autophagosome biogenesis, TBK1 also appears to play a role in autophagosome maturation (Pilli et al., 2012).

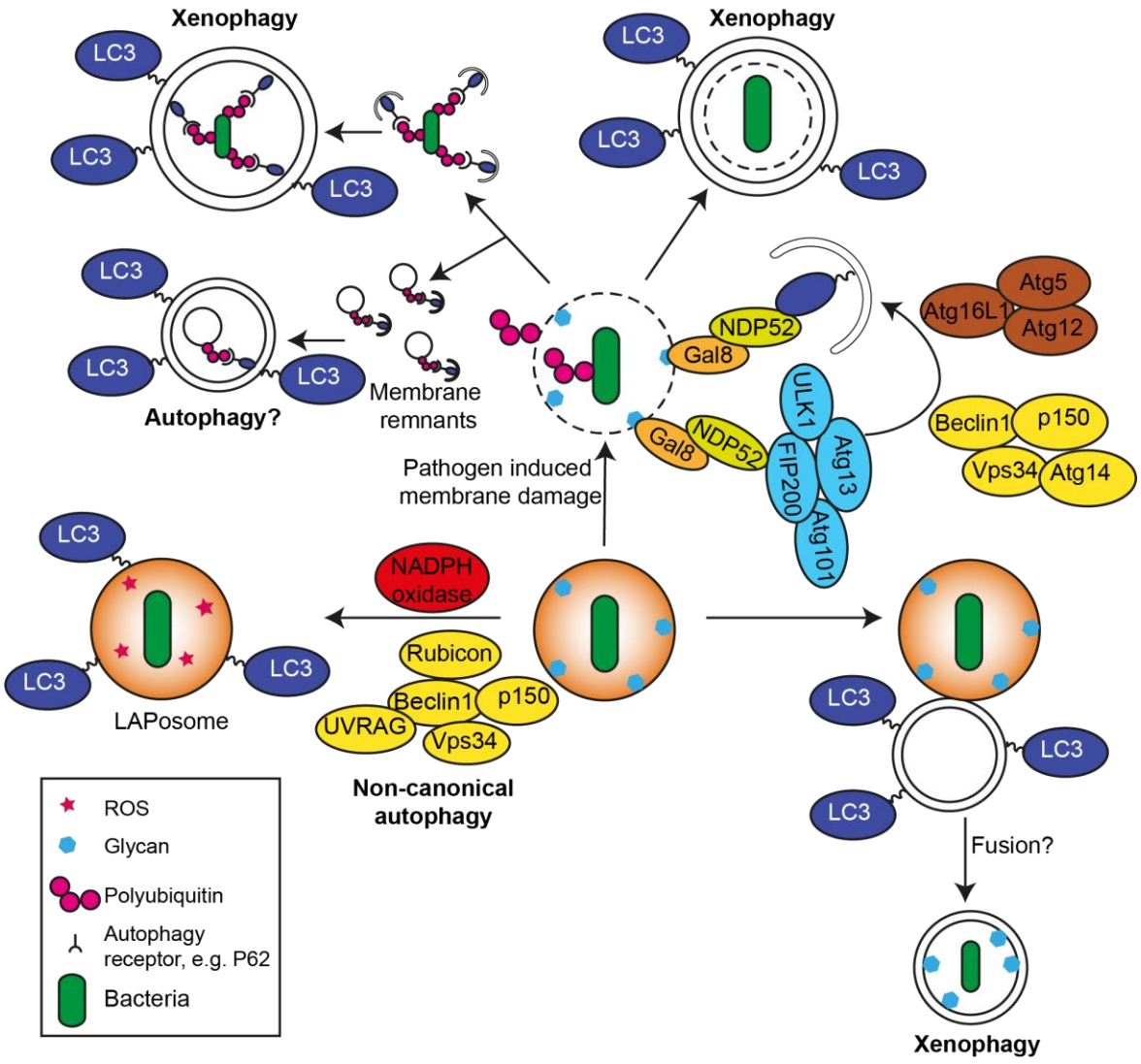

Figure 1.3.3 Pathogen targeting to autophagic compartments. Xenophagy is initiated following membrane damage by the recruitment of Gal8 and polyubiquitin to the damaged membranes and pathogen. Both the pathogen and the phagosome membrane remnants can be targeted for autophagy mediated degradation. Alternatively, LC3 can be fused directly to the phagosome membrane following the recruitment of the NADPH oxidase complex and generation of phagosomal ROS. Direct fusion of phagosomes and autophagosomes or autophagolysosomes would result in pathogens that localise in LC3 positive compartments.

Expansion of the phagophore to engulf large cargoes

Whilst autophagosomes induced by starvation are generally 0.5-2 µm in diameter (Klionsky and Eskelinen, 2014), in order to engulf large cargoes such as mitochondria and bacteria the autophagosomes need to be much larger. During both

mitophagy and xenophagy evidence has emerged for the generation of multiple phagophores or multiple initiation events around the cargo, which should then fuse to form one complete autophagosome (Ravenhill et al., 2019; Dalle Pezze et al., 2020). During the induction of mitophagy, p62 mediates the clustering of mitochondria, however this is not required for mitophagy to occur but may improve efficiency (Narendra et al., 2010).

One of the first live imaging studies of xenophagy was reported with *Salmonella* and clearly shows the steady expansion of the autophagosome around the bacterium (Kageyama et al., 2011). However, there is a lack of studies specifically investigating membrane sources and dynamics during xenophagy. As with starvation induced autophagosome biogenesis, multiple membrane sources are likely to be important.

Xenophagy and Mtb

Following phagosomal rupture, Mtb DNA is released into the cytosol in an ESX-1 dependent manner and is recognised by cyclic GMP-AMP (cGAMP) synthase (cGAS) to elicit the production of cGAMP to activate STING which in turn activates TBK1 (Watson et al., 2012, 2015) (**Figure 1.3.4**). The precise mechanism of Mtb DNA release into the cytosol remains to be defined. As with other pathogens, the activation of TBK1 is crucial for an effective xenophagy response (Watson et al., 2012; Thurston et al., 2009). Additionally, TBK1 phosphorylates interferon regulatory factor (IRF) 3 to promote the transcription of Type I IFNs. Genetic disruption of this pathway at any stage results in decreased ubiquitination, autophagy receptor and LC3 recruitment to Mtb (Watson et al., 2012, 2015). The Type I IFN response is negatively regulated by TRIM14 and TRIM14 KO macrophages show improved control of Mtb replication (Hoffpauir et al., 2020).

The best characterised trigger for xenophagy of Mtb is polyubiquitination. Several E3 ubiquitin ligases are involved in the polyubiquitination response to phagosomal rupture by Mtb including Parkin, SMURF1 and TRIM16 (Manzanillo et al., 2013; Franco et al., 2016; Chauhan et al., 2016). Deletion of any of these E3 ligases attenuates, but does not abolish, autophagic targeting implying redundancy amongst the E3 ligases or, alternatively, ubiquitin independent mechanisms for counteracting

cytosol invading Mtb. In addition to its ubiquitination function, the recruitment of TRIM16 by Gal3 facilitates the recruitment of ULK1 and Beclin1 to Mtb (Chauhan et al., 2016). Additionally, the Mtb protein Rv1468c directly recruits ubiquitin to the bacterial surface leading to p62 recruitment and xenophagy (Chai et al., 2019).

As with other pathogens, several autophagy receptors transduce the ubiquitination signal to the autophagy pathway. NDP52 is important for transduction of cGAS/STING mediated ubiquitination (Watson et al., 2012, 2015). In the zebrafish *M. marinum* model, depletion of either optineurin or p62 increases bacterial burden, whereas their overexpression increases autophagic targeting (Zhang et al., 2019). In murine dendritic cell lines, the receptor p62 colocalises with ubiquitin and LC3 positive Mtb and plays a role in xenophagic targeting (Seto et al., 2013). Both p62 and optineurin, but not NDP52, are phosphorylated upon Mtb infection, which is associated with increased activity (Budzik et al., 2020; Wild et al., 2011; Richter et al., 2016; Pilli et al., 2012). Gal8 recruits TAX1BP1 to Mtb (Bell et al., 2020), where it is also phosphorylated in response to Mtb infection and mouse macrophages lacking TAX1BP1 show disrupted autophagic targeting of Mtb and increased Mtb replication (Budzik et al., 2020).

In addition to ubiquitination, several other proteins have been shown to be important for efficient recognition and capture of Mtb by the autophagy machinery. Ubiquilin1 associates with the surface of Mtb to promote the anti-mycobacterial induction of autophagy by IFN-γ in BMDMs (Sakowski et al., 2015). The DNA damage regulated autophagy modulator protein (DRAM1) is induced by Mtb infection and induces autophagy through both STING and p62 (Van Der Vaart et al., 2014). The knockout of DRAM1 in zebrafish leads to increased macrophage pyroptosis following *M. marinum* infection (Zhang et al., 2020b). The GTPase IRGM is recruited to *M. bovis* BCG phagosomes and likely regulates an effective autophagy response through the recruitment of STX17 for autophagosome maturation (Singh et al., 2006; Kumar et al., 2018). On the other hand, Coronin1a is a negative regulator of autophagic targeting in mouse macrophages, potentially through interfering with the actin cytoskeleton (Seto et al., 2012).

As with other intracellular pathogens, Gal3, Gal8 and Gal9 are recruited to Mtb following phagosomal rupture. The knockout of Gal8 in mouse macrophages leads to improved bacterial replication, whereas its overexpression enhances bacterial control. This effect is mediated, at least in part, through the recruitment of TAX1BP1. Whilst deletion of Gal3 or Gal9 does not affect Mtb replication, Gal9 overexpression improves restriction of Mtb growth in macrophages (Bell et al., 2020). *In vivo*, KO of Gal3 or Gal8 in mice leads to increased Mtb burdens and worse disease outcomes (Chauhan et al., 2016; Jia et al., 2018).

Given studies in other cytosol invading pathogens showing the role of membrane damage in triggering xenophagy (Thurston et al., 2012), the requirement of ESX-1 for cytosolic access of Mtb (van der Wel et al., 2007; Lerner et al., 2017) and autophagic targeting (Watson et al., 2012; Lerner et al., 2016), it is assumed that cytosolic access is required for triggering xenophagy of Mtb. However, the vaccine strain *M. bovis* BCG, which lacks the RD1 region that encodes ESX-1, is targeted to LC3 positive compartments despite not being able to damage membranes or localise to the cytosol (Gutierrez et al., 2004a).

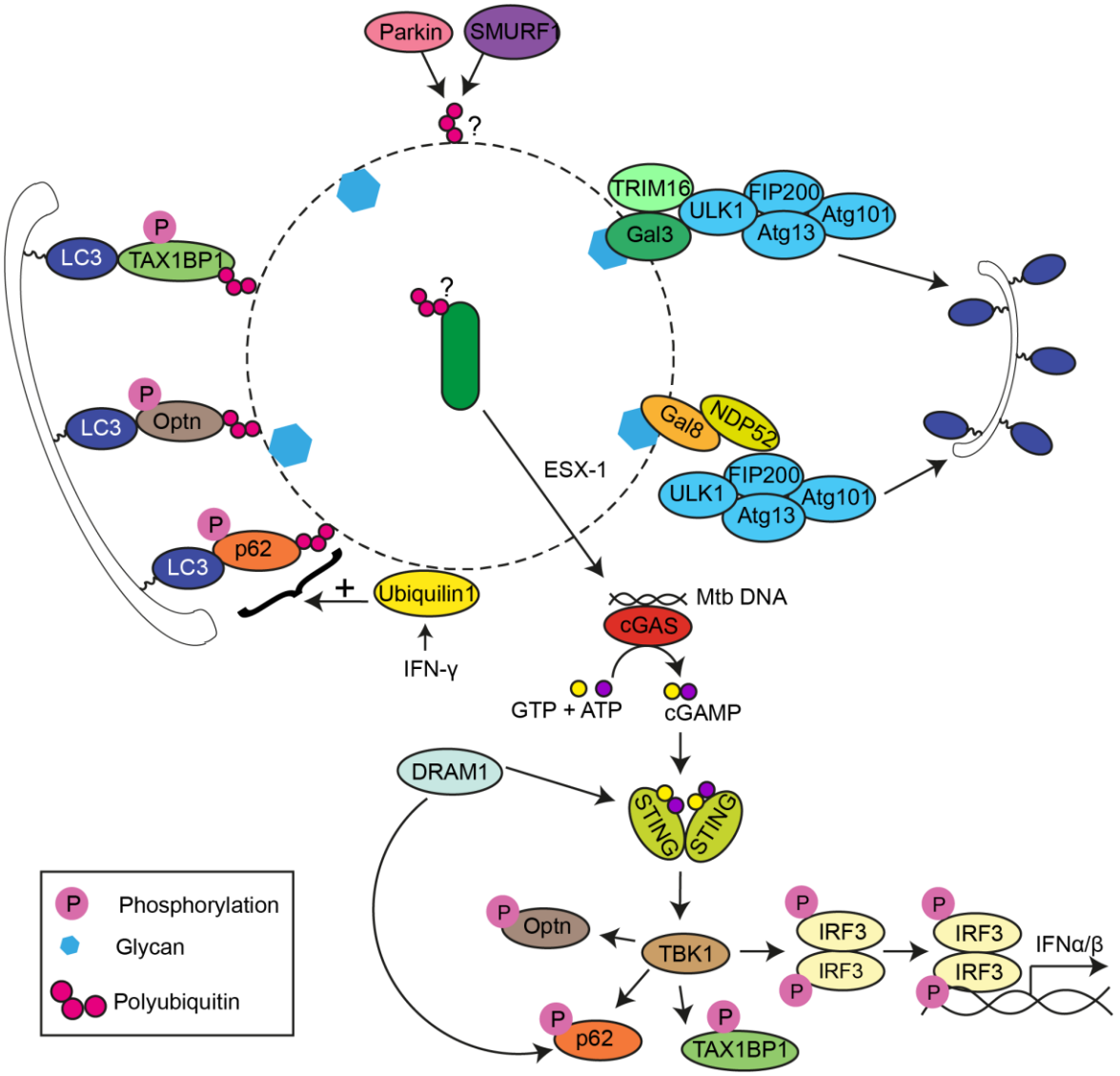

Figure 1.3.4 Xenophagy responses during Mtb infection. Targeting of Mtb by xenophagy is triggered upon phagosome membrane permeabilisation. The release of Mtb DNA into the macrophage cytosol activates the cGAS/STING/TBK1 pathway to trigger type I IFN transcription and promote autophagic targeting, likely through phosphorylation of the autophagy receptors. The ubiquitin ligases Parkin and SMURF1 are responsible for catalysing the assembly of polyubiquitin chains on the membranes and/or bacteria, potentially alongside other unidentified E3 ligases. Ubiquilin1 localises to the phagosome and increases the recruitment of ubiquitin, p62 and LC3. DRAM1 increases xenophagic targeting in a manner dependent on STING and p62. The galectins Gal3 and Gal8 are also involved through the recruitment of the ULK1 kinase complex to trigger local phagophore biogenesis.

Following xenophagy, mycobacteria containing autophagosomes can be endowed with further bactericidal activity through accumulation of antimicrobial peptides. GBPs traffic antimicrobial peptides to Mtb autophagosomes (Kim et al., 2011a) and p62 recruits proteins into vesicles for the generation of antimicrobial peptides (Ponpuak et al., 2010).

The consequence of autophagic targeting appears to be species dependent; in mouse macrophages autophagy induction through starvation or rapamycin treatment leads to restriction of Mtb replication (Gutierrez et al., 2004a), whereas in primary human macrophages autophagy induction by rapamycin increases Mtb replication (Andersson et al., 2016) but in THP-1 cells rapamycin treatment starting at 48 h after infection restricts Mtb (Kumar et al., 2010). Activation of the autophagy pathway in macrophages with IFN-γ or by mTOR inhibition is important for the successful targeting of Mtb to xenophagy in mouse macrophages (Gutierrez et al., 2004a).

Disrupting autophagy *in vitro* in mouse macrophages through knockdown of various autophagy proteins involved in all stages of xenophagy increases Mtb survival (Jayaswal et al., 2010; Watson et al., 2012; Kim et al., 2012b). Whilst myeloid specific Atg5 KO mice show worse disease progression following Mtb infection (Castillo et al., 2012; Kimmey et al., 2015); the knockout of many other autophagy genes, including Atg16L1, did not lead to changes in disease severity (Kimmey et al., 2015). Based on this work, it is postulated that Atg5 is playing an autophagy independent role in limiting Mtb pathogenesis, potentially through control of neutrophilic inflammation (Kimmey et al., 2015). Atg5 is known to have non-autophagic functions *in vivo*, for example it is required for IFN inducible GTPase trafficking to, and rupture of, the parasitophorous vacuole during *Toxoplasma gondii* infection (Zhao et al., 2008). The lack of an *in vivo* phenotype with the majority of autophagy deficient mice could be explained in several ways. Firstly, autophagic control of Mtb replication may not be important *in vivo* as Mtb may already successfully subvert autophagy thus loss of autophagy does not have an effect. Secondly, for some knockouts it is possible that redundant mechanisms exist that

compensate for the loss of one protein. It is also possible that other cell types with intact autophagy are able to complement any loss of function in myeloid lineages. Finally, it is interesting that Gal3 and Gal8 KO mice succumb to Mtb infection more rapidly than their WT littermates (Chauhan et al., 2016; Jia et al., 2018) suggesting that they may have autophagy independent functions that are important *in vivo*. Ultimately, the validity of extrapolating *in vivo* data from mice to human disease needs to be considered given that there are significant differences between the mouse and human disease, and commonly used C57BL/6 mice are mostly resistant to the infection (Kramnik and Beamer, 2016). A genome wide siRNA screen in THP-1 cells showed that autophagy regulating genes were important for control of Mtb infection, although no genes that are essential for autophagy were identified (Kumar et al., 2010).

Subversion of xenophagy by intracellular pathogens

Given the importance of xenophagy in the control of intracellular pathogens, it is not surprising that successful subversion of xenophagy has been implemented by multiple intracellular pathogens as a virulence strategy. For most cytosol dwelling intracellular pathogens, xenophagy subversion may be essential for their successful survival (Upadhyay and Philips, 2019).

Some intracellular pathogens block key steps in the recruitment of the autophagy machinery, for example the *Salmonella* effector SopF can ADP-Ribosylate the v-ATPase to block its interaction with Atg16L1 (Xu et al., 2019). *Salmonella* also employs SseF and SseG to block the activation of Rab1A and inhibit the recruitment of ULK1 (Feng et al., 2018). Additionally, *L. monocytogenes* strains lacking the phospholipase PlcA show increased autophagic targeting; likely to due to an inability to dephosphorylate PI3P, although definitive evidence for this is missing (Mitchell et al., 2015; Birmingham et al., 2007; Mitchell et al., 2017). Some serotypes of GAS secrete a cysteine protease, SpeB, which cleaves the autophagy receptors NDP52, p62 and NBR1 to block autophagic targeting (Barnett et al., 2013). Shigella icsB counteracts the pro-autophagic activity of virG by outcompeting binding of Atg5 (Ogawa et al., 2005) and recruiting Toca-1 (Baxt and Goldberg, 2014).

Other pathogens block the proper functioning of autophagosomes. The *L. pneumophila* protease RavZ cleaves LC3 from autophagosomes preventing their formation and function (Choy et al., 2012). *Yersinia pestis* blocks maturation and acidification of autophagosomes thus rendering them unable to restrict pathogen growth (Pujol et al., 2009).

L. monocytogenes employs several virulence factors to disguise its presence from host cells. *L. monocytogenes* ActA blocks ubiquitination through recruitment of the Arp2/3 complex (Yoshikawa et al., 2009). Expression of inlK by *L. monocytogenes* recruits the host major vault protein (MVP) and bacteria coated with MVP show failure of autophagosomes to form around the bacteria by live cell imaging (Dortet et al., 2011). Additionally, LLO and phospholipase mutants of *L. monocytogenes* show increased localisation in multi-membrane, autophagosome-like compartments potentially implicating these effectors in successful escape from xenophagy (Gedde et al., 2000).

Francisella tularensis O antigen mutants display increased recruitment of ubiquitin and autophagy components however the mechanism behind this is unknown (Case et al., 2014). Legionella sphingosine-1-phosphate lyase alters host cell sphingosine metabolism and subverts autophagy induction (Rolando et al., 2016); indeed sphingolipids are important for many steps in the autophagy pathway (Harvald et al., 2015). Salmonella SpvB is implicated in defects in autophagosome biogenesis in infected cells, potentially through modulation of actin polymerisation (Chu et al., 2016; Li et al., 2016).

Instead of subverting the xenophagy response and evading capture, some pathogens have taken to converting autophagosomes into a replicative niche. *Coxiella burnetii* replicates in an acidified compartment with features reminiscent of autophagosomes, including the presence of LC3 on the vacuole (Berón et al., 2002). Increasing the interaction of the *Coxiella* vacuole with the autophagy pathway led to increased bacterial replication; likely through delivery of nutrients and providing membrane to enlarge the vacuole. (Gutierrez et al., 2005; Winchell et al., 2014). After replication in the cytosol, *F. tularensis* uses autophagy to re-enter the

endolysosomal system in mouse macrophages (Checroun et al., 2006), although the effect of this on the bacteria remains unknown and does not appear to occur in human cells (Akimana et al., 2010). *Yersinia pseudotuberculosis* shows hampered replication during autophagy disruption (Moreau et al., 2010). Through the secretion of a Beclin1 binding protein, to recruit the Atg14 containing PI3K complex, and subsequently preventing lysosomal fusion *Anaplasma phagocytophilum* establishes immature autophagosomes as a niche for replication (Niu et al., 2012, 2008). A similar mechanism is employed by *Staphylococcus aureus* although eventual escape is required to induce host cell death and dissemination (Schnaith et al., 2007).

Unsurprisingly, Mtb has also developed many mechanisms to subvert and supress the xenophagy response at all stages. During Mtb infection of macrophages, various microRNAs targeting autophagy proteins including UVRAG, Atg5, Atg12, LC3B and DRAM2 have been identified as being upregulated (Kim et al., 2015; Ouimet et al., 2016; Kim et al., 2017; Chen et al., 2015). SapM, which is known to interfere with phagosome maturation, is similarly able to inhibit the action of Rab7 in promoting the fusion of autophagosomes with lysosomes (Hu et al., 2015; Chandra et al., 2015). Mtb mediated inhibition of autophagic flux is dependent on ESX-1 (Romagnoli et al., 2012).The role of Mtb Eis appears to be 2 fold; through increasing IL-10 secretion mTOR activity is increased to supress autophagy and through inhibiting ROS production by NADPH oxidase and mitochondria (Duan et al., 2016; Shin et al., 2010). Mtb lacking PE_PGRS47 show increased autophagy induction, LC3 colocalisation and lysosomal targeting in RAW264.7 macrophages (Saini et al., 2016). Whilst not directly shown to have an effect on autophagy, ManLAM inhibits the action of Vps34, the lipid kinase required for autophagosome biogenesis (Vergne et al., 2003). As well as proteins, Mtb lipids can affect autophagic targeting of Mtb. PDIMs block phagosome-damage independent autophagy and sulfoglycolipids act as a TLR2 antagonist to also block this pathway (Bah et al., 2020). Although these methods impair the function of xenophagy to some extent, none of them sufficiently explain why Mtb localises to the cytosol and not immature autophagosomes.

LC3-associated phagocytosis and pathogens

LAP targets a wide range of pathogens including fungi, bacteria, and parasites as well as apoptotic cells (Florey et al., 2011; Martinez et al., 2011, 2015; Hubber et al., 2017; Choi et al., 2014). Maturation of fungi containing LAPosomes in macrophages appears to occur rapidly thus efficiently targeting pathogens for degradation. Disruption of LAP increases *Aspergillus fumigatus* burdens *in vivo* (Martinez et al., 2015; Sanjuan et al., 2007). In dendritic cells, LAP has been shown to slow down phagosome maturation of fungus containing LAPosomes to promote MHC class II antigen presentation (Romao et al., 2013; Ma et al., 2012). Additionally, LAPosome formation in dendritic cells did not affect phagosome maturation or *Saccharomyces cerevisiae* survival (Ma et al., 2012); thus, there appears to be cell-type specific functions of LAP.

Lysosomal swelling, which eventually could induce small amounts of membrane damage, is also known to induce conjugation of LC3 to single membranes (Florey et al., 2015); this has been shown to share some common mechanisms with LAP. Mammalian Atg16L1 contains a C terminal WD40 domain, which is absent in yeast, and is dispensable for macroautophagy. The WD40 domain broadens the functions of Atg16L1 and is required for the induction LAP (Fletcher et al., 2018). Given the WD40 domain dependence and FIP200 independence of v-ATPase mediated recruitment of Atg16L1 in (Xu et al., 2019), the v-ATPase mediated recruitment of Atg16L1 may be required for LAP and not necessarily xenophagy.

As with xenophagy, we have begun to understand mechanisms employed by pathogens to subvert LAP in order to successfully enter and survive within phagocytes. Mtb secretes CpsA to inhibit the function of NADPH oxidase in mouse macrophages, leading to a block in LAP. Mtb lacking CpsA is attenuated *in vitro* and *in vivo* in an NADPH oxidase dependent manner (Köster et al., 2017). Blocking ROS accumulation to prevent LC3 accumulation is also employed by *F. tularensis* (Rabadi et al., 2016) and *Streptococcus suis* (Fang et al., 2015) through the action of bacteria encoded superoxide dismutase; although whether this is LAP or xenophagy remains

elusive. Shigella icsB and virA mutants show increased LC3 recruitment to single membranes (Campbell-Valois et al., 2015).

Autophagy and inflammation

In addition to directly contributing to intracellular pathogen control through xenophagy, the autophagy pathway plays wider roles in immunity through controlling inflammation. Several autophagy genes have polymorphisms that are associated with chronic inflammatory and autoimmune conditions including Chron's disease, systemic lupus, asthma and multiple sclerosis (Martin et al., 2012; Han et al., 2009; Yang et al., 2013; Ramos et al., 2011; Harley et al., 2008; Murthy et al., 2014; Schuster et al., 2015). Moreover, functional non-canonical autophagy, likely LAP, in microglia is required to limit neuroinflammation in a mouse model of multiple sclerosis through clearance of phagocytosed myelin (Berglund et al., 2020).

Increased inflammation as a result of dysfunctional autophagy is linked to inflammasome activation and cytokine secretion. The assembly and activation of the inflammasome, which is essential for processing and secretion of IL-1β and IL-18, is tightly controlled. Mice with reduced levels of Atg16, which serve as a model for Chron's disease, show increased levels of IL-1β and IL-18 with blockade of these cytokines rescuing the disease phenotype (Saitoh et al., 2008; Cadwell et al., 2008). It is thought that dysfunctional mitophagy leads to increased ROS and oxidised mitochondrial DNA, both endogenous inflammasome ligands (Nakahira et al., 2011; Zhou et al., 2011; Matsuzawa-Ishimoto et al., 2018). As well as removing inflammasome activating ligands, autophagy can target core components such as AIM2 and NLRP3 for degradation thus limiting inflammation (Shi et al., 2012).

Additionally, it is known that autophagy limits the induction of Type I IFN. Displacement of Rubicon from the Vps34 complex enhances autophagosome biogenesis to remove cytosolic DNA, the ligand important for cGAS activation and downstream transcriptional responses. The cGAS-STING signalling cascade is further inhibited by autophagy related proteins such as Beclin-1 mediated inhibition of cGAS (Liang et al., 2014) and cGAMP activation of ULK1 to promote autophagy and inhibit STING (Konno et al., 2013).

Autophagy and the adaptive immune response

Compelling evidence indicates that adaptive immune responses are also essential for efficient control of TB. Without the onset of CD4 and CD8 positive T cell mediated immunity individuals are highly susceptible to TB. Mice depleted for T cells by various means are unable to control Mtb replication and rapidly succumb to disease (Orme and Collins, 1984; Tascon et al., 1998; Muller et al., 1987). Moreover, high incidences of new and reactivation of TB in HIV positive individuals is linked to the loss of T cell mediated immunity (Flynn and Chan, 2001a; Selwyn et al., 1989). Here, once again, autophagy has a role to play. Antigen presentation by professional antigen presenting cells, including macrophages, is essential for priming the adaptive immune response. NOX2 dependent formation of autophagosomes stabilises antigens for MHC-II presentation in macrophages (Romao et al., 2013). Moreover autophagy may be important for delivering cytosolic antigens to late endosomes and lysosomes to facilitate loading onto MHC-II (Levine and Deretic, 2007). In dendritic cells autophagy is important for the loading of cytosolic antigens onto MHC-II and delivering internalised antigens to compartments for MHC-I cross-presentation (Matsuzawa-Ishimoto et al., 2018).

Autophagy also plays key roles in regulating T cell functions including, negative selection, priming and activation. During negative selection of self-reactive T cells, autophagy is important for MHC-II mediated cross presentation by thymic epithelial cells and mice with defective thymic autophagy develop fatal multiple organ failure due to cross reactive T cells (Nedjic et al., 2008). CD4+, CD8+ and regulatory T cells (Treg) all show increased apoptosis and dysregulated homeostasis following autophagy disruption, likely due to impaired mitochondrial clearance by mitophagy (Macian, 2019). Whilst effector functions of CD4+ or CD8+ T cells seem to remain intact despite autophagy disruption, memory T cell formation is disrupted (Clarke and Simon, 2019). Moreover, proliferation of T cells following activation by T cell receptor ligation is hampered following deletion of key Atg genes (Macian, 2019). Some phenotypes of autophagy deficient T cells appear to be dependent on the precise gene deleted and the model being investigated, therefore further study will be important to define the mechanism behind these differences.

1.4 In vitro models to study Mtb-macrophage interactions

Despite over a century of research since Mtb was initially discovered by Robert Koch, several aspects of the interaction between the human host and Mtb, such as the cytosolic localisation of Mtb, have only recently become known. Importantly, as an intracellular pathogen, several fundamental questions remain to be answered including: where does Mtb replicate intracellularly, how does its intracellular localisation affect antibiotic efficacy and what intracellular environments are truly capable of restricting Mtb replication? Thus, it is essential that we continue to innovate new approaches to explore the intracellular lifestyle of Mtb and answer questions that hitherto are unresolved.

Mouse macrophage models

Mouse macrophages have been widely used to study Mtb infection and probe the impact of both host and Mtb genetic manipulation on the outcome of infection. Sources of mouse macrophages include (1) cell lines such as RAW264.7 and J774 macrophages and (2) primary cells including BMDMs and peritoneal macrophages. These systems have several advantages including being readily available in large numbers and their genetic tractability. Cell lines are relatively amenable to transfection with plasmid DNA or siRNA and BMDMs can be derived from genetically modified mouse models. Additionally, *in vitro* findings can readily be translated to *in vivo* mouse models.

Immunologically, there are important differences between mouse and human macrophages. In response to immune activation, for example TLR ligation, the two species have unique gene signatures. LPS binding to TLR4 upregulates C-X-C motif chemokine (CXCL) 13 expression in human cells, but this is not seen in mice (Schroder et al., 2012). Inflammasome activation is ATP driven in human cells (Piccini et al., 2008), but cholesterol driven in mouse (Duewell et al., 2010). Non-coding RNAs are also extremely divergent between the two systems. These differences extend to the overall architecture of human and mouse immunology (Mestas and Hughes, 2004). As a result, the response of the two systems to immune challenge is likely to vary substantially.

Whilst many findings in mouse macrophages infected with Mtb can be translated across to human macrophage systems, there are key differences that limit their usefulness. One major difference is in the subcellular localisation of the bacteria. In human macrophages cytosolic Mtb can detected within 4 h of infection (Lerner et al., 2017) whereas in BMDMs no cytosolic bacteria are observed up to 48 h post infection (Schnettger, 2016). However, Mtb can damage membranes and contact the cytosol in mouse macrophages (Schnettger et al., 2017; Simeone et al., 2015). This suggests that mouse macrophages are better able to repair damage inflicted by Mtb or recapture bacteria from the cytosol, as Gal8 and polyubiquitin can still be found colocalising with Mtb (Schnettger et al., 2017). Additionally, the role of NO in Mtb infection may be different. *In vitro*, mouse macrophages produce high, bactericidal levels of NO (Chan et al., 1992) whereas the levels in human macrophages are variable and if NO is required for mycobacterial control remains elusive (Rich et al., 1997; Aston et al., 1998). Overall, the role of NO in human macrophage control of Mtb is still subject to debate and more robust methods to detect NO are required (Chan et al., 2001).

Other innate immune factors are different between human and mouse macrophages. For example, that is the case with two important families of GTPases involved in innate immune defence, the IRGs and GBPs. Whilst the mouse genome encodes for 23 IRGs and 11 GBPs, the human genome only has one IRG – IRGM – and 7 GBPs. Thus, important immunity related proteins may serve different functions in the two models. This is directly relevant for Mtb infection, for example GBP1 and 7 restrict BCG replication in mouse macrophages and IRGM is important for maturation of Mtb containing autophagosomes (Singh et al., 2006).

Human macrophage models

To more accurately reflect Mtb-macrophage interactions in human disease, especially when studying events likely to be affected by the cytosolic localisation of Mtb, it is important to use human macrophages. For this, several cell lines and primary macrophage models are available, each with their own advantages and disadvantages (**Figure 1.4.1**).

Cell lines like the monocyte lines THP-1 (Tsuchiya et al., 1980) and U937 (Sundström and Nilsson, 1976), which can be differentiated to macrophages using phorbol esters, provide a large number of cells for experiments and are relatively easy and cheap to culture. Additionally viral transduction can be used to express fluorescent proteins for live cell imaging or protein knockdown and CRISPR mediated gene editing can be used for generating knockouts (Beckwith et al., 2020). However one major disadvantage with the use of cell lines is the presence of large genetic rearrangements (Odero et al., 2000), which will undoubtedly impact cellular responses to infection. Additionally, the use of phorbol esters such as phorbol 12-myristate 13-acetate (PMA) to trigger the differentiation of the monocytes to macrophages activates the cells, including for example NF-κB, thus priming the macrophages prior to infection and altering the response to subsequent infection. Several signalling pathways, including inflammasome activation, are only partially functional in THP-1 when compared to primary monocytes (Gaidt et al., 2016).

A potential alternative to THP-1 are BlaerE1 cells (Gaidt et al., 2018). These cells were produced from malignant B-lineage cells that can be converted to monocyte/macrophage lineage through inducing nuclear translocation of a C/EBPα transgene. These cells show transcriptional and signalling pathway activity more akin to human monocyte derived macrophages (hMDM) but have the genetic tractability of THP-1 (Gaidt et al., 2018). They are, however, still not a primary macrophage and will eventually contain genetic abnormalities.

In order to obtain karyoptypically normal macrophages, primary cells derived from patients or healthy donors represent a widely used system. The most commonly used approach involves the isolation of monocytes from blood donations and their subsequent differentiation to hMDM with M-CSF or GM-CSF (Lerner et al., 2017). Whilst this yields a large number of cells, there are several limitations. Firstly, it is technically difficult to get blood from the same donor each time and donor-to-donor variability can confound results. Additionally genetic manipulation, for example by CRISPR or siRNA, is challenging with only limited reports of success (Hiatt et al., 2020). Finally, in order to image the dynamics of trafficking events, the expression

of fluorescent proteins and introduction of plasmid DNA to primary human macrophages is challenging and often leads to cell death.

As Mtb initially infects alveolar macrophages these are a highly relevant macrophage to use for *in vitro* studies. These cells can be obtained by bronchoalveolar lavage (BAL) during bronchoscopy. As well as suffering with the genetic intractability seen with hMDM, alveolar macrophages are hard to obtain in sufficient quantities for large scale experiments. Despite this they have been used to study the effect of smoking (O'Leary et al., 2014; Gleeson et al., 2018) and the use of retinoic acid to modulate autophagy in Mtb infection (Coleman et al., 2018).

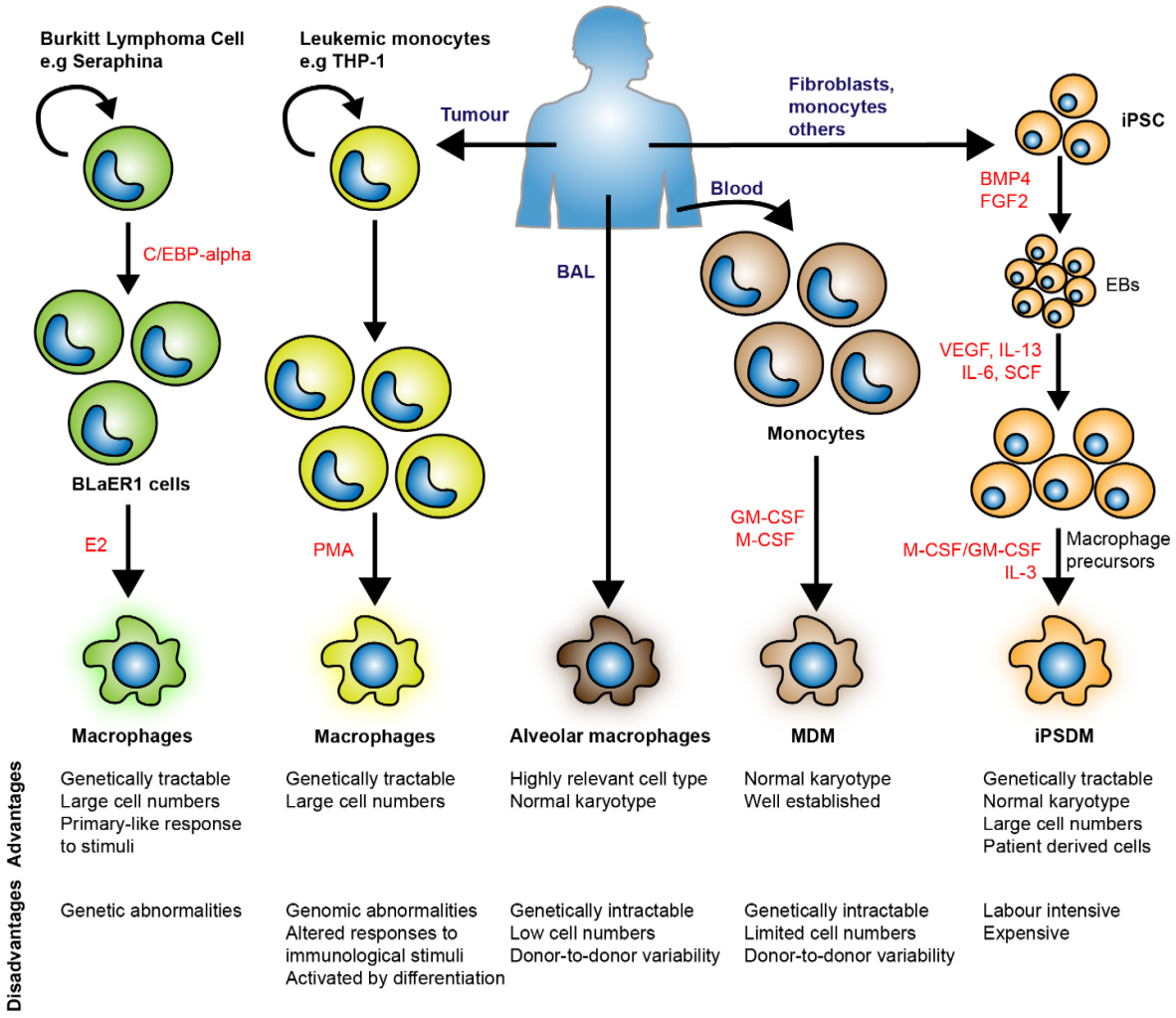

Figure 1.4.1 *In vitro* human macrophage models. Various *in vitro* cellular models exist for human macrophages, including tumour derived cells, primary macrophages from donors and those derived from human stem cells. Each of these models has advantages and disadvantages. The leukemic monocytic cell line THP-1 can be differentiated to adherent macrophage-like cells through the use of phorbol esters such as PMA. B cells can be lineage converted to form macrophages. Primary macrophages can be obtained from bronchoalveolar lavage (BAL) to yield alveolar macrophages or from differentiation of CD14 positive monocytes in the blood. Human induced pluripotent stem cells (iPSC) can be differentiated to macrophages through directed differentiation with cytokines that drive haematopoiesis. Adapted with permission from (Bussi and Gutierrez, 2019).

Altogether there is a clear need for a human macrophage system that combines the benefits of cell lines and primary macrophages to further develop our understanding of host-pathogen interactions in Mtb infection. This system should be genetically tractable, scalable to enable the production of large quantities of homogenous macrophages over time and be capable of reflecting the diversity of macrophages observed *in vivo*.

1.5 Induced pluripotent stem cell derived macrophages

Induced pluripotent stem cells as a revolution in biology

For a number of years researchers have used embryonic stem cells to study human development as well as to generate differentiated cells for studying a wide range of diseases (Ilic and Ogilvie, 2017). However, these come with numerous ethical concerns as their isolation requires the destruction of a human embryo. It is possible to convert fibroblasts into a pluripotent state through the introduction of the transcription factors Oct4, Sox2, c-Myc, and Klf4, now known as the Yamanaka factors, resulting in the production of induced pluripotent stem cells (iPSC) (Takahashi and Yamanaka, 2006). This work has subsequently been expanded upon and we are now able to convert multiple cell types to iPSCs through a variety of methods including Sendai virus and mRNA (Hayes and Zavazava, 2013). Further refinement revealed that excluding Oct4 produces higher quality iPSCs with less epigenetic alterations (Velychko et al., 2019).

After the establishment of robust and reliable protocols to obtain iPSC, these technologies have revolutionised our ability to study human diseases. Somatic cells

isolated from healthy donors or patients with a disease of interest can be reprogramed to iPSCs and then differentiated to a relevant cell type(s) for studies *in vitro*. Ground-breaking studies in developmental biology, neuroscience and cancer have all stemmed from iPSCs in recent years. Building on simple, 2D culture models iPSCs allow the creation of organoids; small miniature organs containing varied cell types and more accurately mimicking structures and physiology found *in vivo* (Bar-Ephraim et al., 2020; Rossi et al., 2018; Kim et al., 2020). Combining these advances, with modern genome engineering techniques to model diseases as well as correcting disease causing genetic mutations has the potential to transform our understanding of many diseases (Cyranoski, 2018; Scudellari, 2016). Moreover, iPSC derived neurons have been used in drug screening to identify novel drug candidates (Lee et al., 2012; Cao et al., 2016).

As well as providing new models to study disease processes, iPSCs are being heralded as a future treatment for many conditions. By generating iPSCs from somatic cells isolated from a patient, correcting genetic mutations causing their condition, differentiating into the right cell type, and transplanting back into the patient we may be able to treat diseases that are currently untreatable. This is particularly feasible for monogenic diseases, such as cystic fibrosis where a single base change – something now readily achievable with CRISPR/Cas9 – can restore production of fully functional proteins. Replenishing RPE cells differentiated from iPSCs have entered into human clinical trials in the USA from the treatment of age related macular degeneration, having shown promise in animal studies (Sharma et al., 2019). One patient has been successfully treated with this before (Cyranoski, 2014; Bragança et al., 2019). Additionally, a trial has started in Japan using iPSC derived dopaminergic neurons to treat Parkinson's disease (Trial ID UMIN000033564) (Stoddard-Bennett and Pera, 2019).

iPSC models of human macrophages

Given the potential of iPSCs to differentiate into any cell type, protocols have emerged to produce macrophages (iPSDM). Since the initial publications demonstrating protocols for the production of macrophages from iPSCs (Kambal et

al., 2011; Choi et al., 2011; Senju et al., 2011) several improved protocols have emerged. Whilst the initial protocols required co-culture with mouse stromal cells or rounds of purification, later protocols used more defined serum and feeder free conditions (van Wilgenburg et al., 2013). Some protocols produce macrophages from a monolayer of iPSCs within a matter of a few weeks but only yield one harvest (Takata et al., 2017), whereas others use embryonic bodies to produce large numbers of macrophages over several months but can take longer to produce cells (van Wilgenburg et al., 2013).

Several studies have sought to compare iPSDM and hMDM, primarily at the transcriptional level, in order to validate them as a relevant system for studying human macrophage biology. Following stimulation with LPS, iPSDM and hMDM show a highly similar response by RNA-seq (Alasoo et al., 2015). Differences include increased changes in antigen presentation, neutrophil attracting chemokine and tissue remodelling genes (Alasoo et al., 2015). Comparing iPSDM and isogenic hMDM revealed that M0, M1 and M2 polarised macrophages from both routes show similar transcriptional and cytokine secretion profiles (Zhang et al., 2015). Both of these studies report increased antigen presentation pathway activation in hMDM compared to iPSDM (Alasoo et al., 2015; Zhang et al., 2015). Further comparison with blood derived monocytes and macrophages revealed significant similarities between iPSDM and hMDM polarised towards M1 or M2 (Cao et al., 2019; Gutbier et al., 2020) and iPSDM recapitulate important alternative splicing events observed in hMDM (Lin et al., 2016).

Whilst iPSDM closely match hMDM at the transcriptional level, they are developmentally more closely related to tissue resident macrophages. Buchrieser and colleagues knocked out either Myb, RUNX1 or SPI1, transcription factors important for macrophage differentiation, in iPSCs prior to macrophage differentiation. Whilst the transcription factor Myb, which is required for monocyte differentiation from haematopoietic stem cells (HSCs), is not important for the production of tissue resident, yolk sac derived macrophages, the transcription factors RUNX1 and SPI1 are required. Knockout of Myb, but not RUNX1, blocks iPSDM

differentiation, thus iPSDM are more closely related to yolk sac derived, tissue resident macrophages (Buchrieser et al., 2017). Indeed, at the transcriptional level the precursors to iPSDM – originally termed monocytes – do not bare much resemblance to CD14+ monocytes isolated from blood, further suggesting these cells have a different developmental origin and should be more correctly called macrophage precursors (Zhang and Reilly, 2017).

An important and debated aspect of *in vitro* studies with macrophages is the generation of the right 'type' of macrophage that mimics the physiological and functional outcomes observed *in vivo*. *In vivo*, macrophages come in various subtypes such as tissue resident and monocyte derived. Additionally, depending on the local microenvironment of the macrophage they have different identities, with unique gene expression profiles and differing responses to infection and other stimuli (Bonnardel et al., 2019; T'Jonck et al., 2018; Bonnardel and Guilliams, 2018; Guilliams and Scott, 2017). Therefore, THP-1 and hMDM are unlikely to be able to recapitulate the wide variety of macrophages found *in vivo*. Through co-culture of iPSDM with cells of the local niche or *in vivo* organ transfer it is possible to generate more specialised macrophage types such as microglia (Takata et al., 2017; Haenseler et al., 2017), thus overcoming this limitation of THP-1 and hMDM. Transplantation of murine iPSDM into a mouse model of pulmonary alveolar proteinosis (PAP) led to long term engraftment, further differentiation to an alveolar macrophage like phenotype – determined by transcriptomics – and reduced disease severity (Mucci et al., 2018).

A further advantage of iPSDM is the ability to make them from genetically modified iPSC to probe the effect of protein knockout or mutagenesis. For example, knockout of LRRK2, a kinase implicated in Parkinson's disease, in iPSDM led to decreased Mtb replication (Härtlova et al., 2018). Further studies have used lentivirus to introduce corrected versions of the GM-CSF receptor alpha gene to iPSC from patients with PAP, which leads to more functional iPSDM (Lachmann et al., 2014). Correction of a mutation involved in chronic granulomatous disease rescued disease relevant phenotypes in iPSDM precursors (Flynn et al., 2015).

A major use of iPSDM to date has been the modelling of diseases using patient derived iPSDM. People with polymorphisms in the IFN-γ receptor show increased susceptibility to mycobacterial disease (Bustamante et al., 2014), this was recapitulated in iPSDM where cells were unable to control *M. bovis* BCG in response to IFN-γ and showed decreased antigen presentation (Neehus et al., 2018; Haake et al., 2020). Other diseases that have been successfully modelled *in vitro* with iPSC include Gaucher disease (Aflaki et al., 2014; Panicker et al., 2012), chronic granulomatous disease (Jiang et al., 2012), Blau syndrome (Takada et al., 2018), and CINCA syndrome (Tanaka et al., 2012).

iPSDM have been infected with multiple pathogens in order to characterise their response. Infection with *Salmonella* identified them as a suitable model (Hale et al., 2015) and further studies identified changes in enhancer priming, as well as a role for IL-10 in supressing prostaglandin E2 to enhance *Salmonella* control (Alasoo et al., 2018; Mukhopadhyay et al., 2020). iPSDM support the replication of *Chlamydia trachomatis* and loss of IRF5 or IL10RA in iPSDM reduces control of the infection (Yeung et al., 2017). iPSDM are also a suitable host for studying viral infection including HIV (van Wilgenburg et al., 2013), zika virus and dengue virus (Lang et al., 2018). Recently, iPSDM were shown to be a naïve macrophage, lacking distinct M1 or M2 polarisation and displaying similarities to macrophages isolated from TB patient lungs (Nenasheva et al., 2020). Notably, these iPSDM failed to show restriction of Mtb replication following IFN-γ treatment. The immunological response of iPSDM to BCG infection has been studied, revealing that TNFα secretion and apoptosis as seen in THP-1 macrophages (Hong et al., 2018).

Human embryonic stem cell derived macrophages have also been used as an *in vitro* drug discovery pipeline with Mtb to identify new molecules capable of restricting intracellular Mtb, including drug resistant strains (Han et al., 2019). The potential for iPSDM as a treatment during infection has been demonstrated in a mouse model of *Pseudomonas aeruginosa* infection whereby large-scale production of iPSDM in a bioreactor followed by intra-pulmonary transplantation reduced bacterial loads (Ackermann et al., 2018).

Altogether, iPSDM are being touted as the future of *in vitro* study of tissue resident macrophages (Lee et al., 2018) as well as for investigating Mendelian factors affecting infection susceptibility (Zhang and Reilly, 2017). With their ability to combine the primary macrophage status of hMDM and the genetic tractability of cell lines they have the potential to transform our ability to understand human macrophage biology.

1.6 Aims of this thesis

Given the limitations of current *in vitro* human macrophage models and ongoing discrepancies regarding the role of the autophagy pathway during Mtb infection, this project aimed to establish human iPSDM as a relevant and valuable model for studying host-pathogen interactions in human macrophages. Following the establishment of the model the aim was to use it to uncover the dynamics of autophagic targeting as well as to dissect the impact of genetic disruption of the autophagy pathway on Mtb replication.

Aim 1: To establish a robust experimental system to work with human macrophages

Given the recent interest in the use of iPSDM to study infection (Hale et al., 2015; Yeung et al., 2017), as well as their potential to overcome some of the limitations of current human macrophage models, I aimed to establish their differentiation within our lab and determine their suitability as a host for studying Mtb infection. Through a variety of cell biology approaches I compared the response of iPSDM to Mtb infection with previously published work probing this interaction in other human macrophage models.

Transcriptomic studies have revealed insights into host defence pathways, and their manipulation, during infection with many intracellular pathogens. The transcriptional response of mouse and human macrophages to Mtb infection has been well studied and provides a useful tool for comparison with iPSDM responses (Papp et al., 2018; Blischak et al., 2015; Silver et al., 2009; Chaussabel et al., 2003; Thuong et al., 2008). Interestingly, no published study compares the response of macrophages to

infection with Mtb WT and the attenuated mutant Mtb ΔRD1, lacking the ESX-1 T7SS. To understand how iPSDM respond to Mtb infection, and the impact of ESX-1 dependent secretion events on this response, we performed bulk RNA-seq on Mtb WT and Mtb ΔRD1 infected iPSDM at 2 h and 48 h post infection.

Aim 2: To analyse the dynamics of xenophagy of Mtb in human macrophages

Whilst the targeting of Mtb to autophagosomes has been widely examined by fixed time point fluorescence studies in mouse macrophages (Watson et al., 2012; Köster et al., 2017), no live cell imaging of this exists in the published literature and a dissection of the pathway in human macrophages is also missing. To fill this gap in knowledge I aimed to utilise iPSDM to study the dynamics of autophagic targeting of Mtb at high spatial and temporal resolution using live cell imaging, partnered with correlative 3D electron microscopy, to define the localisation of Gal8 and LC3B positive membranes as well as Mtb.

Aim 3: To dissect the role of canonical and non-canonical xenophagy of Mtb in human macrophages

Genetic disruption of the autophagy pathway in mouse macrophages *in vitro*, through knockout or knockdown of a range of proteins important for autophagosome biogenesis or cargo recognition, results in reduced control of Mtb (Manzanillo et al., 2013; Franco et al., 2016). However, in mouse models of TB, only Atg5 seem to play a role during infection (Castillo et al., 2012; Kimmey et al., 2015) and only limited studies have examined the role of autophagy in human macrophages during Mtb infection (Kumar et al., 2010). I aimed to study the impact of autophagic disruption, through knockout of Atg7 or Atg14 in iPSDM, on Mtb replication and trafficking.

2. Materials and Methods

2.1 Cell Biology

iPSC culture

hiPSC lines, EIKA2 (European Collection of Authenticated Cell Cultures #66540075), KOLF2_C1 (European Collection of Authenticated Cell Cultures #77650100) and Atg13 KO KOLF2_C1 (a gift from Nick Ksistakis), were maintained in E8 (ThermoFisher Scientific #A1517001) on Vitronectin XF (StemCell Technologies #07180) coated plates at 37°C and 5% CO_2. Cells were passaged 1:6 at confluency using Versene (ThermoFisher Scientific #15040033). Cells were cryopreserved in Knockout Serum Replacement (ThermoFisher Scientific #10828028) + 10% DMSO (Sigma-Aldrich #D2650). On thawing, cells were incubated in E8 + 20 µM Y-27632 (ROCKi) (Tocris #1254) for the first 24 h.

iPSDM differentiation

iPSCs were detached with TryplE Select for 5 min at 37°C (ThermoFisher Scientific #12563011) to form a single cell suspension and seeded at $4x10^6$ cells per well of an AggreWell 800 plate (StemCell Technologies #34815) in E8 + 10 µM ROCKi to form embryonic bodies (EBs). Each day, for three days, two 50% media changes were carried out with E8 + 50 ng/ml bone morphogenic protein 4 (BMP4) (Peprotech #120-05) + 50 ng/ml vascular endothelial growth factor (VEGF) (Peprotech #100-20) + 20 ng/ml stem cell factor (SCF) (Peprotech #300-07). Four days after formation, EBs were flushed out of the wells, washed twice with PBS and seeded at 300 EBs per 225 cm^2 flask (ThermoFisher Scientific #159934) in 30 ml factory media (X-Vivo 15 (Lonza #BEBP02-061Q) + 2 mM Glutamax (ThermoFisher Scientific #35050038) + 50 µM β-Mercaptoethanol (ThermoFisher Scientific #31350010) + 100 ng/ml M-CSF (Peprotech #300-25) + 25 ng/ml IL-3 (Peprotech #200-03)). 20 ml fresh factory media was added each week for 4-5 weeks, until monocytes appeared in the supernatant. Up to 50% of the supernatant containing monocytes was harvested each week, and replaced with 20 ml of factory media. Monocytes were centrifuged at 300 x *g* for 5 min then seeded at $1.2x10^7$ per 15 cm petri dish (StarLabs #CC7672-3614) and differentiated to macrophages in X-Vivo + 2 mM Glutamax + 50 µM β-

Mercaptoethanol + 100 ng/ml M-CSF, a 50% media change was performed on day 3 or 4 of differentiation. For KOLF2_C1 iPSDM, where monocytes were more proliferative, a full media change was performed on day 3 or 4. To detach iPSDM, plates were washed once with PBS then incubated with Versene for 15 min at 37°C and 5% CO_2 before diluting 1:3 with PBS and gently scraping. Macrophages were centrifuged at 300 x *g* for 3 min and plated for experiments in X-Vivo 15 + 2 mM Glutamax + 50 µM β-mercaptoethanol.

Human monocyte derived macrophage differentiation

CD14 positive monocytes were isolated from Leukocyte cones (NHS Blood and Transplant Service, UK) as described previously (Lerner et al., 2017). Red blood cells were removed by centrifugation on Ficoll-Paque (GE Healthcare #28-4039-56 AG) and red cell lysis buffer (Sigma-Aldrich #11814389001) and monocytes positively selected using a magnetic cell separation system with anti-CD14 mAb-coated microbeads (Miltenyi Biotec #130-050-201). Monocytes were seeded into RPMI 1640 (ThermoFisher Scientific #72400054) supplemented with 50 ng/ml M-CSF and allowed to differentiate for 7 days with a 50% media addition on day 3. Macrophages were detached in ice cold 0.5 mM EDTA in PBS (Miltenyi Biotec #130-091-222) and seeded as required.

iPSDM electroporation

iPSDM were electroporated with 1 µg plasmid DNA using the Neon electroporation system (ThermoFisher Scientific #MPK500S). Briefly, iPSDM were harvested, washed in PBS (ThermoFisher Scientific #70011051) and resuspended at $2.5x10^7$ cells/ml in Buffer R and plasmid DNA added. For electroporations using multiple plasmids, equal amounts of each were used to a total of 1 µg. Cells were electroporated at 1700 V for 30 ms, with 1 pulse then plated into dishes as required. Plasmids used are listed in **Table 2.1.1**.

Plasmid	Source	Catalogue Number	Reference
pEGFP-LC3B	Addgene	21073	(Kabeya et al., 2000)
pEGFP-hLC3B	Addgene	24920	(Lee et al., 2008)
RFP-Gal8	In house	N/A	(Bernard et al., 2021)
GFP-Gal8	In house	N/A	This work

Table 2.1.1 Plasmids used for electroporations.

iPSC transduction with lentivirus

EGFP-hLC3B was sub-cloned from Addgene #24920 into pLenti-EF1-MCS-PGK-PURO using NheI and BamHI restriction enzymes and lentivirus particles produced by Alstem Inc (USA). iPSC were seeded in a 6 well plate and transduced with 2 ml E8 + $5x10^5$ IU/ml Lentivirus + 10 µg/ml Polybrene (Sigma-Aldrich #TR-1003-G) overnight. The following day media was changed. After 48 h, cells were harvested and 1500 cells seeded in a 10 cm dish in E8 + CloneR (Stem Cell Technologies #05889). Cells were fed according to CloneR manufacturer's instructions. Individual colonies were picked manually, expanded then sorted by fluorescence-activated cell sorting (FACS) for EGFP positive cells on a FACS Aria III (BD Bioscience) with a 100 µm nozzle.

Atg7 and Atg14 knockout in iPSC by CRISPR/Cas9 editing

Guide RNA design

Considering the transcript architecture of these genes, as well as the downstream screening for putative KO clones it was decided to knockout critical exons for each gene to produce frameshifts that would not lead to functional protein. For Atg7 exons 2 and 3 were chosen for deletion, which removes the start codon and leaves the remaining DNA without an in-frame ATG for an alternative start site (**Table 2.1.2**). For Atg14 exon 5 was chosen for deletion as this will produce a frame shift in the remaining coding sequence and delete key amino acids important for function should a shortened transcript be produced and not removed by nonsense mediated decay (**Table 2.1.3**). Two guide RNAs (gRNA) were designed 5' and 3' of the targeted exons, with protospacer adjacent motifs (PAM) facing in opposite directions to maximise the chances of successful exon deletion (**Table 2.1.4**).

Exon #	Exon/Intron	Start Phase	End Phase	Sequence
1	ENSE00001942132	-	-	GGAAGTTGAGCGGCG
-	Intron 1-2	-	-	gtaagtgagccgcggcgggc...gttattgttta aagagtatagagttccagttttgcaagatgaa aaagttctggagatctgtttcacaacgttgtgatt atacttaatatcacctaactgtttacctcaaaat aatcaagatggtaaagtatatgttatgtgtttctt accacaatccaaaaagaagttgtgtttcaagg tagcctgtaaacatctcattacttttgtttgtttga attaaactttattacaaatgttctttctcaccaggt tttgcatggatatgttattttgctgtgttctgttttgttt tttaatag
2	ENSE00003638636	-	1	GCAAGAAATAATGGCGGCAGCT ACGGGGGATCCTGGACTCTCTA AACTGCAGTTTGCCCCTTTTAGT AGTGCCTTGGATGTTGGGTTTT GGCATGAGTTGACCCAGAAGAA GCTGAACGAGTATCGGCTGGAT GAAGCTCCCAAGGACATTAAGG GTTATTACTACAATG
-	Intron 2-3			gtaggtgattgtaaatttca…gtgataatgcttc tgtccag
3	ENSE00003588186	1	2	GTGACTCTGCTGGGCTGCCAGC TCGCTTAACATTGGAGTTCAGT GCTTTTGACAT
-	Intron 3-4			gtgagtatttatttgttcaaaatctgaagtaaag aatactacttttggcaaggaataagcatgcttg cctccctcataggtggaccacaggaggacta gggaagttcccggtgggcagagtcagccccc ctcatgattctcttatacctcccatagagatgagt gctggatacttaggtctgcctggttaatttttcac cacctatttatcagagtcaattaggtgccaggt gccatctagattgattgagacatagataatatc cctcttgattttgattgtagttaatattttgtgtt...cg tgtttctcttgtatctag
4	ENSE00000902859	2	0	GAGTGCTCCCACCCCAGCCCGT TGCTGCCCAGCTATTGGAACAC TGTATAACACCAACACACTCGA GTCTTTCAAGACTGCAGATAAG AAGCTCCTTTTGGAACAAGCAG CAAATGAG

Table 2.1.2 Atg7 exon and intron sequences. The first 4 exons of Atg7, and their separating introns are shown. The coding sequence is in blue, 5' UTR in red, CRISPR gRNA sequences are highlighted in yellow.

Exon #	Exon/Intron	Start Phase	End Phase	Sequence
4	ENSE00001193872	0	1	AGATGGAAAATAATGTCCTGCA AGATGAGGATTGAACAGTTAAA ACAAACAATATGTAAAGGAAAT GAAGAAATGGAGAAAA
-	Intron 4-5	-	-	gtaagtaattcgtgtccttc...taggaaaatcag gtccttcctgtgctaaacttaaactcgatagttgt tgagtgactccttttactagtgatgattacaaata gagatccagagtcattttaatcatggttctctttg ctttatgtgtaatatctacttgaactaaactctca aattttccacttagtgaacattatattattcaggttt tgctttcagtttagattgcaagggaaaacacgc atgtttgtggggtggagctctgcagtacacagg aactgtttgcagagataattgttgggtgtgattta tttatttttag
5	ENSE00003599053	1	2	ATTCTGAAGGCCTTCTCAAAAC CAAGGAAAAGAATCAGAAGCTT TACAGTCGAGCACAACGGCACC AAGAGAAAAAGGAGAAGATTCA GAGGCATAATCGCAAACTTGGT GACCTGGTAGAAAAAAAGACCA TTGACTTAAGAAGTCATTATGAG CGTCTGGCAAATCTTCGACGAT CCCATATATTAGAGCTCACCTCT GTCATTTTTCCAATCGAGGAAGT AAAGACGGGTGTGAG
-	Intron 5-6	-	-	gtacattaagcaagtcttttgactccaggaata gatcaagttccaaatacttttaaagtatgtcatt accttatttattgggtcttattctagggtcattggttt tcctggtgatggaacataagtcttatctgtttcaa caaacagtacgcaccgcagaaagctgggg aggcagcgaggtgaggggtggggcccaca cttgtgtactgtcctagagcttctagatgaggtg ctgactcacactcctgattaagaaccatctgat ggctgggagtggtggctcacgcctataatccc ag...gtgtgtcttcctacttgtag

6	ENSE00003490931	2	1	AGACCCCGCAGATGTGTCTTCA GAGAGTGACAGTGCCATGACCT CCAGCACTGTGAGCAAGCTTGC TGAAGCCCGGAGGACAACTTAC CTCTCAGGACGATGGGTCTGTG ACGATCACAACGGAGACACCAG CATTAGCATTACAGGGCCTTGG ATTAGCCTCCCTAACAATGGGG ACTACTCTGCCTACTACAGCTG GGTGGAGGAGAAGAAAACAAC CCAGGGGCCTG

Table 2.1.3. Atg14 exon and intron sequences. The 4th, 5th and 6th exons of Atg14, and their separating introns are shown. The coding sequence is in blue, CRISPR gRNA sequences are highlighted in yellow.

Gene	gRNA number	gRNA-sequence
Atg7	1	UUAUUUUGAGGUAAACAGUU
	2	UAACAUAUCCAUGCAAAACC
	3	CUCCCUCAUAGGUGGACCAC
	4	AUCAGAGUCAAUUAGGUGCC
Atg14	1	AUCGAGUUUAAGUUUAGCAC
	2	AACCAUGAUUAAAAUGACUC
	3	UAAGCAAGUCUUUUGACUCC
	4	GGGUCUUAUUCUAGGGUCAU

Table 2.1.4. gRNAs used for knockout of Atg7 and Atg14 in hiPSC.

Targeting of iPSC

Cas9 ribonucleoprotein complexes were formed using 5 µg Cas9 (IDT #1081059) and 4 µg modified synthetic gRNA (Synthego Corporation, USA) at room temperature for 15 min. A single cell suspension of iPSC was generated with TryplE for 5 min at 37°C. $1x10^6$ cells were suspended in 100 µl buffer P3 (Lonza #V4XP-3024) and added to preformed ribonucleoprotein complexes of four gRNAs per gene. Cells were nucleofected using the Amaxa 4D (Lonza) program CA137 and plated in one well of a 6 well plate in E8 + 10 µM ROCKi. The following day, media was changed to E8 without ROCKi and cells were fed until confluent.

Single cell cloning

Once confluent, cells were harvested as a single cell suspension using TryplE and 2000 cells seeded in a 10 cm dish coated with Vitronectin XF in E8 + CloneR. Cells were fed 2 days post seeding with a full change with E8 + CloneR and 25% of initial media volume of E8 + CloneR was added on day 3. On day 4, media was changed to E8 alone. Once colonies formed, they were manually picked into duplicate 96 well plates. Successful KO clones were screened by PCR and picked for expansion.

Screening for KO clones

Following expansion of the duplicate 96 well plates, cells from one plate were lysed in 80 µl cell lysis buffer (50 mM KCl + 10 mM Tris pH 8 + 2 mM $MgCl_2$ + 0.45% NP40 + 0.45% Tween20 + Proteinase K) at 65°C for 2 h to extract genomic DNA (gDNA). Proteinase K was inactivated at 80°C for 15 min and lysates diluted 1:10 with nuclease free water then used for a PCR screen to test for putative knockout clones. Using primers flanking the deleted exons (**Table 2.1.5**), gDNA was amplified that would give a 1500 base pair (bp) fragment for the WT gene but a shorter product, 700 bp for Atg7 and 1000 bp for Atg14, if exon deletion had been successful. Fragments were amplified using EconoTaq polymerase master mix (Lucigen #30033-1), 1 µM of each primer (IDT) and 2.5 µl gDNA. PCR cycles were run as follows: 98°C for 2 min, then 35 cycles of 98°C 20 sec, 57°C 15 sec, 72°C 80 sec, and a final extension of 5 min at 72°C. Samples were run on 1% Agarose gels for analysis.

Primer name	Sequence	Purpose
Atg7_GF2	AGGATGGTTTTCAAAGTTGTGTCTT	Amplifying Atg7 gDNA around exons 2&3
Atg7_GR2	ACAGTGGCTTGTATACAGAAGTAGA	
Atg14_GF1	TCTGTCTGAGAGTTTACAGCTTGTT	Amplifying Atg14 gDNA around exon 5
Atg14_GR1	TGCCTCACAACACACAACTAATAAA	

Table 2.1.5 PCR primers for amplifying Atg7 KO and Atg14 KO regions.

2.2 Microbiology

Mtb strains

Mtb H37Rv WT (Mtb WT) and Mtb H37Rv ΔRD1 (Mtb ΔRD1) were kindly provided by Prof. Douglas Young (The Francis Crick Institute, UK) and Dr Suzie Hingley-Wilson (University of Surrey, UK) respectively. Fluorescent Mtb strains were generated as previously reported (Lerner et al., 2016). E2Crimson Mtb was generated by transformation with pTEC19, a gift from Prof. Lalita Ramakrishnan (Addgene 30178). Strains were verified by sequencing and tested for PDIM positivity by thin layer chromatography (TLC) of lipid extracts from Mtb cultures (**Figure 2.2.1**), purified PDIM (BEI Resources NR-20328) and lipid extracts from Mtb ΔPDIM (Lerner et al., 2018) were used as positive and negative controls respectively. Mtb strains were cultured in Middlebrook 7H9 supplemented with 0.2% glycerol, 0.05% Tween-80 and 10% albumin dextrose catalase (ADC). For E2Crimson strains 7H9 was supplemented with 50 µg/ml hygromycin (Life Technologies 10687010).

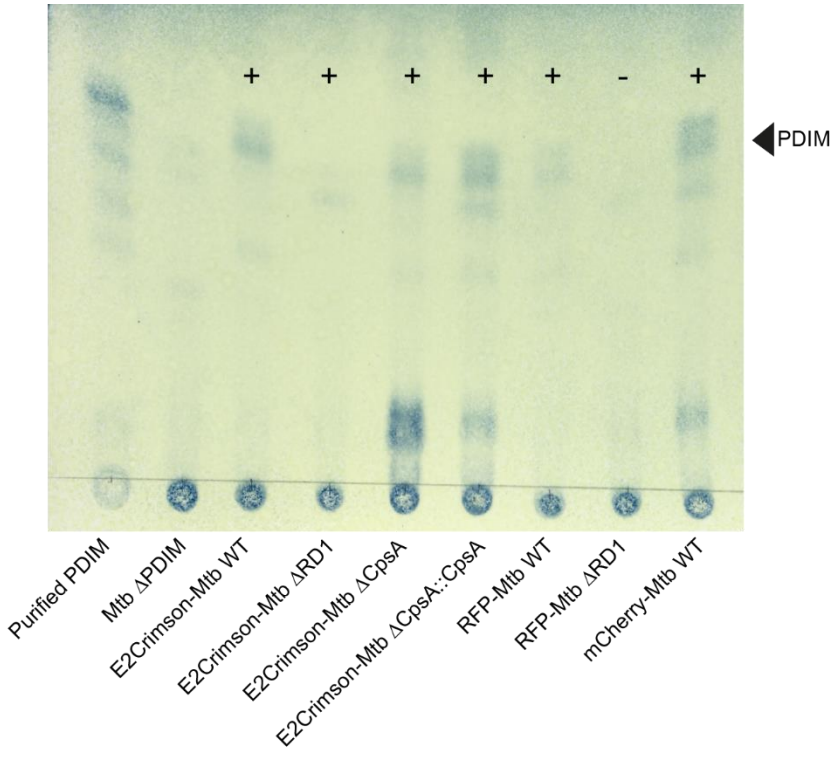

Figure 2.2.1 TLC for PDIMs in Mtb strains used. Lipid extracts from all Mtb strains used were subjected to TLC to check for the presence of PDIMs. Arrowhead indicates the band corresponding to PDIMs. Strains deemed PDIM positive are marked (+) and negative (-).

cpsA rv3484 mutant construction in *Mycobacterium tuberculosis*

The gene *cpsA* (*rv3484*) (**Figure 2.2.2**) was deleted from Mtb H37Rv WT using the ORBIT method (Murphy et al., 2018). Briefly, Mtb WT was transformed with the plasmid pKM461 (a gift from Kenan Murphy Addgene plasmid #108320) that allowed for the expression of the RecT annealase and the BxB1 phage integrase upon addition of 500 ng/ml anhydrotetracycline (ATc) (Sigma Aldrich 37919). Next, ATc-induced Mtb was co-transformed with an oligonucleotide targeting the gene *cpsA* (gcgcgccagttggttcgacggcgcctggccgaggcatatgatggcgcgttctgagggcaatcgcccacgcGG TTTGTCTGGTCAACCACCGCGGTCTCAGTGGTGTACGGTACAAACCatcgatggc ggcggcgtgccctgcgtgaactaggtaagttatccgaccactccacgcagcccgtcggcgc) and the plasmid pKM496 (a gift from Kenan Murphy (Addgene plasmid #109301) carrying the BxB1 phage *attP* and *attB* sites respectively. RecT mediates the annealing of the oligonucleotide to the lagging strand during replication, leading to the replacement of the targeted genomic region by the BxB1 phage *attP* site. Subsequently, the integrase mediated recombination of the *attP* and *attB* sites leads to the introduction of the zeocin resistance marker at the deleted locus. The transformants were verified by PCR for the deletion of *cpsA* and the plasmid pKM461 was lost by counter selection on sucrose. The final clone was confirmed by whole genome sequencing. The resulting strain (Mtb ΔCpsA) was cultured in the presence of 25 µg/ml zeocin (Gibco R25001).

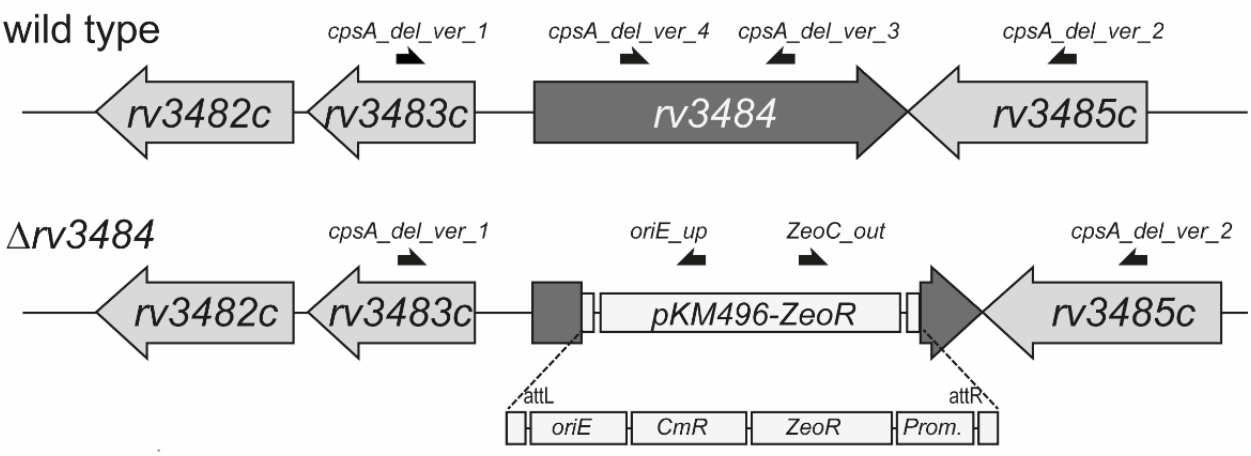

Figure 2.2.2 Genomic arrangement of cpsA (rv3484). *Mycobacterium tuberculosis cpsA (rv3484)* locus in the wild type strain and the deletion mutant strain generated by using the ORBIT method.

Black half-arrows depict the position of the primers used for validation PCR. *oriE*: origin of replication for plasmid replication in Escherichia coli, *CmR*: gene encoding resistance to chloramphenicol, *ZeoR*: gene encoding resistance to zeocin, *Prom*.: groEL promoter, *attL* and *attR*: *att* sites resulting from the recombination of Bxb1 *attB* and *attP* sites.

Successful knockout was validated by PCR using the primers detailed in **Table 2.2.1** and shown in **Figure 2.2.2**. Results confirming successful deletion of CpsA are shown in **Figure 2.2.3**.

Primer name	Sequence
cpsA_delver_1	CGTCTTGCACCGTCACCAG
cpsA_delver_2	GCGGTTCGTTCGTCGGCATC
cpsA_delver_3	TGGCGGTGGGTGCGGTCCAG
cpsA_delver_4	GAAAGAGCTCGAGACCCGGG
ZeoN-out	GGCACTGGTCAACTTGGCCAT
ZeoC-out	GCAACTGCGTGCACTTCGTG
oriE-up	ACGCCTGGTATCTTTATAGTCC

Table 2.2.1 Primers used to validate deletion of *cpsA*.

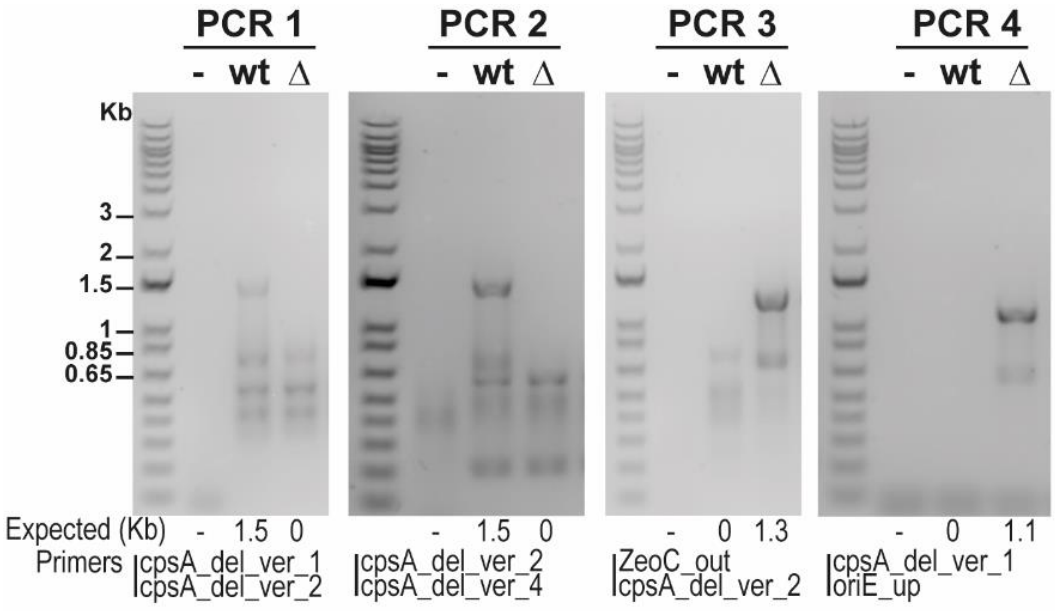

Figure 2.2.3 Validation of deletion of *cpsA* (*rv3484*) from *M. tuberculosis*. Purified Mtb DNA from the indicated strains was analysed by PCR using the primers shown. The expected product size from each PCR in each strain is indicated. - : no DNA, wt: Mtb WT, Δ: Mtb ΔCpsA.

For complementation the gene *cpsA* has been amplified from Mtb WT using primers cpsA-rev-munI (gcgccaattgaaagcttatttaaatctagttca) and phsp60-fw-ecorV (gcgcgatatcttaaactctagacggtgaccac) and Phusion High Fidelity polymerase (NEB M0531). The fragment and the recipient vector pML2375 (a gift from Michael Niederweiss) cut by MunI (NEB R3589S) and EcoRV (NEB R3195S) were ligated with T4 DNA ligase (NEB M0202S) to yield pMS6K-Phsp60-cpsA placing the expression of *cpsA* under the control of the strong *hsp60* promoter from the MS6 site in the mycobacterial chromosome. The resulting strain (Mtb ΔCpsA::CpsA) was cultured in the presence of 25 µg/ml zeocin + 25 µg/ml kanamycin (Sigma Aldrich, K4000).

PDIM extraction and visualisation

All strains used for infection were checked for the presence of PDIMs. Bacteria from 10 ml of logarithmic culture were inactivated for 2 h at 95°C in 1 mL PBS. After 3 washes in water, supernatants from successive incubations in chloroform:methanol (2:1) and methanol:chloroform (1:1) were pooled and dried at 55°C. Dried lipids were further resuspended in chloroform, resolved on a silica gel plate with a petroleum ether:ethyl acetate (98:2) solvent mix and visualized with 5% phosphomolybdic acid in ethanol.

Macrophage infection with Mtb

The day before infection, cells were seeded into dishes as required. iPSDM and hMDM were seeded at a density of 50,000 cells per well of a 96 well plate, 150,000 cells per well of a 24 well plate or per Mattek gridded dish (Mattek Corporation P35G-1.5-14-CGRD), 500,000 cells per well of a 12 well plate, $1x10^6$ cells per well of a 6 well plate. Mid-logarithmic phase bacterial cultures (OD_{600} 0.5-1.0) were centrifuged at 2000 x *g* for 5 min and washed twice in PBS. Pellets were then shaken vigorously for 1 min with 2.5-3.5 mm glass beads (VWR 332124G) and bacteria resuspended in 10 ml macrophage culture media before being centrifuged at 300 x *g* for 5 min to remove large clumps. The top 7 ml of bacterial suspension was taken, the OD_{600} recorded and diluted appropriately for infection. The inoculum was added at the correct MOI, assuming OD_{600} of 1 is $1x10^8$ bacteria/ml. Infections were carried out

in a volume of 50 µl in a 96 well plate, 300 µl in a 24 well plate, 500 µl in a 12 well plate or 1 ml in a 6 well plate. After 2 h of uptake extracellular bacteria were removed with two washes in PBS and macrophages incubated for the required time points in macrophage media. At the required time post infection cells were harvested as appropriate. For infections in the presence of IFN-γ, cells were incubated with 20 ng/ml IFN-γ following the washes to remove extracellular bacteria for the remainder of the infection. An MOI of 1 was used for all replication experiments, for all other experiments an MOI of 2 was used unless stated differently in the figure legend.

2.3 Imaging

Indirect immunofluorescence

Cells were fixed in 4% paraformaldehyde (PFA) (Electron Microscopy Sciences #15710) in PBS overnight at 4°C. Aldehydes were quenched in 50 mM NH_4Cl, membranes permeabilised in PBS/0.1% BSA (Cell Signaling Technology 9998S)/0.05% Saponin (Sigma Aldrich 47036) for 10 min and blocked in PBS/0.1% BSA for 5 min. Antibodies, indicated in **Table 2.3.1**, were then added sequentially for 1 h at room temperature. Between antibodies, cells were washed three times in PBS. Nuclei were stained with DAPI (ThermoFisher D1306) diluted 1:10000 in PBS for 10 min. Coverslips were mounted on glass slides with DAKO mounting medium (DAKO #S3023). Coverslips were imaged using a Leica SP5 or SP8 inverted confocal microscope (Leica Microsystems, Germany) with a 63X 1.4NA oil immersion objective. 96 well glass bottom Viewplates (Perkin Elmer 6005430) were imaged on an Opera Phenix high content imaging system (Perkin Elmer, Germany) with either a 40X 1.1NA or 63X 1.15NA water immersion objective. Images were acquired in confocal mode, with 2 x binning and Two Peak autofocus.

For imaging on the Leica SP5 or SP8 DAPI was excited at 405 nm using a Diode, Alexa 488 was excited at 488 nm with an Argon laser, RFP was excited at 561 nm using a DPSS laser, and E2Crimson was excited at 633 nm with a HeNe laser. Fluorescence was detected using HyD detectors. Laser and detector settings were kept constant between conditions for each biological replicate of an experiment.

For imaging on the Opera Phenix DAPI was excited at 405 nm and emission detected from 435-480 nm, Alexa 488 was excited at 488 nm and emission detected from 500-550 nm, E2Crimson was excited at 633 nm and emission detected from 650-760 nm. Fluorescence was detected using a 16 bit scMOS camera.

Antibody	Supplier	Catalogue Number	Dilution
LC3B	MBL	PM036	1:100
LAMP-1	Abcam	ab24170	1:100
Gal8	RnD Systems	AF1305	1:100
p40 Phox	Millipore	07-503	1:100
EEA1	BD Bioscience	610457	1:100
Anti-rabbit AlexaFluor 488	ThermoFisher Scientific	A11034	1:800
Anti-mouse AlexaFluor 488	ThermoFisher Scientific	A11029	1:800
Anti-goat AlexaFluor 488	ThermoFisher Scientific	A11055	1:800

Table 2.3.1 Antibodies used for indirect immunofluorescence.

Live cell imaging

iPSDM were seeded in a Mattek gridded dish and infected with Mtb. Immediately after addition of bacteria, Mattek gridded dishes were sealed with parafilm, loaded into a holder and imaged on a laser scanning confocal microscope (Leica SP5, Leica Microsystems, Germany) at 37°C/5% CO_2 using a custom-made environmental chamber from EMBL. Samples were imaged using a 63x 1.4NA oil immersion objective. For live imaging of Lysotracker, cells were stained for 15 min with 50 nM Lysotracker Green DND-26 (ThermoFisher Scientific #L7526) at 37°C/5% CO_2 before removal of media and addition of Mtb and immediate transfer to the microscope and imaging as described above. Time frames for each movie are detailed in figure legends.

Alexa 488 and Lysotracker Green were excited at 488 nm with an Argon laser, mCherry was excited at 561 nm using a DPSS laser, and E2Crimson was excited at 633 nm with a HeNe laser. Fluorescence was detected using HyD detectors in BrightR mode. Laser and detector settings were kept constant between conditions for each biological replicate of an experiment.

Transmission electron microscopy

Sample preparation

Cells were washed in PBS and then fixed in 2.5% glutaraldehyde (GA) (Sigma Aldrich 1121790025) in 200 mM HEPES pH 7.4 for 30 min at room temperature then overnight at 4°C. The following day the fixative was exchanged for 1% glutaraldehyde. After several washes in 200 mM HEPES buffer, samples were processed in a Pelco Biowave Pro (Ted Pella, USA) with use of microwave energy and vacuum. Samples were fixed and stained using a reduced osmium, thiocarbohydrazine, osmium (ROTO)/en bloc lead aspartate protocol. Samples for stereological analysis were dehydrated using an ethanol series of 50, 75, 90 and 100% then lifted from the tissue culture plastic with propylene oxide, washed 4 times in dry acetone and transferred to 1.5 ml microcentrifuge tubes. Samples were infiltrated with a dilution series of 50, 75, 100% of Ultra Bed Low Viscosity Epoxy (Electron Microscopy Sciences 14310) resin to acetone mix and centrifuged at 600 x *g* between changes. Finally, samples were cured for a minimum of 48 h at 60°C before trimming and sectioning.

Sectioning and imaging

Ultrathin sections (~50 nm) were cut with an EM UC7 Ultramicrotome (Leica Microsystems, Germany) using an oscillating ultrasonic 35° diamond Knife (DiaTOME, Switzerland) at a cutting speed of 0.6 mm/sec, a frequency set by automatic mode and, a voltage of 6.0 V. Images were acquired using a 120 kV Tecnai G2 Spirit BioTwin (FEI company, USA) with an Orius CCD camera (Gatan Inc., USA).

Correlative live cell fluorescence and focused ion beam scanning electron microscopy (FIB SEM)

Sample preparation

iPSDM expressing GFP-LC3B and/or RFP-Gal8 were imaged live as described above before a final high-resolution Z stack was acquired. Samples were fixed in 4% PFA overnight at 4°C before high resolution Z stacks of the fixed cells were acquired. Cells were then fixed in 2.5% GA for 15 min at room temperature before being processed for EM as described above, with the exception of using Durcupan resin. Samples were processed in a Pelco Biowave Pro as described above except only being washed twice with dry acetone. In the next steps samples were infiltrated with a dilution series of 50, 75 and 100% of Durcupan resin (Sigma Aldrich 44610) to acetone mix.

Image acquisition

Focused ion beam scanning electron microscopy (FIB SEM) data was collected using a Crossbeam 540 FIB SEM with Atlas 5 for 3-dimensional tomography acquisition (Zeiss, Cambridge). The grid square containing the cell of interest was trimmed from the resin block, mounted on a standard 12.7 mm SEM stub using silver paint, and coated with a 5 nm layer of platinum. The specific cell of interest was relocated in the SEM by imaging through the platinum coating at an accelerating voltage of 10 kV and correlating to previously acquired fluorescence microscopy images. After preparation for milling and tracking, electron micrographs were acquired at 5 nm isotropic resolution throughout each region of interest, using a 9 or 10 µs dwell time. During acquisition, the SEM was operated at an accelerating voltage of 1.5 kV with 1 nA current. The EsB detector was used with a grid voltage of 1,200 V. Ion beam milling was performed at an accelerating voltage of 30 kV and current of 700 pA.

Image processing and alignment

After cropping to each region of interest, the datasets were aligned (register virtual stack slices, translation, default settings; Fiji), and batch processed to supress noise,

and enhance sharpness and contrast (gaussian blur [0.8 pixel radius], smart sharpen [60 percent, 10 pixel radius], smart sharpen [100 percent, 2 pixel radius], medium contrast curve; Adobe Photoshop CC 2015.5). For viewing, and to mitigate any misalignment with respect to the light microscopy orientation that was introduced during specimen mounting, each dataset was rotated and resliced in XY and YZ planes to flatten the volume with respect to the coverslip surface. The volume was then resliced in the XZ plane, perpendicular to the coverslip surface, to enable direct correlation of light and electron microscopy images.

Scanning electron microscopy

iPSDM were treated with an inoculum of Mtb WT at an MOI of 10 for 20 min on 13 mm glass coverslips. Samples where then fixed with a mixture of 4% PFA, 1.25% GA, 0.04 M sucrose in 200 mM HEPES pH 7.4 overnight at 4°C. A Pelco Biowave Pro was used to process the samples as follows. Samples were washed twice in HEPES at 250 W for 40 s and post-fixed in 2% osmium tetroxide (Taab). Samples were washed in 200 mM HEPES then dehydrated using a step-wise ethanol series of 50, 75, 90 and 100 % at 250 W for 40 s per step. Samples were critical point dried using an EM CPD300 (Leica Microsystems, Germany) and acetone as the solvent. The samples were coated with 2 nm gold before imaging on a Quanta SEM (FEI, United States).

2.4 Image Analysis

Stereology analysis

Fixed cells were pelleted at 600 x *g* after detachment from tissue culture plastic prior to embedding. At least 24 different infected cells per sample were imaged at ×3,900 magnification by systematic and random sampling. Cross points of the stereological test grid over bacteria were counted with regard to the subcellular localization of bacteria, which was determined from images taken at minimum magnification of ×16,000. Percentages were calculated from total counts per sample. The following criteria were followed for the assessment of subcellular membrane involvement: (a) Single surrounding membrane; bacteria were, at least partially, tightly surrounded by a phospholipid bilayer, representing the phagosomal membrane (b) cytosolic;

bacteria were surrounded by ribosomes, representing the cytoplasm with no indication of the phagosomal membrane; (c) Multiple surrounding membranes; bacteria were enveloped by double or multiple membrane structures.

FIB SEM segmentation

Datasets were imported into IMOD (Kremer et al., 1996) and manually segmented. The cytosol facing membranes were outlined. Where gaps existed in membranes or there was ambiguity as to the presence or location of a membrane they were introduced into the model and left as holes. Where the sample was torn during coverslip detachment and this affected sample preservation a hole was left.

Fluorescence-EM correlation

3D alignment of the fluorescence and FIB SEM image was performed using BigWarp. Fluorescence and FIB SEM files were converted to TIFF files and linear adjustments made to brightness and contrast using Fiji. The BigDataViewer and BigWarp plugin (Pietzsch et al., 2015) were used to align the two datasets. The FIB SEM stack was set as the ‘target’ and the light microscopy stack as the ‘moving dataset’. In landmark mode, a minimum of ten fiducials were placed in the first instance, across six axes (x, y, z, pitch, yaw, roll) for the initial alignment. Further points were chosen to increase the accuracy using a thin-plate spline method.

2D correlative light and electron microscopy (CLEM) of single slices from the fluorescence and FIB SEM was performed in Icy (BioImage Analysis Unit, Institut Pasteur, Paris, France) using the ecCLEM plugin (Paul-Gilloteaux et al., 2017). The fluorescence image was deformed to map onto the unaltered FIB SEM slice using non rigid transformation. Bacteria and clearly defined LC3 positive structures were used as landmarks.

Fixed cell image analysis

To quantify Mtb replication, images were acquired on an Opera Phenix using a 40x 1.1NA objective with at least 15 fields of view per well with a 10% overlap between adjacent fields, 3 wells per condition per experiment. Data was analysed in Harmony (version 4.9, Perkin Elmer Inc., Germany). Maximum projections of all planes, a total

of 4 with each 1 µm apart, were produced. Fields were stitched together to create a global image with dynamic binning and cells were segmented based on DAPI, excluding any cells touching the edge of the imaged area. Bacteria were detected using the 'Find Spots' or 'Calculate Image' building block of Harmony to produce a mask of the bacteria. The total bacterial area in each cell was then determined by Harmony. To calculate change in Mtb area/cell the mean Mtb area per cell at each time point was divided by the mean Mtb area per cell at 2 h. Uninfected cells, that is those with an Mtb area of 0, were excluded from analysis.

To quantify marker association to Mtb from images acquired using the Leica SP5 or SP8 on glass coverslips images from at least 10 fields of view per replicate, acquired on a 63X objective, were loaded into Fiji and the mean fluorescence intensity (MFI) in an area marked by a mask of the bacteria was determined, as previously reported (Lerner et al., 2016; Schnettger and Gutierrez, 2017). Briefly, a manual threshold was determined to produce a mask of the bacteria then the 'Analyse Particles' function of Fiji, with size 0.5-Infinity and circularity 0.00-1.00, was used to measure the properties of the marker channel in the mask created. The MFI of manually selected marker positive and negative bacteria was calculated and used to determine a cut-off MFI for positive bacteria and the percentage of positive bacteria determined from this. Due to the nature of the LAMP-1 staining, automatic quantification was unreliable and so the number of positive and negative bacteria were counted manually.

To quantify marker association to Mtb from images acquired using the Opera Phenix, cells were stained in 96 well glass Viewplates and imaged on a 63X 1.15NA water immersion objective. Following acquisition, images were evaluated using Harmony. Bacteria were identified using the 'Find Spots' building block and the mean fluorescence intensity of the marker in in each identified bacterial 'spot' calculated. The resulting analysis was examined to identify an appropriate cut off to distinguish bacteria positive and negative for the marker. This threshold was then used to compute the number of positive bacteria and thus the percentage of bacteria positive for the marker.

Live cell image analysis

To quantify Lysotracker association, bacteria of interest were duplicated from the field of view and a mask of the bacteria and a ring of pixels around the bacteria was generated. To do this the bacteria containing channel was thresholded using a manually determined range and a single ‘Dilate’ command applied to expand the mask by 1 pixel in Fiji Is Just Image (v1.53c). This mask was then used to measure the mean fluorescence intensity of pixels in the green (Lysotracker) channel in the area defined by the mask using ‘Measure’ as previously reported (Schnettger and Gutierrez, 2017).

2.5 Molecular Biology

SDS-PAGE and Western blot

Cells were lysed in RIPA buffer (Millipore #20-188) containing protease and phosphatase inhibitor cocktail (ThermoFisher Scientific #78445) for 10 min on ice. LDS sample buffer (ThermoFisher Scientific #NP008) and NuPage Sample Reducing Agent (ThermoFisher Scientific #NP009) were added and samples boiled at 95°C for 20 min if infected with Mtb, otherwise 10 min. Samples were loaded into 4-12% Bis-Tris SDS-PAGE gels (ThermoFisher Scientific #WG1403BOX, #NP0322BOX, #NP0321BOX) at 200 V for 35 min. Proteins were transferred to PVDF membranes (ThermoFisher Scientific #IB24002, #IB24001) on an iBlot2 (ThermoFisher Scientific #IB21001) using program P0. Membranes were blocked in 5% skimmed milk (VWR B008KK2DMK) in PBS + 0.01% Tween 20 (PBS-T) for 1 h at room temperature with shaking. Primary antibodies, diluted in blocking buffer as indicated in **Table 2.5.1**, were incubated with membranes overnight at 4°C with shaking. Blots were washed three times in PBS-T and incubated with HRP-conjugated secondary antibodies for 1 h at room temperature. Blots were developed with ECL (Millipore, WBULF0500) and imaged on a GE Amersham Imager 680 (GE Healthcare, U.K.). Molecular weight ladder (Abcam, #116028).

Antibody	Dilution	Supplier	Catalogue Number
LC3B	1:1000	Abcam	ab48394
p62	1:1000	Cell Signaling Technology	#5114
Atg7	1:1000	Cell Signaling Technology	#8558
Atg14	1:1000	Cell Signaling Technology	#5504S
IDO	1:1000	Cell Signaling Technology	#12006
iNOS	1:250	Novus Biologicals	NBP1-67618
Ubiquitin	1:1000	Cell Signaling Technology	#3936
β-actin-HRP	1:5000	Cell Signaling Technology	#12262
Anti-rabbit HRP	1:10000	Promega	W4011
Anti-mouse HRP	1:10000	Promega	W4021

Table 2.5.1 Antibodies used for Western blotting.

Analysis of autophagic flux by Western blot

iPSC or iPSDM were seeded into 6 well or 12 well plates respectively and iPSC allowed to grow to confluency. Cells were washed twice with PBS then incubated for 2 h in full medium or starved of amino acids with Hanks Balanced Salt Solution (HBSS, ThermoFisher Scientific #14170088) with or without 100 nM Bafilomycin A1 (Merck B1793-10UG) or 50 µM monensin (Sigma Aldrich M5273-5G) as detailed in figure legends. Samples were processed for SDS-PAGE and Western blot as described above.

Flow cytometry

Cells were stimulated with 20 ng/ml IFN-γ (Peprotech #300-02) + 500 ng/ml LPS (Sigma-Aldrich #) overnight. Cells were collected and incubated in PBS/0.1% BSA + 5 µl FC block per million cells for 20 min. 50 µl of cells were then incubated with 50 µl antibody cocktail diluted in PBS/0.1% BSA for 20 min on ice in the dark. Cells were washed in 2 ml PBS and fixed in 2% PFA prior to analysis. Cells were analysed on an LSRII flow cytometer (Becton, Dickinson and Company (BD), USA). Antibodies were purchased from BD and are detailed in **Table 2.5.2**. Flow cytometry data was analysed and plotted in FlowJo (BD, USA).

Antibody	Clone	Volume used (µl)	Catalogue Number
CD14-Alexa647	MΦP9	5	562690
CD119-PE	GIR-208	5	558934
CD86-BV421	2331	5	562433
CD11b-APC	ICRF44	20	561015
CD163-FITC	GHI/61	5	563697
CD169-PE	7-239	5	565248
CD206-BV421	19.2	5	564062
IgG1κ-PE	-	20	554680
IgG1κ-FITC	-	5	554679
IgG1κ-APC	-	20	555751
IgG1κ-BV421	-	5	562438
IgG2bκ-Alexa647	-	5	557903

Table 2.5.2 Antibodies used for Flow Cytometry.

Cytokine measurement

200 µl of supernatant from infected cells in a 96 well plate was collected and filtered twice through 0.2 µm PVDF membranes and stored at -80°C. Cytokine levels were analysed using a 20plex human inflammation panel from Invitrogen (EPX200-12185-901) according to the manufacturer's instructions. Samples were analysed on a Bio-Plex 200 (BioRad).

Plasmid cloning and purification

Human LGALS8 was sub-cloned from pET-Galectin-8 FL (Addgene #68805) into pmRFP-C1 (Clontech) or pEGFP-C1 (Clontech) using BglII (ThermoFisher Scientific #FD0083) and KpnI (ThermoFisher Scientific #FD0524). All plasmids were transformed into TOP10 chemically competent *E.coli* (ThermoFisher Scientific

#C404010) and cultured in LB with appropriate antibiotic. Plasmids were purified by miniprep (Qiagen #27104).

Nitric oxide detection

200 µl of supernatant was collected from iPSDM treated with 500 ng/ml LPS, 20 ng/ml IFN-γ or both in combination overnight in 96 well plates. Samples were then analysed for levels of nitrite and nitrate using Nitric Oxide Assay Kit (ThermoFisher Scientific EMSNO) following the manufacturer's instructions.

RNA-seq gene expression analysis of iPSDM infected with Mtb

RNA-sequencing sample preparation

$1x10^6$ EIKA2 iPSDM were seeded in 6 well plates and infected at an MOI of 2 for 2 h. Extracellular bacteria were removed with 2 PBS washes and cells were then incubated in macrophage media for 2 h or 48 h. At the respective time point samples were incubated in 1 ml TriZol (ThermoFisher Scientific #15596026) at room temperature for 5 min. Samples were stored at -80°C until ready for library preparation. 3 biological replicates were performed.

RNA-seq library preparation

RNA libraries were constructed using TruSeq Stranded Total RNA Library Prep Gold kit (Illumina #20020596) where ribosomal and mitochondrial RNA were depleted by RiboZero beads according to manufacturer's protocol. The final libraries were assessed using TapeStation 2200 System (Agilent). All libraries were sequenced on an Illumina Hi-Seq 4000 instrument with SR75 reactions.

RNA-seq data analysis

The quality of the sequencing fastq files was analysed using FastQC (v0.11.5) and low-quality samples were excluded from further differential gene expression analysis. Sequence reads were adapter- and quality- trimmed using Trimmomatic (v0.36) before aligning to the human genome (Ensembl GRCh38 build 88) using STAR aligner (v2.5.2a). Gene expression was quantified using RSEM (v.1.2.29) and differential gene expression analysis was performed using DESeq2 (v1.20.0) with default parameters. DESeq2 uses a generalized linear model to estimate log2 fold

change (log2FC) between comparison groups and the Benjamini-Hochberg false discovery rate was applied for multiple testing corrections, resulting in an adjusted p-value (padj) for each gene per comparison. Functional canonical pathways and disease networks associated with the differentially expressed genes were identified using Ingenuity IPA (Qiagen) with a cut off of padj<0.01 for differentially expressed genes.

RNA-seq data availability

RNA-seq data is published in (Bernard et al., 2021) and has been deposited to the Gene Expression Omnibus with accession number GSE132283.

Graph plotting and statistical analysis

Violin plots were produced using RStudio (The R Project for Statistical Computing) and the ggplot2 package. All other graphs, including heatmaps, were produced in GraphPad Prism V9.0 (GraphPad Software LLC, USA). Statistical analyses, as detailed in figure legends, was carried out in GraphPad Prism V9.0. Figures were compiled using Adobe Illustrator 2020 V24.3 (Adobe Inc. USA).

3. Results

3.1 Set up and characterisation of human iPSDM as an in vitro model of Mtb infection

Given that the available human macrophage models for studying host-pathogen interactions, especially in the context of Mtb infection, were not suitable to answer the questions in the aims of this thesis, iPSDM were chosen as the model of choice for this work.

Their normal karyotype, ability to reflect primary human macrophage responses to immunological stimuli (Lin et al., 2016; Zhang et al., 2015; Alasoo et al., 2015) and amenability to CRISPR mediated genome engineering (Härtlova et al., 2018) provided an opportunity to explore as-yet unanswered questions. As this model was not established in the lab, nor had it been used to study the cell biology of Mtb infection before, it was important to characterise the differentiation status and cellular responses of iPSDM after Mtb infection.

Production and characterisation of iPSDM

Several published protocols were available for deriving macrophages from iPSCs (Lee et al., 2018), here a well characterised protocol that allowed long-term production of cells over approximately 4 months was followed. Initially, embryonic bodies were formed and then differentiated towards haematopoietic lineages through the use of BMP4, VEGF and SCF. Then, in flasks, haematopoietic cells were stimulated to differentiate and generate monocytes through the use of IL-3 and M-CSF (van Wilgenburg et al., 2013) as outlined in **Figure 3.1.1**. Although labour intensive, this system reproducibly yielded large volumes of pure macrophages for downstream experiments. The initial set up of the iPSDM model was performed in the EIKA2 hiPSC line, which is derived from a healthy white adult male between 45 and 49 years of age. This line had the whole genome sequence available, successfully differentiated to macrophages in other laboratories (Alasoo et al., 2018), and displayed a normal karyotype.

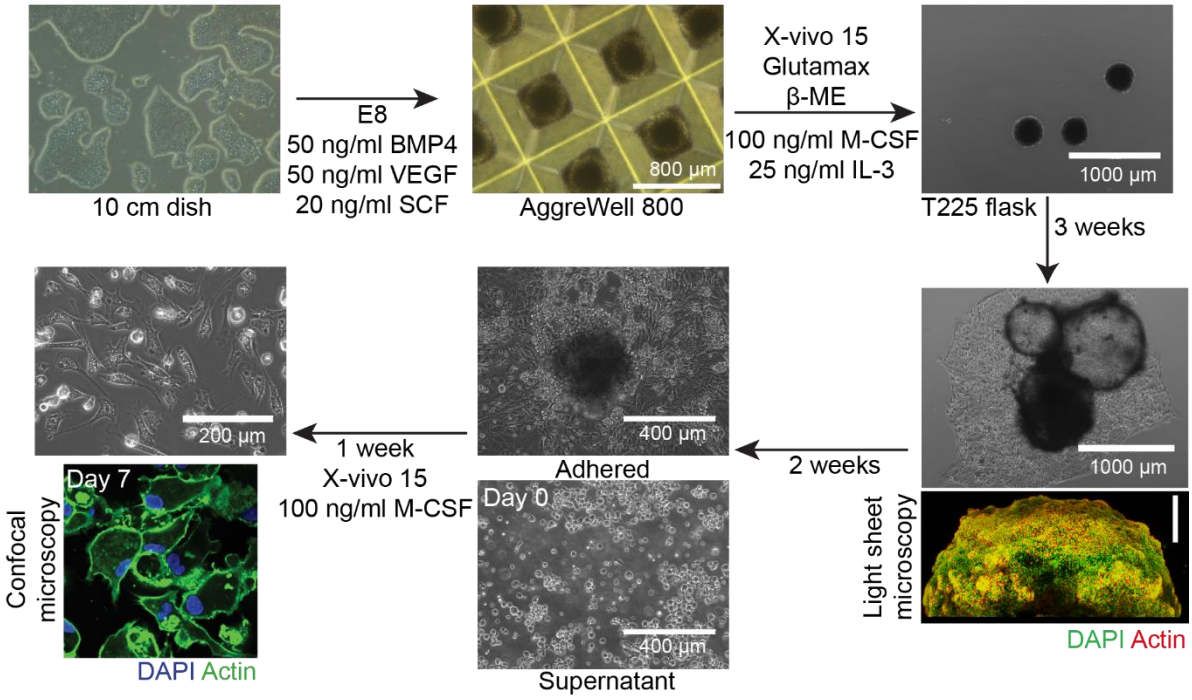

Figure 3.1.1 Differentiation of hiPSC to iPSDM. Human EIKA2 iPSC are cultured to confluency then seeded into AggreWell800 dishes to form embryonic bodies. Addition of BMP4, VEGF and SCF for 3 days begins the differentiation process before ~300 EBs are seeded into T225 cm^2 flasks for monocyte factory production. After 4-5 weeks monocytes appear in the supernatant, from which they can be harvested and terminally differentiated to macrophages with M-CSF. Following differentiation macrophages display dense cortical actin staining. Scale bar in light sheet micrograph 300 µm.

Flow cytometry analysis of the monocytes showed high levels of CD14 and moderate levels of CD11b surface expression along with low levels of CD86 and high levels of CD119 surface expression (**Figure 3.1.2A**). The phagocytic receptors CD169, CD163 and CD206 were all expressed to varying degrees on the surface of the monocytes (**Figure 3.1.2A**). Following 7 days of differentiation in M-CSF, the macrophages upregulated CD11b surface expression but showed little CD14 at the cell surface. The levels of CD86 surface expression remained moderate whilst CD119 was high; following classical LPS and IFN-γ stimulation the levels of CD86 increased and CD119 was undetectable. After differentiation, CD169 was the only one of the three phagocytic receptors examined detectable at the cell surface. Overall, this analysis was consistent with previous reports in human macrophages (Schulz et al., 2019). To complement this analysis, RNA-seq was performed and

reads for macrophage specific transcription factors and differentiation markers analysed. Reads mapping to macrophage specific transcription factors including *PPARG*, *RUNX3*, *ID2*, *ID3* and *MEF2C* (Lee et al., 2018) were detected. Moreover *RUNX1 was also detected* whereas *Myb* was not detectable by this method (**Figure 3.1.2B**), a finding that was consistent with previous reports that iPSDM production is RUNX1 dependent and Myb independent (Buchrieser et al., 2017). When compared to AmpliSeq data from hMDM and human alveolar macrophages (Papp et al., 2018), a broadly similar expression of transcription factors was observed (**Figure 3.1.2C&D**). Transcript analysis for common macrophage markers, including the surface markers in the flow cytometry analysis, revealed the expression of many common macrophage markers including *CD14*, *CD16*, *CD68*, *CD11b* and *CD119*. In contrast, reads mapping to stem cell markers, such as *CD34*, *Oct4* and *Nanog*, were not detected (**Figure 3.1.2E**).

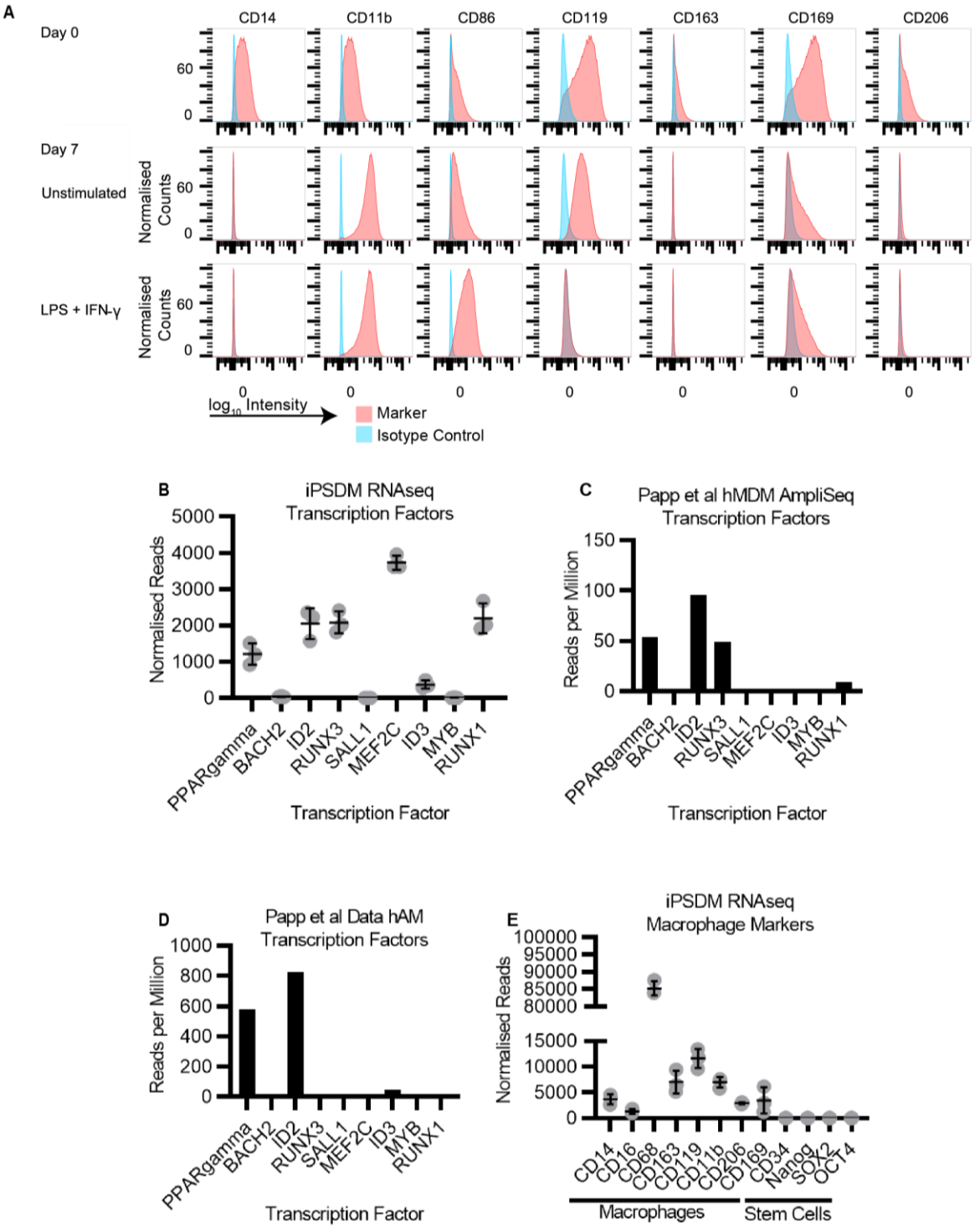

Figure 3.1.2 Human iPSDM express a range of macrophage markers. A. iPSDM were analysed by flow cytometry on day of harvest (Day 0) or after 7 days of differentiation in M-CSF for surface expression of several monocyte and macrophage markers. Macrophages were left unstimulated or activated overnight with 50 ng/ml LPS and 20 ng/ml IFN-γ prior to flow cytometry analysis as indicated. Data representative of 2 biological replicates. **B.** RNA-seq data from 2 h uninfected iPSDM

was examined for reads mapping to macrophage specific transcription factors. Data are mean ± SD from 3 biological replicates. Each point represents an independent biological replicate. **C & D.** AmpliSeq data from hMDM (**C**) and human alveolar macrophages (hAM) (**D**) in Papp et al. 2018 was analysed for reads mapping to the same transcription factors as in **B**. **E.** RNA-seq data from 2 h uninfected iPSDM was examined for reads mapping to common macrophage and stem cell markers. Data are mean ± SD from 3 biological replicates. Each point represents an independent biological replicate.

At the functional level, iPSDM were observed to have classical phagocytic and macropinocytic features when infected with Mtb and examined by scanning electron microscopy (SEM) (**Figure 3.1.3A**). In response to LPS and IFN-γ treatment, iPSDM expressed both indoleamine-2,3-dioxygenase (IDO) and inducible nitric oxide synthase (iNOS), however it was not possible to detect nitric oxide in the cell culture supernatant (**Figure 3.1.3B&C**), as has previously been reported in THP-1 and human alveolar macrophages (Roshick et al., 2006; Gross et al., 2014).

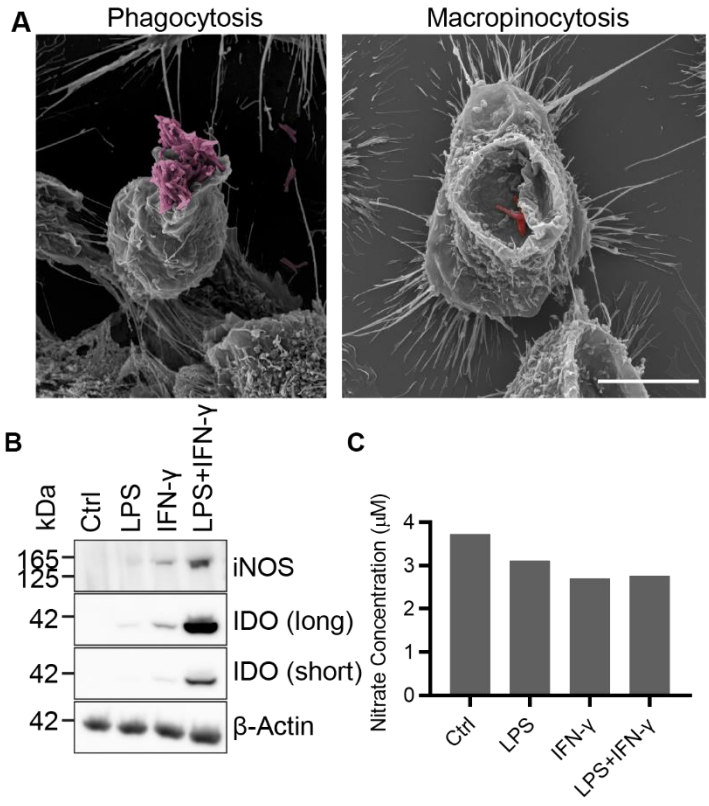

Figure 3.1.3 Human iPSDM are phagocytic and express iNOS and IDO in response to LPS and IFN-γ treatment. A. iPSDM were incubated with Mtb WT at an MOI of 10 for 20 min before being examined by SEM. Representative images of phagocytosis and micropinocytosis-like events are shown. Scale bar 5 μm. **B & C.** iPSDM were treated overnight with 50 ng/ml LPS, 20 ng/ml IFN-γ or both before Western blotting for IDO and iNOS (**B**) or analysing the concentration of nitrates in the cell culture supernatant (**C**). Data representative of 1 biological replicate.

Response of iPSDM after infection with Mtb

After infection of iPSDM with Mtb stably expressing the fluorophore E2Crimson (E2Crimson-Mtb), confocal microscopy showed Mtb was intracellular between 2 h and 72 h of infection, indicating that iPSDM were able to phagocytose Mtb. After 72 h of infection, Mtb WT replicated approximately 4-fold when compared to the uptake, while the attenuated mutant Mtb ΔRD1 only replicated 2-fold (**Figure 3.1.4**). When infected cells were incubated with exogenous IFN-γ for the course of the infection there was no difference observed in the replication of Mtb WT or Mtb ΔRD1, as was recently reported in iPSDM (Nenasheva et al., 2020) and has been previously reported in hMDMs (Lerner et al., 2017). Whether the observed replication defects

could be rescued through complementation with the RD1 region could not be confirmed due to technical limitations with the Mtb ΔRD1 complemented strain.

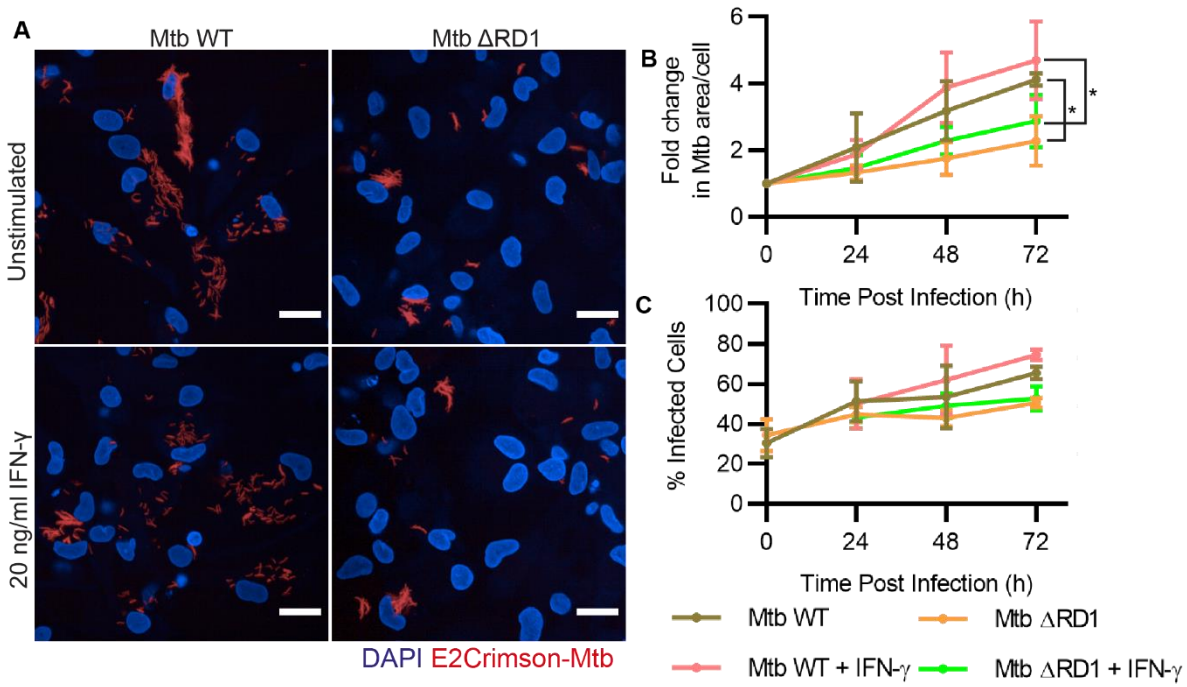

Figure 3.1.4 Mtb WT replicates efficiently in iPSDM. iPSDM were infected with E2Crimson expressing Mtb WT or Mtb ΔRD1 at an MOI of 1 and incubated with media with or without 20 ng/ml IFN-γ throughout the infection period. Cells were fixed at indicated time points and imaged on an Opera Phenix microscope. **A.** Representative confocal micrographs of iPSDM after 72 h of infection. Scale bar 10 µm **B.** Fold change in mean Mtb area per infected cell over time from 3 biological replicates each with 3 technical replicates. Data are mean ± SD. Data analysed by one way ANOVA with Holm-Sidak's multiple comparisons test, * $p<0.05$. **C.** Change in % of infected cells over time for each strain and stimulation from the same experiments plotted in **B**. Data are mean ± SD of 3 biological replicates.

At the subcellular level, both Mtb WT and Mtb ΔRD1 were observed to reside within membrane bound compartments that were positive for the late endosomal marker LAMP-1 (**Figure 3.1.5C-D**). In contrast, no colocalisation with the early endosomal marker EEA1 was observed (**Figure 3.1.5 A-B**). In agreement with these localisation studies and consistent with previous reports of cytosolic access by Mtb in human cells (van der Wel et al., 2007; Lerner et al., 2017), Mtb WT localised to the cytosol of iPSDM as early as 2 h post infection and by 48 h the majority of Mtb WT was

cytosolic (**Figure 3.1.5E&F**). In contrast, Mtb ΔRD1 was found within single membranes up to 48 h post infection (**Figure 3.1.5F**).

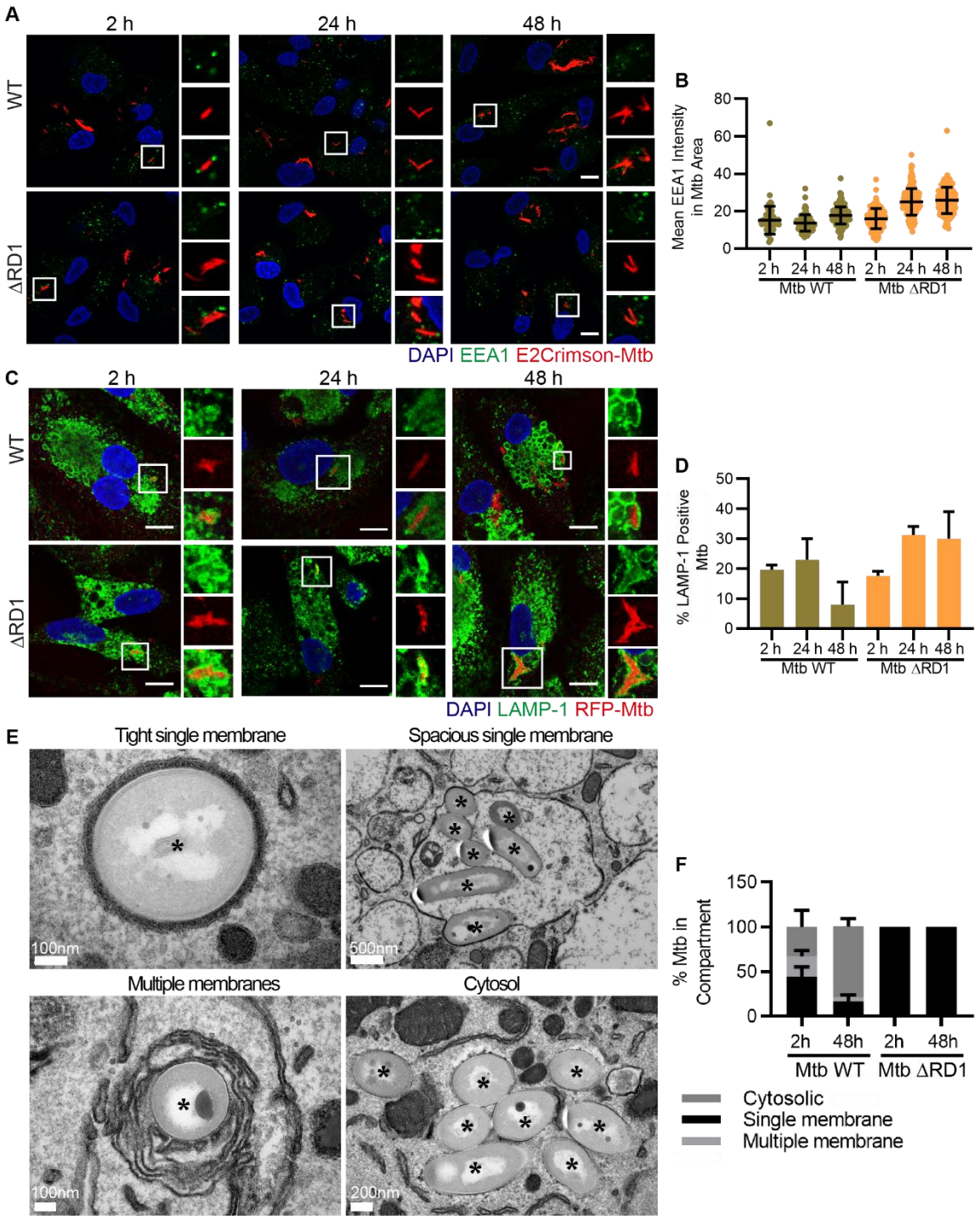

Figure 3.1.5 Mtb localises to heterogeneous subcellular environments in iPSDM. A&C. iPSDM infected with fluorescently labelled Mtb WT or Mtb ΔRD1 at an MOI of 2 for 2 h, 24 h or 48 h were subjected to immunofluorescence for EEA1 (**A**) or LAMP1 (**C**). Scale bar 10 µm. Zooms of the areas

marked by white boxes are shown to the right of each main image. **B.** Quantification of the mean EEA1 intensity in each bacterial object. Data are mean ± SD from 1 biological replicate, representative of 3. **D.** Quantification of the percentage of LAMP1 positive bacteria from images represented in **C**. Data are mean ± SD of 2 biological replicates. **E.** Representative transmission electron micrographs of Mtb WT at 48 h post infection in iPSDM. Mtb bacilli are indicted by *. **F.** Stereological analysis of transmission electron micrographs represented in **E** to identify subcellular localisation of the bacteria. Data are mean ± SEM of 2 biological replicates. At least 49 infected cells were analysed for each condition.

The lysosomotropic dye Lysotracker (LTR) accumulates in endolysosomes where it is irreversibly protonated and is unable to cross the endolysosomal membrane. If there is a compromise in endomembrane integrity, LTR leaks out and thus can be used to monitor membrane integrity (Repnik et al., 2017; Schnettger et al., 2017). After infection of iPSDM with RFP-Mtb WT, distinct profiles of LTR association with mycobacteria were observed by live cell imaging. In some cases, LTR positive Mtb lost the fluorescent signal and this was not recovered during the duration of imaging (**Figure 3.1.6A&B**). On the other hand, in some cases Mtb transiently lost LTR straining followed by a re-accumulation and dissociation, suggesting rounds of damage, recapture and re-escape (**Figure 3.1.6C&D**). A proportion of the bacteria retained LTR signal throughout the imaging period (**Figure 3.1.6E&F**). LTR positive vacuoles appeared in the vicinity of, but not directly around, Mtb WT in some cells suggesting normal LTR accumulation in membrane bound compartments around the bacteria (**Figure 3.1.6G**).

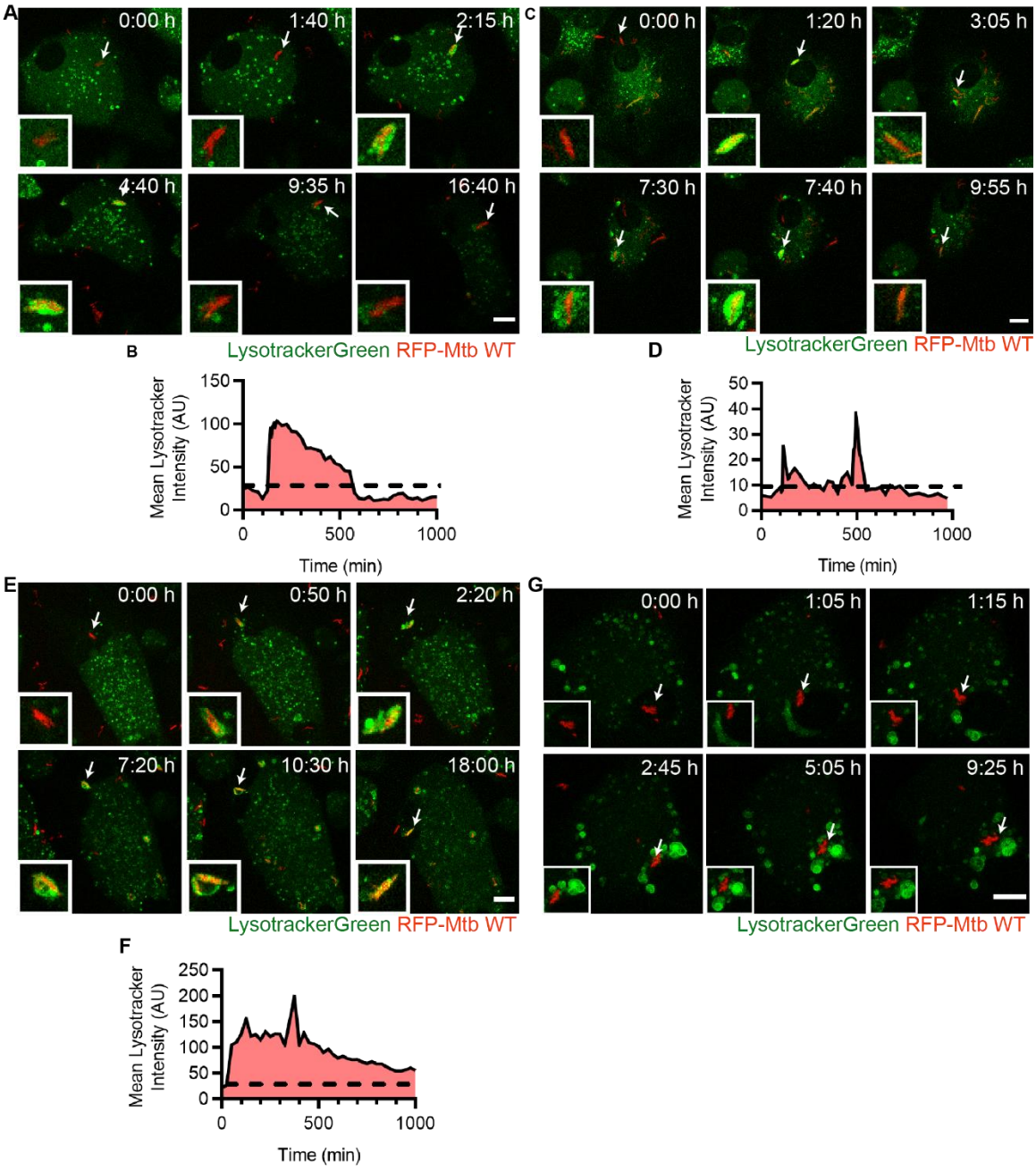

Figure 3.1.6 Mtb can fluctuate between Lysotracker positive and negative compartments. iPSDM stained with Lysotracker Green DND-26 were infected with RFP-Mtb WT at an MOI of 2 and imaged live with frames every 5 min for 24 h. **A, C, E & G.** Stills presented as maximum projections with linear adjustments made to brightness and contrast. Scale bar 10 µm. Arrows indicate the bacterium to follow, insets show a zoom of this bacterium at each time point. **A.** Mtb WT is able to damage the phagosomal membrane, leading to a loss of Lysotracker Green staining that does not recover. **B.** Quantification of Lysotracker association to the bacterium indicated in panel **A**. dashed line indicates cut off for bacteria to be considered Lysotracker negative. **C.** Mtb WT goes through

multiple rounds of cytosolic access, recapture and acidification and further membrane damage. **D.** Quantification of Lysotracker association to the bacterium indicated in panel **C**. **E.** Mtb WT localises to Lysotracker positive compartments for several hours. **F.** Quantification of Lysotracker association to the bacterium indicated in panel **E**. **G.** Mtb WT induced the formation of large Lysotracker positive vacuoles.

RNA-seq analysis of the iPSDM response to Mtb infection

The transcriptional response in the blood of TB patients has been widely studied and revealed a predominant Type I IFN signature during active disease (Berry et al., 2010; Singhania et al., 2018). *In vitro* transcriptomic analysis has been performed in murine and human macrophages infected with Mtb WT (Andreu et al., 2017; Thuong et al., 2008; Papp et al., 2018), and some studies have compared responses to Mtb WT and attenuated mutants such as H37Ra (Silver et al., 2009; Blischak et al., 2015). However, a detailed comparison between infection of macrophages with Mtb WT and the attenuated mutant Mtb ΔRD1, which lacks a functional ESX-1 secretion system, were not available. This comparison can help to identify host transcriptional responses linked to RD1 dependent process, such as membrane damage and cytosolic access. To define the response, iPSDM were infected with Mtb WT or Mtb ΔRD1 for 2 h or 48 h and analysed by bulk host RNA-seq. The 2 h time point was chosen to probe early changes when the bacterial burden was similar (**Figure 3.1.4**), but RD1 dependent differences, such as subcellular localisation (**Figure 3.1.5**), have begun to emerge. The 48 h time point was chosen to reflect changes as a result of the growth and manipulation of the macrophages by Mtb WT, whilst Mtb ΔRD1 has only undergone minimal replication.

At 2 h post infection, both Mtb WT and Mtb ΔRD1 infected iPSDM showed differential expression of circa 5000 genes compared to uninfected controls. However, there were no significant differences in gene expression when Mtb WT and Mtb ΔRD1 infected cells were compared (**Figure 3.1.7**). By 48 h, the response of iPSDM to Mtb WT increased with circa 9000 differentially expressed genes (DEG) whereas the response to Mtb ΔRD1 infection decreased to 800 DEGs (**Figure 3.1.7**). When comparing the Mtb ΔRD1 to Mtb WT infected iPSDM at 48 h, 8000 DEGs were found,

with the majority being expressed at lower levels in Mtb ΔRD1 infected macrophages (**Figure 3.1.7 and Figure 3.1.10A**).

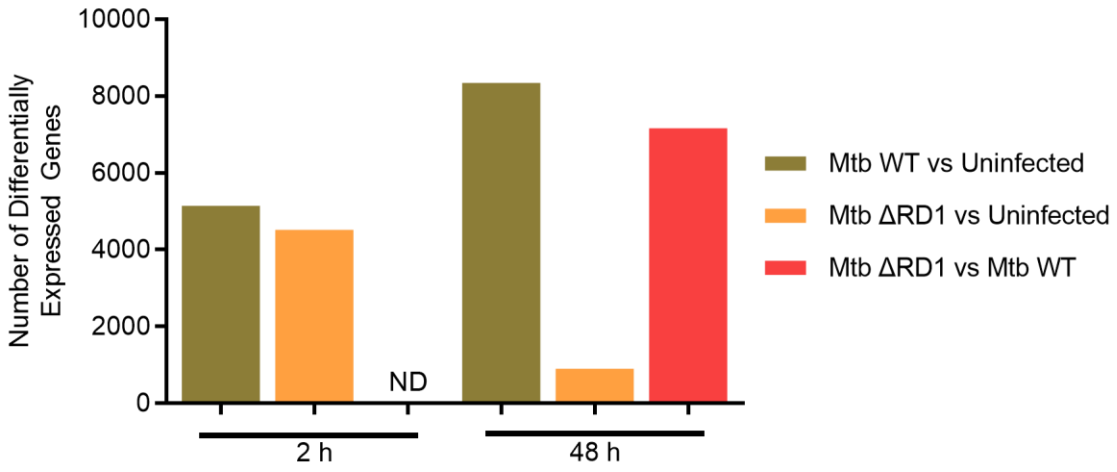

Figure 3.1.7 Mtb WT induces sustained changes in gene expression over the first 48 h of infection in iPSDM. EIKA2 iPSDM were infected with RFP-Mtb WT or Mtb ΔRD1 at an MOI of 2 for 2 h or 48 h before total RNA was isolated and analysed by RNA-seq. The number of differentially expressed genes for each infection condition and time point compared to uninfected controls or each other is presented. Data from 3 independent biological replicates. ND: none detected.

At 2 h post infection the most upregulated genes (defined by p value or fold change) were immune modulators and immune signalling genes known to have a function in defence against pathogens (**Figure 3.1.8A**). Transcripts for cytokines such as *TNFα*, *IL-6*, *IL-1α*, and *IL-1β* were highly upregulated in both Mtb WT and Mtb ΔRD1 infected iPSDM (**Figure 3.1.8A**). Other transcripts that were highly upregulated include those for proteins that serve to transduce and respond to the activation of pattern recognition receptors such as *IRAK2* and *PTX3* and molecules involved in inducing chemotaxis like *CCL4L2* and *CCL20* (**Figure 3.1.8A**). DEGs were analysed using Ingenuity Pathway Analysis (IPA) and this also reflected a major early response to infection being immunomodulatory. Signaling through the TNF receptors, TLRs, NF-κB and interferon signalling were amongst the most significantly upregulated pathways (**Figure 3.1.8B&C**). An interesting finding was the identification of actin nucleation by the ARP-WASP complex, suggesting changes in cell motility or potentially phagocytosis in response to infection (**Figure 3.1.8B&C**).

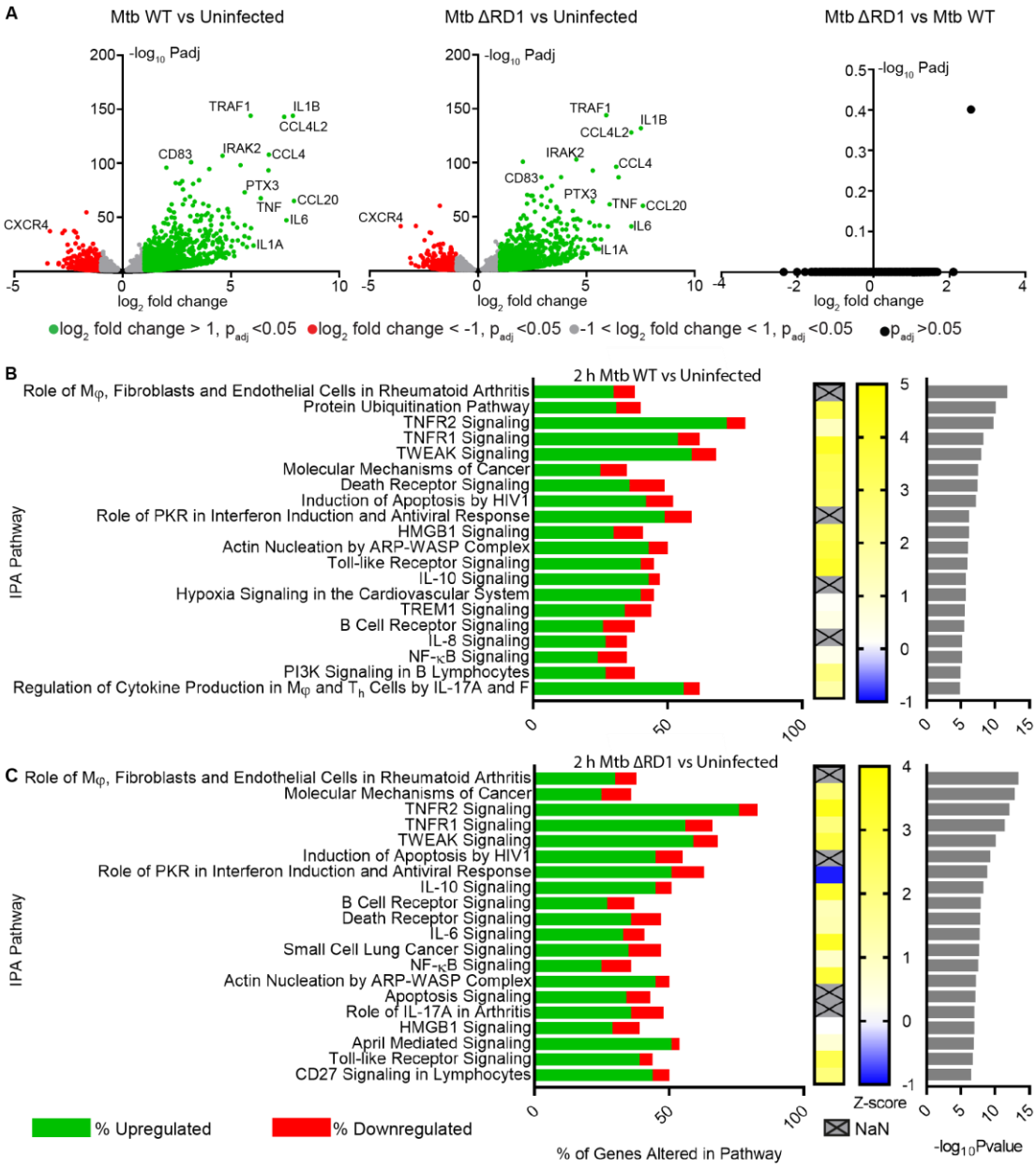

Figure 3.1.8 Mtb WT and Mtb ΔRD1 induce a similar transcriptional response in iPSDM at 2 h post infection. A. All detected genes from the 2 h time point of the RNA-seq study were plotted on volcano plots for each comparison made. Green points indicate upregulated genes with a fold change > 2, red spots down regulated genes with a fold change <-2, grey spots indicate differentially expressed genes with a fold change between -2 and 2, black spots indicate not significantly changed genes. **B&C.** Differentially expressed genes from the 2 h time point, with a cut off of $p < 0.01$, were analysed by IPA to identify common pathways that were altered in Mtb WT (**B**) or Mtb ΔRD1 (**C**) infected compared to uninfected cells. Left hand bar chart indicates the top 20 dysregulated pathways by P value with the percentage of upregulated genes in green and downregulated in red. Right hand

bar chart indicates the P value for each pathway. Heat map shows activation status of the pathway by Z score, grey boxes indicate an incomputable Z score.

At 48 h post infection, a strong immune activation signature was still present in the Mtb WT infected iPSDM with the most highly upregulated genes including *CCL4*, *CLEC4E*, *SEMA4A* and *NCF1* (**Figure 3.1.9A**). IPA analysis also showed highly activated pathways such as interferon signalling, antigen presentation and TREM1 signalling (**Figure 3.1.9B**). Additionally, the top dysregulated pathway in Mtb WT infected iPSDM at 48 h was EIF2 signalling, which was significantly downregulated implying disruption of mRNA translation (**Figure 3.1.9B**). Protein ubiquitination was significantly activated in the iPSDM infected with Mtb WT but not Mtb ΔRD1 (**Figure 3.1.9B**). In the Mtb ΔRD1 infected iPSDM at 48 h the transcriptional signature changed towards being more immunosuppressive with upregulation of genes such as *TIFAB*, *PLA2GD*, *RARRES2* and *LILRB2* (**Figure 3.1.9A**). Whilst IPA analysis revealed a degree of immune-related pathway activation, such as interferon signalling and antigen presentation, in these Mtb ΔRD1 infected iPSDM a metabolic reprogramming signature was also clear. Genes involved in lipid metabolism were upregulated with cholesterol biosynthesis and LXR/RXR activation both predicted to be activated by Z score (**Figure 3.1.9C**). Another significant signal was the priming of the adaptive immune response with antigen presentation, OX40 signalling and communication between innate and adaptive immune cells among the pathways that were upregulated in iPSDM infected with Mtb ΔRD1 at 48 h (**Figure 3.1.9C**).

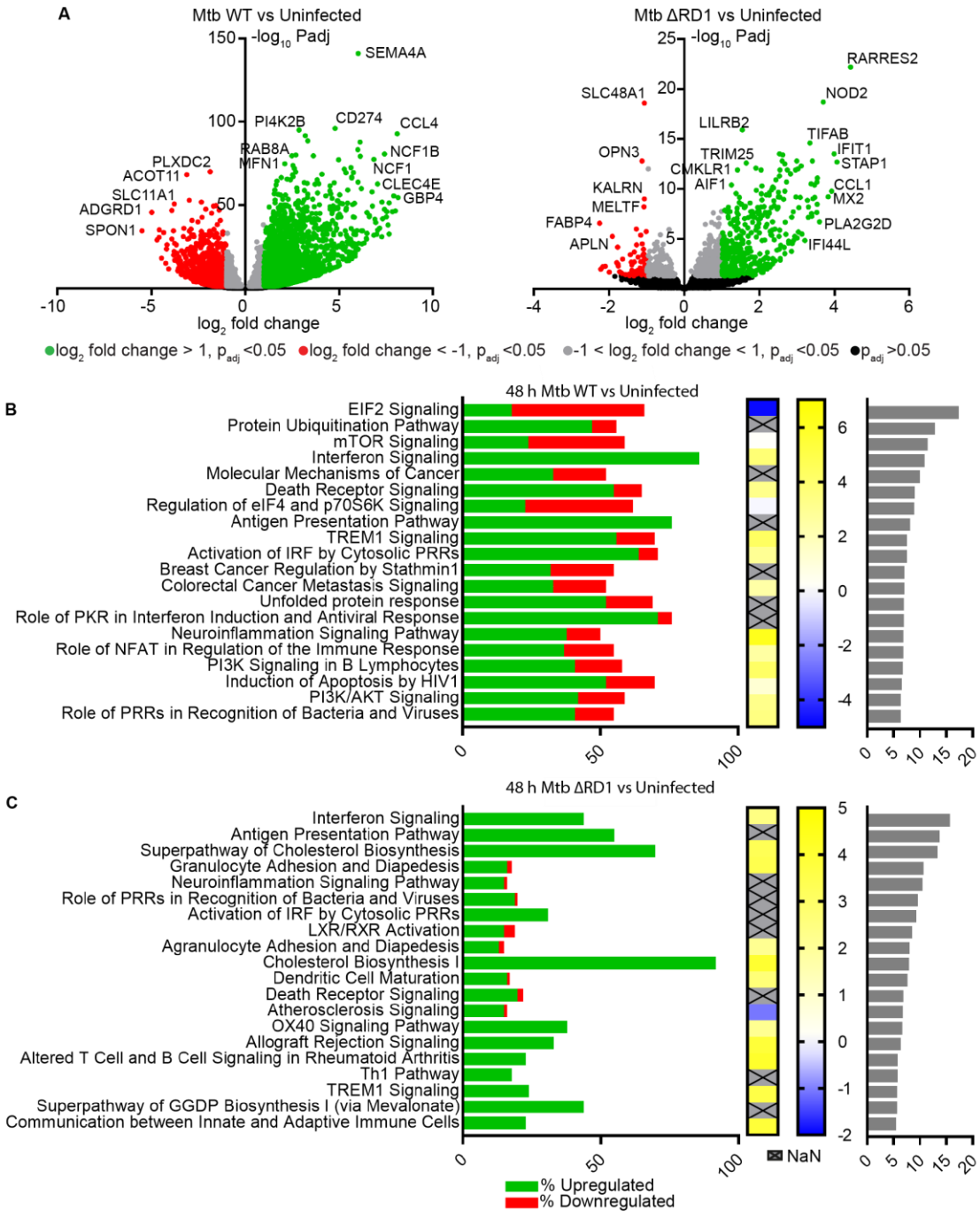

Figure 3.1.9 Mtb WT leads to sustained changes in gene expression over the first 48 h of infection whereas Mtb ΔRD1 infection leads to lower levels of transcriptional dysregulation. A. All detected genes from the 48 h time point of the RNA-seq study were plotted on volcano plots comparing each infection to the uninfected controls. Green points indicate upregulated genes with a fold change > 2, red spots down regulated genes with a fold change <-2, grey spots indicate differentially expressed genes with a fold change between -2 and 2, black spots indicate not significantly changed genes. **B&C.** Differentially expressed genes from the 48 h time point, with a cut

off of $p < 0.01$, were analysed by IPA to identify common pathways that were altered in Mtb WT (**B**) or Mtb ΔRD1 (**C**) infected vs uninfected cells. Left hand bar chart indicates the top 20 dysregulated pathways by P value with the percentage of upregulated genes in green and downregulated in red. Right hand bar chart indicates the P value for each pathway. Heat map shows activation status of the pathway by Z score, grey boxes indicate an incomputable Z score.

When comparing the transcriptional response of iPSDM infected with Mtb WT and Mtb ΔRD1 at 48 h the majority of dysregulated pathways were downregulated in Mtb ΔRD1 infected cells (**Figure 3.1.10B**). Many of these downregulated pathways were immune related, reflecting the lower degree of immune activation in macrophages infected with Mtb ΔRD1 **(Figure 3.1.10B**). Indeed, genes downregulated in macrophages infected with Mtb ΔRD1 were immunomodulatory such as *SEMA4A*, *CD274*, *IDO* and *CXCL11* (**Figure 3.1.10A**).

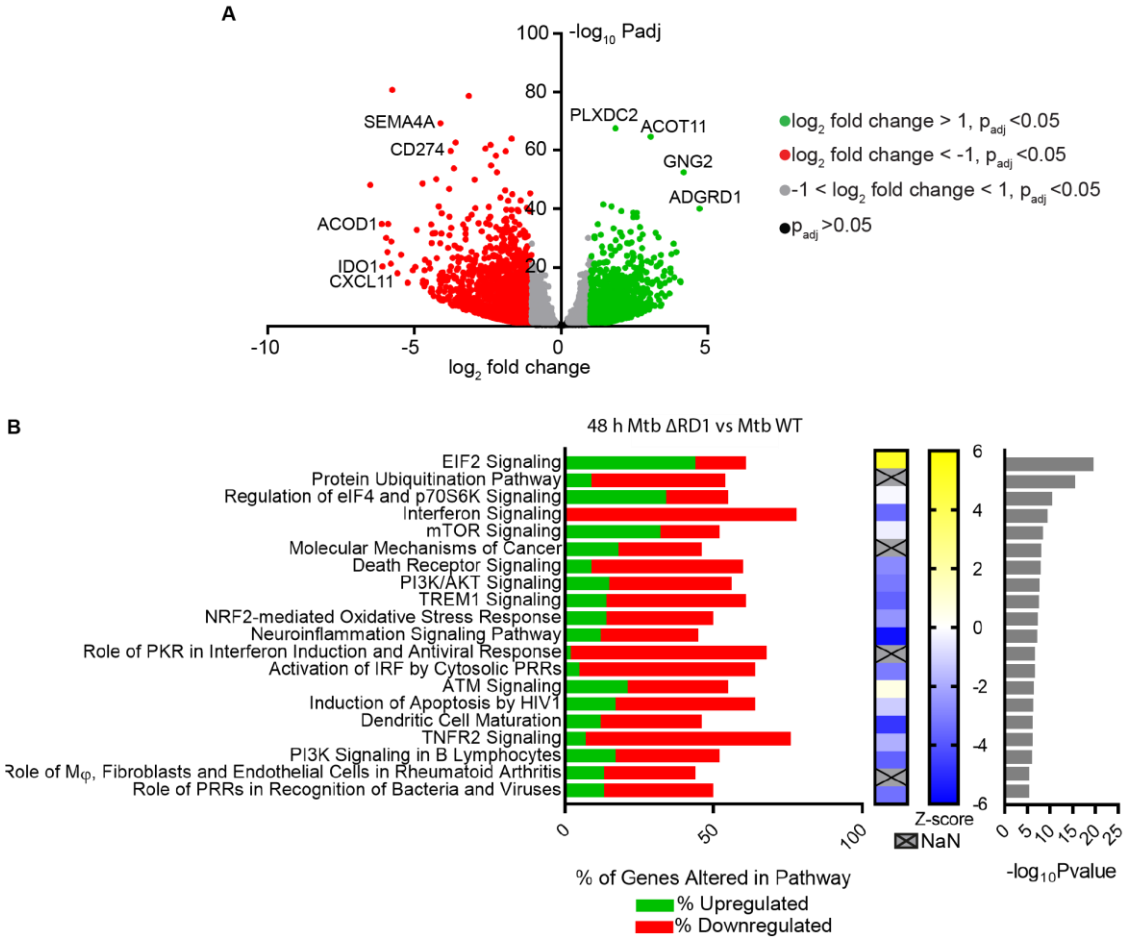

Figure 3.1.10 iPSDM infected with Mtb ΔRD1 at 48 h have lower expression of key immune defence genes and lower activation of immune defence pathways than Mtb WT infected macrophages. A. Volcano plot showing changes in all genes detected when comparing Mtb ΔRD1 to Mtb WT infected iPSDM at 48 h. Green points indicate upregulated genes with a fold change > 2, red spots down regulated genes with a fold change <-2, grey spots indicate differentially expressed genes with a fold change between -2 and 2, black spots indicate not significantly changed genes. **B.** Differentially expressed genes from the 48 h time point when comparing Mtb ΔRD1 and WT infected iPSDM, with a cut off of $p < 0.01$, were analysed by IPA to identify common pathways that were altered. Left hand bar chart indicates the top 20 dysregulated pathways by P value with the percentage of upregulated genes in green and downregulated in red. Right hand bar chart indicates the P value for each pathway. Heat map shows activation status of the pathway by Z score, grey boxes indicate an incomputable Z score.

Whilst many immune-related pathways remained activated in the Mtb ΔRD1 infected iPSDM at 48 h, the degree of activation was far lower than in the Mtb WT infected cells (**Figure 3.1.11A**). Furthermore, transcription of pro-inflammatory cytokine

encoding genes including *IFNA, IFNB, IL6, CCL2, CCL3, CCL4 and TNF* was robustly upregulated at 48 h in Mtb WT but not Mtb ΔRD1 infected iPSDM. This increased transcription was reflected in increased secretion of pro-inflammatory cytokines after infection with Mtb WT at 48 h (**Figure 3.1.11B**). The secretion of IFN-α, one of the type I IFNs, was entirely ESX-1 dependent (**Figure 3.1.11B**), as has been previously reported (Stanley et al., 2007). The secretion of other cytokines important in the immune response to TB *in vivo*, such as TNFα and IL-1α, was also upregulated in iPSDM infected with Mtb WT infected cells more than in Mtb ΔRD1 infected iPSDM, although this did not reach statistical significance. Overall, many of the cytokines were found at higher concentrations in supernatant from iPSDM infected with Mtb WT than Mtb ΔRD1, however this did not always reach statistical significance (**Figure 3.1.11B**).

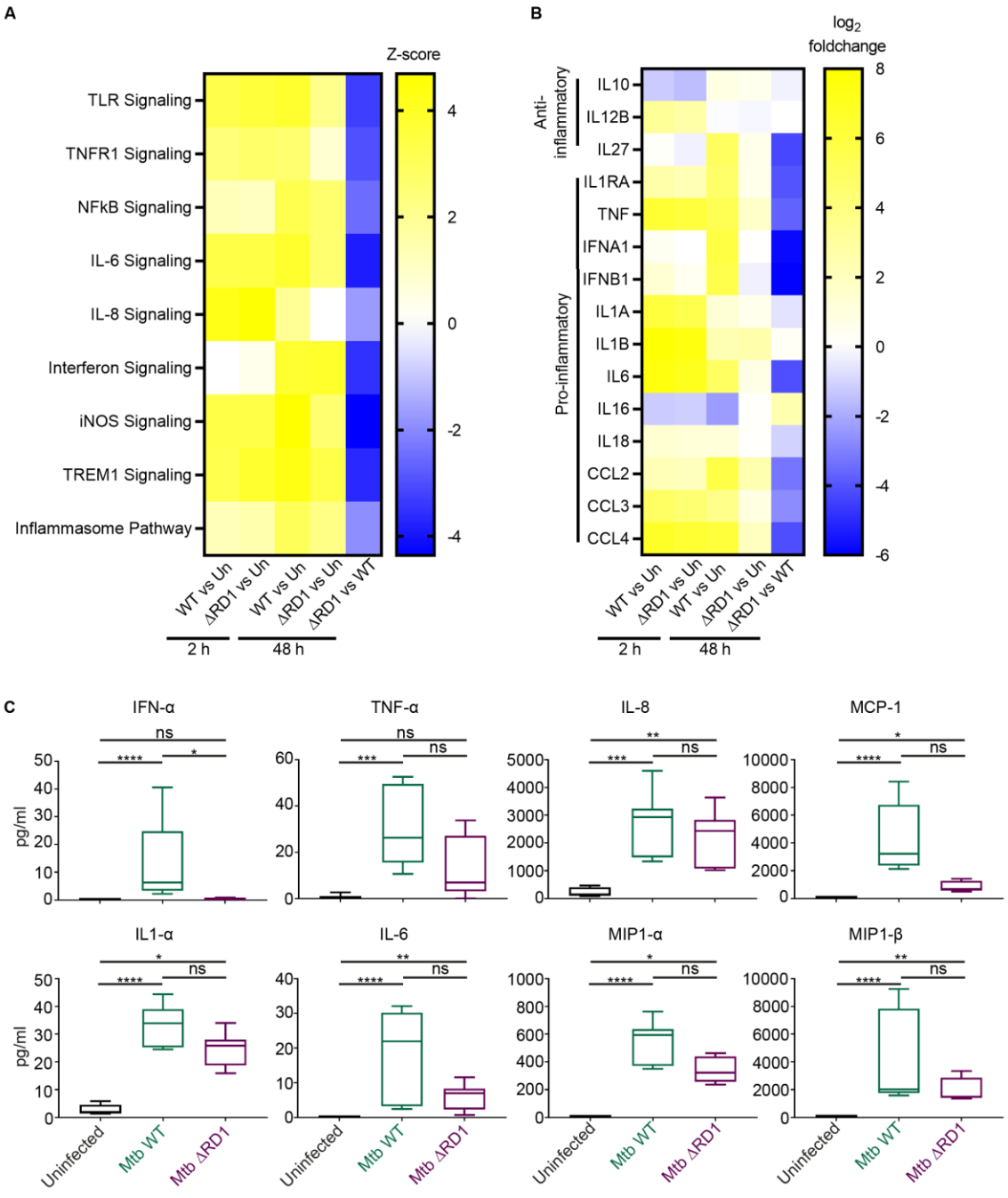

Figure 3.1.11 Mtb WT infection leads to a sustained immune defence response in iPSDM that is reduced in Mtb ΔRD1 infected cells. A. Heat map showing activation status, by Z score, of selected immune signalling pathways from IPA analysis of DEGs from the RNA-seq dataset for comparisons indicated. **B.** Heat map showing log_2foldchange for selected cytokines from the RNA-seq dataset for comparisons indicated. Un: uninfected. **C.** Supernatant from iPSDM infected with Mtb WT or Mtb ΔRD1 for 48 h at an MOI of 2 was analysed by Luminex for inflammatory cytokines shown. Data are medians from 3 biological replicates, each with 3 technical replicates with whiskers indicating

the maximum and minimum. Analysed by one way ANOVA and Dunn's multiple comparisons test ns not significant, * $p < 0.05$, ** $p < 0.01$, *** $p < 0.001$, **** $p < 0.0001$.

Genes in the protein ubiquitination pathway were upregulated in Mtb WT infected iPSDM at both 2 h and 48 h post infection (**Figure 3.1.12A**). These genes included ubiquitin itself as well as a range of E2 and E3 ligases (**Figure 3.1.12B**). The E2 UBE2QL1, which is required for efficient lysophagy (Koerver et al., 2019), and the E3 SMURF1, which conjugates polyubiquitin for xenophagy initiation during Mtb infection (Franco et al., 2016), were both upregulated. PRKN, which codes for the E3 ligase Parkin that also plays a role in xenophagy induction during Mtb infection (Manzanillo et al., 2013), was downregulated after 48 h of infection with Mtb WT. Western blot analysis showed that Mtb WT infected iPSDM at 48 h had an increased level of polyubiquitnated proteins whereas Mtb ΔRD1 infected cells showed no changes compared to uninfected controls (**Figure 3.1.12C**).

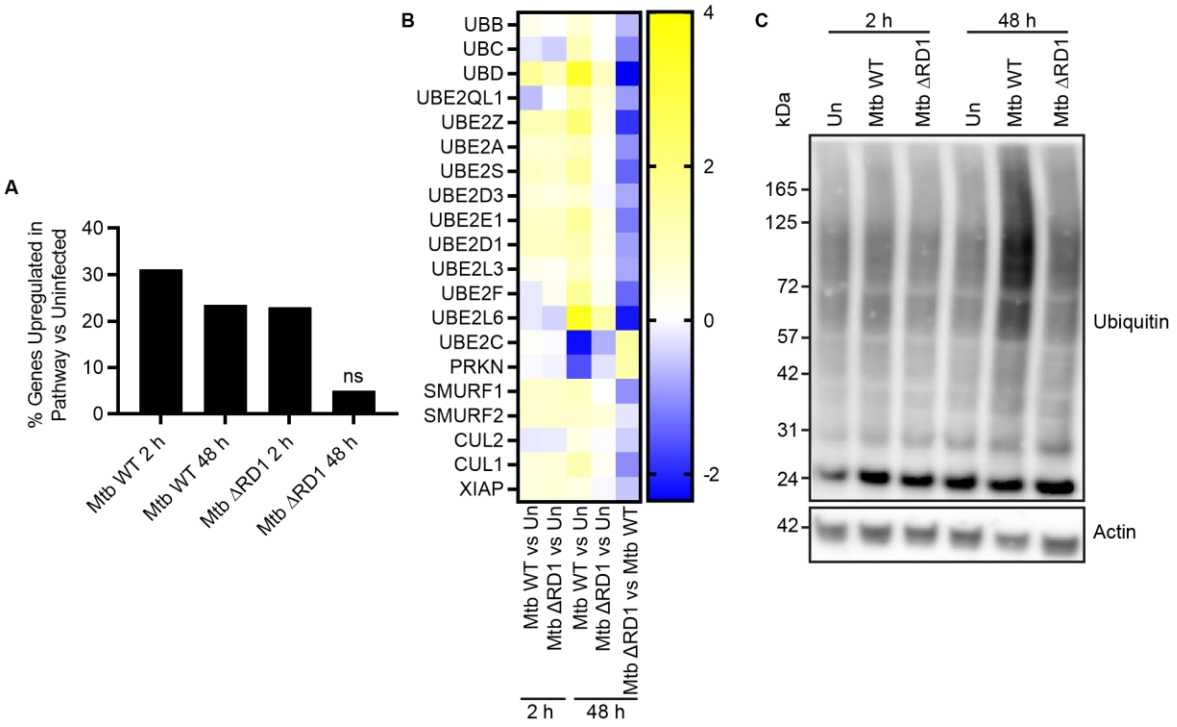

Figure 3.1.12 Mtb WT infection induces accumulation of polyubiquitnated proteins in iPSDM. **A.** Bar chart showing percentage of genes upregulated in the protein ubiquitination pathway when compared to uninfected controls. ns: not significant. **B.** Heat map showing selected genes from the ubiquitination pathway identified by RNA-seq showing log_2fold change in all comparisons made. **C.**

iPSDM were infected with RFP-Mtb WT or Mtb ΔRD1 at an MOI of 2 for 2 h or 48 h and subjected to Western blotting for ubiquitin. Image representative of 3 biological replicates. Un: uninfected.

In summary, the data presented in this chapter showed the establishment of protocols to reliably produce human macrophages from iPSCs that recapitulate many well-established interactions with Mtb reported with other *in vitro* systems. The RNA-seq analysis showed immunomodulatory changes in iPSDM infected with Mtb and highlighted important differences specifically triggered by the Mtb ESX-1 system. Changes in gene expression were initially common between Mtb WT and Mtb ΔRD1 infection but diverged by 48 h post infection with Mtb WT infected cells more strongly maintaining their immune activation status.

3.2 Mtb induces dynamic rearrangement of the autophagy machinery upon phagosome membrane damage

Many of the previous studies of autophagy during Mtb infection have used snapshot imaging to determine bacterial localisation over the course of hours at specific time points (Watson et al., 2012; Manzanillo et al., 2013; Gutierrez et al., 2004a). When beginning this work, there were no studies looking at the spatiotemporal dynamics of the process at high resolution in human macrophages. Moreover, it was yet to be established how, following membrane damage, Mtb was able to access the cytosol without being captured by the autophagy machinery. Thus, having established iPSDM as a relevant model for studying Mtb infection, this system was used to probe autophagic targeting of Mtb through correlative live cell imaging and electron microscopy approaches.

The dynamics of membrane damage during Mtb infection of iPSDM

Following phagocytic uptake, Mtb damages the phagosomal membrane, a process that exposes carbohydrates on the luminal surface (Thurston et al., 2012). This is recognised by Gal8 in both mouse macrophages and human lymphatic endothelial cells (Schnettger et al., 2017; Lerner et al., 2018). To validate that this also occurs in human macrophages, iPSDM were infected with Mtb WT or Mtb ΔRD1 and the distribution of endogenous Gal8 was analysed. Mtb WT colocalisation with Gal8 peaked at early time points post infection, with 10.3 ± 1.8% (mean ± SD) of Mtb positive at 2 h and this decreased over time with 5.2 ± 0.8% positive at 48 h (**Figure 3.2.1**). Whilst a small number of Mtb ΔRD1 colocalised with Gal8, 0.2 ± 0.3% at 2 h, this was to a much lower extent than Mtb WT.

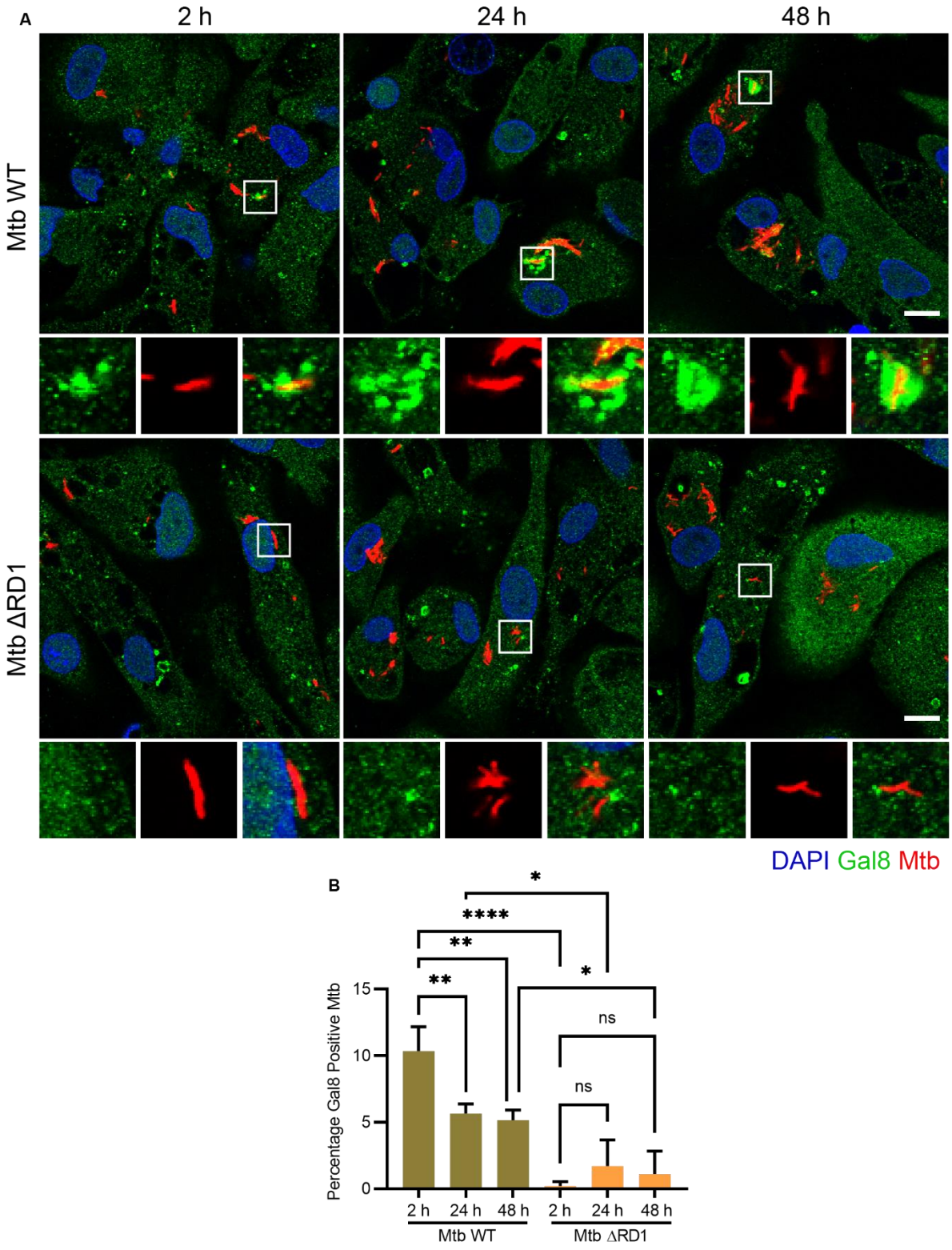

Figure 3.2.1 Mtb WT association with Gal8 is significantly higher than Mtb ΔRD1. iPSDM infected with E2Crimson Mtb WT or Mtb ΔRD1 at an MOI of 2 for 2 h, 24 h or 48 h were examined by

immunofluorescence for Gal8 recruitment. **A.** Representative confocal images of Gal8 recruitment to Mtb, representative of 3 biological replicates. Scale bar 10 µm. Zooms of regions highlighted in white squares are shown below each main image. **B.** Quantification of the percentage of Gal8 positive bacteria for each condition. Graph shows mean ± SD of 3 biological replicates. Data analysed by one way ANOVA and Holm-Sidak's multiple comparison test, ns not significant, * $p<0.05$, ** $p<0.01$, **** $p<0.0001$.

As observed previously in hMDMs, THP-1 and dendritic cells (Lerner et al., 2017; Simeone et al., 2012; van der Wel et al., 2007), Mtb WT was able to localise to the cytosol of iPSDM (**Figure 3.1.5**); suggesting a failure of the autophagy machinery to capture Mtb as it ruptures the phagosomal membrane. In order to test this hypothesis, iPSDM transiently expressing EGFP-Gal8 were infected with mCherry Mtb WT and analysed by live cell imaging to explore the dynamics of membrane damage during Mtb infection. Following phagocytosis, Mtb WT was rapidly recognised by EGFP-Gal8 (**Figure 3.2.2A**) and over the course of several hours EGFP-Gal8 dissociated, forming distinct vesicles (**Figure 3.2.2A**). When examined by electron microscopy the bacteria that dissociated from Gal8 (Bacteria 2) localised in the cytosol (**Figure 3.2.2A&B**). Bacteria that had not associated with Gal8 (Bacteria 3) were localised within a single membrane bound compartment (**Figure 3.2.2A&C**). These observations are consistent with Gal8 recognising damaged phagosomes, suggesting Mtb is able to shed the damaged membranes to access the macrophage cytosol.

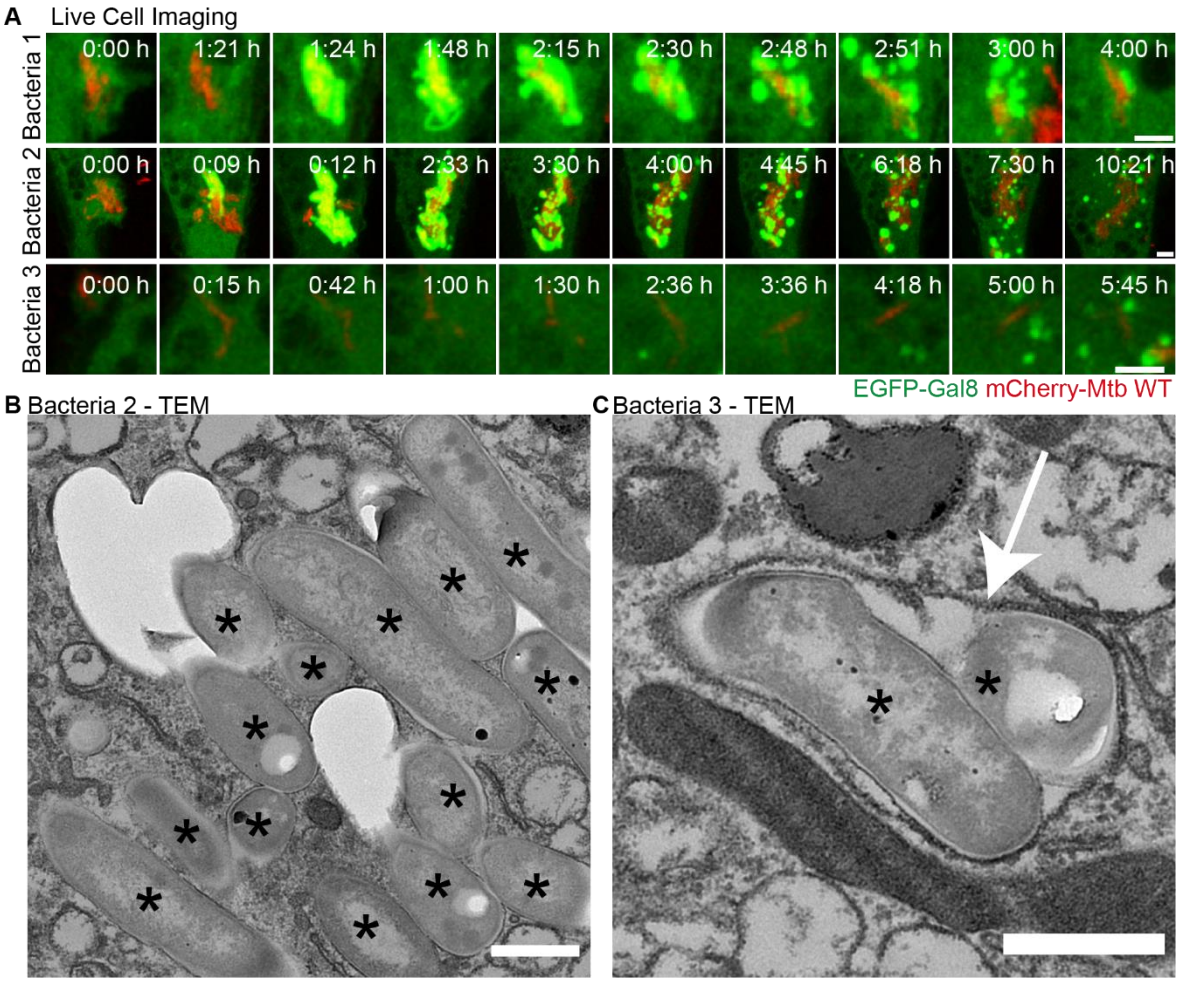

Figure 3.2.2 Mtb WT accesses the cytosol following membrane damage in iPSDM. iPSDM expressing EGFP-Gal8 were infected with mCherry-Mtb WT at an MOI of 2 and imaged live with frames every 3 min. **A.** Maximum projection stills from live cell imaging of 3 different bacteria in one cell, time 0 represents the phagocytosis event for each bacterium. Images processed by Gaussian blur of radius 1. Scale bar 3 µm. Images representative of 2 biological replicates. **B & C.** TEM images of bacterium 2 (**B**) and bacterium 3 (**C**) from panel **A**. Scale bar 500 nm. * indicates Mtb. Arrow indicates phagosomal membrane.

Mtb impairs autophagic flux at 24 h and 48 h post infection in iPSDM

Previous reports indicated that Mtb efficiently blocks autophagic flux in human macrophages (Chandra et al., 2015; Romagnoli et al., 2012). Western blotting for the autophagy markers LC3B and p62 in iPSDM infected with Mtb WT or Mtb ΔRD1 revealed no changes at 2 h post infection. In contrast, at 24 h and 48 h post infection, LC3-II and p62 accumulated in iPSDM infected with Mtb WT but not with Mtb ΔRD1.

As expected, the accumulation of LC3B-II and p62 was further enhanced by BafA1 treatment but no more so than observed in uninfected controls suggesting the increase observed in Mtb WT infected iPSDM at 48 h was due to a blockade in autophagic flux rather than an induction of autophagosome biogenesis (**Figure 3.2.3**).

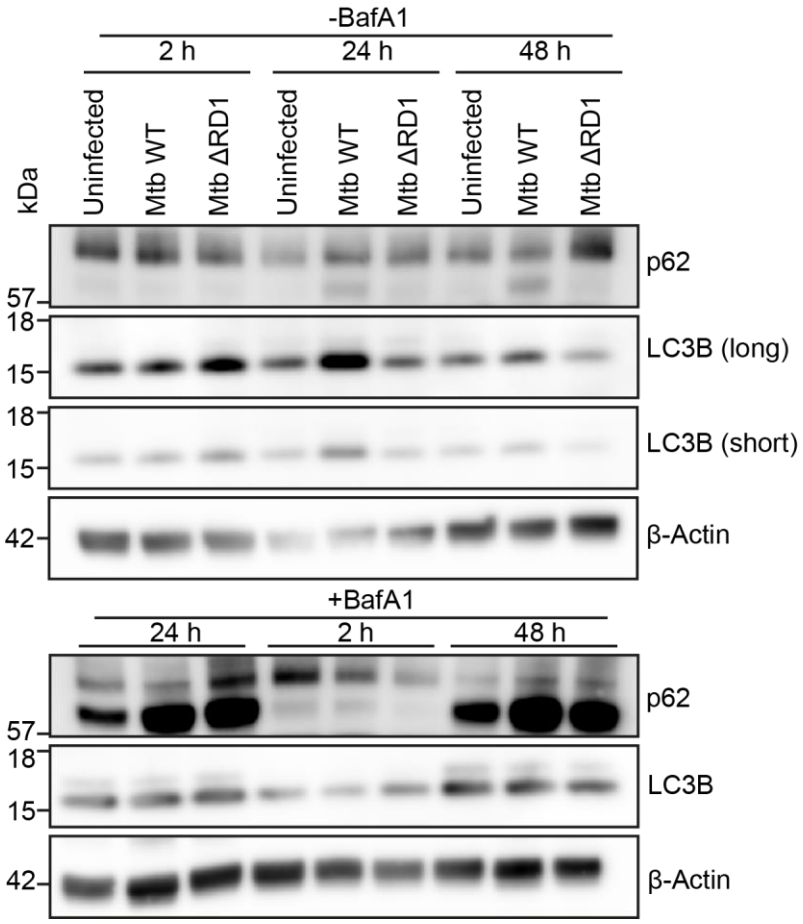

Figure 3.2.3 Mtb WT impairs autophagic flux in iPSDM. Protein extracts from iPSDM infected with Mtb WT or Mtb ΔRD1 at an MOI of 2 for 2 h, 24 h or 48 h in the absence or presence of 100 nM Bafilomycin A1 (BafA1) were subjected to Western blotting for autophagy markers p62 and LC3B. Blots representative of 3 biological replicates.

Mtb induces LC3B tubulovesicular structures in human macrophages

Given that Gal8 functions to recruit the autophagy machinery for xenophagic targeting (Thurston et al., 2012) but Mtb was able to shed EGFP-Gal8 positive membranes to enter the cytosol (**Figure 3.2.2**), the dynamics of the autophagy machinery during Mtb infection were examined in more detail. Live cell imaging of

iPSDM transiently expressing EGFP-LC3B and infected with Mtb WT revealed a striking, dynamic rearrangement of autophagosomes whereby EGFP-LC3B rapidly localised to large tubular and swollen autophagosomes several microns in size (**Figure 3.2.4A**) (Bernard et al., 2021). These autophagic structures were observed to persist for several hours (**Figure 3.2.4A**). Given the similarities between these structures and those observed during starvation and calcium phosphate precipitate induced autophagy and during Hepatitis B virus infection (Gao et al., 2010; Inoue et al., 2015), we name them LC3 tubulovesicular structures (LC3-TVS). Over time, it was observed that Mtb shed these LC3-TVS and dissociated from EGFP-LC3B. During this process, the vacuoles shrank and by end of the imaging period were no longer present in the macrophages (**Figure 3.2.4A**). In addition to the large EGFP-LC3B positive structures, thinner and more transient EGFP-LC3B positive tubules were observed to protrude from the LC3-TVS (4:45 h image in **Figure 3.2.4A**). The induction of autophagy and LC3-TVS was only observed in Mtb WT infected cells, those infected with Mtb ΔRD1 showed no changes in the autophagy machinery over the first 24 h of infection (**Figure 3.2.4B**). The scattered autophagosomes, visible as LC3B puncta, moved throughout the Mtb ΔRD1 infected macrophages as expected but did not clearly associate with the mycobacteria.

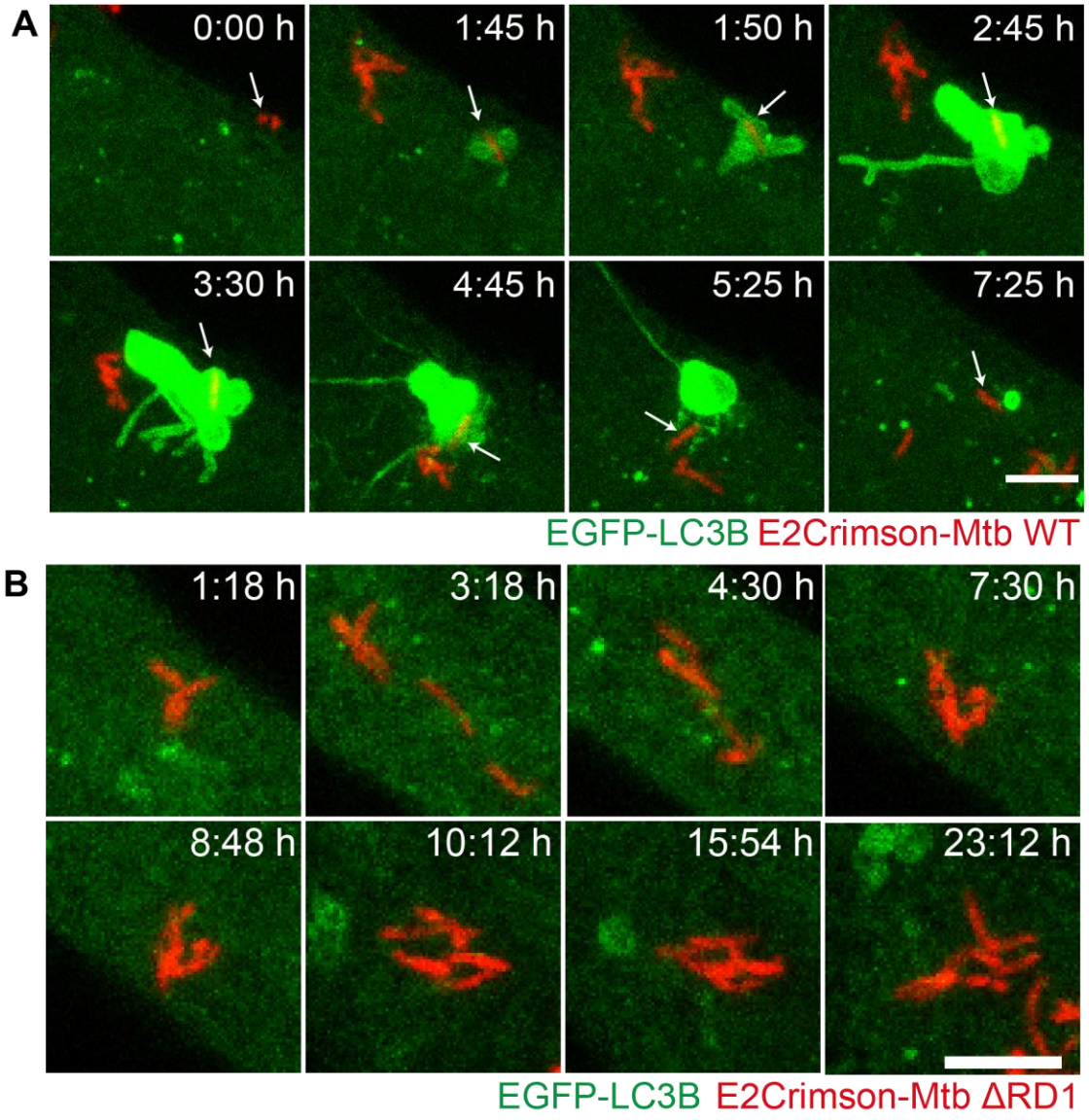

Figure 3.2.4 Mtb induces the formation of large, EGFP-LC3B positive vacuoles and tubules in an RD1 dependent manner. **A & B.** iPSDM expressing EGFP-LC3B were infected with E2Crimson-Mtb WT (**A**) or E2Crimson-Mtb ΔRD1 (**B**) at an MOI of 2 and imaged live with frames every 5 min for **A** and 3 min for **B**. Images are maximum projection stills, with time 0 being the frame of phagocytosis. Arrows in **A** indicate bacteria of interest. Scale bar 5 µm.

To define whether the observed EGFP-LC3B dynamics were caused by high levels of overexpression or the introduction of DNA into the macrophage cytosol, likely stimulating an induction of Type I IFN prior to infection, KOLF2 iPSDM stably expressing EGFP-hLC3B were infected with Mtb WT and examined by live cell imaging. Similar EGFP-LC3B dynamics to those observed in **Figure 3.2.4** were found, with transient production of LC3-TVS, which are lost over time (**Figure 3.2.5**).

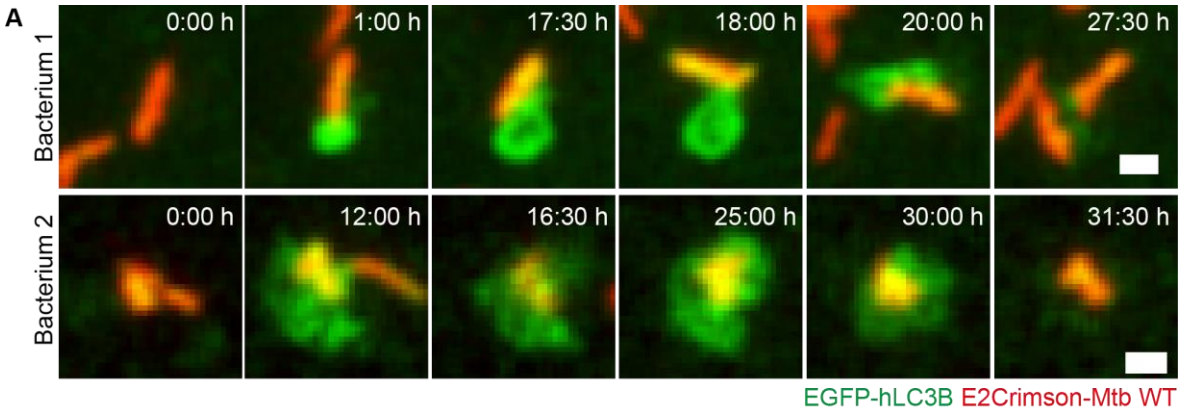

Figure 3.2.5 iPSDM stably expressing EGFP-hLC3B also show induction of large LC3B positive vacuoles during Mtb WT infection. KOLF2 iPSDM stably expressing EGFP-hLC3B were infected with E2Crimson-Mtb WT at an MOI of 1 and imaged live with frames every 30 min. Images are maximum projection stills of two different bacteria in two cells, representative of 2 biological replicates. Scale bar 5 µm. Images were processed with the Smooth function in FIJI.

Interestingly, as well as single LC3-TVS induction events, some Mtb WT were observed to trigger two consecutive rounds of LC3-TVS (**Figure 3.2.6**). Approximately 1.5 h after phagocytosis an initial, relatively small induction of LC3-TVS was observed and after a further 3 h the bacterium was observed to be LC3 negative. An hour later, a second, large induction of LC3-TVS was observed; suggesting the trigger for LC3-TVS can occur multiple times around one bacterium.

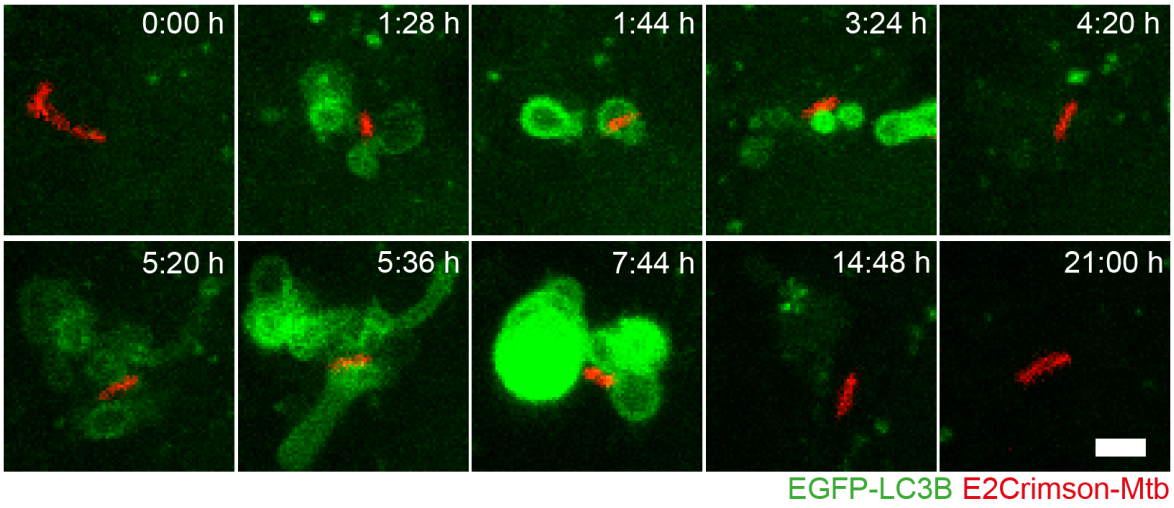

Figure 3.2.6 Mtb WT is able to induce multiple rounds of LC3-TVS formation. iPSDM transiently expressing EGFP-LC3B and infected with E2Crimson Mtb WT at an MOI of 2 were imaged live with frames every 4 min. Images are maximum projection stills from this live cell movie and are a zoom of one bacterium from one cell followed over time, with time 0 being the frame of the phagocytic event. Scale bar 2 µm.

Moreover, when examining endogenous LC3B in iPSDM infected with Mtb, large LC3B positive membranes juxtaposing Mtb WT were observed but were absent in the Mtb ΔRD1 infected cells (**Figure 3.2.7A**). These structures were found at 2 h, 24 h and 48 h after infection with circa 40% of all LC3B positive Mtb WT showing this phenotype (**Figure 3.2.7B**). Given the similarity of these structures to those observed in the live cell imaging (**Figure 3.2.4-6**) it is likely these structures formed even under endogenous levels of LC3B expression and were not a consequence of overexpression artefacts. To exclude the possibility this is a phenomenon solely observed in the iPSDM model, the localisation of endogenous LC3B was analysed in hMDM infected with Mtb WT or Mtb ΔRD1. Similar tubular and vacuolar LC3B positive structures were observed at 2 h post infection. However, at 24 h of infection these structures were no longer observed (**Figure 3.2.7C&D**). TEM analysis also revealed a very complex membranous organisation in iPSDM infected with Mtb WT, showing multi-lamellar compartments, sometimes containing organelles such as lipid droplets, adjacent to Mtb bacilli (**Figure 3.2.7E**).

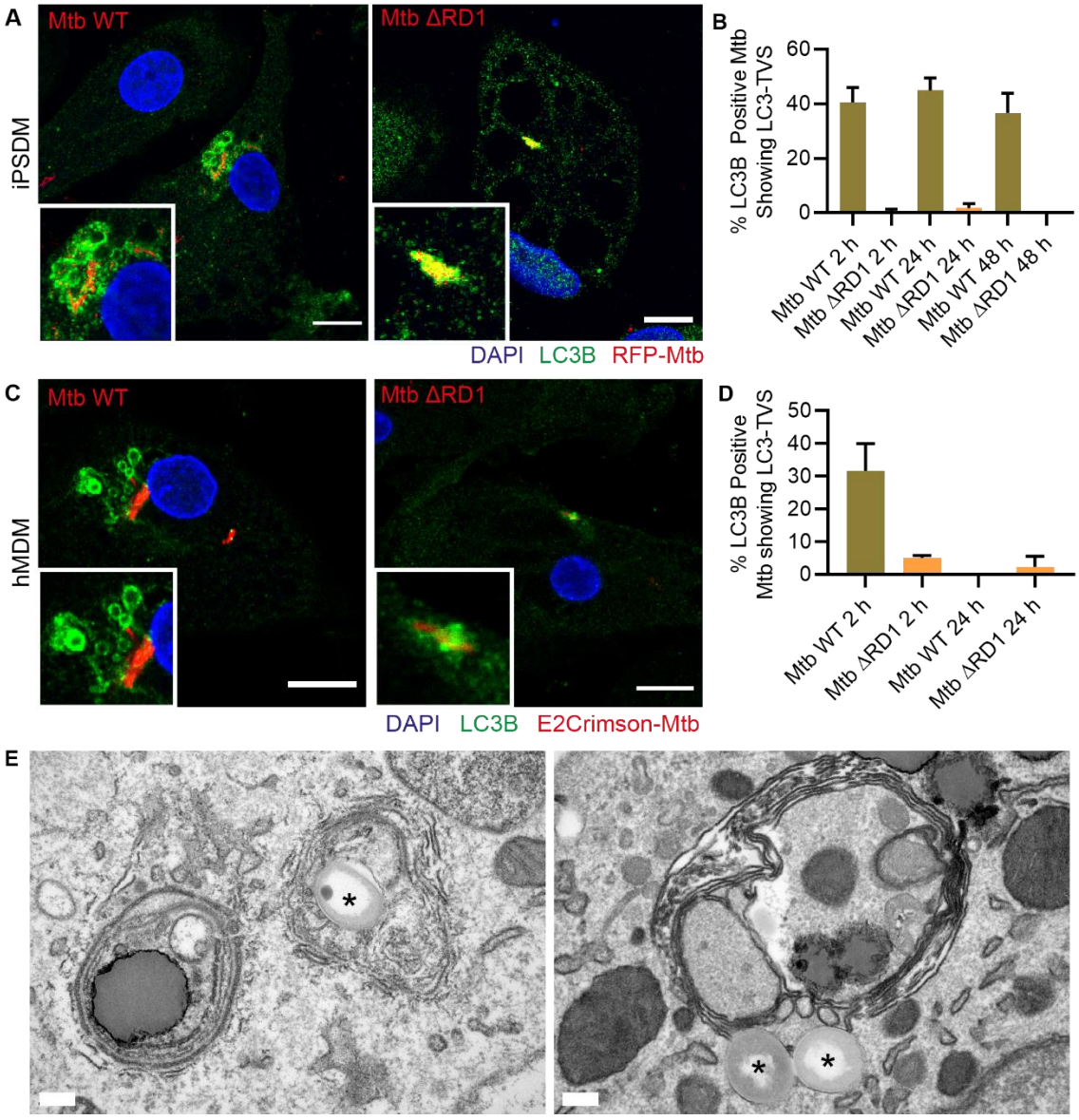

Figure 3.2.7 Large LC3B positive vacuoles are observed in both iPSDM and hMDM infected with Mtb WT. A. iPSDM were infected with RFP-Mtb WT or ΔRD1 at an MOI of 2 and examined by immunofluorescence of LC3B at 48 h post infection. Scale bar 10 µm. **B.** Manual quantification of the percentage of LC3B positive Mtb in iPSDM showing enlarged LC3B positive vacuoles adjacent to the bacteria as shown in **A**. Data are mean ± SD from 3 biological replicates. **C.** hMDM were infected with E2Crimson-Mtb WT or Mtb ΔRD1 at an MOI of 2 and examined by immunofluorescence of LC3B at 2 h post infection. Representative images of 2 biological replicates. **D.** Manual quantification of the percentage of LC3B positive Mtb in hMDM showing enlarged LC3B positive vacuoles adjacent to the bacteria as shown in **C**. Data are mean ± SEM from 2 biological replicates. **E.** TEM images of iPSDM infected with RFP-Mtb WT at 48 h post infection. Scale bar 200 nm. Asterisks indicate Mtb.

Phagosome membrane damage precedes LC3-TVS formation

The RD1 dependency of the observations in **Figures 3.2.4-7**, and the similarity of some aspects with the live cell imaging of EGFP-Gal8 in **Figure 3.2.3**, indicated this rearrangement of the autophagy machinery was likely triggered by phagosome membrane damage. Live cell imaging of iPSDM co-expressing EGFP-LC3B and RFP-Gal8 infected with E2Crimson-Mtb WT showed association of RFP-Gal8 immediately prior to recruitment of EGFP-LC3B (**Figure 3.2.8A**). Confirming the previous results, EGFP-LC3B was recruited to large LC3-TVS, some of which were positive for RFP-Gal8. Interestingly, some of the large EGFP-LC3B tubules originating for the vacuoles were RFP-Gal8 negative. After chemical fixation, it was still possible to visualise the LC3B positive vacuoles and tubules (**Figure 3.2.8B**). However, due to the time from imaging to fixation, some structures changed between the last frame of the live cell imaging, likely due to the protracted time to fix the sample in a BSL3 laboratory. Following fixation, the sample was imaged by focussed ion beam scanning electron microscopy (FIB SEM), a technique previously used to image subcellular structures at ultra-high resolution in infection (Weiner and Enninga, 2019; Fredlund et al., 2018). 3D correlative light and FIB SEM analysis revealed that the EGFP-LC3B positive membranes were large, multi-membranous structures (**Figure 3.2.8C**). Although fixation and processing artefacts cannot be excluded, these swollen autophagosomes had regions of electron dense lumen and electron-lucent areas. Segmentation of the FIB SEM data revealed an incomplete double membrane surrounding the bacteria (**Figure 3.2.8D**), suggesting a partially formed autophagosome. Whilst in some sections, a complete double membrane resembling an autophagosome was observed around the bacteria (**Figure 3.2.8Di**) in other areas well-defined ends of the double membrane were clear (**Figure 3.2.8Dii**). Notably, this three dimensional analysis showed the localisation of lipid droplets to the EGFP-LC3B positive structures, suggesting a potential induction of lipophagy during Mtb infection (**Figure 3.2.8E**).

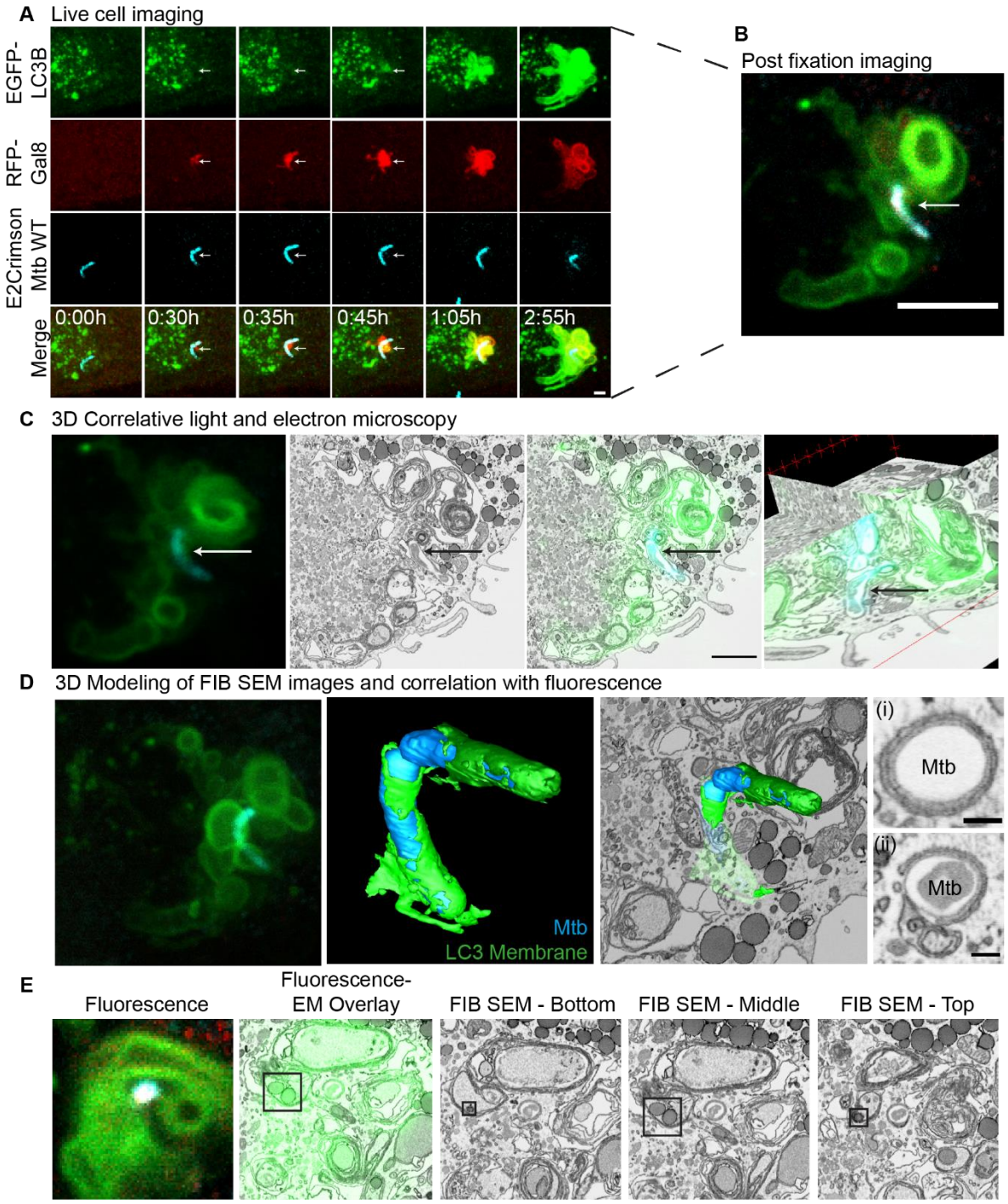

Figure 3.2.8 Gal8 recruitment after membrane damage precedes the formation of Mtb-induced LC3-TVS. iPSDM expressing EGFP-LC3B and RFP-Gal8 infected with E2Crimson Mtb WT were imaged live with frames every 5 min. **A.** Maximum projection stills from live cell imaging. Images were filtered using the Smooth function in FIJI. Representative of 2 biological replicates. **B.** Single Z slice from post-fixation confocal imaging of cell shown in **A**. **C.** 3D CLEM of post fixation Z stack and FIB SEM of cell in panels **A** and **B**. Scale bar 2 µm, arrow indicates Mtb. **D.** Segmentation of FIB SEM

dataset showing the partial encasement of bacteria (cyan) in **A&B** in double membrane structures (green), that are LC3B positive. Fluorescence image is a 3D projection of the post fixation Z stack. (i) Shows a slice through the bacteria from the FIB SEM where the double membrane appears complete. (ii) Shows a slice through the bacteria from the FIB SEM where the double membrane appears incomplete. Scale bar 0.2 µm. **E.** Correlation of fluorescence with FIB SEM section showing lipid droplets (black square) in a double membrane LC3 positive compartment.

Mtb spatially segregates from LC3B positive damaged membranes

The shedding of the EGFP-LC3B positive membranes observed in **Figure 3.2.4-6** along with the partial envelopment of the bacteria in double membranes in **Figure 3.2.8** suggested that Mtb may use this to evade successful capture by the autophagy machinery. Live cell imaging of EGFP-LC3B expressing iPSDM enabled the identification of bacteria that had undergone different EGFP-LC3B dynamics (**Figure 3.2.9A&B**). Whilst some bacteria managed to shed the EGFP-LC3B positive membranes (**Figure 3.2.9A**) others still showed partial colocalisation (**Figure 3.2.9B**). Imaging immediately prior to fixation also identified bacteria entirely coated with EGFP-LC3B (**Figure 3.2.9C&G**). FIB SEM analysis of the bacteria that was completely EGFP-LC3B negative (ROI1 in **Figure 3.2.9C**) showed cytosolic bacteria contacting organelles such as lipid droplets and in close apposition to mitochondria (**Figure 3.2.9D**). The EGFP-LC3B membranes shed from the bacteria were complex, multi-membraned structures as previously observed in **Figure 3.2.8** (**Figure 3.2.9E**). The 3D FIB SEM reconstruction of the bacilli partially surrounded by an EGFP-LC3B positive membrane showed that the majority of the bacterial surface was exposed to the cytosol with one pole being enwrapped in a double membrane (**Figure 3.2.9F**). Within this double membrane there were small intraluminal vesicles. Mtb entirely enclosed by an EGFP-LC3B positive membrane in the image prior to fixation were localised within a partially complete double membrane, which also contained ER-like sheets of membrane (**Figure 3.2.9G**).

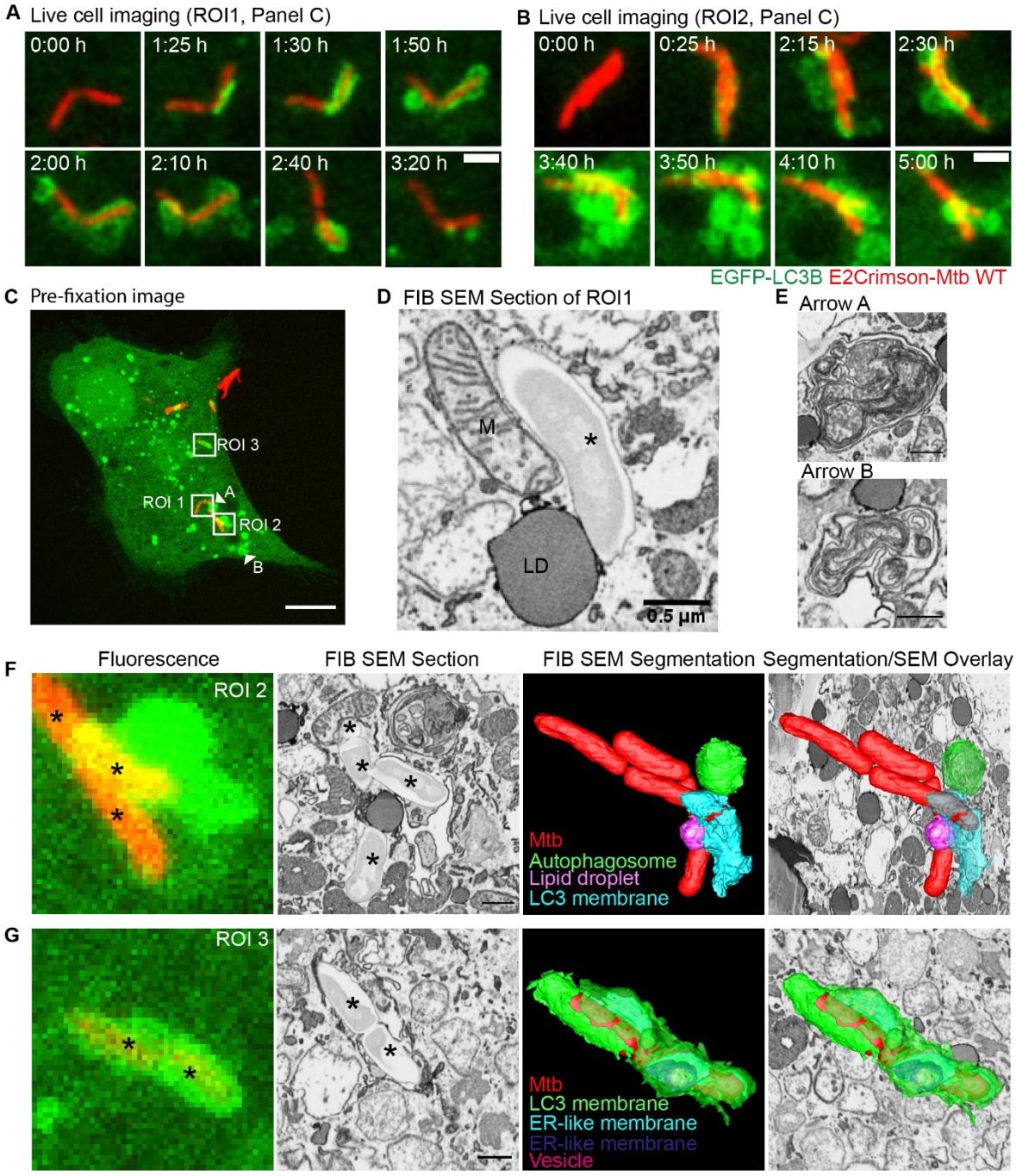

Figure 3.2.9 Mtb WT escapes LC3-TVS to reside in the cytosol. iPSDM expressing GFP-LC3B (green) and infected with E2Crimson-Mtb WT (red) were followed by confocal live cell imaging **A & B** with frames every 5 min. Images are maximum projection stills, filtered with a Gaussian blur, radius 0.8, showing 2 small clumps of bacteria. Scale bar 2 µm. **C.** Maximum projection of 15 Z slice image of cell shown in **A** and **B** taken immediately prior to fixation. Scale bar 10 µm. ROI1, 2 and 3 are shown in detail in panels **D**, **F** and **G** respectively. Arrowheads A and B indicate LC3 positive membranes that were previously associated with Mtb and are shown in detail in panel **E**. **D.** Section

from FIB SEM showing one of the bacteria (*) in ROI1 in the cytosol in contact with a lipid droplet (LD) and a mitochondrion (M). **E.** Section from FIB SEM showing LC3 positive membranes (indicated by arrowheads in **C**) that have been shed from Mtb in ROI2. **F.** Correlative light and FIB-SEM of ROI2 in **C**. Scale bar in FIB SEM section 0.5 µm. **G.** Correlative light and FIB-SEM of ROI3 in **C**. Scale bar in FIB SEM section 0.5 µm.

In conclusion, the data presented in this chapter demonstrated that Mtb induced phagosome damage leads to targeting of the damaged phagosomal remnants for autophagy. Additionally, the induction of large LC3-TVS is associated with successful evasion of autophagic targeting and localisation of Mtb in the cytosol of macrophages. Altogether, the ultrastructure analysis revealed a very complex autophagic membrane reorganisation after Mtb infection of iPSDM.

3.3 An autophagy independent role for Atg14 in restricting Mtb replication in iPSDM

Having demonstrated the effective evasion of autophagic capture by Mtb in human macrophages in chapter 3.2, it was of interest to dissect the impact of autophagy disruption in iPSDM on Mtb replication. I next capitalised on the main advantage of iPSC to knockout specific genes by CRISPR and test the function of autophagy deficient iPSDM. As both canonical and non-canonical autophagy have been implicated in controlling bacterial infections, including Mtb (Köster et al., 2017; Gutierrez et al., 2004a), it was important to develop tools to dissect both pathways.

iPSDM express a truncated and functional form of Atg13

In order to harness this potential, readily available Atg13 knockout (KO) in the KOLF2_C1 iPSC background (Nicholas Ksistakis, Babraham Institute, Cambridge, U.K.) were used to probe the effect of canonical autophagy disruption on Mtb infection induced autophagy and Mtb replication. As expected, the Atg13 KO iPSCs showed impaired starvation-induced autophagy and did not accumulate LC3-II in response to BafA1 treatment (**Figure 3.3.1A**). Unexpectedly, the Atg13 KO macrophages showed a normal autophagy response to starvation (**Figure 3.3.1B**). Western blotting analysis for Atg13 showed that in the WT iPSCs the main band was at approximately 60 kDa, the predicted molecular weight of the full-length protein, with a faint band at around 50 kDa (**Figure 3.3.1A**). In the iPSDM the 60 kDa band diminished and the 50 kDa band became the predominant band (**Figure 3.3.1B**). Analysis of the gene and transcript architecture on Ensembl showed there was an alternative start site in the gene within Exon 4 that would produce a truncated protein missing the first 79 amino acids with a predicted molecular weight of 51 kDa (**Figure 3.3.1C**). The gRNA used to make the knockout aligns within Exon 4 and is 5’ to the alternative start site. Therefore following macrophage differentiation the dominant isoform of Atg13 is still expressed and the cells show no defects in autophagy.

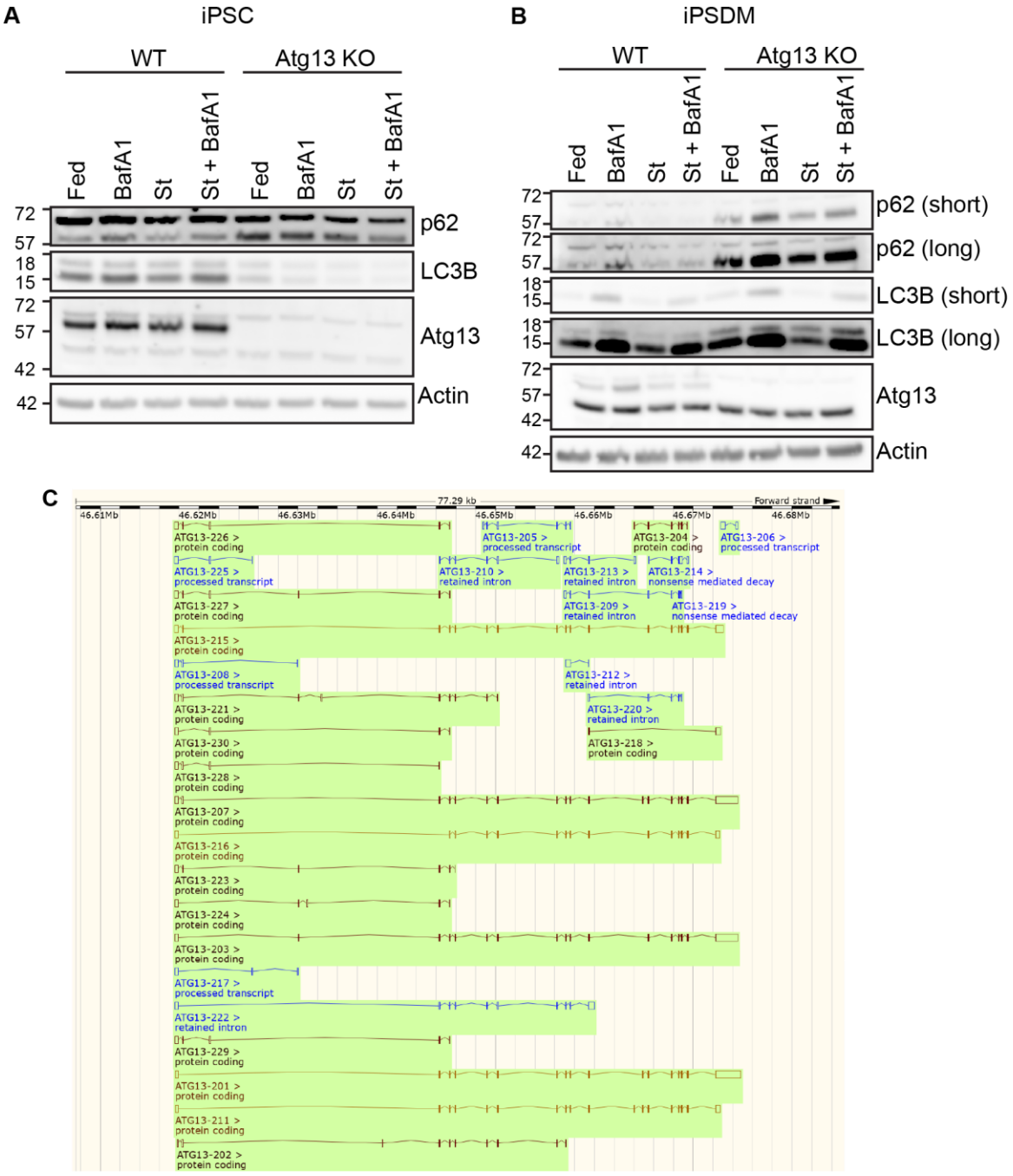

Figure 3.3.1 iPSDM express a truncated form of Atg13 that is capable of supporting starvation induced autophagy. iPSDM were derived from WT or Atg13 KO KOLF iPSCs and their autophagy response to canonical autophagy stimuli was examined by Western blot. **A.** KOLF WT and Atg13 KO iPSCs were treated as indicated for 2 h and subjected to Western blot analysis for Atg13, p62 and LC3B. Fed: full media, St: starvation, BafA1: bafilomycin A1. Blot representative of 2 biological replicates **B.** KOLF WT and Atg13 KO iPSDM were treated as indicated for 2 h and examined by Western blot for Atg13, p62 and LC3B. Blot representative of 1 biological replicate. **C.** Ensembl

transcript tracks for human Atg13. Transcript Atg13-216 represents a truncated form of the protein that is observed to be abundantly expressed in macrophages.

Indeed, during Mtb infection, autophagy induction still occurred at 48 h post infection (**Figure 3.3.2**). Thus, the predominant isoform of Atg13 that is expressed in iPSDM is a truncated 50 kDa version that retains functionality in autophagosome biogenesis and supports both starvation- and Mtb infection-induced autophagy. Therefore, these macrophages were not suitable for studying the effects of autophagy disruption.

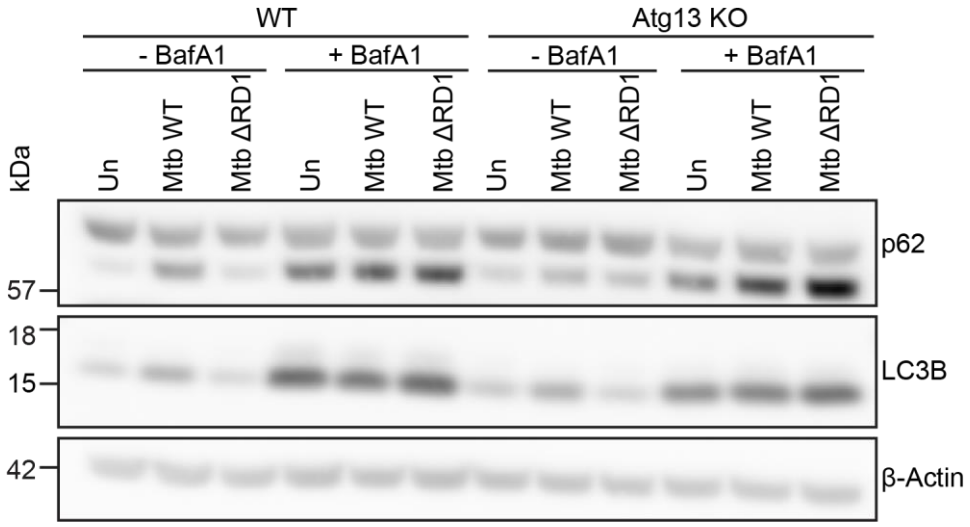

Figure 3.3.2 The truncated form of Atg13 is able to support autophagy induction by Mtb infection. WT and Atg13 KO KOLF iPSDM were infected with Mtb WT or Mtb ΔRD1 at an MOI of 2. Western blot of LC3B and p62 at 48 h post infection. BafA1: bafilomycin A1, Un: uninfected. Representative of 3 biological replicates.

Generation and characterisation of Atg7 and Atg14 KO iPSDM

In parallel to the studies with Atg13, autophagy knockouts were made in both EIKA2 and KOLF2 iPSCs to disrupt either canonical and non-canonical autophagy, or canonical autophagy alone. In order to disrupt all autophagic processes Atg7 KO iPSCs were generated, as this has previously been widely reported to disrupt both canonical and non-canonical autophagy (Martinez et al., 2015, 2011; Tanida et al., 1999; Kim et al., 1999). This also avoids the complications of the autophagy independent phenotype, shown in mice with genetic deletions of Atg5 infected with Mtb (Kimmey et al., 2015). In order to specifically disrupt canonical autophagy, whilst

leaving non-canonical autophagy functional, Atg14 was selected (Martinez et al., 2015).

Following clonal isolation, PCR screens were used to identify homozygous KO clones; that is those only producing only the shorter product. This identified six homozygous Atg14 KO clones in the KOLF2 (**Figure 3.3.3A**), six Atg14 KO clones in the EIKA2 (**Figure 3.3.3D**) and one Atg7 KO clone in the EIKA2 (**Figure 3.3.3C**). No homozygous Atg7 KO clones were identified in the KOLF2 (**Figure 3.3.3B**), this is likely due to a heterozygous SNP within one of the 5’ gRNAs and the other guide not being as efficient at generating a cut.

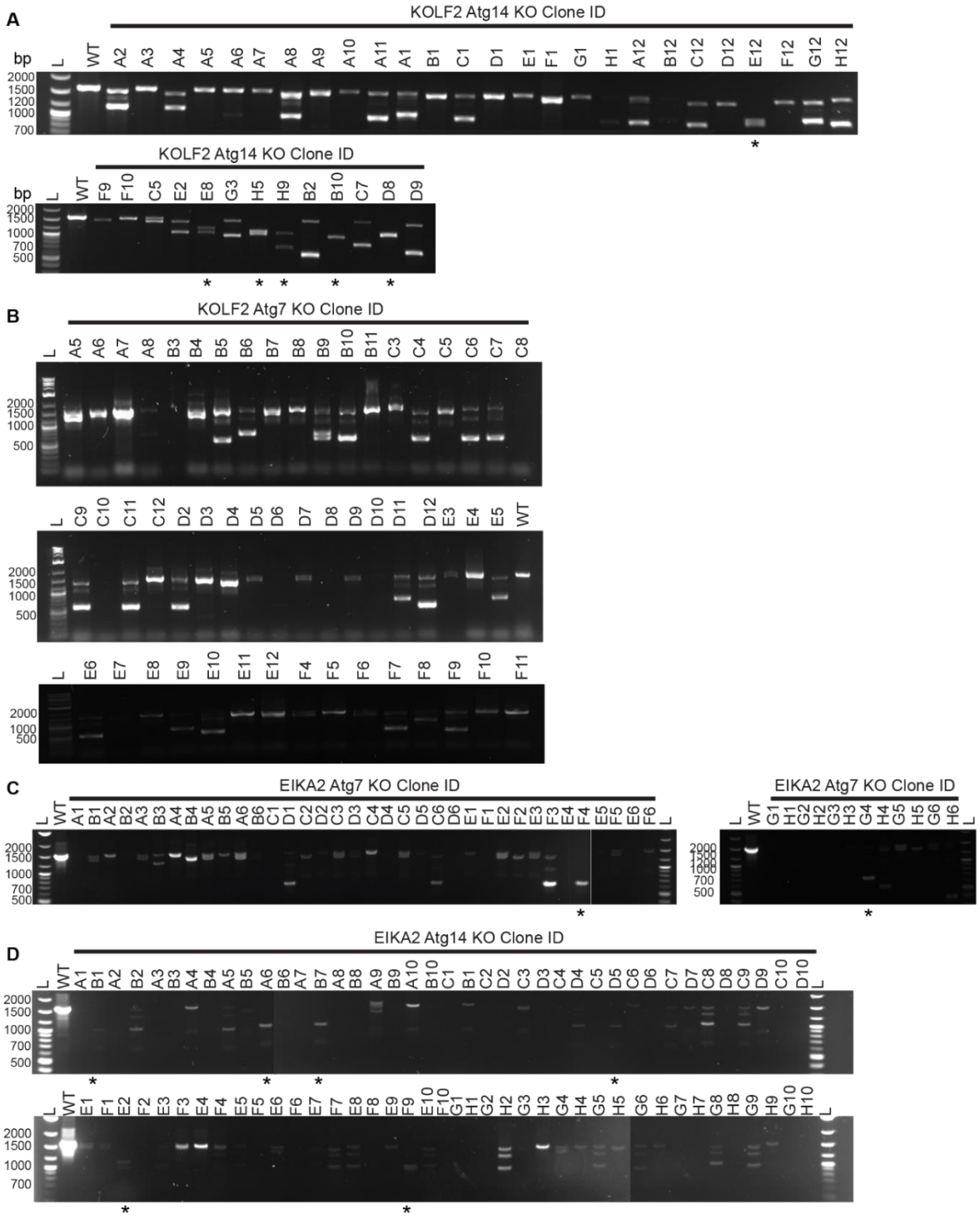

Figure 3.3.3 PCR screen identifies Atg7 KO and Atg14 KO iPSCs. PCR amplication of gDNA extracted from single clones of KOLF2 (**A&B**) or EIKA2 (**C&D**) iPSCs following CRISPR/Cas9 targeting for deletion of exons in Atg7 (**B&C**) or Atg14 (**A&D**). Amplification of Atg7 around the cut sites (**B&C**) yields a band of approximately 1500 bp in WT cells and a band of approximately 700 bp following successful gene editing. Amplification of Atg14 (**A&D**) yields a band band of approximately

1500 bp in WT cells and a band of approximately 1000 bp following successful gene editing. * indicate homozygous KO clones.

Selected PCR validated KO clones were expanded and screened by Western blot for the autophagy response and loss of the corresponding protein. EIKA WT iPSCs accumulated LC3-II in response to canonical autophagy induction by starvation, blockade of autophagosome degradation by BafA1 or induction of non-canonical autophagy by monensin treatment (Florey et al., 2015) (**Figure 3.3.4A**). In contrast, the Atg7 KO EIKA iPSCs had undetectable levels of LC3-II under fed or starvation conditions however, BafA1 or monensin treatment led to detectable levels of LC3B at 15kDa, albeit much lower than is seen in the WT cells (**Figure 3.3.4A**). Additionally, Atg7 KO iPSCs showed accumulation of p62 under all conditions when compared with WT iPSCs. p62 levels were not altered by BafA1 or monensin treatment; whereas WT iPSCs accumulated p62 following both of these treatments (**Figure 3.3.4A**). As expected, the Atg14 KO iPSCs showed increased p62 over WT cells, even in the fed condition, and failed to alter levels of LC3-II in response to either starvation or BafA1 (**Figure 3.3.4B**). In contrast, monensin treatment led to an increase in LC3-II levels and undetectable levels of LC3-I in with WT and Atg14 KO iPSCs indicating functional non-canonical autophagy in these cells (**Figure 3.3.4B**). Altogether, these data showed that Atg7 KO iPSCs are defective in both canonical and non-canonical autophagy, whereas the Atg14 KO iPSCs were only defective in canonical autophagy.

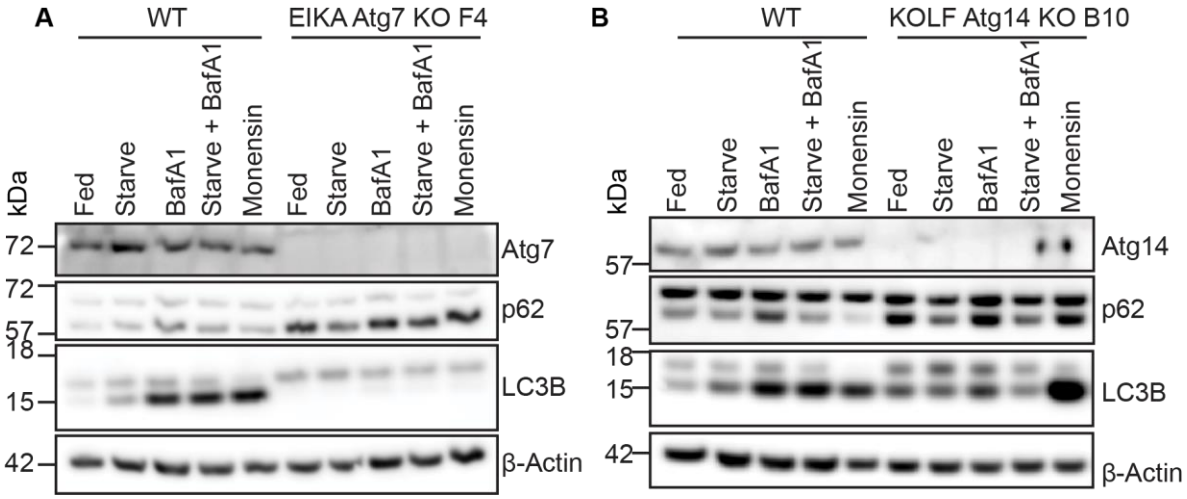

Figure 3.3.4 Characterisation of the autophagy response in Atg7 KO and Atg14 KO iPSC. A. Western blot of Atg7, p62 and LC3B in EIKA WT and EIKA Atg7 KO F4 iPSCs following treatment with starvation, bafilomycin A1 or monensin for 2 h. **B.** Western blot of Atg14, p62 and LC3B in KOLF WT and KOLF Atg14 KO B10 iPSCs following treatment with starvation, bafilomycin A1 or monensin for 2 h. Blots representative of 3 biological replicates. BafA1: bafilomycin.

To test if macrophage differentiation affected the autophagy phenotypes of the Atg7 and Atg14 KOs the same experiment as in **Figure 3.3.4** was repeated in the iPSDM. Atg7 protein was not detected in the Atg7 KO iPSDM (**Figure 3.3.5A**) and Atg7 KO iPSDM showed two bands for LC3B, one at 15 kDa and one at 18 kDa. A small increase in LC3-II was observed after treatment with BafA1, although the effect was lower when compared with WT iPSDM (**Figure 3.3.5A**). The autophagy receptor p62 levels were higher in Atg7 KO iPSDM under resting conditions (**Figure 3.3.5A**). Unfortunately, the Atg14 antibody failed to detect Atg14 in WT macrophages so it was not possible to validate the loss of protein at this stage. Functionally, however, the Atg14 KO macrophages showed no significant changes in LC3B processing after starvation and only minor changes after BafA1 treatment. Following induction of non-canonical autophagy with monensin a small induction of LC3-II was observed, which was to a similar level as in the WT iPSDM (**Figure 3.3.5B**). The levels of p62 remained largely unchanged in both WT and Atg14 KO iPSDM under all conditions tested (**Figure 3.3.5B**).

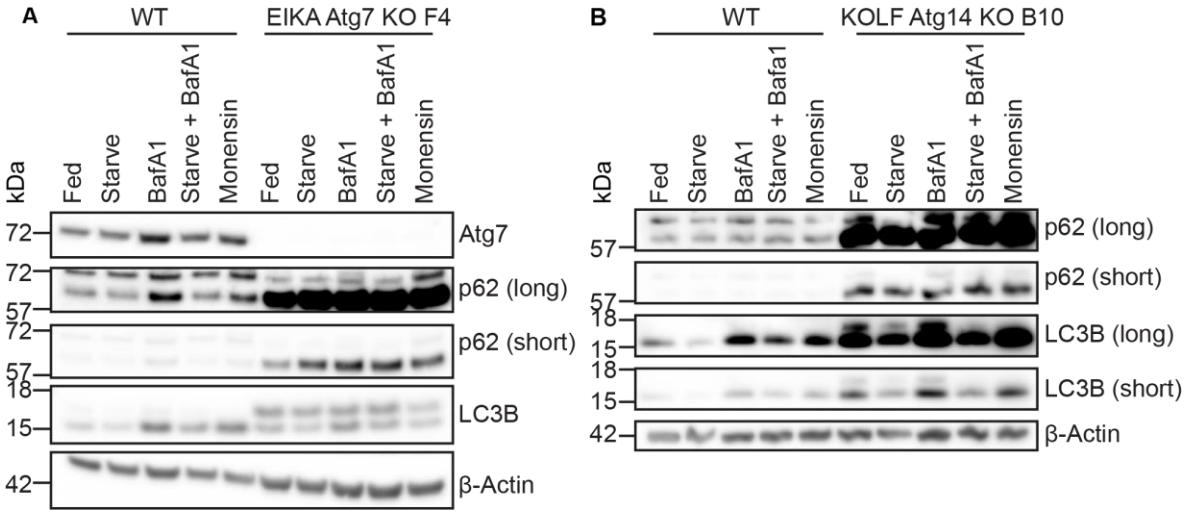

Figure 3.3.5 Characterisation of the autophagy response in Atg7 and Atg14 KO iPSDM. A. Western blot of Atg7, p62 and LC3B in EIKA WT and EIKA Atg7 KO F4 iPSDM following treatment with starvation, bafilomycin A1 or monensin for 2 h. Data representative of 2 biological replicates **B.** Western blot of p62 and LC3B in KOLF WT and KOLF Atg14 KO B10 iPSDM following treatment with starvation, bafilomycin A1 or monensin for 2 h. Data representative of 1 biological replicate. BafA1: bafilomycin.

Mtb lacking the protein CpsA is attenuated in human macrophages

Deletion of the protein CpsA (rv3484), a member of the LytR-CpsA-Psr (LCP) domain containing family, impaired Mtb replication in BMDM and THP-1. In mouse macrophages this restriction is associated with an enhanced recruitment of NADPH oxidase and induction of LAP, a form of non-canonical autophagy (Köster et al., 2017). Using the Atg7 and Atg14 KO iPSDM in combination with two mutant strains of Mtb, Mtb ΔRD1 and Mtb ΔCpsA, which are unable to induce canonical or to block non-canonical autophagy respectively, I aimed to dissect the roles of canonical and non-canonical autophagy in Mtb infection.

The growth of Mtb WT, Mtb ΔRD1, Mtb ΔCpsA and Mtb ΔCpsA::CpsA in 7H9 broth was similar (**Figure 3.3.6**). It was initially important to validate that Mtb ΔCpsA replication was restricted in iPSDM. Whilst uptake of Mtb was unaffected by CpsA or RD1 deletion, replication of Mtb ΔCpsA and Mtb ΔRD1 – as shown before (**Figure 3.1.4**) – was significantly attenuated in iPSDM (**Figure 3.3.7**). This replication defect was rescued through complementation of CpsA with integration of the gene at a

different chromosomal locus and expression driven by a constitutive promoter (Mtb ΔCpsA::CpsA). As growth in broth was not altered (**Figure 3.3.6**), the deletion of CpsA specifically affects intracellular bacterial replication.

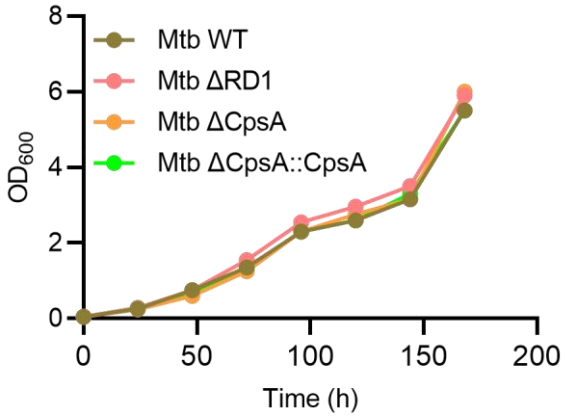

Figure 3.3.6 Mtb CpsA does not show a growth defect in broth. Mtb strains were grown to exponential phase before dilution down to OD_{600} 0.05 and monitoring Mtb growth by recording the OD_{600} every 24 h. Data from one representative experiment of 2 biological replicates

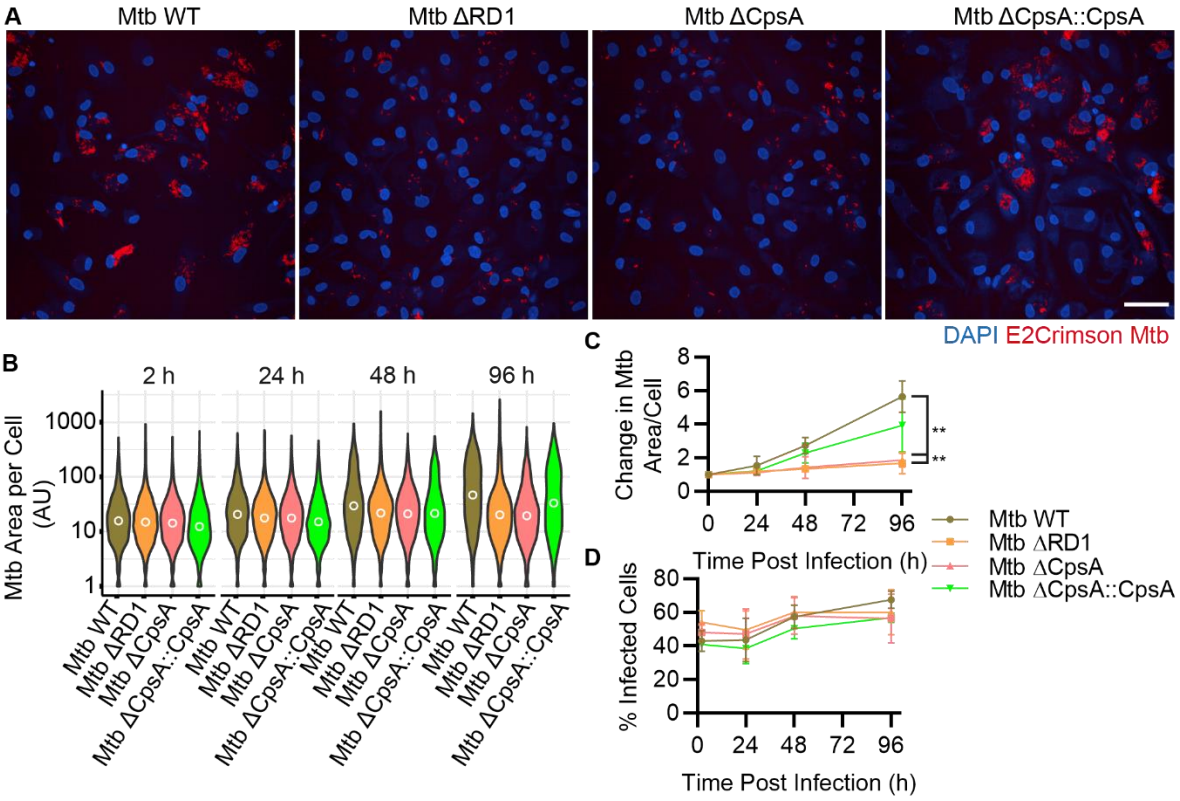

Figure 3.3.7 Mtb ΔCpsA replication is attenuated in iPSDM. iPSDM infected with Mtb WT, Mtb ΔRD1, Mtb ΔCpsA or Mtb ΔCpsA::CpsA were analysed for Mtb replication by confocal microscopy at 2 h, 24 h, 48 h and 96 h pot infection. **A**. Representative micrographs of iPSDM infected with each strain for 96 h. Scale bar 50 µm. **B.** Violin plot of Mtb area per cell from one representative biological replicate of 3. White circles indicate mean Mtb area/cell. **C.** Change in Mtb area per cell over 96 h is shown for all strains, data represented as mean ± SD of 3 biological replicates. ** $p < 0.01$. Data were analysed by one way ANOVA with Holm-Sidak's multiple comparisons test. **D.** Percentage of infected cells from the same 3 biological replicates in **C.** Data are mean ± SD.

Next, to examine if the observed attenuation of Mtb ΔCpsA in iPSDM was potentially linked with NADPH oxidase, the recruitment of the endogenous, membrane associated subunit p40 Phox to Mtb was monitored by confocal microscopy. No differences in the recruitment of p40 Phox to Mtb WT and Mtb ΔCpsA were observed after 2 h of infection (**Figure 3.3.8**). However, at 48 h post infection, the levels of association of p40 Phox with Mtb ΔCpsA were significantly higher when compared to Mtb WT in infected iPSDM.

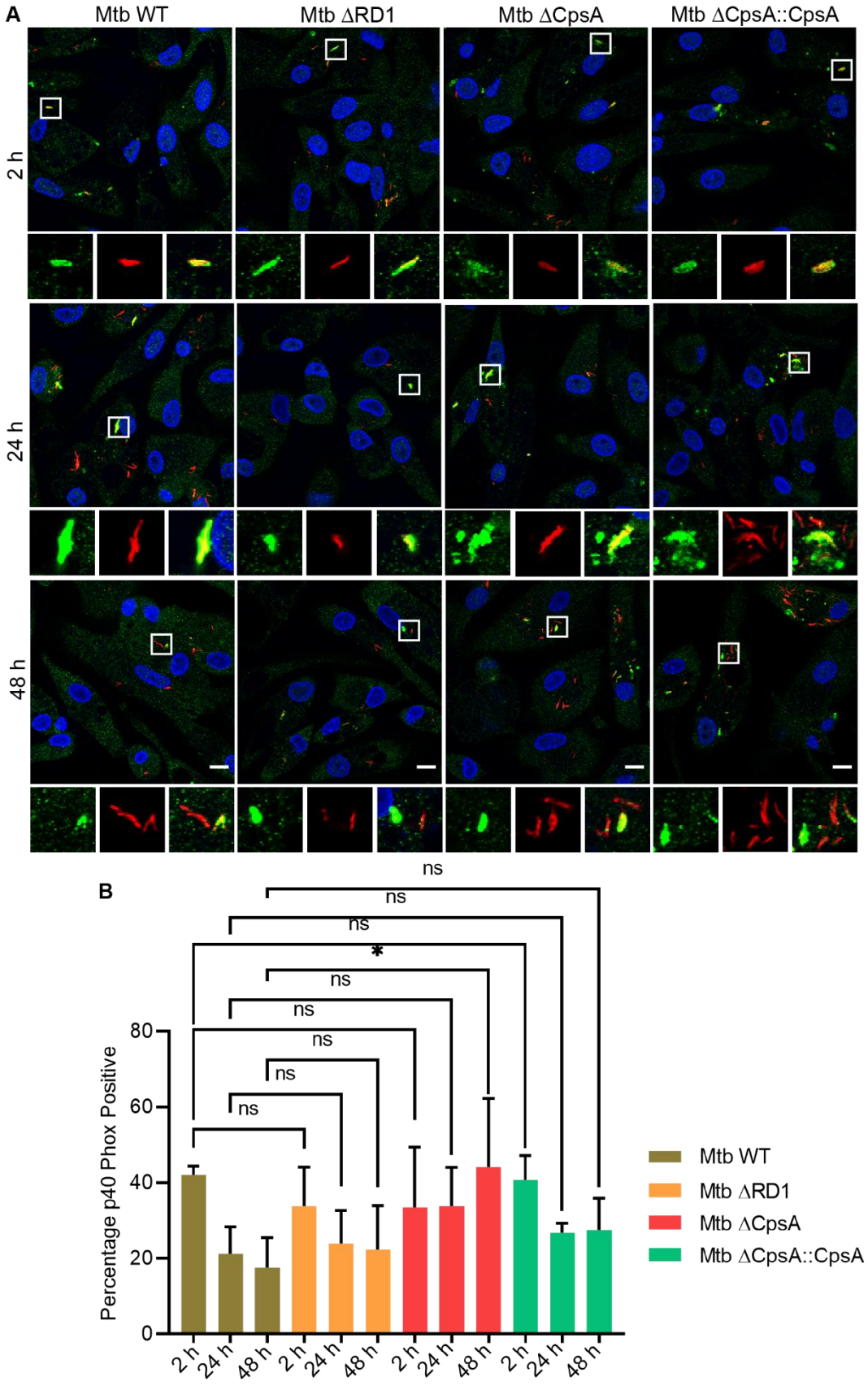
A
Mtb WT
Mtb ΔRD1
Mtb ΔCpsA
Mtb ΔCpsA::CpsA
2 h
24 h
48 h
B
ns
ns
ns
*
ns
ns
ns
ns
ns
Percentage p40 Phox Positive
0
20
40
60
80
2 h
24 h
48 h
Mtb WT
Mtb ΔRD1
Mtb ΔCpsA
Mtb ΔCpsA::CpsA

Figure 3.3.8 Mtb ΔCpsA retains p40 Phox recruitment at 48 h post infection. iPSDM infected with Mtb WT, Mtb ΔRD1, Mtb ΔCpsA or Mtb ΔCpsA::CpsA for 2-48 h were stained for p40 Phox by immunofluorescence. **A.** Representative images of p40 Phox recruitment to each strain, at each time point. Images representative of 3 biological replicates. Scale bar 10 μm. Close-ups of region marked by white box are shown below each main image. **B.** Quantification of p40 Phox recruitment to Mtb from images represented in **A**. Data are mean ± SD of 3 biological replicates. Data analysed by one way ANOVA and Holm-Sidak's multiple comparisons test, ns not significant, * $p < 0.05$.

Proteins with an LCP domain are responsible for cell wall biosynthetic processes in many Gram-positive bacteria, as well as in Mtb. In Mtb both CpsA and rv3267 are the LCP domain containing proteins responsible for conjugation of arabinogalactan to peptidoglycan in the bacterial cell wall (Harrison et al., 2016; Grzegorzewicz et al., 2016). It is possible that CpsA deletion may subtly impact cell wall constituents and thus affect the assembly of secretion systems, including ESX-1, and other membrane proteins and complexes. To examine if the Mtb ΔCpsA mutant was defective in its ability to induce phagosome membrane damage, recruitment of Gal8 was monitored as described before (**Figure 3.2.1**). No differences in Gal8 recruitment were observed between Mtb WT and Mtb ΔCpsA (**Figure 3.3.9**), suggesting no defects in phagosome damage by Mtb ΔCpsA compared with Mtb WT.

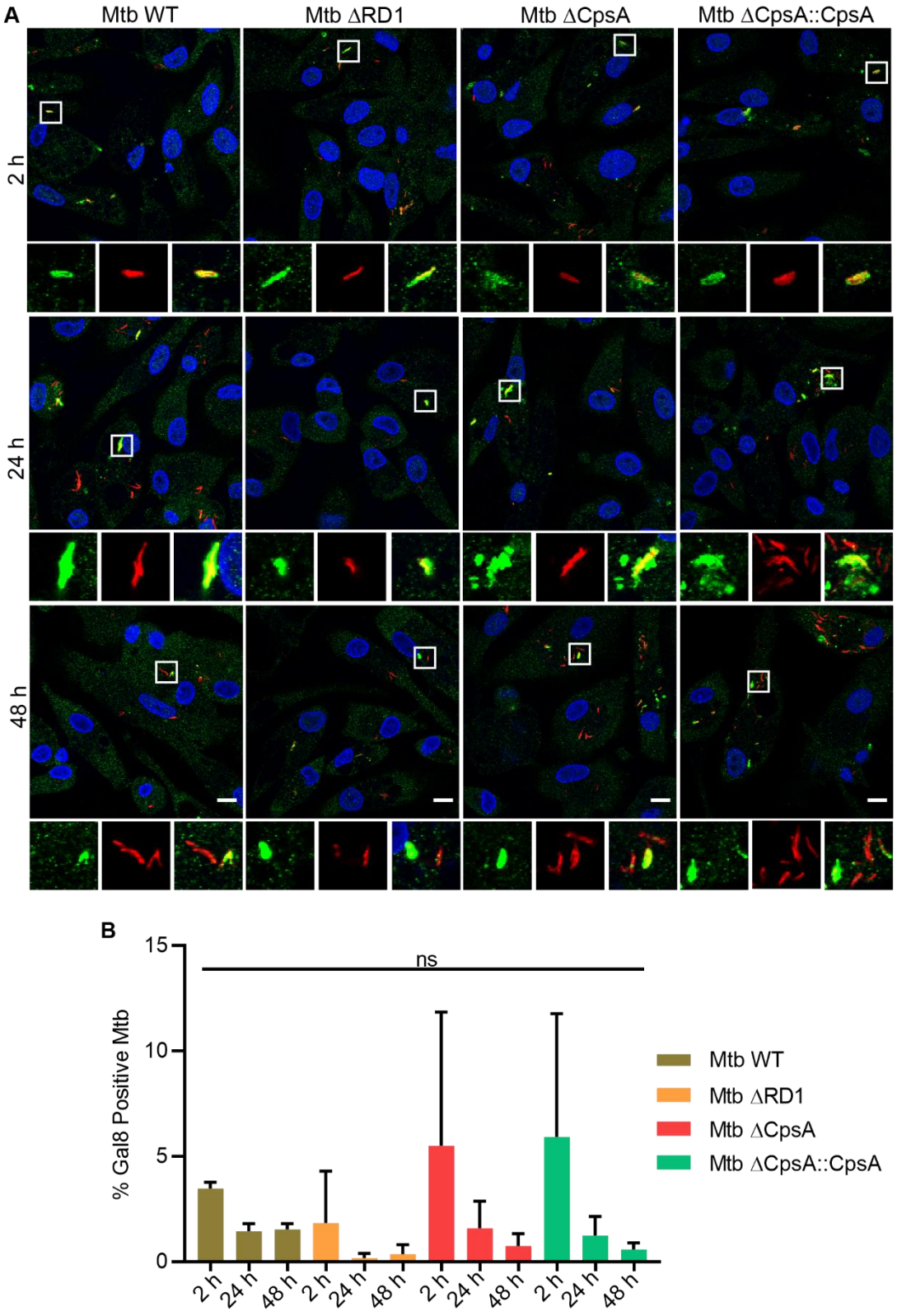
A
Mtb WT
Mtb ΔRD1
Mtb ΔCpsA
Mtb ΔCpsA::CpsA
2 h
24 h
48 h
B
% Gal8 Positive Mtb
15
10
5
0
ns
2 h
24 h
48 h
Mtb WT
Mtb ΔRD1
Mtb ΔCpsA
Mtb ΔCpsA::CpsA

Figure 3.3.9 Mtb CpsA is able to damage the phagosomal membrane. iPSDM infected with Mtb WT, Mtb ΔRD1, Mtb ΔCpsA or Mtb ΔCpsA::CpsA for 2 h, 24 h or 48 h were analysed for Gal8 recruitment by immunofluorescence. **A.** Representative images, insets highlight examples of positive bacteria marked by white square in main image. Scale bar 10 µm. **B.** Quantification of percentage of Gal8 positive Mtb for each condition shown in **A.** Data are mean ± SD of 3 biological replicates. Analysed by one way ANOVA, ns not significant.

Western blot analysis of Mtb infected iPSDM showed no differences in LC3B lipidation at 2 h post infection when comparing Mtb WT and Mtb ΔCpsA infected cells. After 48 h of infection, an accumulation of p62 was observed in Mtb WT, but not Mtb ΔRD1 infected iPSDM (**Figure 3.3.10**), as shown previously in **Figure 3.2.3**. Whilst a small RD1 dependent increase in LC3-II levels was observed here, it was not as pronounced as observed in **Figure 3.2.3**. Mtb ΔCpsA and Mtb ΔCpsA::CpsA infected iPSDM also showed an accumulation of LC3-II and p62, suggesting that CpsA is dispensable for blockade of autophagic flux by Mtb.

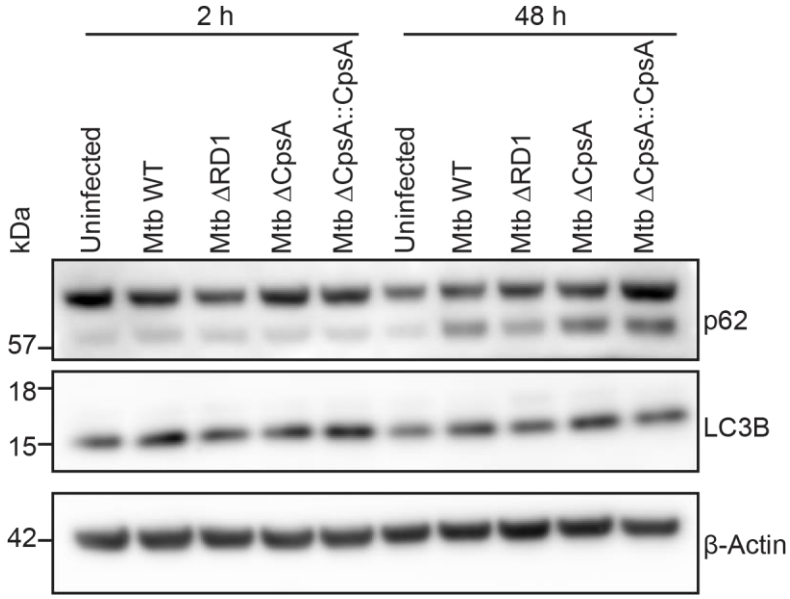

Figure 3.3.10 Mtb CpsA is not required for blockade of autophagic flux after infection. Protein extracts from iPSDM infected with Mtb WT, Mtb ΔRD1, Mtb ΔCpsA or Mtb ΔCpsA::CpsA for 2 h or 48 h were examined for changes in autophagy induction by Western blot. Blots are representative of 3 biological replicates.

Mtb replication is not affected in Atg7 KO iPSDM

To determine if the Mtb infection induced accumulation of LC3-II (**Figure 3.2.3**) was blocked in Atg7 KO iPSDM, macrophages were infected for 48 h and LC3B and p62 analysed by Western blot (**Figure 3.3.11**). The accumulation of LC3-II in Mtb WT infected iPSDM was blocked in Atg7 KO macrophages (**Figure 3.3.11**) whereas the accumulation of p62 was enhanced (**Figure 3.3.11**). No changes in LC3-II or p62 were observed after infection of WT or Atg7 KO iPSDM with Mtb ΔRD1 when compared to the uninfected control.

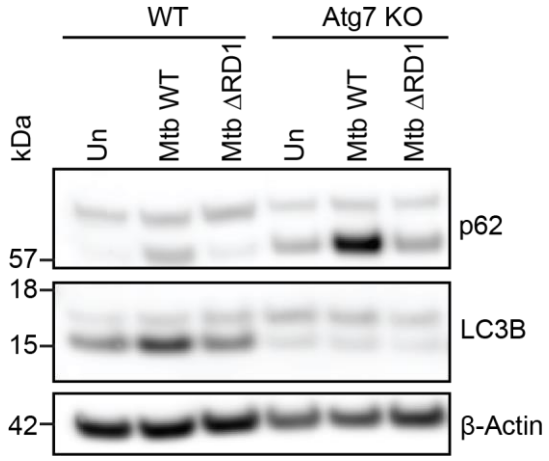

Figure 3.3.11 Atg7 KO iPSDM do not accumulate LC3-II following Mtb infection. Protein extracts from EIKA WT or Atg7 KO iPSDM infected with Mtb WT or Mtb ΔRD1 for 48 h were subjected to Western blotting for LC3B and p62. Data are representative of 3 biological replicates. Un: uninfected.

Whilst disruption of the autophagy pathway through knockout of key selective autophagy genes in mouse macrophages *in vitro* enhances Mtb replication (Köster et al., 2017; Manzanillo et al., 2013; Franco et al., 2016; Watson et al., 2012); a genetic approach targeting the autophagy machinery has not, to the best of our knowledge, been used in human macrophage models. An siRNA screen in THP-1 cells to identify host proteins required to control an established infection did not identify any Atg proteins as being required (Kumar et al., 2010). After 96 h of infection, no differences in replication of Mtb WT or Mtb ΔRD1 were observed when comparing WT and Atg7 KO iPSDM (**Figure 3.3.12A-C**). The lack of observed differences was not due to a change in bacterial uptake or dissemination in Atg7 KO iPSDM as the bacterial area per cell at uptake and percentage of infected cells at all

time points was similar in both cell types (**Figure 3.3.12D-F**). Of note, in one of the two biological replicates, total cell numbers (as measured by number of nuclei counted) were lower in Atg7 KO iPSDM infected with Mtb WT at 96 h. It is therefore possible that there is increased cell death in the Atg7 KO and this may mask any differences in Mtb replication. However, at least up until 48 h post infection no differences were observed in cell number.

Interestingly, whilst Atg7 KO BMDM were unable to restrict Mtb ΔCpsA up to 72 h post infection (Köster et al., 2017), we were unable to repeat this findings in iPSDM (**Figure 3.3.12A-C**). Mtb ΔCpsA showed attenuated replication in the Atg7 KO iPSDM, which cannot carry out either LAP of xenophagy. This suggests that neither canonical nor non-canonical autophagy were responsible for the restriction of Mtb ΔCpsA replication in human macrophages.

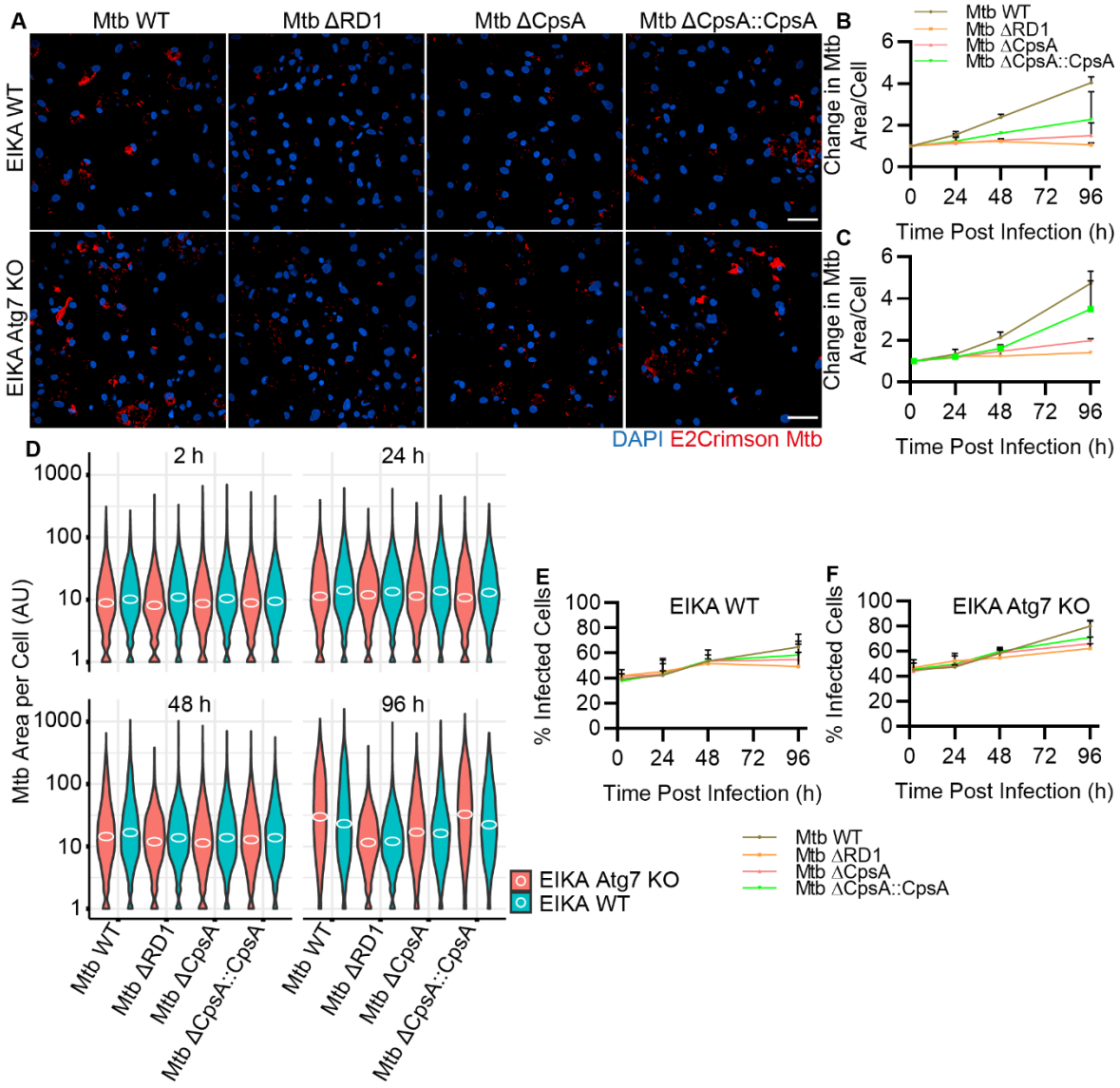

Figure 3.3.12 Mtb replication is unaltered in Atg7 KO iPSDM. EIKA2 WT and Atg7 KO iPSDM were infected with Mtb WT, Mtb ΔRD1, Mtb ΔCpsA or Mtb ΔCpsA::CpsA for 2 h, 24 h, 48 h or 96 h and Mtb replication analysed by confocal microscopy. **A.** Representative confocal fluorescence images at 96 h post infection. Scale bar 50 µm. **B&C.** Quantification of the change in Mtb area per cell, relative to uptake, in WT (**B**) or Atg7 KO (**C**) iPSDM. Data are mean + SD of 2 biological replicates. **D.** Violin plot of Mtb area per cell from 1 biological replicate, representative of 2. White circles represent the mean Mtb area per cell for each condition. **E&F.** Percentage of infected cells at each time point for WT (**E**) and Atg7 KO (**F**) iPSDM. Data are mean + SD of 2 biological replicates.

Atg14 is required in iPSDM to control Mtb replication

In order to determine if non-canonical autophagy was induced at 48 h post infection and at all responsible for the increased LC3-II seen previously (**Figure 3.2.3**), Atg14 KO iPSDM infected with Mtb WT, Mtb ΔRD1, Mtb ΔCpsA or Mtb ΔCpsA::CpsA were subjected to Western blotting. Atg14 KO iPSDM showed higher LC3-II levels compared to WT macrophages under resting conditions. Notably, after infection of Atg14 KO iPSDM with Mtb WT there was no induction of LC3 processing, suggesting that LC3B-II accumulation in WT iPSDM is due to a blockade of canonical autophagic flux (**Figure 3.3.12**). The levels of p62 in Atg14 KO iPSDM were higher compared to WT iPSDM in all conditions tested (**Figure 3.3.13**).

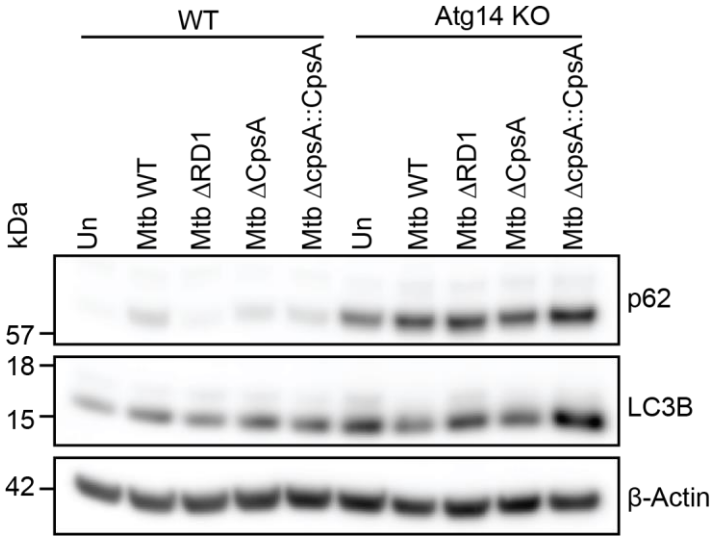

Figure 3.3.13 Atg14 KO iPSDM do not accumulate LC3-II or p62 following Mtb WT infection. Protein extracts from KOLF WT or Atg14 KO iPSDM infected with Mtb WT, Mtb ΔRD1, Mtb ΔCpsA or Mtb ΔCpsA::CpsA for 48 h were Western blotted for LC3B and p62. Image is representative of 2 biological replicates. Un: uninfected.

Reports in Atg14 KO murine BMDMs and mice with a myeloid specific deletion of Atg14 showed a small, but not significant, increase in bacterial burden (Kimmey et al., 2015; Köster et al., 2017). Whether Atg14 is required to restrict Mtb replication in human macrophages is unknown and, given that Atg7 KO iPSDM showed no differences in Mtb burden up to 96 h of infection, any differences would likely be independent of an autophagic function of Atg14. Thus, KOLF WT and Atg14 KO

(clone B10, see **Figure 3.3.3**) iPSDM were infected for up to 96 h with Mtb WT, Mtb ΔRD1, Mtb ΔCpsA or Mtb ΔCpsA::CpsA and their replication analysed. Replication of Mtb WT was significantly enhanced in Atg14 KO iPSDM compared with WT macrophages, showing 10 fold compared to 4 fold replication over 96 h (**Figure 3.3.14A-E**). This difference was not related to differences in phagocytosis as a similar proportion of cells were infected in both genetic backgrounds, and the bacterial area per cell was similar at 2 h of infection (**Figure 3.3.14D, F&G**). Mtb ΔRD1, Mtb ΔCpsA and Mtb ΔCpsA::CpsA also showed a slight, but not statistically significant, increase in replication over 96 h in Atg14 KO iPSDM (**Figure 3.3.14A-E**).

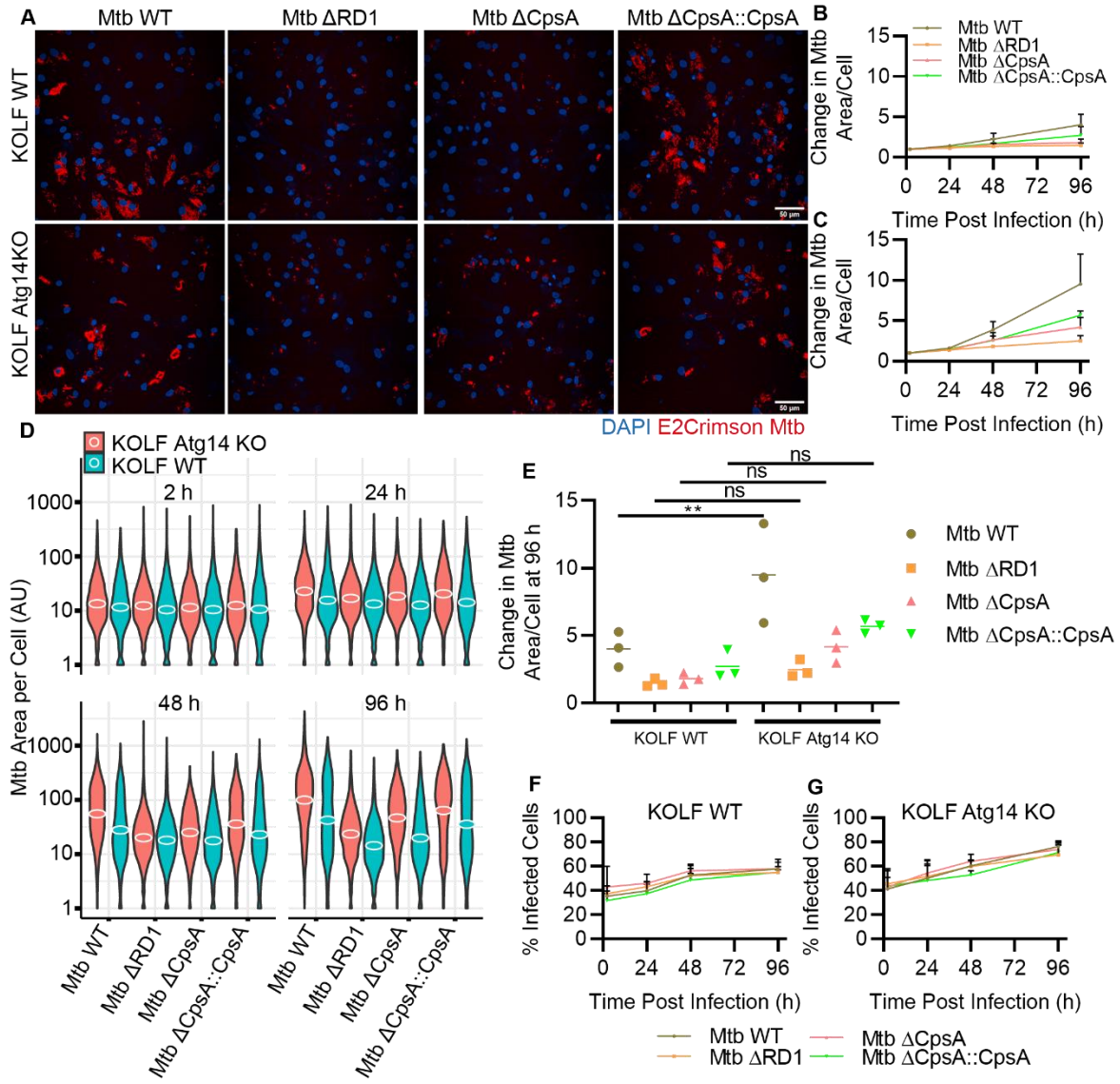

Figure 3.3.14 Mtb replication is enhanced in Atg14 KO iPSDM. KOLF WT and Atg14 KO iPSDM were infected with Mtb WT, Mtb ΔRD1, Mtb ΔCpsA or Mtb ΔCpsA::CpsA for 2 h, 24 h, 48 h or 96 h and Mtb replication analysed by confocal microscopy. **A.** Representative confocal fluorescence images at 96 h post infection. Scale bar 50 µm. **B&C.** Quantification of the change in Mtb area per cell, relative to uptake, in WT (**B**) or Atg14 KO (**C**) iPSDM. Data are mean + SD of 3 biological replicates. **D.** Violin plot of Mtb area per cell from 1 biological replicate, representative of 3. White circles represent the mean Mtb area per cell for each condition. **E.** Plot of the change in Mtb area per cell at 96 h, relative to uptake for the 3 biological replicates shown in **B&C**. Line represents the mean of each condition, each point represents one biological replicate. Data analysed by one way ANOVA and Holm-Sidak's multiple comparison, ns not significant, ** p<0.01. **F&G.** Percentage of infected cells at each time point for WT (**F**) and Atg14 KO (**G**) iPSDM. Data are mean + SD of 3 biological replicates.

In conclusion, data presented in this chapter revealed that the LAP mediated restriction of Mtb ΔCpsA observed in BMDM by (Köster et al., 2017) was not recapitulated in human macrophages. Moreover, genetic dissection of autophagy through two specific Atg knockouts revealed that blockade of all LC3 lipidation dependent autophagic process had no effect on Mtb replication but a potential autophagy independent role for Atg14 in restricting Mtb replication was identified.

4. Discussion

4.1 iPSDM as a human macrophage model for studying Mtb infection

The study of human macrophage-Mtb interactions has largely been hampered by the lack of a scalable, genetically tractable source of karyotypically normal, primary-like human macrophages (Bussi and Gutierrez, 2019). Whilst hMDM and cell lines such as THP-1, alongside studies in mouse macrophages, have enabled the dissection of certain key aspects of these interactions, neither provides the opportunity for reverse genetics in fully functional human macrophages, or the generation of specialised tissue-resident like macrophages. Herein, I have established and utilised iPSDM to overcome some of these limitations revealing previously unknown dynamics and roles of the canonical and non-canonical autophagy pathways during Mtb infection.

The establishment of iPSDM production (**Figure 3.1.1**) yielded large numbers of macrophages week-on-week enabling reproducible, large scale experiments. The macrophages expressed classical markers by FACS, such as CD11b, CD86 and CD119 on their surface and mRNA for these and other markers, such as CD14, CD16 and CD68, were also detected by RNA-seq (**Figure 3.1.2**), consistent with previous reports in human macrophages (Lerner et al., 2017; Schulz et al., 2019). Importantly, reads for stem cell markers were largely absent indicating thorough, pure differentiation. As previously reported, iPSDM expressed the transcription factor RUNX1 but not Myb, indicative of an ontogeny similar to tissue resident macrophages (Buchrieser et al., 2017).

iPSDM were able to support the intracellular replication of Mtb WT, whilst restricting the replication of Mtb ΔRD1 (**Figure 3.1.4**), as happens in other human macrophage models (Lerner et al., 2017). IFN-γ, a potent activator of macrophages (Nathan et al., 1983), that is important for control of Mtb infection in mouse macrophages (Gutierrez et al., 2004a; Flesch and Kaufmann, 1987) as well as for protecting against mycobacterial infection in humans (Bustamante et al., 2014), was unable to

restrict the replication of Mtb WT in iPSDM. These data are in agreement with a recent study in iPSDM (Nenasheva et al., 2020) as well has previous studies with hMDM (Douvas et al., 1985; Lerner et al., 2017), where IFN-γ treatment had no effect on or marginally increased Mtb replication. The reason for this apparent species-dependent difference may be several fold. IFN-γ stimulation markedly alters the transcriptional and functional landscape of macrophages (Ehrt et al., 2001; Nathan et al., 1983) and the human and mouse genomes encode different interferon responsive genes, e.g. IRGs (Hunn et al., 2011). Many of the proteins encoded by these genes have unknown functions and could potentially be implicated in the restrictive effect of IFN-γ in mouse macrophages. Mtb infected human macrophages have also been shown to be refractory to induction of transcriptional changes following IFN-γ treatment (Ting et al., 1999). Mouse macrophages induce iNOS expression and NO production following LPS and IFN-γ stimulation (Kamijo et al., 1994; Gross et al., 2014) and the production of NO is capable of restricting Mtb replication (Chan et al., 1992). However, human macrophages either do not induce iNOS expression and NO production following IFN-γ and LPS treatment due to epigenetic silencing (Gross et al., 2014) or any NO produced is insufficient to restrict Mtb (Rich et al., 1997; Aston et al., 1998) (**Figure 3.1.3**). Thus, an important effector of IFN-γ mediated restriction of Mtb in mouse macrophages, NO (Ehrt et al., 2001), is not active in the human system. The production of Type I IFN generates macrophages that are resistant to IFN-γ mediated restriction of Mtb replication and this may play a role in this *in vitro* system (Lienard et al., 2016). Additional studies probing the effect of treatment of iPSDM with IFN-γ before infection will be useful in determining if pre-activated human macrophages are more capable of restricting Mtb replication, however no difference was observed in hMDM (Lerner et al., 2017).

Cytosolic access of Mtb WT was observed within 2 h post infection and proceeded to become the dominant subcellular location of Mtb in iPSDM after 48 h of infection (**Figure 3.1.5**). This early cytosolic access is observed in other human *in vitro* models, including macrophages, dendritic cells and endothelial cells (van der Wel et al., 2007; Simeone et al., 2012; Lerner et al., 2016). The iPSDM show a greater proportion of cytosolic bacteria at early time points than seen in other models;

however, hMDM and lymphatic endothelial cells show approximately 50% and 75% of Mtb in the cytosol at 48 h respectively (Lerner et al., 2016, 2017), which is more similar to what is seen in iPSDM. The reasons behind the high level of early cytosolic access are unknown, and warrant further investigation. It is important to note, that EM requires chemical fixation and some membranes could be altered by this process. It is therefore possible that the proportion of bacteria in the cytosol could be either under- or over- estimated in some conditions. The definitive proof will come from high pressure freezing studies, which allow for better membrane preservation (Tsang et al., 2018), but these approaches are currently not possible because of the lack of these technologies in BSL3 laboratories. Importantly, we do not know the precise proportion of cytosolic bacteria in macrophages within the lungs of patients with TB thus it is not possible to conclude which model most accurately reflects what is seen in macrophages in, for example, granulomas. The increasing proportion of cytosolic bacteria over time could be explained by either continuous phagosome damage and escape of more bacteria, or preferential replication of bacteria following cytosolic access, as has been observed in hLEC (Lerner et al., 2020). Whilst recruitment of Gal8 to Mtb WT at 24 h and 48 h after infection is observed (**Figure 3.2.1**), providing evidence of continuing phagosome damage, the relatively low percentage is unlikely to account for the large increase in the proportion of cytosolic bacteria. Evidence that the cytosol may support enhanced replication of Mtb comes from a study in hLEC whereby smuggling of Mtb ΔRD1 into the cytosol by coinfection with Mtb WT leads to increased replication and cording of the attenuated mutant (Lerner et al., 2020). Indeed, for other intracellular pathogens such as *Salmonella*, cytosolic access leads to increased bacterial replication (Knodler et al., 2010; Malik-Kale et al., 2012) and it has recently been reported that cytosolic *Salmonella* have greater access to nutrients (Roder et al., 2020). The response of Mtb to successful cytosolic access at the transcriptional and metabolic level is yet to be fully understood and is an area that requires significant tool development to explore.

One important question that remains to be answered is which environments promote Mtb re-localisation into the cytosol? Additionally, what is the stimulus that triggers Mtb to attempt cytosolic access rather than hide in the maturation-arrested

phagosome? Whilst much work is still required to establish when ESX-1 transcription, translation and activation occur *in cellulo* it is known that the system is functional in conventional culture conditions in broth (Chen et al., 2013). Interestingly, the PhoPR system, which regulates several key ESX-1 genes (Kumar et al., 2016; Frigui et al., 2008), is activated by low pH *in vitro* (Abramovitch et al., 2011). Mtb with mutations or loss of PhoP are unable to secrete ESAT-6 due to loss of expression of key components of the secretion system (Ryndak et al., 2008). Thus, in response to the low pH of the lysosome transcription of key ESX-1 components should be upregulated, and thus ESAT-6 secretion, should theoretically be enhanced however direct proof of this is missing. Although an acidic pH enhances the membrane damaging function of ESAT-6 *in vitro* (De Jonge et al., 2007), this is not required in THP-1 macrophages infected with *M. marinum* (Conrad et al., 2017) and neutralising lysosomal pH enhances cytosolic access in RAW264.7 mouse macrophages infected with Mtb (Simeone et al., 2015). The loss of LTR association with Mtb *in cellulo* in both mouse macrophages (Schnettger et al., 2017) and iPSDM (**Figure 3.1.6**) suggests that Mtb is able to damage phagosomal membranes following phagosome maturation and potentially acidification. In iPSDM, some bacteria in intact compartments that retained LTR were able to cause leakage of LTR staining that did not re-accumulate during the time course of the experiment. This suggests that these bacteria have successfully escaped from the phagolysosome or, if the membrane has been repaired, the phagosome or autophagosome does not mature. The presence of bacteria that underwent multiple rounds of LTR accumulation and leakage suggests that Mtb can return to intact membrane bound compartments in iPSDM. The mechanisms implicated in the dynamics of phagosome repair and recapture of cytosolic bacteria in human macrophages warrants further study, however ESCRT mediated repair (López-Jiménez et al., 2018; Mittal et al., 2018), Rab20 mediated endosomal fusion (Schnettger et al., 2017), and autophagy (Kreibich et al., 2015) may all play a role. Because some bacilli eventually remain LTR negative, this implies Mtb is able to subvert, potentially through subsequent rounds of membrane damage, this repair and/or recapture to reside in a non-acidified environment. Meanwhile, those bacteria

that accumulate and retain LTR likely represent a subset of bacilli that are unable to arrest phagosome maturation or damage the phagosomal membrane, potentially due to being in a different metabolic or replicative state.

As well as providing a model capable of reflecting many well-known and established findings in the context of Mtb-human macrophage interactions, iPSDM have the ability to open new avenues and uncover novel biology. Through co-culture of iPSDM with cell types relevant to the tissue niche of interest – either *in vitro* or *in vivo* – it is possible to induce differentiation to a more tissue resident like state (Takata et al., 2017; Haenseler et al., 2017). Moreover, the potential for use of macrophages differentiated from patient derived iPSC to study the mechanisms of inherited susceptibility to diseases and infections will help uncover the underlying cause, as has already been done with IFN-γ receptor polymorphisms (Neehus et al., 2018; Haake et al., 2020). The relative ease of genome engineering in these cells has the potential to facilitate studies requiring genetic knock-in or knockout (Härtlova et al., 2018; Lee et al., 2020; Hall-Roberts et al., 2020) (**Figure 3.3.3**) that, to date, have not been feasible in primary human macrophages; an important aspect that is discussed further below. Combining these technologies with recently developed models, such as the lung on a chip (Thacker et al., 2020), provides an exciting opportunity to investigate the interaction of Mtb with multiple cell types in more physiologically relevant conditions.

There are, of course, disadvantages to the use of iPSDM. The process of differentiation is expensive, especially given the large volumes and high concentration of M-CSF containing media required, hence making it difficult to do all experiments in multiple genetic backgrounds or with multiple clones. Recent developments have facilitated cost reductions, as well as more definition of media components (Vaughan-Jackson et al., 2020), and further cost reductions are likely to come as the technology develops. Whilst it is possible to produce very high yields of iPSDM each week – in the order of $1x10^7$ per T225 cm^2 flask – this requires time consuming tissue culture and this must be considered when considering the feasibility of experiments.

4.2 The ESX-1 T7SS dependent transcriptional response of human macrophages to Mtb infection

The use of RNA-seq approaches has significantly improved our understanding of cellular responses to stimuli over recent decades. However, the majority of studies into the macrophage response to Mtb infection have used microarrays to study the transcriptional landscape (Silver et al., 2009; Chaussabel et al., 2003). The major disadvantage of this approach is that it is limited to the pre-selected transcripts in the microarray and may miss novel transcripts as well as having a smaller dynamic range and decreased sensitivity. Thus, our study is one of the first to use bulk RNA-seq analysis to identify RD1 dependent changes in the human macrophage transcriptome. This RD1 dependent signature is likely the result of the action of the ESX-1 T7SS as loss of the RD1 region results in the loss of essential components of this complex (Pym et al., 2002; Majlessi et al., 2005; Brodin et al., 2006). iPSDM displayed a common response to infection with both Mtb WT or Mtb ΔRD1 at 2 h of infection (**Figure 3.1.8**). A novel but clear ESX-1 dependent signature became apparent at 48 h post infection (**Figure 3.1.10**).

As expected, the initial response of iPSDM to Mtb infection, either with virulent Mtb WT or the attenuated mutant Mtb ΔRD1, is to upregulate immune sensing and defence pathways in order to combat the infection (**Figure 3.1.8**). This largely reflects the response observed in hMDM and human alveolar macrophages infected with Mtb WT where the top activated pathways were related to the immune response (Papp et al., 2018). Some of the most highly upregulated pathways include TNF-α signalling, which is important for Mtb defence *in vivo* (Flynn et al., 1995), and transduction of signals following PRR ligation such as TLR and NF-κB signalling.

The absence of a differential response to Mtb WT and Mtb ΔRD1 at 2 h was initially surprising. Given that Mtb WT has elicited membrane damage (**Figure 3.2.1**) and translocated into the cytosol (**Figure 3.1.5**) by this time point, it was predicted that a differential transcriptional response may be evident. For example, cytosolic Mtb will activate different PRRs e.g. through cytosolic DNA and RNA sensing (Watson et al., 2015; Cheng and Schorey, 2018), and thus elicit an altered transcriptional response.

It is possible that this time point is too early to see some of these changes and any subtle differences may be masked by the activation of similar signalling pathways by other PRRs. It also suggests that responses elicited through extracellular recognition of Mtb do not diverge due to the loss of RD1. Indeed, other RNA-seq studies comparing the response of hMDM to infection with Mtb WT, heat killed Mtb or attenuated mycobacteria such as *M. bovis* BCG and *M. smegmatis* have shown that the transcriptional response is largely driven by antigens rather than strain specific virulence factors (Blischak et al., 2015). However, as we report here, Blischak et al., also observed a greater transcriptional dysregulation in cells infected with virulent, rather than killed or attenuated mycobacteria and were able to identify genes only showing altered transcription following infection with virulent Mtb at 18 h and 48 h after infection.

A major signalling pathway activated in the iPSDM at both 2 h and 48 h post infection was IFN signalling (**Figure 3.1.9**), likely through the action of Mtb induced secretion of IFNs, including IFN-α (**Figure 3.1.11**), on the macrophages. Indeed, IFN signalling was more activated in Mtb WT than Mtb ΔRD1 infected iPSDM at 48 h, tallying with the increased concentration of IFN-α in the supernatant of Mtb WT infected iPSDM. IFN signalling, from both Type I and II IFN, is a transcriptional signature seen in patients with active TB (Berry et al., 2010). The action of Type I IFN has been demonstrated to have both beneficial and detrimental impacts on the outcome of Mtb infection, overall hyper activation of Type I IFN secretion and signalling is likely to be harmful to the host (Moreira-Teixeira et al., 2018), potentially through driving the expression of IL-1 receptor antagonist (IL-1Ra) to block the action of IL-1β, an important cytokine in TB infection (Ji et al., 2019). Type I IFN signalling in macrophages has been linked to induction of a regulatory macrophage phenotype that are unable to restrict Mtb replication (Lienard et al., 2016) and induction of macrophage cell death (Zhang et al., 2020a). Thus, the identification of RD1 dependent Type I IFN secretion (**Figure 3.1.11**) and IFN signalling (**Figure 3.1.10**) in iPSDM recapitulates a well-known response to Mtb infection.

Dysregulated protein ubiquitination was observed at 48 h post infection with Mtb WT (**Figure 3.1.12**). In addition to its role in xenophagy targeting (Fujita et al., 2013), ubiquitination of *Salmonella* recruits the proteasome to the bacterial surface to restrict its replication (Perrin et al., 2004). Moreover, protein ubiquitination is important for modifying the proteome through proteasomal degradation, modulating endosomal sorting and modifying protein function (Komander and Rape, 2012). Alterations in multiple post-translational modifications have been observed in primary mouse macrophages infected with Mtb and multiple other pathogens (Budzik et al., 2020; Johnson et al., 2020). Differentially ubiquitinated proteins identified included many involved in the immune response such as Clec4e, Il1b, Nos2 and Ifit1, as well as proteins important for autophagy (Budzik et al., 2020). When comparing protein ubiquitination in Mtb WT and Mtb ΔESX-1 infected macrophages, proteins in macroautophagy, lysosome function, defence response and regulation of innate immunity were all altered more in Mtb WT infected macrophages (Johnson et al., 2020). It will be important and interesting to determine which proteins are differentially ubiquitinated in the iPSDM following Mtb infection as well as the effect this has on their abundance and function. Further, some of these ubiquitinated proteins are likely to be important for xenophagic targeting through autophagy receptor recruitment and thus will enhance our understanding of how ubiquitin regulates selective autophagy.

EIF2 signalling is an important component of the stress response and reprograms the transcriptional and translational landscape to cope with cellular stress as well as being important for the assembly of stress granules (Pakos-Zebrucka et al., 2016). Therefore, its predicted inactivation following 48 h of Mtb WT infection was very interesting (**Figure 3.1.9**). For instance, EIF2 signalling is important for NF-κB signalling and changes in translation, for example the increased production of pro-inflammatory cytokines, and this is inhibited by the *Yersinia* effector YopJ (Shrestha et al., 2012). Macrophages in Mtb lesions in mice show increased staining for phosphorylated EIF2α, which is required for stress induced transcriptional and translational changes, due to induction of ER stress (Seimon et al., 2010).

Over time, Mtb WT infected iPSDM increased the number of DEGs, whereas this was decreased in Mtb ΔRD1 infected macrophages (**Figure 3.1.7**). Overall, this suggests that macrophages infected with Mtb ΔRD1 are transcriptionally switching to a more resting-like state by 48 h after infection whereas Mtb WT infected macrophages remain activated. This response translates as, for example, sustained activation of immune signalling pathways and pro-inflammatory cytokine transcription and secretion in Mtb WT infected macrophages (**Figure 3.1.11**). These observations are in agreement with microarray data showing that Mtb H37Rv is able to induce stronger pro-inflammatory responses in human alveolar macrophages when compared with attenuated Mtb H37Ra, which has mutations in the PhoP subunit of two component systems that are required for virulence (Silver et al., 2009; Zheng et al., 2008). Many of the pro-inflammatory cytokines and chemokines detected play an important role during TB disease. IL-1α and TNF-α are both important for protection against TB, whereas increased IFN-α appears to play a detrimental role in disease progression (Flynn et al., 1995; Di Paolo et al., 2015). Many of these cytokines, including IL-6, have previously been shown to be secreted by hMDM following Mtb infection (Giacomini et al., 2001).

In iPSDM infected with Mtb ΔRD1, the 48 h pathway analysis revealed changes in transcripts for proteins involved in lipid metabolism (**Figure 3.1.9**). These transcripts mapped to pathways including cholesterol biosynthesis and LXR/RXR activation. The lipidomic profile of human macrophages infected with Mtb WT shows increased triacylglycerols and sterols after 96 h of infection (Greenwood et al., 2019). Moreover, host cholesterol consumption by Mtb is implicated in bacterial dormancy (Pandey and Sassetti, 2008), thus the observed transcriptional response to Mtb ΔRD1 infection may be linked to replenishing cholesterol consumed by the bacilli. Importantly, cholesterol metabolic pathways were also altered in Mtb WT infected cells at 48 h post infection and these pathways were not differentially affected by RD1 dependent responses. Transcriptional profiling alone is insufficient to determine the changes in lipid profiles, thus a full lipidomic analysis is required to validate these hypotheses.

Going forward, it will be important to investigate the importance of these pathways during Mtb infection through biochemical analysis. Proteomic analysis of post-translational modifications, as performed in mouse macrophages (Budzik et al., 2020), will aid in the identification of novel ubiquitinated proteins for further investigation. With respect to EIF2 signalling, the changes in pathway activity will need formal validation for example by Western blot of relevant transcripts and proteins. Next mechanisms and consequences of this altered activation can be deciphered, potentially through genetic manipulation of the pathway.

4.3 Mtb effectively avoids xenophagic capture

For bacterial pathogens such as *Salmonella* the recruitment of galectins, especially Gal8, is intimately linked with efficient targeting to xenophagy to prevent cytosolic access (Thurston et al., 2012). Meanwhile, for professional cytosol dwelling pathogens like *Listeria* and *Shigella*, these damaged membranes can be shed to escape successful xenophagy (Mitchell et al., 2015; Dupont et al., 2009). In the context of Mtb infection, Gal8 is recruited in both mouse macrophages and hLEC (Schnettger et al., 2017; Lerner et al., 2018) and mediates the recruitment of autophagy receptors including TAX1BP1 following membrane damage (Bell et al., 2020). However, given that successful cytosolic localisation is observed in human but not mouse macrophages (Lerner et al., 2017; Schnettger, 2016) it is important to understand the dynamics of membrane damage and subsequent autophagy activation in human experimental systems.

Experiments in chemically fixed cells showed that membrane damage predominantly occurs at 2 h after infection in iPSDM but also continues at least over the first 48 h (**Figure 3.2.1**), as has been previously reported in other cellular models (Lerner et al., 2018; Schnettger et al., 2017; Bell et al., 2020). Interestingly, we identified a small subset of Mtb ΔRD1 that also colocalised with Gal8, which has not been observed in human macrophages before. It is possible this is due to the presence of PDIM in this Mtb ΔRD1 strain, whereas previous strains used were PDIM negative. As Mtb ΔRD1 was not found in the cytosol of iPSDM (**Figure 3.1.5**), any membrane damage that does occur likely is efficiently repaired to prevent translocation of Mtb

ΔRD1 into the cytosol. This implies that Mtb WT may block host-dependent repair pathways, such as the Rab20 mediated fusion of endosomes, which are not disrupted by Mtb ΔRD1 (Schnettger et al., 2017). Indeed, in Rab20 KO macrophages, Mtb ΔRD1 was observed to colocalise with Gal8 suggesting that Mtb ΔRD1 is able to damage membranes, albeit inefficiently, and this damage is efficiently repaired (Schnettger, 2016).

Live cell imaging of EGFP-Gal8 during Mtb infection of iPSDM revealed that within hours of phagocytosis Mtb is able to induce membrane damage that is recognised by EGFP-Gal8. Then, over the course of several hours this EGFP-Gal8 coat is shed in vesicles (**Figure 3.2.2**). Correlative electron microscopy revealed that shedding of the damaged membranes and EGFP-Gal8 coat correlated with cytosolic localisation of the bacilli. Thus, in human macrophages Mtb is able to efficiently shed damaged phagosomal membranes to access the cytosol. One important remaining question is the long-term fate of these phagosomal remnants following shedding from Mtb. Live imaging of iPSDM co-expressing RFP-Gal8 and EGFP-LC3 revealed that LC3 is recruited to these damaged membranes, suggesting a role for autophagy in targeting them for removal (**Figure 3.2.8**), as occurs during *Shigella* infection (Dupont et al., 2009). The shedding of host proteins in this manner is also seen in *Shigella* infection whereby a coat of GBPs, which assemble directly on the bacterial surface to restrict replication and activate pyroptosis (Wandel et al., 2020), is shed following ubiquitination by an E3 ligase secreted by *Shigella* (Wandel et al., 2017).

Live cell imaging of the autophagic targeting of bacteria, or indeed most other large cargoes, is largely absent in the literature. In mouse embryonic fibroblasts infected with *Salmonella* live cell imaging showed the formation of an autophagosome tightly associated to the bacterial surface (Kageyama et al., 2011). Additionally, Ivermectin induced mitophagy leads to the formation of a tight autophagosome around fragmented mitochondria (Zachari et al., 2019). Both of these live imaging experiments show autophagosome formation appearing to complete over timescales in the order of 10 minutes. iPSDM infected with Mtb WT did not show such a simple recruitment of the autophagy machinery following phagosome damage. Instead,

large tubulovesicular autophagosomes, LC3-TVS, formed around the bacteria (**Figure 3.2.8**). These unusual autophagic structures have also been observed in THP-1 cells infected with Mtb (Beckwith et al., 2020). Additionally, various patterns of LC3 recruitment to *M. marinum* in *D. discoideum* have been reported, including coats, patches and dots (Cardenal-Muñoz et al., 2017) with some of these observations resembling our live and fixed cell imaging observations (**Figure 3.2.4 and Figure 3.2.7**). Moreover, during starvation and calcium phosphate precipitate induced autophagy and hepatitis B virus (HBV) infection such LC3-TVS have been observed (Gao et al., 2010; Inoue et al., 2015). In the context of HBV infection, LC3-TVS increase lysosomal delivery and reduce the secretion of virions (Inoue et al., 2015). Finally, during *Plasmodium berghei* infection, autophagy proteins, including LC3, are directed into a tubulovesicular network highly reminiscent of those described here, before being shed as vesicles into the cytoplasm; a process that is important for completion of the liver stage of the parasite lifecycle (Agop-Nersesian et al., 2017). The role of the LC3 positive tubulovesicular structures, which seem to be a general response during infection with various pathogens, will be an interesting area of research.

Our correlative FIB SEM analysis revealed the striking membrane complexity generated following phagosomal damage and autophagy activation. The damaged RFP-Gal8 and EGFP-LC3B positive membranes were highly complex with multiple internal membranes and vesicles (**Figure 3.2.8**). Similar observations were made during FIB SEM analysis of Mtb in THP-1 following Gal3 recruitment (Beckwith et al., 2020) and the damaged *M. marinum* vacuole and recruited autophagy machinery in *D. discoideum* revealed structures very similar to those seen here (López-Jiménez et al., 2018). Moreover, dense membrane structures containing ubiquitinated host and bacterial proteins have been observed in primary mouse macrophages infected with *M. marinum* (Collins et al., 2009). Finally, in BMDM infected with Mtb multi-membrane structures, which were p62 positive, were observed (Schnettger et al., 2017). The multi-membrane nature of these structures, together with the observed membrane damage event prior to their formation strongly suggests this process is linked to xenophagy rather than a form of non-canonical autophagy.

Some of the autophagic compartments generated by Mtb contained organelles such as lipid droplets, suggesting a possible induction of lipophagy (**Figure 3.2.9**). A similar observation has previously been reported in *D. discoideum* infected with *M. marinum* (Barisch and Soldati, 2017a), suggesting lipophagy as a mechanism for trafficking lipid droplets to the *M. marinum* phagosome. Recently, lipid droplets in human macrophages were shown to dramatically change their protein content following immune stimuli, such as LPS treatment, in order to become immune signalling hubs and adopt antibacterial properties (Bosch et al., 2020). Furthermore, lipid droplets serve as a reservoir for accumulation of the antibiotic bedaquiline and can transfer the antibiotic to Mtb (Greenwood et al., 2019). Thus, targeting lipid droplets for autophagic degradation may work to reduce their ability to contribute to immune responses. Whether this targeting of lipid droplets is selective and specific, or the result of them being coincidentally close upon LC3-TVS formation is unknown. Moreover, it is unclear if other organelles can also be wrapped and contained within LC3-TVS.

The ultrastructural analysis of this work showed that Mtb comes into intimate contact with organelles, including lipid droplets, following cytosolic access (**Figure 3.2.9**). Contact between mycobacteria and lipid droplets have been reported previously and are known to contribute a source of lipids that support bacterial growth (Barisch and Soldati, 2017b; Barisch et al., 2015). Mtb has also been shown to contact lipid droplets, and even be localised within them, in human PBMCs (Peyron et al., 2008). The close proximity of Mtb and mitochondria seen here (**Figure 3.2.9**) has not previously been reported and suggests that mitochondria interact with bacteria localised in the cytosol. Whilst cellular metabolism (Pisu et al., 2020) and mitochondrial function (Abarca-Rojano et al., 2003) are altered following Mtb infection, the precise mechanisms behind this are largely unknown and whether direct contact plays a role requires further functional studies. Moreover, direct contact of Mtb with the plasma membrane is reported to induce damage and cell death (Beckwith et al., 2020), thus Mtb-mitochondrial contact may damage the mitochondrial membrane leading to alterations in cellular metabolism and possibly induction of mitophagy. Indeed, infection of macrophages with Mtb H37Rv but not

the attenuated strain Mtb H37Ra leads to increased cytochrome c release in macrophages, (Abarca-Rojano et al., 2003). As release of cytochrome c requires permeabilisation of the mitochondrial outer membrane (Garrido et al., 2006) it is possible that Mtb-mitochondrial contact could disrupt the mitochondrial membrane to facilitate this release and induce apoptosis.

The formation of such large membranous structures containing internal membranes (**Figure 3.2.8**) is likely to require an influx of membrane from sources other than the phagosome or *de novo* membrane synthesis. There are several potential sources for this membrane e.g. endosomes, lysosomes and the ER. As a large, widely distributed organelle the ER is a likely candidate as a membrane source. During autophagosome biogenesis, Atg2 transfers lipids from the ER into the growing autophagosome (Maeda et al., 2019; Valverde et al., 2019; Tang et al., 2019) and Atg9 distributes them between the inner and outer leaflets (Matoba et al., 2020; Maeda et al., 2020). *De novo* autophagosome biogenesis following pathogen mediated vacuolar rupture has been reported during *Salmonella* infection of epithelial cells (Ravenhill et al., 2019). Thus, assuming some of the observed LC3-TVS are the result of autophagosome formation, it is likely Atg2 mediated lipid transfer from the ER provides lipids for the expansion of these membranes. The biochemical analysis of LC3-TVS by (Gao et al., 2010) revealed membrane trafficking proteins were associated with these structures, including Rab5 and Rab7, which are important for endosome and lysosome fusion. Assuming these structures are similar to those observed during Mtb infection, it is possible that endosomal fusion provides membranes to the growing LC3-TVS.

Over the course of the live cell imaging experiments, the LC3 positive membranes shed from the bacteria disappeared (**Figure 3.2.4**). This could be explained by de-lipidation of LC3 from the membrane, as happens during *Legionella* infection through the action of the effector RavZ (Choy et al., 2012), or Atg4 activity during other canonical autophagy processes (Kauffman et al., 2018; Agrotis et al., 2019). However, as these LC3 positive membranes consist of LC3 conjugated to lipids in both the outer and inner membrane it is unlikely that de-lipidation alone can explain

the loss of EGFP signal. Given that EGFP is quenched in acidic environments it is tempting to speculate that these damaged membranes fuse with lysosomes for degradation. Indeed, during live cell imaging with LTR, large, acidified membranous vacuoles – reminiscent of these LC3 positive vacuoles – appeared adjacent to some bacteria (**Figure 3.1.6**). Thus, it is likely that damaged phagosomal remnants are targeted for lysosome mediated degradation through the autophagy pathway as observed during *Shigella* infection of epithelial cells (Dupont et al., 2009). Further live cell imaging experiments, for example with a GFP-RFP-LC3B reporter (Kimura et al., 2007) or EGFP-LC3B and a lysosomal marker such as LTR would be helpful here. Live imaging with the GFP-RFP-LC3B flux reporter was attempted during this thesis work, however relatively rapid bleaching of the RFP fluorophore made it difficult to conclude if the LC3-TVS acidify or not.

An interesting idea raised by the data presented in Chapter 2 is that Mtb may block the completion of the formation of the autophagosome. For example, bacteria that were completely coated by LC3 in fluorescence microscopy did not have a complete double membrane around them when examined by FIB SEM (**Figure 3.2.9**). It is not possible to rule out these gaps being due to artefacts introduced by the chemical fixation and EM processing. How Mtb might block closure of autophagosomes is unknown. However, Mtb is known to block the action of the ESCRT machinery through secretion of EsxG and EsxH (Mehra et al., 2013; Mittal et al., 2018) and the ESCRT machinery is required for autophagosome closure (Takahashi et al., 2018; Zhou et al., 2019; Zhen et al., 2020). Therefore, it is possible that local secretion of these proteins blocks the action of the ESCRT machinery in closing the autophagosome and inhibiting efficient targeting of Mtb by xenophagy.

As well as potentially blocking autophagosomal closure it is likely that Mtb secretes other, unknown factors to facilitate the shedding of the membranes. Unlike *Shigella* and *Listeria*, which polymerise actin at their poles in order to move within and between cells, Mtb is non-motile and therefore cannot actively move away from the damaged phagosome or forming autophagic membranes. In the case of *Listeria* it is the secretion of the phospholipase PlcA and the actin assembling protein ActA that

are important for xenophagy evasion after vacuolar rupture (Mitchell et al., 2015). It would be interesting to identify if there are Mtb factors required for the successful shedding of LC3 positive membranes, and if so the potential host targets.

The fate of Mtb following escape from autophagic targeting and cytosolic access was not examined here but requires follow up work. It would be interesting to determine if, following escape, the bacteria are able to replicate more efficiently than those that do not damage membranes and remain inside the phagosome. Whilst this was attempted, the relatively low expression of EGFP-LC3B in the stably transduced macrophages meant high laser powers were required and bacterial replication over several days could not be observed. It will be important to generate new stable EGFP-LC3B lines using a stronger promoter, such as CMV, to facilitate these experiments.

Finally, it would be interesting to determine if a stimulus prior to infection, such as rapamycin or IFN-γ, may increase the efficiency and effectiveness of xenophagic targeting. If so this could still make xenophagy an interesting target of host-directed therapies.

4.4 Role of membrane tubulation in the membrane damage response

In addition to the large tubular and vesicular autophagic structures that displayed a degree of stability lasting several hours, more transient EGFP-LC3B tubulation events were also observed (**Figure 3.2.4**). Some of these tubules were very thin and extended over several microns before either retracting or disconnecting. Such tubulation events have been observed in response to other membrane damaging stimuli. In *Staphylococcus aureus* infection the pore forming toxin α-haemolysin has been linked with the formation of large networks of LC3B, Rab7 and Rab1b positive tubules (López de Armentia et al., 2017). The formation of these tubules requires microtubules and the motor protein kinesin 1 suggesting some force generation by this motor may be involved in elongating the membrane. Whether these have a role in the formation of tubules during Mtb infection warrants further investigation. Additionally, following lysosomal damage by LLOMe, the kinase LRRK2 regulates

the microtubule and motor protein dependent formation of tubules from damaged lysosomes, which get scissioned to form vesicles that go on to contact other lysosomes, potentially as a mechanism of membrane recycling (Bonet-Ponce et al., 2020). Moreover, calcium phosphate precipitate induced endosomal damage is associated with LC3 tubule formation (Chen et al., 2014). Overall, data presented here combined with the literature suggests a role for membrane tubulation during the endomembrane damage response that requires further study.

The observed membrane tubulation may be as a result of attempts by the cell to repair the damage. It is plausible that following membrane rupture the tubules form to remove the pore forming toxins from the main organelle in order to restore membrane integrity and functioning of the organelle. For example, in the context of lysosomal damage removing the holes or pores and resealing the membrane would facilitate the restoration of a proton gradient and acidification. Alternatively, components of the autophagy machinery have been reported to seal damaged membranes during *Salmonella* infection (Kreibich et al., 2015), and whilst this did not involve tubulation there could be similar mechanisms operating here.

Tubulation of autophagic membranes also occurs during autophagic lysosome reformation (ALR) (Yu et al., 2010). As the terminal step of autophagy involves fusion with lysosomes, it is important to regenerate new lysosomes for continued degradation of endocytic and autophagic cargoes. This can be achieved through ALR, whereby Kinesin 1 dependent production of tubules from autolysosomes leads to the formation of small proto-lysosomes, which acidify and acquire degradative properties (Du et al., 2016; Yu et al., 2010). These tubules may be different to those observed in (Bonet-Ponce et al., 2020) as ALR tubules are LAMP-1 positive, whereas those induced by LLOMe treatment appear to be negative for the endolysosomal protein LAMP-1. The tubules observed during ALR are highly reminiscent of the thin, highly dynamic EGFP-LC3B tubules seen emerging from the large, more stable LC3-TVS (**Figure 3.2.4**) as well as those seen in (López de Armentia et al., 2017). Notably, however, during ALR tubules are LC3 negative, therefore the LC3 tubules observed here likely form independently of ALR and may

be more akin to those observed during LLOMe induced damage to endolysosomes (Bonet-Ponce et al., 2020).

Membrane tubulation has a well described role in sorting cargoes from endosomes (McNally and Cullen, 2018). The Retromer complex, along with sorting nexin and bar domain (SNX-BAR) proteins are important for the formation of these tubules, whether such membrane deforming proteins are required for the formation of EGFP-LC3B tubules warrants further study. Interestingly, BAR domain containing proteins have been proposed to be important for the tubulation of macropinosomes following osmotically driven shrinking (Freeman et al., 2020). Thus, instead of removing damaged membranes, the membrane tubulation observed here could result in the removal of intact membranes and proteins for recycling.

4.5 Mtb ΔCpsA attenuation is autophagy independent in iPSDM

The Mtb protein CpsA is one of 3 proteins of the LCP family encoded by the Mtb genome. Their function in Mtb is mainly associated with the conjugation of arabinogalactan to peptidoglycan during cell wall biosynthesis (Harrison et al., 2016) and mutants lacking rv3267, one of the LCP proteins, but not CpsA show significant growth defects in broth and a double knockout is lethal (Grzegorzewicz et al., 2016). In both mouse and human macrophages, growth of CpsA knockout Mtb is attenuated (Köster et al., 2017) (**Figure 3.3.6**). In mouse macrophages this attenuation has been shown to be due to increased NADPH oxidase recruitment and phagosomal ROS production leading to LAP. However, if this attenuation was due to ROS and LAP was not shown in human macrophages (Köster et al., 2017).

Here, it is shown that NADPH oxidase is retained on the Mtb ΔCpsA phagosome up to 48 h post infection, whereas Mtb WT shows decreased colocalisation as the infection progresses (**Figure 3.3.7**). In primary mouse macrophages, Mtb ΔCpsA recruited NADPH oxidase more efficiently than Mtb WT at 2 h post infection (Köster et al., 2017) however this was not observed in the iPSDM system (**Figure 3.3.7**). Interestingly, this could not be linked to the reported LAP dependent restriction of Mtb ΔCpsA as replication was not rescued in Atg7 KO iPSDM, where both canonical and non-canonical autophagy are disrupted (**Figure 3.3.12**). Additionally, no

changes in LC3-II levels were detected by Western blot of Mtb ΔCpsA infected iPSDM at 2 h post infection, indicating no significant changes in LC3 lipidation (**Figure 3.3.10**). It is possible that no changes are seen due to LC3 lipidation occurring only on a subset of Mtb containing phagosomes in the approximately 40% of infected cells at this time point, thus any changes may be below detection limits of Western blotting on the population level. By 48 h post infection with Mtb ΔCpsA, the levels of p62 and LC3B-II were similar to cells infected with Mtb WT, indicating that CpsA is dispensable for the blockade of autophagic flux by Mtb.

Mtb ΔCpsA is able to induce membrane damage, as indicated by Gal8 recruitment (**Figure 3.3.9**), implying that the ESX-1 secretion system is likely functional in this mutant. It remains to be clarified if this membrane damage is sufficient to facilitate cytosolic localisation, or whether this damage is efficiently repaired leading to phagosomal localisation and the observed growth restriction.

Overall, much of the experimental work to date on LAP has relied on mouse macrophage models including BMDM and RAW264.7 (Martinez et al., 2011, 2015, 2016; Sanjuan et al., 2007; Cunha et al., 2018) as well as murine fibroblasts (Fletcher et al., 2018). The related process of LANDO has also been characterised in mouse macrophages and microglia (Heckmann et al., 2019). It is therefore important to validate these findings relating to LAP in a human macrophage system. There is some evidence for LAP in human monocytes playing a role in protection from liver inflammation (Wan et al., 2020), however it is unclear if the process also applied to fully differentiated macrophages. NADPH oxidase dependent recruitment of LC3 to phagosomes in human macrophages is, however, important for antigen presentation (Romao et al., 2013).

Regarding the Mtb ΔCpsA strain generated here, it will be important to validate the mechanism of its restriction in human macrophages. Firstly, does the increased NADPH oxidase recruitment correlate with increased ROS and does altering NADPH oxidase recruitment rescue Mtb ΔCpsA replication? The activation of NADPH oxidase can be assayed using the phosphorylation status of p40phox and phagosomal ROS measured with probes such as DCFDA. Secondly, is there

increased endogenous LC3 recruitment to Mtb ΔCpsA phagosomes? Thirdly, is Mtb ΔCpsA impaired in its ability to access the cytosol and is it therefore restricted through phagosome maturation? EM studies of Mtb ΔCpsA in iPSDM, combined with confocal microscopy to examine recruitment of phagosome maturation markers such as LAMP-1 will help answer this question. Overall, establishing the mechanism of attenuation of Mtb ΔCpsA will reveal how this protein subverts the macrophage response to enable Mtb survival and replication.

4.6 Autophagy deficient human macrophages display no defects in Mtb control

Disruption of the proper functioning of the autophagy pathway through a variety of genetic knockout approaches significantly enhances Mtb replication in mouse macrophages *in vitro* (Manzanillo et al., 2013; Franco et al., 2016; Watson et al., 2012). Whether knocking out these autophagy genes brings about these effects by directly removing xenophagy or by disrupting other functions of the autophagy pathway that are important for bacterial control is unknown. Moreover, many of the knockouts that have the greatest effect, such as Atg5, will affect both xenophagy and non-canonical autophagy so it could be either pathway that is important for restricting Mtb replication. The situation is further complicated by the fact that most of these knockouts, except Atg5, have no effect *in vivo* as measured by colony forming units (CFU) (Kimmey et al., 2015; Watson et al., 2012; Castillo et al., 2012). Moreover, as previously discussed, the ability of mouse macrophages to reflect events occurring in human macrophages is variable and needs to be considered in this context.

Initially work was carried out in Atg13 KO iPSCs and iPSDM however these were found to have been ineffectively knocked out. Whilst the iPSC are unable to initiate changes in LC3 lipidation in response to starvation or BafA1 treatment, the WT and Atg13 KO iPSDM have similar LC3 processing responses (**Figure 3.3.1**). This cell-type specific response can be explained by an apparent difference in dominant transcripts. Whilst Western blotting of the iPSCs for Atg13 revealed a major band at 60 kDa in the WT cells that was absent in the KO, the WT iPSDM mainly expressed

a 50 kDa version (**Figure 3.3.1**). Interestingly, differentiation of these iPSCs into neurons yielded cells that were still defective in canonical autophagy (Nicholas Ksistakis, unpublished). It remains to be investigated why this truncated, yet apparently fully functional, form of Atg13 is the predominant form in macrophages.

One of the aims of this thesis was to evaluate the role of both canonical and non-canonical autophagy. To this end, Atg7 KO iPSCs were produced as a tool to block all forms of LC3-lipidation dependent autophagy. Validation of the Atg7 KO iPSC revealed, as expected, no Atg7 protein and LC3 processing is severely impaired under resting or starvation conditions (**Figure 3.3.4**). Interestingly, following BafA1 or monensin treatment a faint band of LC3 at 15 kDa could be observed, suggesting that blockade of lysosomal function leads to accumulation of a form of LC3 at this molecular weight. Following macrophage differentiation, the band at 15 kDa, the molecular weight of LC3-II, was observed in all conditions (**Figure 3.3.5**). Given that Atg7 is absolutely required for LC3 lipidation, it is possible this band represents the pro form of LC3, prior to cleavage by Atg4, which also runs at 15 kDa (Agrotis et al., 2019). This could be checked using immunofluorescence for LC3 puncta, however it should be noted that LC3 puncta can form even without LC3 lipidation (Runwal et al., 2019). Importantly, both WT and Atg7 KO iPSC and iPSDM showed a large accumulation of p62, even under resting conditions, due to being unable to degrade the protein by autophagy.

In iPSDM lacking Atg7, there was no detectable LC3 processing after infection with Mtb (**Figure 3.3.11**). There is a significantly larger accumulation of the autophagy receptor p62 in the Mtb WT infected, Atg7 KO iPSDM compared to the WT iPSDM controls, suggesting further blockade of p62 degradation. When examining the RNA-seq data, the expression of p62 was upregulated at 48 h post infection in an RD1 dependent manner. The observed accumulation of p62 is likely due to increased *de novo* synthesis of the protein, which is unable to be degraded by the autophagy pathway.

Atg7 KO cells are capable of forming autophagosomes around NBR1 puncta without lipidation of any Atg8s (Ohnstad et al., 2020). Whether this process of

autophagosome formation is sufficient to selectively target large cargoes, such as Mtb, is unclear. The reported Atg7-independent autophagy relies on the autophagy receptor TAX1BP1 and the kinase TBK1, both of which are involved in xenophagy of Mtb (Bell et al., 2020; Budzik et al., 2020; Watson et al., 2012). Thus, it is important to consider that Mtb targeting to autophagy may not be completely inhibited in Atg7 KO iPSDM and could explain the *in vivo* data (Kimmey et al., 2015).

In vitro, knockdown of Atg7 in BMDM did not alter Mtb replication after 3 days of infection (Köster et al., 2017), however Atg7 knockdown in *ex-vivo* alveolar or peritoneal murine macrophages did increase Mtb replication (Sivangala Thandi et al., 2020). Overall, Köster et al., do not observe large differences in Mtb WT replication upon disruption of the autophagy machinery by KO or KD of several proteins, including Atg5. *In vivo,* mice lacking Atg7 expression in myeloid cells show no alteration in Mtb burden or pathology (Kimmey et al., 2015). Interestingly, Atg7 KO mice were more susceptible to *M. bovis* BCG infection, likely due to increased uptake of mycobacteria (Bonilla et al., 2013). Whilst knockdown of Atg7 in U937 cells decreases maturation of *M. bovis* BCG phagosomes, the authors did not correlate this with an impact on intracellular survival or replication (Singh et al., 2006). In the context of Atg7 independent autophagosome formation (Ohnstad et al., 2020) it is possible that the lack of phenotypes observed in some of these studies could be due to continued autophagic targeting of mycobacteria.

Disruption of the E3 like complex of Atg5-12-16L1 is frequently used to produce models that are defective in all forms of autophagy. Atg5 KO mice and cell lines consistently show an increase in Mtb replication, bacterial burdens and pathology (Castillo et al., 2012; Manzanillo et al., 2013). However, the *in vivo* pathology is mostly due to increased neutrophilic inflammation and is due to an autophagy independent function of Atg5, the mechanism of which is yet to be described (Kimmey et al., 2015). Atg5 is implicated in the induction of apoptosis, independently of its autophagic function (Yousefi et al., 2006). Thus KO of Atg5 may result in a more pro-inflammatory mode of cell death, such as necrosis or pyroptosis, following

Mtb infection thus leading to the observed increase in pathology (Kimmey et al., 2015).

In Atg7 KO iPSDM, Mtb replication was unaffected by autophagy disruption (**Figure 3.3.12**). Whilst this finding requires validation in additional genetic backgrounds and clones, it provides an interesting insight into the possibility that autophagic processes are sufficiently subverted by Mtb that their blockade by Atg7 KO does not enhance the effect. Indeed, Mtb is known to subvert autophagy flux, that process by which autophagosomes fuse with lysosomes for degradation (Chandra et al., 2015). Moreover, data presented here shows that Mtb is able to escape from the forming autophagosome to enter the cytosol (**Figure 3.2.9**). Given the discovery of Atg7 independent autophagy (Ohnstad et al., 2020) it may be necessary to produce iPSDM with KO of both Atg7 and FIP200 to block both LC3 lipidation dependent and independent autophagy to probe the effect on Mtb replication.

4.7 Atg14 restricts Mtb replication in an autophagy independent manner

Specific disruption of canonical autophagy, requiring the *de novo* formation of autophagosomes, whilst leaving non-canonical, single membrane autophagy intact was achieved through knockout of Atg14 (Martinez et al., 2015). Atg14 KO iPSCs and iPSDM do not respond to canonical autophagy stimuli, such as starvation, but are able to activate non-canonical autophagy, for example in response to monensin (**Figure 3.3.4&5**). Following 48 h of Mtb WT infection, no increased LC3 lipidation was seen in the Atg14 KO iPSDM suggesting that the induction of LC3-II is due to canonical autophagy at this time point (**Figure 3.3.13**). Thus, these cells provide a tool to examine the effect of canonical autophagy disruption and the role of non-canonical autophagy during Mtb infection.

To date, limited work has used genetics to specifically examine the role of canonical autophagy in Mtb infection. Mice with a genetic knockout of Atg14 in myeloid cells showed a small, statistically not significant, increase in Mtb burden in the lungs (Kimmey et al., 2015) and a similar pattern was observed in BMDMs (Köster et al., 2017). The *in vivo* analysis was performed using two mice per condition (Kimmey et

al., 2015), increasing this, and thus the statistical power, may reveal a statistically and biologically relevant difference.

Surprisingly, whilst the Atg7 KO macrophages showed no change in Mtb replication, the knockout of Atg14, which disrupts canonical autophagy but leaves non-canonical autophagy intact, led to increased replication of Mtb (**Figure 3.3.14**). Thus, either non-canonical autophagy promotes Mtb growth whilst canonical autophagy is restrictive so blocking both pathways, as in Atg7 KO, leads to no net change or Atg14 has an autophagy independent function in controlling Mtb replication in iPSDM. A role for LAP in establishing a niche for bacterial replication is observed with *L. monocytogenes*, where LAP contributes to the formation of spacious *Listeria* containing phagosomes (SLAPs) (Lam et al., 2013). Bacteria in SLAPs, which appear to be those expressing low levels of LLO, replicate more slowly and establish a persistent infection (Birmingham et al., 2008).

As well as its role in the Vps34 lipid kinase complex and autophagosome biogenesis, Atg14 acts as a tether interacting with the STX17 and SNAP29 t-SNARE on autophagosomes to prime it for VAMP8 binding and fusion (Diao et al., 2015). Atg14 regulates endosome maturation through binding to the fusogenic SNARE effector protein Snapin, and this was independent of its ability to bind to Beclin1 (Kim et al., 2012a). If Atg14 plays a similar role during phagosome maturation in macrophages is unknown but differences in phagosome maturation could explain the higher replication rates of not only Mtb WT but also the small improvement in replication of the attenuated mutants Mtb ΔRD1 and Mtb ΔCpsA. Atg5 and Atg7, thus LC3 lipidation, are not important for phagosome maturation of zymosan particles in murine fibroblasts or primary macrophages (Cemma et al., 2016), thus any effect of Atg14 on phagosome maturation is likely to be independent of autophagosome biogenesis. Whilst this contradicts the findings of (Martinez et al., 2011, 2015; Sanjuan et al., 2007), it is possible this is due to the models used, for example endogenous versus overexpressed LC3.

Further validation of the observed replication phenotype in additional Atg14 KO clones and genetic backgrounds will be important. Following this, it will be interesting

to consider the mechanism behind these observations. Firstly, it will be important to examine if, and how, Atg14 is recruited to phagosomes. Assuming Atg14 is recruited to the phagosome it will be important to confirm this process is not related to autophagy induction e.g. occurring without downstream LC3 lipidation and independently of the formation of the complex with Beclin1 and Vps34. Finally, recruitment of effectors potentially regulating phagosome maturation, such as STX17 and Snapin, should be examined. Should these effectors not prove to be the mediators, a screen to find novel interacting partners, e.g. through proximity biotinylation studies (Rhee et al., 2013), will be informative to define potential autophagy independent Atg14 pathways.

4.8 Conclusions

In this thesis, I set up and validate iPSDM as a new model for studying Mtb-human macrophage interactions, especially at the cell biology level. Through a combination of techniques, including an in-depth RNA-seq study, I reveal their ability to recapitulate previously reported macrophage responses to Mtb infection. This RNA-seq data also revealed a novel, ESX-1 dependent, transcriptional signature at 48 h post infection yielding potentially interesting, virulence associated host pathways for further study.

Through correlative live cell imaging and 3D electron microscopy I uncover a novel rearrangement of the autophagy machinery as a result of phagosome damage by Mtb that correlates with autophagy evasion and cytosolic access by virulent Mtb (**Figure 4.8.1**).

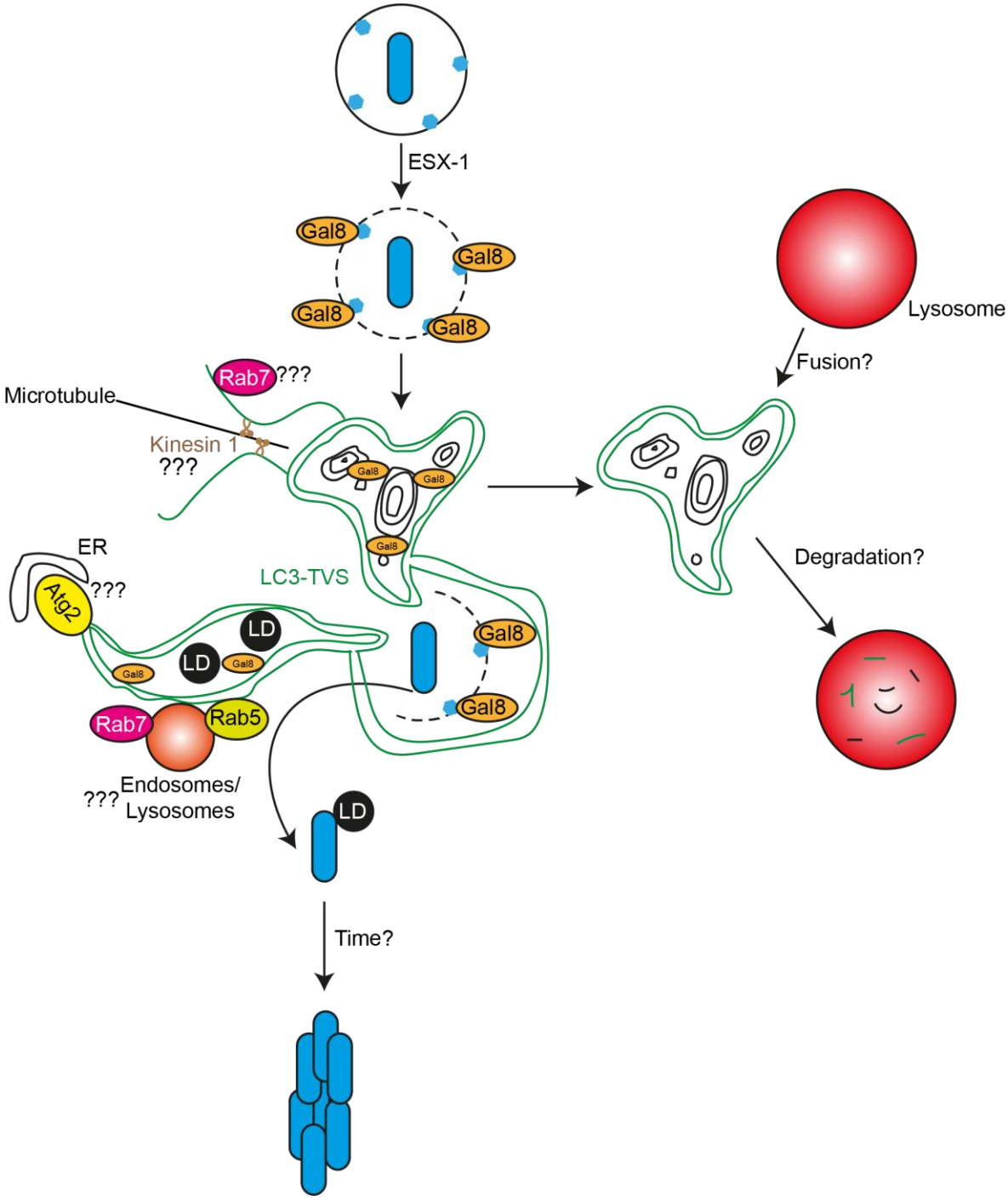

Figure 4.8.1 Model of LC3-TVS formation and xenophagy evasion by Mtb. After recognition of ESX-1 dependent phagosome membrane damage by Gal8, large LC3-TVS are formed, which can contain organelles such as lipid droplets (LD). Potential membrane sources for LC3-TVS include the ER and endosomes and lysosomes. From these LC3-TVS thin, LC3B positive tubules emerge and this may be driven by Kinesin 1 and Rab7. Over time, Mtb dissociates from these LC3-TVS to reside

in the cytosol where it might replicate, whilst the LC3 positive membranes may fuse with lysosomes to be degraded.

Finally, by using the genetic tractability of iPSCs, I produced iPSDM with homozygous knockout of the autophagy proteins Atg7 and Atg14 to disrupt canonical and non-canonical autophagy. Pairing these macrophage knockouts, with Mtb KOs that are unable to block autophagy, I probed the role of these separate arms of the autophagy pathway during Mtb infection. The Mtb mutant ΔCpsA shows restricted replication in iPSDM, however this is not rescued by autophagy disruption through knockout of Atg7 suggesting the restriction is likely mediated by a pathway that is not autophagy. Neither Mtb WT nor Mtb ΔRD1 showered altered intracellular growth in Atg7 KO iPSDM; whereas both these strains and Mtb ΔCpsA showed increased replication upon knockout of Atg14. These findings suggest an autophagy independent role for Atg14 in controlling Mtb replication, potentially through regulating phagosome maturation.

5. Future perspectives

Going forward, there are several questions raised by the work contained in this thesis that are worthy of further investigation.

1. Expansion of the iPSDM model to reflect alternative macrophage subtypes.
2. What are the mechanisms driving LC3-TVS formation and xenophagy evasion by Mtb?
3. What is the mechanism of Atg14 mediated restriction of Mtb replication?

The potential of iPSDM to reflect tissue resident macrophages has already been described for microglia *in vitro* and alveolar macrophages *in vivo*. It would be helpful to determine if *in vitro* co-culture of iPSDM with Type I and II alveolar epithelial cells, the major cell types found in alveoli, was enough to reprogram the iPSDM to better reflect this cell type. Moreover, iPSDM could be incorporated into lung organoids or organs on a chip to examine how they interact with these cell types during infection.

Many questions remain regarding the formation and shedding of LC3-TVS. It would be interesting to identify what host and bacterial effectors are required for their formation and dissociation. A study of the membrane sources required could yield insights into how the large tubules are formed. Moreover, the formation of the thin, transient tubules may be reliant on kinesins and microtubules and this could be studied further.

The mechanism behind Atg14 mediated restriction of Mtb replication in iPSDM may be due to defects in phagosome maturation. Live imaging experiments examining Atg14 localisation during infection will help understand if Atg14 acts at the phagosome. Moreover, rescue of the Atg14 KO iPSC with WT, Beclin1 or Snapin binding deficient mutants of Atg14 (Kim et al., 2012a) would determine which of these interactions is important. Alternatively, studying phagosome maturation by using alternative models, such as latex beads, will help decipher the role of Atg14 in phagosome maturation.

6. References

Abarca-Rojano, E., P. Rosas-Medina, P. Zamudio-Cortéz, R. Mondragón-Flores, and F.J. Sánchez-García. 2003. Mycobacteriurn tuberculosis virulence correlates with mitochondrial cytochrome c release in infected macrophages. *Scand. J. Immunol.* 58:419–427. doi:10.1046/j.1365-3083.2003.01318.x.

Abramovitch, R.B., K.H. Rohde, F.-F. Hsu, and D.G. Russell. 2011. aprABC: a Mycobacterium tuberculosis complex-specific locus that modulates pH-driven adaptation to the macrophage phagosome. *Mol. Microbiol.* 80:678–694. doi:10.1111/j.1365-2958.2011.07601.x.

Ackermann, M., H. Kempf, M. Hetzel, C. Hesse, A.R. Hashtchin, K. Brinkert, J.W. Schott, K. Haake, M.P. Kühnel, S. Glage, C. Figueiredo, D. Jonigk, K. Sewald, A. Schambach, S. Wronski, T. Moritz, U. Martin, R. Zweigerdt, A. Munder, and N. Lachmann. 2018. Bioreactor-based mass production of human iPSC-derived macrophages enables immunotherapies against bacterial airway infections. *Nat. Commun.* 9:5088. doi:10.1038/s41467-018-07570-7.

Aflaki, E., B.K. Stubblefield, E. Maniwang, G. Lopez, N. Moaven, E. Goldin, J. Marugan, S. Patnaik, A. Dutra, N. Southall, W. Zheng, N. Tayebi, and E. Sidransky. 2014. Macrophage models of gaucher disease for evaluating disease pathogenesis and candidate drugs. *Sci. Transl. Med.* 6:1–14. doi:10.1126/scitranslmed.3008659.

Agop-Nersesian, C., M. De Niz, L. Niklaus, M. Prado, N. Eickel, and V.T. Heussler. 2017. Shedding of host autophagic proteins from the parasitophorous vacuolar membrane of Plasmodium berghei. *Sci. Rep.* 7:1–14. doi:10.1038/s41598-017-02156-7.

Agrotis, A., N. Pengo, J.J. Burden, and R. Ketteler. 2019. Redundancy of human ATG4 protease isoforms in autophagy and LC3/GABARAP processing revealed in cells. *Autophagy*. 15:976–997. doi:10.1080/15548627.2019.1569925.

Akimana, C., S. Al-Khodor, and Y.A. Kwaik. 2010. Host factors required for modulation of phagosome biogenesis and proliferation of francisella tularensis within the cytosol. *PLoS One*. 5. doi:10.1371/journal.pone.0011025.

Alasoo, K., F.O. Martinez, C. Hale, S. Gordon, F. Powrie, G. Dougan, S. Mukhopadhyay, and D.J. Gaffney. 2015. Transcriptional profiling of macrophages derived from monocytes and iPS cells identifies a conserved response to LPS and novel alternative transcription. *Sci. Rep.* 5:1–12. doi:10.1038/srep12524.

Alasoo, K., J. Rodrigues, S. Mukhopadhyay, A.J. Knights, A.L. Mann, K. Kundu, C. Hale, G. Dougan, and D.J. Gaffney. 2018. Shared genetic effects on chromatin and gene expression indicate a role for enhancer priming in immune response. *Nat. Genet.* 50:424–431. doi:10.1038/s41588-018-0046-7.

Andersson, A.-M., B. Andersson, C. Lorell, J. Raffetseder, M. Larsson, and R.

Blomgran. 2016. Autophagy induction targeting mTORC1 enhances Mycobacterium tuberculosis replication in HIV co-infected human macrophages. *Sci. Rep.* 6:28171. doi:10.1038/srep28171.

Andreu, N., J. Phelan, P.F. de Sessions, J.M. Cliff, T.G. Clark, and M.L. Hibberd. 2017. Primary macrophages and J774 cells respond differently to infection with Mycobacterium tuberculosis. *Sci. Rep.* 7:42225. doi:10.1038/srep42225.

Armstrong, J.A., and P. D'Arcy Hart. 1975. Phagosome-Lysosome Interactions in Cultured Macrophages Infected with Virulent Tubercle Bacilli. *J. Exp. Med.* 142.

Aston, C., W.N. Rom, A.T. Talbot, and J. Reibman. 1998. Early inhibition of mycobacterial growth by human alveolar macrophages is not due to nitric oxide. *Am. J. Respir. Crit. Care Med.* 157:1943–1950. doi:10.1164/ajrccm.157.6.9705028.

Atri, C., F.Z. Guerfali, and D. Laouini. 2018. Role of human macrophage polarization in inflammation during infectious diseases. *Int. J. Mol. Sci.* 19. doi:10.3390/ijms19061801.

Augenstreich, J., A. Arbues, R. Simeone, E. Haanappel, A. Wegener, F. Sayes, F. Le Chevalier, C. Chalut, W. Malaga, C. Guilhot, R. Brosch, and C. Astarie-Dequeker. 2017. ESX-1 and phthiocerol dimycocerosates of Mycobacterium tuberculosis act in concert to cause phagosomal rupture and host cell apoptosis. *Cell. Microbiol.* 19:1–19. doi:10.1111/cmi.12726.

Augenstreich, J., E. Haanappel, G. Ferré, G. Czaplicki, F. Jolibois, N. Destainville, C. Guilhot, A. Milon, C. Astarie-Dequeker, and M. Chavent. 2019. The conical shape of DIM lipids promotes Mycobacterium tuberculosis infection of macrophages. *Proc. Natl. Acad. Sci. U. S. A.* 116:25649–25658. doi:10.1073/pnas.1910368116.

Augenstreich, J., E. Haanappel, F. Sayes, R. Simeone, V. Guillet, S. Mazeres, C. Chalut, L. Mourey, R. Brosch, C. Guilhot, and A. Catherine. 2020. Phthiocerol dimycocerosates from Mycobacterium tuberculosis increase the membrane activity of bacterial effectors and host receptors. *bioRxiv*.

Axe, E.L., S.A. Walker, M. Manifava, P. Chandra, H.L. Roderick, A. Habermann, G. Griffiths, and N.T. Ktistakis. 2008. Autophagosome formation from membrane compartments enriched in phosphatidylinositol 3-phosphate and dynamically connected to the endoplasmic reticulum. *J. Cell Biol.* 182:685–701. doi:10.1083/jcb.200803137.

Babst, M., D.J. Katzmann, E.J. Estepa-Sabal, T. Meerloo, and S.D. Emr. 2002a. Escrt-III: An Endosome-Associated Hetreooligomeric Protein Complex Requied for MVB Sorting. *Dev. Cell*. 3:271–282. doi:10.1016/S1534-5807(02)00220-4.

Babst, M., D.J. Katzmann, W.B. Snyder, B. Wendland, and S.D. Emr. 2002b. Endosome-associated complex, ESCRT-II, recruits transport machinery for protein sorting at the multivesicular body. *Dev. Cell*. 3:283–289. doi:10.1016/S1534-5807(02)00219-8.

Bach, H., K.G. Papavinasasundaram, D. Wong, Z. Hmama, and Y. Av-Gay. 2008. Mycobacterium tuberculosis Virulence Is Mediated by PtpA Dephosphorylation of Human Vacuolar Protein Sorting 33B. *Cell Host Microbe*. 3:316–322. doi:10.1016/j.chom.2008.03.008.

Bagaitkar, J., E.A. Barbu, L.J. Perez-Zapata, A. Austin, G. Huang, S. Pallat, and M.C. Dinauer. 2017. PI(3)P-p40 phox binding regulates NADPH oxidase activation in mouse macrophages and magnitude of inflammatory responses in vivo . *J. Leukoc. Biol.* 101:449–457. doi:10.1189/jlb.3ab0316-139r.

Bah, A., M. Sanicas, J. Nigou, C. Guilhot, C. Astarie-Dequeker, and I. Vergne. 2020. The Lipid Virulence Factors of Mycobacterium tuberculosis Exert Multilayered Control over Autophagy-Related Pathways in Infected Human Macrophages. *Cells*. 9:666. doi:10.3390/cells9030666.

Bar-Ephraim, Y.E., K. Kretzschmar, and H. Clevers. 2020. Organoids in immunological research. *Nat. Rev. Immunol.* 20:279–293. doi:10.1038/s41577-019-0248-y.

Barczak, A.K., R. Avraham, S. Singh, S.S. Luo, W.R. Zhang, M.A. Bray, A.E. Hinman, M. Thompson, R.M. Nietupski, A. Golas, P. Montgomery, M. Fitzgerald, R.S. Smith, D.W. White, A.D. Tischler, A.E. Carpenter, and D.T. Hung. 2017. Systematic, multiparametric analysis of Mycobacterium tuberculosis intracellular infection offers insight into coordinated virulence. *PLoS Pathog.* 13:1–27. doi:10.1371/journal.ppat.1006363.

Barisch, C., P. Paschke, M. Hagedorn, M. Maniak, and T. Soldati. 2015. Lipid droplet dynamics at early stages of Mycobacterium marinum infection in Dictyostelium. *Cell. Microbiol.* 17:1332–1349. doi:10.1111/cmi.12437.

Barisch, C., and T. Soldati. 2017a. Breaking fat! How mycobacteria and other intracellular pathogens manipulate host lipid droplets. *Biochimie*. 141:54–61. doi:10.1016/j.biochi.2017.06.001.

Barisch, C., and T. Soldati. 2017b. Mycobacterium marinum Degrades Both Triacylglycerols and Phospholipids from Its Dictyostelium Host to Synthesise Its Own Triacylglycerols and Generate Lipid Inclusions. *PLoS Pathog.* 13:1–30. doi:10.1371/journal.ppat.1006095.

Barnett, T.C., D. Liebl, L.M. Seymour, C.M. Gillen, J.Y. Lim, C.N. LaRock, M.R. Davies, B.L. Schulz, V. Nizet, R.D. Teasdale, and M.J. Walker. 2013. The Globally Disseminated M1T1 Clone of Group A Streptococcus Evades Autophagy for Intracellular Replication. *Cell Host Microbe*. 14:675–682. doi:10.1016/j.chom.2013.11.003.

Baxt, L.A., and M.B. Goldberg. 2014. Host and bacterial proteins that repress recruitment of LC3 to Shigella early during infection. *PLoS One*. 9. doi:10.1371/journal.pone.0094653.

Beckwith, K.S., M.S. Beckwith, S. Ullmann, R.S. Sætra, H. Kim, A. Marstad, S.E. Åsberg, T.A. Strand, M. Haug, M. Niederweis, H.A. Stenmark, and T.H. Flo.

2020. Plasma membrane damage causes NLRP3 activation and pyroptosis during Mycobacterium tuberculosis infection. *Nat. Commun.* 11:2270. doi:10.1038/s41467-020-16143-6.

Bell, S.L., K.L. Lopez, J.S. Cox, K.L. Patrick, and R.O. Watson. 2020. Galectin-8 senses phagosomal damage and recruits selective autophagy adapter TAX1BP1 to control Mycobacterium tuberculosis infection in macrophages. *bioRxiv*.

Berglund, R., A.O. Guerreiro-Cacais, M.Z. Adzemovic, M. Zeitelhofer, H. Lund, E. Ewing, S. Ruhrmann, E. Nutma, R. Parsa, M. Thessen-Hedreul, S. Amor, R.A. Harris, T. Olsson, and M. Jagodic. 2020. Microglial autophagy–associated phagocytosis is essential for recovery from neuroinflammation. *Sci. Immunol.* 5:eabb5077. doi:10.1126/sciimmunol.abb5077.

Bernard, E.M., A. Fearns, C. Bussi, P. Santucci, C.J. Peddie, R.J. Lai, L.M. Collinson, and M.G. Gutierrez. 2021. M. tuberculosis infection of human iPSC-derived macrophages reveals complex membrane dynamics during xenophagy evasion. *J. Cell Sci.* 134:jcs252973. doi:10.1242/jcs.252973.

Bernardini, M.L., J. Mounier, H. D'Hauteville, M. Coquis-Rondon, and P.J. Sansonetti. 1989. Identification of icsA, a plasmid locus of Shigella flexneri that governs bacterial intra- and intercellular spread through interaction with F-actin. *Proc. Natl. Acad. Sci. U. S. A.* 86:3867–3871. doi:10.1073/pnas.86.10.3867.

Berón, W., M.G. Gutierrez, M. Rabinovitch, and M.I. Colombo. 2002. Coxiella burnetii localizes in a Rab7-labeled compartment with autophagic characteristics. *Infect. Immun.* 70:5816–5821. doi:10.1128/IAI.70.10.5816-5821.2002.

Berry, M.P.R., C.M. Graham, F.W. McNab, Z. Xu, S.A.A. Bloch, T. Oni, K.A. Wilkinson, R. Banchereau, J. Skinner, R.J. Wilkinson, C. Quinn, D. Blankenship, R. Dhawan, J.J. Cush, A. Mejias, O. Ramilo, O.M. Kon, V. Pascual, J. Banchereau, D. Chaussabel, and A. O'Garra. 2010. An interferon-inducible neutrophil-driven blood transcriptional signature in human tuberculosis. *Nature*. 466:973–977. doi:10.1038/nature09247.

Biazik, J., P. Ylä-Anttila, H. Vihinen, E. Jokitalo, and E.L. Eskelinen. 2015. Ultrastructural relationship of the phagophore with surrounding organelles. *Autophagy*. 11:439–451. doi:10.1080/15548627.2015.1017178.

Bielecki, J., P. Youngman, P. Connelly, and D.A. Portnoy. 1990. Bacillus subtilis expressing a haemolysin gene from Listeria monocytogenes can grow in mammalian cells. *Nature*. 345:175–176. doi:10.1038/345175a0.

Birmingham, C.L., V. Canadien, E. Gouin, E.B. Troy, T. Yoshimori, P. Cossart, D.E. Higgins, and J.H. Brumell. 2007. Listeria monocytogenes evades killing by autophagy during colonization of host cells. *Autophagy*. 3:442–451. doi:10.4161/auto.4450.

Birmingham, C.L., V. Canadien, N.A. Kaniuk, B.E. Steinberg, D.E. Higgins, and J.H.

Brumell. 2008. Listeriolysin O allows Listeria monocytogenes replication in macrophage vacuoles. *Nature*. 451:350–354. doi:10.1038/nature06479.

Birmingham, C.L., A.C. Smith, M.A. Bakowski, T. Yoshimori, and J.H. Brumell. 2006. Autophagy controls Salmonella infection in response to damage to the Salmonella-containing vacuole. *J. Biol. Chem.* 281:11374–11383. doi:10.1074/jbc.M509157200.

Blischak, J.D., L. Tailleux, A. Mitrano, L.B. Barreiro, and Y. Gilad. 2015. Mycobacterial infection induces a specific human innate immune response. *Sci. Rep.* 5:1–16. doi:10.1038/srep16882.

Blocker, A., P. Gounon, E. Larquet, K. Niebuhr, V. Cabiaux, C. Parsot, and P. Sansonetti. 1999. The Tripartite Type III Secreton of Shigella flexneri Inserts IpaB and IpaC into Host Membranes. *J. Cell Biol.* 147:683–693.

Bonecini-Almeida, M.G., S. Chitale, I. Boutsikakis, J. Geng, H. Doo, S. He, and J.L. Ho. 1998. Induction of in vitro human macrophage anti-Mycobacterium tuberculosis activity: requirement for IFN-gamma and primed lymphocytes. *J. Immunol.* 160:4490–9.

Bonet-Ponce, L., A. Beilina, C.D. Williamson, E. Lindberg, J.H. Kluss, S. Saez-Atienzar, N. Landeck, R. Kumaran, A. Mamais, C.K.E. Bleck, Y. Li, and M.R. Cookson. 2020. LRRK2 mediates tubulation and vesicle sorting from lysosomes. *Sci. Adv.* 6:eabb2454. doi:10.1126/sciadv.abb2454.

Bonilla, D.L., A. Bhattacharya, Y. Sha, Y. Xu, Q. Xiang, A. Kan, C. Jagannath, M. Komatsu, and N.T. Eissa. 2013. Autophagy regulates phagocytosis by modulating the expression of scavenger receptors. *Immunity*. 39:537–547. doi:10.1016/j.immuni.2013.08.026.

Bonnardel, J., and M. Guilliams. 2018. Developmental control of macrophage function. *Curr. Opin. Immunol.* 50:64–74. doi:10.1016/j.coi.2017.12.001.

Bonnardel, J., W. T'Jonck, D. Gaublomme, R. Browaeys, C.L. Scott, L. Martens, B. Vanneste, S. De Prijck, S.A. Nedospasov, A. Kremer, E. Van Hamme, P. Borghgraef, W. Toussaint, P. De Bleser, I. Mannaerts, A. Beschin, L.A. van Grunsven, B.N. Lambrecht, T. Taghon, S. Lippens, D. Elewaut, Y. Saeys, and M. Guilliams. 2019. Stellate Cells, Hepatocytes, and Endothelial Cells Imprint the Kupffer Cell Identity on Monocytes Colonizing the Liver Macrophage Niche. *Immunity*. 51:638-654.e9. doi:10.1016/j.immuni.2019.08.017.

Bosch, M., M. Sánchez-Álvarez, A. Fajardo, R. Kapetanovic, B. Steiner, F. Dutra, L. Moreira, J.A. López, R. Campo, M. Marí, F. Morales-Paytuví, O. Tort, A. Gubern, R.M. Templin, J.E.B. Curson, N. Martel, C. Català, F. Lozano, F. Tebar, C. Enrich, J. Vázquez, M.A. Del Pozo, M.J. Sweet, P.T. Bozza, S.P. Gross, R.G. Parton, and A. Pol. 2020. Mammalian lipid droplets are innate immune hubs integrating cell metabolism and host defense. *Science (80-.).* 370:eaay8085. doi:10.1126/science.aay8085.

Botella, H., J. Vaubourgeix, M.H. Lee, N. Song, W. Xu, H. Makinoshima, M.S.

Glickman, and S. Ehrt. 2017. Mycobacterium tuberculosis protease MarP activates a peptidoglycan hydrolase during acid stress . *EMBO J.* 36:536–548. doi:10.15252/embj.201695028.

Bragança, J., J.A. Lopes, L. Mendes-Silva, and J.M.A. Santos. 2019. Induced pluripotent stem cells, a giant leap for mankind therapeutic applications. *World J. Stem Cells*. 11:421–430. doi:10.4252/wjsc.v11.i7.421.

Brodin, P., L. Majlessi, L. Marsollier, M.I. De Jonge, D. Bottai, C. Demangel, J. Hinds, O. Neyrolles, P.D. Butcher, C. Leclerc, S.T. Cole, and R. Brosch. 2006. Dissection of ESAT-6 system 1 of Mycobacterium tuberculosis and impact on immunogenicity and virulence. *Infect. Immun.* 74:88–98. doi:10.1128/IAI.74.1.88-98.2006.

Brumell, J.H., P. Tang, M.L. Zaharik, and B.B. Finlay. 2002. Disruption of the Salmonella-Containing Vacuole Leads to Increased Replication of. *Society*. 70:3264–3270. doi:10.1128/IAI.70.6.3264.

Buchrieser, J., W. James, and M.D. Moore. 2017. Human Induced Pluripotent Stem Cell-Derived Macrophages Share Ontogeny with MYB-Independent Tissue-Resident Macrophages. *Stem Cell Reports*. 8:334–345. doi:10.1016/j.stemcr.2016.12.020.

Budzik, J.M., D.L. Swaney, D. Jimenez-Morales, J.R. Johnson, N.E. Garelis, T. Repasy, A.W. Roberts, L.M. Popov, T.J. Parry, D. Pratt, T. Ideker, N.J. Krogan, and J.S. Cox. 2020. Dynamic post-translational modification profiling of m. Tuberculosis-infected primary macrophages. *Elife*. 9:1–30. doi:10.7554/eLife.51461.

Bussi, C., and M.G. Gutierrez. 2019. *Mycobacterium tuberculosis* infection of host cells in space and time. *FEMS Microbiol. Rev.* 1–21. doi:10.1093/femsre/fuz006.

Bustamante, J., S. Boisson-Dupuis, L. Abel, and J.L. Casanova. 2014. Mendelian susceptibility to mycobacterial disease: Genetic, immunological, and clinical features of inborn errors of IFN-γ immunity. *Semin. Immunol.* 26:454–470. doi:10.1016/j.smim.2014.09.008.

Buter, J., T.-Y. Cheng, M. Ghanem, A.E. Grootemaat, S. Raman, X. Feng, A.R. Plantijn, T. Ennis, J. Wang, R.N. Cotton, E. Layre, A.K. Ramnarine, J.A. Mayfield, D.C. Young, A. Jezek Martinot, N. Siddiqi, S. Wakabayashi, H. Botella, R. Calderon, M. Murray, S. Ehrt, B.B. Snider, M.B. Reed, E. Oldfield, S. Tan, E.J. Rubin, M.A. Behr, N.N. van der Wel, A.J. Minnaard, and D.B. Moody. 2019. Mycobacterium tuberculosis releases an antacid that remodels phagosomes. *Nat. Chem. Biol.* 15:889–899. doi:10.1038/s41589-019-0336-0.

Cadwell, K., J.Y. Liu, S.L. Brown, H. Miyoshi, J. Loh, J.K. Lennerz, C. Kishi, W. Kc, J.A. Carrero, S. Hunt, C.D. Stone, E.M. Brunt, R.J. Xavier, B.P. Sleckman, E. Li, N. Mizushima, T.S. Stappenbeck, and H.W. Virgin IV. 2008. A key role for autophagy and the autophagy gene Atg16l1 in mouse and human intestinal

Paneth cells. *Nature*. 456:259–263. doi:10.1038/nature07416.

Cambier, C.J., S.M. O'Leary, M.P. O'Sullivan, J. Keane, and L. Ramakrishnan. 2017. Phenolic Glycolipid Facilitates Mycobacterial Escape from Microbicidal Tissue-Resident Macrophages. *Immunity*. 47:552-565.e4. doi:10.1016/j.immuni.2017.08.003.

Cambier, C.J., K.K. Takaki, R.P. Larson, R.E. Hernandez, D.M. Tobin, K.B. Urdahl, C.L. Cosma, and L. Ramakrishnan. 2014. Mycobacteria manipulate macrophage recruitment through coordinated use of membrane lipids. *Nature*. 505:218–222. doi:10.1038/nature12799.

Campbell-Valois, F.X., M. Sachse, P.J. Sansonetti, and C. Parsot. 2015. Escape of actively secreting shigella flexneri from ATG8/LC3-Positive vacuoles formed during cell-to-cell spread is facilitated by IcsB and VirA. *MBio*. 6:1–11. doi:10.1128/mBio.02567-14.

Cao, L., A. McDonnell, A. Nitzsche, A. Alexandrou, P.-P. Saintot, A.J.C. Loucif, A.R. Brown, G. Young, M. Mis, A. Randall, S.G. Waxman, P. Stanley, S. Kirby, S. Tarabar, A. Gutteridge, R. Butt, R.M. McKernan, P. Whiting, Z. Ali, J. Bilsland, and E.B. Stevens. 2016. Pharmacological reversal of a pain phenotype in iPSC-derived sensory neurons and patients with inherited erythromelalgia. *Sci. Transl. Med.* 8:ra56335ra56. doi:10.1126/scitranslmed.aad7653.

Cao, X., G.K. Yakala, F.E. van den Hil, A. Cochrane, C.L. Mummery, and V. V. Orlova. 2019. Differentiation and Functional Comparison of Monocytes and Macrophages from hiPSCs with Peripheral Blood Derivatives. *Stem Cell Reports*. 12:1282–1297. doi:10.1016/j.stemcr.2019.05.003.

Cardenal-Muñoz, E., S. Arafah, A.T. López-Jiménez, S. Kicka, A. Falaise, F. Bach, O. Schaad, J.S. King, M. Hagedorn, and T. Soldati. 2017. Mycobacterium marinum antagonistically induces an autophagic response while repressing the autophagic flux in a TORC1- and ESX-1-dependent manner. *PLoS Pathog.* 13:1–28. doi:10.1371/journal.ppat.1006344.

Carlton, J.G., and J. Martin-serrano. 2007. Parallels Between Cytokinesis and the ESCRT Machinery. *Science (80-.).* 316:1908–1912. doi:10.1126/science.1143422.

Case, E.D.R., A. Chong, T.D. Wehrly, B. Hansen, R. Child, S. Hwang, H.W. Virgin, and J. Celli. 2014. The Francisella O-antigen mediates survival in the macrophage cytosol via autophagy avoidance. *Cell. Microbiol.* 16:862–877. doi:10.1111/cmi.12246.

Case, E.D.R., J.A. Smith, T.A. Ficht, J.E. Samuel, and P. De Figueiredo. 2016. Space: A Final Frontier for Vacuolar Pathogens. *Traffic*. 17:461–474. doi:10.1111/tra.12382.

Castillo, E.F., A. Dekonenko, J. Arko-Mensah, M.A. Mandell, N. Dupont, S. Jiang, M. Delgado-Vargas, G.S. Timmins, D. Bhattacharya, H. Yang, J. Hutt, C.R. Lyons, K.M. Dobos, and V. Deretic. 2012. Autophagy protects against active

tuberculosis by suppressing bacterial burden and inflammation. *Proc. Natl. Acad. Sci.* 109:E3168-76. doi:10.1073/pnas.1210500109.

Cemma, M., S. Grinstein, and J.H. Brumell. 2016. Autophagy proteins are not universally required for phagosome maturation. *Autophagy*. 12:1–7. doi:10.1080/15548627.2016.1191724.

Cemma, M., P.K. Kim, and J.H. Brumell. 2011. The ubiquitin-binding adaptor proteins p62/SQSTM1 and NDP52 are recruited independently to bacteria-associated microdomains to target Salmonella to the autophagy pathway. *Autophagy*. 7:341–345. doi:10.4161/auto.7.3.14046.

Chai, Q., X. Wang, L. Qiang, Y. Zhang, P. Ge, Z. Lu, Y. Zhong, B. Li, J. Wang, L. Zhang, D. Zhou, W. Li, W. Dong, Y. Pang, G.F. Gao, and C.H. Liu. 2019. A Mycobacterium tuberculosis surface protein recruits ubiquitin to trigger host xenophagy. *Nat. Commun.* 10. doi:10.1038/s41467-019-09955-8.

Chan, E.D., J. Chan, and N.W. Schluger. 2001. What is the role of nitric oxide in murine and human host defense against tuberculosis? Current knowledge. *Am. J. Respir. Cell Mol. Biol.* 25:606–612. doi:10.1165/ajrcmb.25.5.4487.

Chan, J., Y. Xing, R.S. Magliozzo, and B.R. Bloom. 1992. Killing of Virulent Mycobacterium tuberculosis by Reactive Nitrogen Intermediates Produced by Activated Murine Macrophages. *J. Exp. Med.* 175:1111–1122.

Chandra, P., S. Ghanwat, S.K. Matta, S.S. Yadav, M. Mehta, Z. Siddiqui, A. Singh, and D. Kumar. 2015. Mycobacterium tuberculosis Inhibits RAB7 Recruitment to Selectively Modulate Autophagy Flux in Macrophages. *Sci. Rep.* 5:16320. doi:10.1038/srep16320.

Chauhan, S., S. Kumar, A. Jain, M. Ponpuak, M.H. Mudd, and T. Kimura. 2016. TRIMs and Galectins Globally Cooperate and TRIM16 and Galectin-3 Co-direct Autophagy in Endomembrane Damage Homeostasis. *Dev. Cell*. 39:1–15. doi:10.1016/j.devcel.2016.08.003.

Chaussabel, D., R.T. Semnani, M.A. McDowell, D. Sacks, A. Sher, and T.B. Nutman. 2003. Unique gene expression profiles of human macrophages and dendritic cells to phylogenetically distinct parasites. *Blood*. 102:672–681. doi:10.1182/blood-2002-10-3232.

Checroun, C., T.D. Wehrly, E.R. Fischer, S.F. Hayes, and J. Celli. 2006. Autophagy-mediated reentry of Francisella tularensis into the endocytic compartment after cytoplasmic replication. *Proc. Natl. Acad. Sci.* 103:14578–14583. doi:10.1073/pnas.0601838103.

Chen, J.M., M. Zhang, J. Rybniker, L. Basterra, N. Dhar, A.D. Tischler, F. Pojer, and S.T. Cole. 2013. Phenotypic profiling of mycobacterium tuberculosis espa point mutants reveals that blockage of ESAT-6 and CFP-10 secretion in vitro does not always correlate with attenuation of virulence. *J. Bacteriol.* 195:5421–5430. doi:10.1128/JB.00967-13.

Chen, X., B. Khambu, H. Zhang, W. Gao, M. Li, X. Chen, T. Yoshimori, and X.M. Yin. 2014. Autophagy induced by calcium phosphate precipitates targets damaged endosomes. *J. Biol. Chem.* 289:11162–11174. doi:10.1074/jbc.M113.531855.

Chen, Z., Y. Hu, B.M. Cumming, P. Lu, L. Feng, J. Deng, A.J.C. Steyn, and S. Chen. 2016. Mycobacterial WhiB6 Differentially Regulates ESX-1 and the Dos Regulon to Modulate Granuloma Formation and Virulence in Zebrafish. *Cell Rep.* 16:2512–2524. doi:10.1016/j.celrep.2016.07.080.

Chen, Z., T. Wang, Z. Liu, G. Zhang, J. Wang, S. Feng, and J. Liang. 2015. Inhibition of autophagy by MiR-30A induced by Mycobacteria tuberculosis as a possible mechanism of immune escape in human macrophages. *Jpn. J. Infect. Dis.* 68:420–424. doi:10.7883/yoken.JJID.2014.466.

Cheng, Y., and J.S. Schorey. 2018. Mycobacterium tuberculosis – induced IFN-β production requires cytosolic DNA and RNA sensing pathways. *J. Exp. Med.* 215:2919–2935.

Choi, J., S. Park, S.B. Biering, E. Selleck, C.Y. Liu, X. Zhang, N. Fujita, T. Saitoh, S. Akira, T. Yoshimori, L.D. Sibley, S. Hwang, and H.W. Virgin. 2014. The parasitophorous vacuole membrane of toxoplasma gondii is targeted for disruption by ubiquitin-like conjugation systems of autophagy. *Immunity*. 40:924–935. doi:10.1016/j.immuni.2014.05.006.

Choi, K.D., M. Vodyanik, and I.I. Slukvin. 2011. Hematopoietic differentiation and production of mature myeloid cells from human pluripotent stem cells. *Nat. Protoc.* 6:296–313. doi:10.1038/nprot.2010.184.

Choy, A., J. Dancourt, B. Mugo, T.J. O'Connor, R.R. Isberg, T.J. Melia, and C.R. Roy. 2012. The Legionella Effector RavZ Inhibits Host Autophagy Through Irreversible Atg8 Deconjugation. *Science (80-.).* 338:1072–1076. doi:10.1126/science.1227026.

Chu, Y., S. Gao, T. Wang, J. Yan, G. Xu, Y. Li, H. Niu, R. Huang, and S. Wu. 2016. A novel contribution of spvB to pathogenesis of Salmonella Typhimurium by inhibiting autophagy in host cells. *Oncotarget*. 7:8295–8309. doi:10.18632/oncotarget.6989.

Clarke, A.J., and A.K. Simon. 2019. Autophagy in the renewal, differentiation and homeostasis of immune cells. *Nat. Rev. Immunol.* 19:170–183. doi:10.1038/s41577-018-0095-2.

Clay, H., J.M. Davis, D. Beery, A. Huttenlocher, S.E. Lyons, and L. Ramakrishnan. 2007. Dichotomous Role of the Macrophage in Early Mycobacterium marinum Infection of the Zebrafish. *Cell Host Microbe*. 2:29–39. doi:10.1016/j.chom.2007.06.004.

Clay, H., H.E. Volkman, and L. Ramakrishnan. 2008. TNF signaling mediates resistance to mycobacteria by inhibiting bacterial growth and macrophage death but not tuberculous granuloma formation. *Immunity*. 29:283–294.

doi:10.1016/j.immuni.2008.06.011.TNF.

Clemens, D.L., and M. a Horwitz. 1995. Characterization of the Mycobacterium mberctdosis Phagosome and Evidence that Phagosomal Maturation Is Inhibited. *J. Exp. Med.* 181:257–270.

Cohen, S.B., B.H. Gern, J.L. Delahaye, K.N. Adams, C.R. Plumlee, J.K. Winkler, D.R. Sherman, M.Y. Gerner, and K.B. Urdahl. 2018. Alveolar Macrophages Provide an Early Mycobacterium tuberculosis Niche and Initiate Dissemination. *Cell Host Microbe*. 24:439-446.e4. doi:10.1016/j.chom.2018.08.001.

Coleman, M.M., S.A. Basdeo, A.M. Coleman, C.N. Cheallaigh, C.P. De Castro, A.M. McLaughlin, P.J. Dunne, J. Harris, and J. Keane. 2018. All-trans retinoic acid augments autophagy during intracellular bacterial infection. *Am. J. Respir. Cell Mol. Biol.* 59:548–556. doi:10.1165/rcmb.2017-0382OC.

Collins, C.A., A. De Mazière, S. Van Dijk, F. Carlsson, J. Klumperman, and E.J. Brown. 2009. Atg5-independent sequestration of ubiquitinated mycobacteria. *PLoS Pathog.* 5. doi:10.1371/journal.ppat.1000430.

Conrad, W.H., M.M. Osman, J.K. Shanahan, F. Chu, K.K. Takaki, J. Cameron, D. Hopkinson-Woolley, R. Brosch, and L. Ramakrishnan. 2017. Mycobacterial ESX-1 secretion system mediates host cell lysis through bacterium contact-dependent gross membrane disruptions. *Proc. Natl. Acad. Sci.* 114:1371–1376. doi:10.1073/pnas.1620133114.

Cooper, A.M., K.D. Mayer-Barber, and A. Sher. 2011. Role of innate cytokines in mycobacterial infection. *Mucosal Immunol.* 4:252–260. doi:10.1038/mi.2011.13.

Cox, J.S., B. Chess, M. McNeil, and W.R. Jacobs. 1999. Complex lipid determines tissue-specific replication of Mycobacterium tuberculosis in mice. *Nature*. 402:79–83. doi:10.1038/47042.

Crowle, A.J., R. Dahl, E. Ross, and M.H. May. 1991. Evidence that vesicles containing living, virulent Mycobacterium tuberculosis or Mycobacterium avium in cultured human macrophages are not acidic. *Infect. Immun.* 59:1823–1831. doi:10.1128/iai.59.5.1823-1831.1991.

Cunha, L.D., M. Yang, R. Carter, C. Guy, L. Harris, J.C. Crawford, G. Quarato, E. Boada-Romero, H. Kalkavan, M.D.L. Johnson, S. Natarajan, M.E. Turnis, D. Finkelstein, J.T. Opferman, C. Gawad, and D.R. Green. 2018. LC3-Associated Phagocytosis in Myeloid Cells Promotes Tumor Immune Tolerance. *Cell*. 175:429-441.e16. doi:10.1016/j.cell.2018.08.061.

Cyranoski, D. 2014. Japanese woman is first recipient of next-generation stem cells. *Nature*. doi:10.1038/nature.2014.15915.

Cyranoski, D. 2018. The cells that sparked a revolution. *Nature*. 555:428–430.

Dalle Pezze, P., E. Karanasios, V. Kandia, M. Manifava, S.A. Walker, N. Gambardella Le Novère, and N.T. Ktistakis. 2020. ATG13 dynamics in nonselective autophagy and mitophagy: insights from live imaging studies and

mathematical modeling. *Autophagy*. 00:1–11. doi:10.1080/15548627.2020.1749401.

Davis, J.M., and L. Ramakrishnan. 2009. The Role of the Granuloma in Expansion and Dissemination of Early Tuberculous Infection. *Cell*. 136:37–49. doi:10.1016/j.cell.2008.11.014.

Day, T.A., J.E. Mittler, M.R. Nixon, C. Thompson, M.D. Miner, M.J. Hickey, R.P. Liao, J.M. Pang, D.M. Shayakhmetov, and D.R. Sherman. 2014. Mycobacterium tuberculosis strains lacking surface lipid phthiocerol dimycocerosate are susceptible to killing by an early innate host response. *Infect. Immun.* 82:5214–5222. doi:10.1128/IAI.01340-13.

Diao, J., R. Liu, Y. Rong, M. Zhao, J. Zhang, Y. Lai, Q. Zhou, L.M. Wilz, J. Li, S. Vivona, R.A. Pfuetzner, A.T. Brunger, and Q. Zhong. 2015. ATG14 promotes membrane tethering and fusion of autophagosomes to endolysosomes. *Nature*. 520:563–566. doi:10.1038/nature14147.

Dooley, H.C., M. Razi, H.E.J. Polson, S.E. Girardin, M.I. Wilson, and S.A. Tooze. 2014. WIPI2 Links LC3 Conjugation with PI3P, Autophagosome Formation, and Pathogen Clearance by Recruiting Atg12-5-16L1. *Mol. Cell*. 55:238–252. doi:10.1016/j.molcel.2014.05.021.

Dortet, L., S. Mostowy, A.S. Louaka, E. Gouin, M.A. Nahori, E.A.C. Wiemer, O. Dussurget, and P. Cossart. 2011. Recruitment of the major vault protein by inlk: A listeria monocytogenes strategy to avoid autophagy. *PLoS Pathog.* 7. doi:10.1371/journal.ppat.1002168.

Douvas, G.S., D.L. Looker, A.E. Vatter, and A.J. Crowle. 1985. Gamma interferon activates human macrophages to become tumoricidal and leishmanicidal but enhances replication of macrophage-associated mycobacteria. *Infect. Immun.* 50:1–8. doi:10.1128/iai.50.1.1-8.1985.

Draijer, C., L.R.K. Penke, and M. Peters-Golden. 2019. Distinctive Effects of GM-CSF and M-CSF on Proliferation and Polarization of Two Major Pulmonary Macrophage Populations. *J. Immunol.* 202:2700–2709. doi:10.4049/jimmunol.1801387.

Du, W., Q.P. Su, Y. Chen, Y. Zhu, D. Jiang, Y. Rong, S. Zhang, Y. Zhang, H. Ren, C. Zhang, X. Wang, N. Gao, Y. Wang, L. Sun, Y. Sun, and L. Yu. 2016. Kinesin 1 Drives Autolysosome Tubulation. *Dev. Cell*. 37:326–336. doi:10.1016/j.devcel.2016.04.014.

Duan, L., M. Yi, J. Chen, S. Li, and W. Chen. 2016. Mycobacterium tuberculosis EIS gene inhibits macrophage autophagy through up-regulation of IL-10 by increasing the acetylation of histone H3. *Biochem. Biophys. Res. Commun.* 473:1229–1234. doi:10.1016/j.bbrc.2016.04.045.

Duewell, P., H. Kono, K.J. Rayner, C.M. Sirois, G. Vladimer, F.G. Bauernfeind, G.S. Abela, L. Franchi, G. Nũez, M. Schnurr, T. Espevik, E. Lien, K.A. Fitzgerald, K.L. Rock, K.J. Moore, S.D. Wright, V. Hornung, and E. Latz. 2010. NLRP3

inflammasomes are required for atherogenesis and activated by cholesterol crystals. *Nature*. 464:1357–1361. doi:10.1038/nature08938.

Dupont, N., S. Lacas-Gervais, J. Bertout, I. Paz, B. Freche, G.T. Van Nhieu, F.G. van der Goot, P.J. Sansonetti, and F. Lafont. 2009. Shigella Phagocytic Vacuolar Membrane Remnants Participate in the Cellular Response to Pathogen Invasion and Are Regulated by Autophagy. *Cell Host Microbe*. 6:137–149. doi:10.1016/j.chom.2009.07.005.

Durgan, J., A.H. Lystad, K. Sloan, S.R. Carlsson, M.I. Wilson, E. Marcassa, R. Ulferts, J. Webster, A.F. Lopez-Clavijo, M.J. Wakelam, R. Beale, A. Simmonsen, D. Oxley, and O. Florey. 2020. Non-canonical autophagy drives alternative ATG8 conjugation to phosphatidylserine. *bioRxiv*.

Ehrt, S., D. Schnappinger, S. Bekiranov, J. Drenkow, S. Shi, T.R. Gingeras, T. Gaasterland, G. Schoolnik, and C. Nathan. 2001. Reprogramming of the macrophage transcriptome in response to interferon-γ and mycobacterium tuberculosis: Signaling roles of nitric oxide synthase-2 and phagocyte oxidase. *J. Exp. Med.* 194:1123–1139. doi:10.1084/jem.194.8.1123.

Ellison, C.J., W. Kukulski, K.B. Boyle, S. Munro, and F. Randow. 2020. Transbilayer Movement of Sphingomyelin Precedes Catastrophic Breakage of Enterobacteria- Containing Vacuoles. *Curr. Biol.* 30:1–10. doi:10.1016/j.cub.2020.05.083.

Eriksson, I., P. Wäster, and K. Öllinger. 2020. Restoration of lysosomal function after damage is accompanied by recycling of lysosomal membrane proteins. *Cell Death Dis.* 11. doi:10.1038/s41419-020-2527-8.

Eskelinen, E.L., and P. Saftig. 2009. Autophagy: A lysosomal degradation pathway with a central role in health and disease. *Biochim. Biophys. Acta*. 1793:664–673. doi:10.1016/j.bbamcr.2008.07.014.

Eum, S.Y., J.H. Kong, M.S. Hong, Y.J. Lee, J.H. Kim, S.H. Hwang, S.N. Cho, L.E. Via, and C.E. Barry. 2010. Neutrophils are the predominant infected phagocytic cells in the airways of patients with active pulmonary TB. *Chest*. 137:122–128. doi:10.1378/chest.09-0903.

Famelis, N., A. Rivera-Calzada, G. Degliesposti, M. Wingender, N. Mietrach, J.M. Skehel, R. Fernandez-Leiro, B. Böttcher, A. Schlosser, O. Llorca, and S. Geibel. 2019. Architecture of the mycobacterial type VII secretion system. *Nature*. 576:321–325. doi:10.1038/s41586-019-1633-1.

Fang, L., H. Shen, Y. Tang, and W. Fang. 2015. Superoxide dismutase of Streptococcus suis serotype 2 plays a role in anti-autophagic response by scavenging reactive oxygen species in infected macrophages. *Vet. Microbiol.* 176:328–336. doi:10.1016/j.vetmic.2015.02.006.

Feeley, E.M., D.M. Pilla-Moffett, E.E. Zwack, A.S. Piro, R. Finethy, J.P. Kolb, J. Martinez, I.E. Brodsky, and J. Coers. 2017. Galectin-3 directs antimicrobial guanylate binding proteins to vacuoles furnished with bacterial secretion

systems. *Proc. Natl. Acad. Sci.* 114:E1698–E1706. doi:10.1073/pnas.1615771114.

Feil, S.C., D.B. Ascher, M.J. Kuiper, R.K. Tweten, and M.W. Parker. 2014. Structural Studies of Streptococcus pyogenes Streptolysin O Provide Insights into the Early Steps of Membrane Penetration. *J. Mol. Biol.* 426:785–792. doi:10.1016/j.jmb.2013.11.020.

Feng, Z.Z., A.J. Jiang, A.W. Mao, Y. Feng, W. Wang, J. Li, X. Zhang, K. Xing, and X. Peng. 2018. The Salmonella effectors SseF and SseG inhibit Rab1A-mediated autophagy to facilitate intracellular bacterial survival and replication. *J. Biol. Chem.* 293:9662–9673. doi:10.1074/jbc.M117.811737.

Fisch, D., B. Clough, M. Domart, V. Encheva, H. Bando, A.P. Snijders, L.M. Collinson, M. Yamamoto, A.R. Shenoy, and E.-M. Frickel. 2020. Human GBP1 Differentially Targets Salmonella and Toxoplasma to License Recognition of Microbial Ligands and Caspase-Mediated Death. *Cell Rep.* 32:108008. doi:10.1016/j.celrep.2020.108008.

Fiskin, E., T. Bionda, I. Dikic, and C. Behrends. 2016. Global Analysis of Host and Bacterial Ubiquitinome in Response to Salmonella Typhimurium Infection. *Mol. Cell*. 62:967–981. doi:10.1016/j.molcel.2016.04.015.

Flannagan, R.S., V. Jaumouillé, and S. Grinstein. 2012. The cell biology of phagocytosis. *Annu. Rev. Pathol. Mech. Dis.* 7:61–98. doi:10.1146/annurev-pathol-011811-132445.

Flesch, I., and S.H. Kaufmann. 1987. Mycobacterial growth inhibition by interferon-gamma-activated bone marrow macrophages and differential susceptibility among strains of Mycobacterium tuberculosis. *J. Immunol.* 138:4408–13.

Fletcher, K., R. Ulferts, E. Jacquin, T. Veith, N. Gammoh, J.M. Arasteh, U. Mayer, S.R. Carding, T. Wileman, R. Beale, and O. Florey. 2018. The WD40 domain of ATG16L1 is required for its non-canonical role in lipidation of LC3 at single membranes. *EMBO J.* e97840. doi:10.15252/embj.201797840.

Florey, O., N. Gammoh, S.E. Kim, X. Jiang, and M. Overholtzer. 2015. V-ATPase and osmotic imbalances activate endolysosomal LC3 lipidation. *Autophagy*. 11:88–99. doi:10.4161/15548627.2014.984277.

Florey, O., S.E. Kim, C.P. Sandoval, C.M. Haynes, and M. Overholtzer. 2011. Autophagy machinery mediates macroendocytic processing and entotic cell death by targeting single membranes. *Nat. Cell Biol.* 13:1335–1343. doi:10.1038/ncb2363.

Flynn, J.A.L., M.M. Goldstein, J. Chan, K.J. Triebold, K. Pfeffer, C.J. Lowenstein, R. Schrelber, T.W. Mak, and B.R. Bloom. 1995. Tumor necrosis factor-α is required in the protective immune response against mycobacterium tuberculosis in mice. *Immunity*. 2:561–572. doi:10.1016/1074-7613(95)90001-2.

Flynn, J.L., and J. Chan. 2001a. Immunology of Tuberculosis. *Annu. Rev. Immunol.*

19:93–129.

Flynn, J.L., J. Chan, and P.L. Lin. 2011. Macrophages and control of granulomatous inflammation in tuberculosis. *Mucosal Immunol.* 4:271–278. doi:10.1038/mi.2011.14.

Flynn, J.O.A.L., and J. Chan. 2001b. Tuberculosis: Latency and Reactivation. *Infect. Immun.* 69:4195–4201. doi:10.1128/IAI.69.7.4195–4201.2001.

Flynn, R., A. Grundmann, P. Renz, W. Hänseler, W.S. James, S.A. Cowley, and M.D. Moore. 2015. CRISPR-mediated genotypic and phenotypic correction of a chronic granulomatous disease mutation in human iPS cells. *Exp. Hematol.* 43:838-848.e3. doi:10.1016/j.exphem.2015.06.002.

Franco, L.H., V.R. Nair, C.R. Scharn, R.J. Xavier, J.R. Torrealba, M.U. Shiloh, and B. Levine. 2016. The Ubiquitin Ligase Smurf1 Functions in Selective Autophagy of Mycobacterium tuberculosis and Anti-tuberculous Host Defense. *Cell Host Microbe*. 21:1–14. doi:10.1016/j.chom.2016.11.002.

Fratti, R.A., J.M. Backer, J. Gruenberg, S. Corvera, and V. Deretic. 2001. Role of phosphatidylinositol 3-kinase and Rab5 effectors in phagosomal biogenesis and mycobacterial phagosome maturation arrest. *J. Cell Biol.* 154:631–644. doi:10.1083/jcb.200106049.

Fratti, R.A., J. Chua, I. Vergne, and V. Deretic. 2003. Mycobacterium tuberculosis glycosylated phosphatidylinositol causes phagosome maturation arrest. *Proc. Natl. Acad. Sci.* 100:5437–5442. doi:10.1073/pnas.0737613100.

Fredlund, J., and J. Enninga. 2014. Cytoplasmic access by intracellular bacterial pathogens. *Trends Microbiol.* 22:128–137. doi:10.1016/j.tim.2014.01.003.

Fredlund, J., J.C. Santos, V. Stévenin, A. Weiner, P. Latour-Lambert, K. Rechav, A. Mallet, J. Krijnse-Locker, M. Elbaum, and J. Enninga. 2018. The entry of Salmonella in a distinct tight compartment revealed at high temporal and ultrastructural resolution. *Cell. Microbiol.* 20:1–13. doi:10.1111/cmi.12816.

Freeman, S.A., S. Uderhardt, A. Saric, R.F. Collins, C.M. Buckley, S. Mylvaganam, P. Boroumand, J. Plumb, R.N. Germain, D. Ren, and S. Grinstein. 2020. Lipid-gated monovalent ion fluxes regulate endocytic traffic and support immune surveillance. *Science (80-.).* 367:301–305. doi:10.1126/science.aaw9544.

Frigui, W., D. Bottai, L. Majlessi, M. Monot, E. Josselin, P. Brodin, T. Garnier, B. Gicquel, C. Martin, C. Leclerc, S.T. Cole, and R. Brosch. 2008. Control of M. tuberculosis ESAT-6 secretion and specific T cell recognition by PhoP. *PLoS Pathog.* 4. doi:10.1371/journal.ppat.0040033.

Fujita, N., T. Itoh, H. Omori, M. Fukuda, T. Noda, and T. Yoshimori. 2008. The Atg16L Complex Specifies the Site of LC3 Lipidation for Membrane Biogenesis in Autophagy. *Mol. Biol. Cell*. 19:2092–2100. doi:10.1091/mbc.e07-12-1257.

Fujita, N., E. Morita, T. Itoh, A. Tanaka, M. Nakaoka, Y. Osada, T. Umemoto, T. Saitoh, H. Nakatogawa, S. Kobayashi, T. Haraguchi, J.-L.L. Guan, K. Iwai, F.

Tokunaga, K. Saito, K. Ishibashi, S. Akira, M. Fukuda, T. Noda, and T. Yoshimori. 2013. Recruitment of the autophagic machinery to endosomes during infection is mediated by ubiquitin. *J. Cell Biol.* 203:115–128. doi:10.1083/jcb.201304188.

van Furth, R., and Z.A. Cohn. 1968. The Origin and Kinetics of Mononuclear Phagocytes. *J. Exp. Med.* 128:415–435. doi:10.1017/CBO9781107415324.004.

Gaidt, M.M., T.S. Ebert, D. Chauhan, T. Schmidt, J.L. Schmid-Burgk, F. Rapino, A.A.B. Robertson, M.A. Cooper, T. Graf, and V. Hornung. 2016. Human Monocytes Engage an Alternative Inflammasome Pathway. *Immunity*. 44:833–846. doi:10.1016/j.immuni.2016.01.012.

Gaidt, M.M., F. Rapino, T. Graf, and V. Hornung. 2018. Modeling Primary Human Monocytes with the Trans--Differentiation Cell Line BLaER1. *In* Innate Immune Activation: Methods and Protocols. D. De Nardo and C.M. De Nardo, editors. Springer New York, New York, NY. 57–66.

Gaillard, J.L., P. Berche, J. Mounier, S. Richard, and P. Sansonetti. 1987. In vitro model of penetration and intracellular growth of Listeria monocytogenes in the human enterocyte-like cell line Caco-2. *Infect. Immun.* 55:2822–2829. doi:10.1128/iai.55.11.2822-2829.1987.

Ganbat, D., S. Seehase, E. Richter, E. Vollmer, N. Reiling, K. Fellenberg, K.I. Gaede, C. Kugler, and T. Goldmann. 2016. Mycobacteria infect different cell types in the human lung and cause species dependent cellular changes in infected cells. *BMC Pulm. Med.* 16:1–16. doi:10.1186/s12890-016-0185-5.

Gao, J., L. Langemeyer, D. Kümmel, F. Reggiori, and C. Ungermann. 2018. Molecular mechanism to target the endosomal Mon1-Ccz1 GEF complex to the pre-autophagosomal structure. *Elife*. 7:1–18. doi:10.7554/eLife.31145.

Gao, W., J.H. Kang, Y. Liao, W.X. Ding, A.A. Gambotto, S.C. Watkins, Y.J. Liu, D.B. Stolz, and X.M. Yin. 2010. Biochemical isolation and characterization of the tubulovesicular LC3-positive autophagosomal compartment. *J. Biol. Chem.* 285:1371–1383. doi:10.1074/jbc.M109.054197.

Garrido, C., L. Galluzzi, M. Brunet, P.E. Puig, C. Didelot, and G. Kroemer. 2006. Mechanisms of cytochrome c release from mitochondria. *Cell Death Differ.* 13:1423–1433. doi:10.1038/sj.cdd.4401950.

Gedde, M.M., D.E. Higgins, L.G. Tilney, and D.A. Portnoy. 2000. Role of listeriolysin O in cell-to-cell spread of Listeria monocytogenes. *Infect. Immun.* 68:999–1003. doi:10.1128/IAI.68.2.999-1003.2000.

Giacomini, E., E. Iona, L. Ferroni, M. Miettinen, L. Fattorini, G. Orefici, I. Julkunen, and E.M. Coccia. 2001. Infection of Human Macrophages and Dendritic Cells with Mycobacterium tuberculosis Induces a Differential Cytokine Gene Expression That Modulates T Cell Response . *J. Immunol.* 166:7033–7041. doi:10.4049/jimmunol.166.12.7033.

Ginhoux, F., and M. Guilliams. 2016. Tissue-Resident Macrophage Ontogeny and Homeostasis. *Immunity*. 44:439–449. doi:10.1016/j.immuni.2016.02.024.

Gleeson, L.E., S.M. O'Leary, D. Ryan, A.M. McLaughlin, F.J. Sheedy, and J. Keane. 2018. Cigarette smoking impairs the bioenergetic immune response to mycobacterium tuberculosis infection. *Am. J. Respir. Cell Mol. Biol.* 59:572–579. doi:10.1165/rcmb.2018-0162OC.

Goren, M.B., O. Brokl, and W.B. Schaefer. 1974. Lipids of Putative Relevance to Virulence in Mycobacterium tuberculosis: Phthiocerol Dimycocerosate and the Attenuation Indicator Lipid. *Infect. Immun.* 9:150–158.

Greenwood, D.J., M.S. Dos Santos, S. Huang, M.R.G. Russell, L.M. Collinson, J.I. MacRae, A. West, H. Jiang, and M.G. Gutierrez. 2019. Subcellular antibiotic visualization reveals a dynamic drug reservoir in infected macrophages. *Science (80-.).* 364:1279–1282. doi:10.1126/science.aat9689.

Gross, T.J., K. Kremens, L.S. Powers, B. Brink, T. Knutson, F.E. Domann, R.A. Philibert, M.M. Milhem, and M.M. Monick. 2014. Epigenetic Silencing of the Human NOS2 Gene: Rethinking the Role of Nitric Oxide in Human Macrophage Inflammatory Responses . *J. Immunol.* 192:2326–2338. doi:10.4049/jimmunol.1301758.

Grzegorzewicz, A.E., C. De Sousa-D'Auria, M.R. McNeil, E. Huc-Claustre, V. Jones, C. Petit, S.K. Angala, J. Zemanová, Q. Wang, J.M. Belardinelli, Q. Gao, Y. Ishizaki, K. Mikušová, P.J. Brennan, D.R. Ronning, M. Chami, C. Houssin, and M. Jackson. 2016. Assembling of the Mycobacterium tuberculosis cell wall core. *J. Biol. Chem.* 291:18867–18879. doi:10.1074/jbc.M116.739227.

Guilliams, M., I. De Kleer, S. Henri, S. Post, L. Vanhoutte, S. De Prijck, K. Deswarte, B. Malissen, H. Hammad, and B.N. Lambrecht. 2013. Alveolar macrophages develop from fetal monocytes that differentiate into long-lived cells in the first week of life via GM-CSF. *J. Exp. Med.* 210:1977–1992. doi:10.1084/jem.20131199.

Guilliams, M., and C.L. Scott. 2017. Does niche competition determine the origin of tissue-resident macrophages? *Nat. Rev. Immunol.* 17:451–460. doi:10.1038/nri.2017.42.

Gutbier, S., F. Wanke, N. Dahm, A. Rümmelin, S. Zimmermann, K. Christensen, F. Köchl, A. Rautanen, K. Hatje, B. Geering, J.D. Zhang, M. Britschgi, S.A. Cowley, and C. Patsch. 2020. Large-scale production of human IPSC-derived macrophages for drug screening. *Int. J. Mol. Sci.* 21:1–23. doi:10.3390/ijms21134808.

Gutierrez, M., S. Master, and S. Singh. 2004a. Autophagy Is a Defense Mechanism Inhibiting BCG and Mycobacterium tuberculosis Survival in Infected Macrophages. *Cell*. 119:753–766.

Gutierrez, M.G., and J.G. Carlton. 2018. ESCRTs offer repair service. *Science (80-.).* 360:33–34. doi:10.1126/science.aat2630.

Gutierrez, M.G., D.B. Munafó, W. Berón, and M.I. Colombo. 2004b. Rab7 is required for the normal progression of the autophagic pathway in mammalian cells. *J. Cell Sci.* 117:2687–97. doi:10.1242/jcs.01114.

Gutierrez, M.G., C.L. Vázquez, D.B. Munafó, F.C.M. Zoppino, W. Berón, M. Rabinovitch, and M.I. Colombo. 2005. Autophagy induction favours the generation and maturation of the Coxiella-replicative vacuoles. *Cell. Microbiol.* 7:981–993. doi:10.1111/j.1462-5822.2005.00527.x.

Haake, K., A.-L. Neehus, T. Buchegger, M.P. Kühnel, P. Blank, F. Philipp, C. Oleaga-Quintas, A. Schulz, M. Grimley, R. Goethe, D. Jonigk, U. Kalinke, S. Boisson-Dupuis, J.-L. Casanova, J. Bustamante, and N. Lachmann. 2020. Patient iPSC-Derived Macrophages to Study Inborn Errors of the IFN-γ Responsive Pathway. *Cells*. 9:483. doi:10.3390/cells9020483.

Haenseler, W., S.N. Sansom, J. Buchrieser, S.E. Newey, C.S. Moore, F.J. Nicholls, S. Chintawar, C. Schnell, J.P. Antel, N.D. Allen, M.Z. Cader, R. Wade-Martins, W.S. James, and S.A. Cowley. 2017. A Highly Efficient Human Pluripotent Stem Cell Microglia Model Displays a Neuronal-Co-culture-Specific Expression Profile and Inflammatory Response. *Stem Cell Reports*. 8:1727–1742. doi:10.1016/j.stemcr.2017.05.017.

Hale, C., A. Yeung, D. Goulding, D. Pickard, K. Alasoo, F. Powrie, G. Dougan, and S. Mukhopadhyay. 2015. Induced pluripotent stem cell derived macrophages as a cellular system to study Salmonella and other pathogens. *PLoS One*. 10:1–20. doi:10.1371/journal.pone.0124307.

Hall-Roberts, H., D. Agarwal, J. Obst, T.B. Smith, J. Monzón-Sandoval, E. Di Daniel, C. Webber, W.S. James, E. Mead, J.B. Davis, and S.A. Cowley. 2020. TREM2 Alzheimer's variant R47H causes similar transcriptional dysregulation to knockout, yet only subtle functional phenotypes in human iPSC-derived macrophages. *Alzheimers. Res. Ther.* In Press.

Hämälistö, S., J.L. Stahl, E. Favaro, Q. Yang, B. Liu, L. Christoffersen, B. Loos, C. Guasch Boldú, J.A. Joyce, T. Reinheckel, M. Barisic, and M. Jäättelä. 2020. Spatially and temporally defined lysosomal leakage facilitates mitotic chromosome segregation. *Nat. Commun.* 11. doi:10.1038/s41467-019-14009-0.

Hamasaki, M., N. Furuta, A. Matsuda, A. Nezu, A. Yamamoto, N. Fujita, H. Oomori, T. Noda, T. Haraguchi, Y. Hiraoka, A. Amano, and T. Yoshimori. 2013. Autophagosomes form at ER-mitochondria contact sites. *Nature*. 495:389–393. doi:10.1038/nature11910\rnature11910 [pii].

Han, H.W., H.H. Seo, H.Y. Jo, H.J. Han, V.C.A. Falcão, V. Delorme, J. Heo, D. Shum, J.H. Choi, J.M. Lee, S.H. Lee, H.R. Heo, S.H. Hong, M.H. Park, R.K. Thimmulappa, and J.H. Kim. 2019. Drug Discovery Platform Targeting M. tuberculosis with Human Embryonic Stem Cell-Derived Macrophages. *Stem cell reports*. 13:980–991. doi:10.1016/j.stemcr.2019.10.002.

Han, J.W., H.F. Zheng, Y. Cui, L.D. Sun, D.Q. Ye, Z. Hu, J.H. Xu, Z.M. Cai, W. Huang, G.P. Zhao, H.F. Xie, H. Fang, Q.J. Lu, J.H. Xu, X.P. Li, Y.F. Pan, D.Q. Deng, F.Q. Zeng, Z.Z. Ye, X.Y. Zhang, Q.W. Wang, F. Hao, L. Ma, X.B. Zuo, F.S. Zhou, W.H. Du, Y.L. Cheng, J.Q. Yang, S.K. Shen, J. Li, Y.J. Sheng, X.X. Zuo, W.F. Zhu, F. Gao, P.L. Zhang, Q. Guo, B. Li, M. Gao, F.L. Xiao, C. Quan, C. Zhang, Z. Zhang, K.J. Zhu, Y. Li, D.Y. Hu, W.S. Lu, J.L. Huang, S.X. Liu, H. Li, Y.Q. Ren, Z.X. Wang, C.J. Yang, P.G. Wang, W.M. Zhou, Y.M. Lv, A.P. Zhang, S.Q. Zhang, D. Lin, Y. Li, H.Q. Low, M. Shen, Z.F. Zhai, Y. Wang, F.Y. Zhang, S. Yang, J.J. Liu, and X.J. Zhang. 2009. Genome-wide association study in a Chinese Han population identifies nine new susceptibility loci for systemic lupus erythematosus. *Nat. Genet.* 41:1234–1237. doi:10.1038/ng.472.

Hankins, H.M., R.D. Baldridge, P. Xu, and T.R. Graham. 2015. Role of Flippases, Scramblases and Transfer Proteins in Phosphatidylserine Subcellular Distribution. *Traffic*. 16:35–47. doi:10.1111/tra.12233.

Harley, J.B., M.E. Alarcón-Riquelme, L.A. Criswell, C.O. Jacob, R.P. Kimberly, K.L. Moser, B.P. Tsao, T.J. Vyse, C.D. Langefeld, S.K. Nath, J.M. Guthridge, B.L. Cobb, D.B. Mirel, M.C. Marion, A.H. Williams, J. Divers, W. Wang, S.G. Frank, B. Namjou, S.B. Gabriel, A.T. Lee, P.K. Gregersen, T.W. Behrens, K.E. Taylor, M. Fernando, R. Zidovetzki, P.M. Gaffney, J.C. Edberg, J.D. Rioux, J.O. Ojwang, J.A. James, J.T. Merrill, G.S. Gilkeson, M.F. Seldin, H. Yin, E.C. Baechler, Q.Z. Li, E.K. Wakeland, G.R. Bruner, K.M. Kaufman, and J.A. Kelly. 2008. Genome-wide association scan in women with systemic lupus erythematosus identifies susceptibility variants in ITGAM, PXK, KIAA1542 and other loci. *Nat. Genet.* 40:204–210. doi:10.1038/ng.81.

Harrison, J., G. Lloyd, M. Joe, T.L. Lowary, E. Reynolds, H. Walters-Morgan, A. Bhatt, A. Lovering, G.S. Besra, and L.J. Alderwick. 2016. Lcp1 is a phosphotransferase responsible for ligating arabinogalactan to peptidoglycan in mycobacterium tuberculosis. *MBio*. 7:1–12. doi:10.1128/mBio.00972-16.

Härtlova, A., S. Herbst, J. Peltier, A. Rodgers, O. Bilkei-Gorzo, A. Fearns, B.D. Dill, H. Lee, R. Flynn, S.A. Cowley, P. Davies, P.A. Lewis, I.G. Ganley, J. Martinez, D.R. Alessi, A.D. Reith, M. Trost, and M.G. Gutierrez. 2018. LRRK2 is a negative regulator of Mycobacterium tuberculosis phagosome maturation in macrophages . *EMBO J.* 37:1–17. doi:10.15252/embj.201798694.

Harvald, E.B., A.S.B. Olsen, and N.J. Færgeman. 2015. Autophagy in the light of sphingolipid metabolism. *Apoptosis*. 20:658–670. doi:10.1007/s10495-015-1108-2.

Hayashi-Nishino, M., N. Fujita, T. Noda, A. Yamaguchi, T. Yoshimori, and A. Yamamoto. 2010. Electron tomography reveals the endoplasmic reticulum as a membrane source for autophagosome formation. *Autophagy*. 6:301–303. doi:10.4161/auto.6.2.11134.

Hayes, M., and N. Zavazava. 2013. Strategies to Generate Induced Pluripotent Stem Cells. *In* Embryonic Stem Cell Immunobiology: Methods and Protocols. N. Zavazava, editor. Humana Press, Totowa, NJ. 77–92.

Heckmann, B.L., B.J.W. Teubner, B. Tummers, E. Boada-Romero, L. Harris, M. Yang, C.S. Guy, S.S. Zakharenko, and D.R. Green. 2019. LC3-Associated Endocytosis Facilitates β-Amyloid Clearance and Mitigates Neurodegeneration in Murine Alzheimer's Disease. *Cell*. 1–16. doi:10.1016/j.cell.2019.05.056.

Hegedus, K., S. Takats, A. Boda, A. Jipa, P. Nagy, K. Varga, A.L. Kovacs, and G. Juhasz. 2016. The Ccz1-Mon1-Rab7 module and Rab5 control distinct steps of autophagy. *Mol. Biol. Cell*. 27:3132–3142. doi:10.1091/mbc.E16-03-0205.

Helming, L., and S. Gordon. 2008. The molecular basis of macrophage fusion. *Immunobiology*. 212:785–793. doi:10.1016/j.imbio.2007.09.012.

Herbst, S., P. Campbell, J. Harvey, E.M. Bernard, V. Papayannopoulos, N.W. Wood, H.R. Morris, and M.G. Gutierrez. 2020. LRRK2 activation controls the repair of damaged endomembranes in macrophages. *EMBO J.* 44:1–14. doi:10.15252/embj.2020104494.

Hettinger, J., D.M. Richards, J. Hansson, M.M. Barra, A.C. Joschko, J. Krijgsveld, and M. Feuerer. 2013. Origin of monocytes and macrophages in a committed progenitor. *Nat. Immunol.* 14:821–830. doi:10.1038/ni.2638.

Hiatt, J., D.A. Cavero, M.J. Mcgregor, D.E. Gordon, W. Zheng, J.M. Budzik, T.L. Roth, K.M. Haas, U. Rathore, A. Mayer-Franke, M.S. Bouzidi, J.F. Hultquist, J.A. Wojcechowskyj, K.A. Fontaine, S.K. Pillai, J.S. Cox, J.D. Ernst, N.J. Krogan, and A. Marson. 2020. Efficient Generation of Isogenic Primary Human Myeloid Cells using CRISPR-Cas9 Ribonucleoproteins. *bioRxiv*.

High, N., J. Mounier, M.C.C. Prévost, and P.J.J. Sansonetti. 1992. IpaB of Shigella flexneri causes entry into epithelial cells and escape from the phagocytic vacuole. *EMBO J.* 11:1991–1999. doi:10.1002/j.1460-2075.1992.tb05253.x.

Hoffpauir, C.T., S.L. Bell, K.O. West, T. Jing, S. Odio-torres, S. Cox, A.P. West, P. Li, K.L. Patrick, and R.O. Watson. 2020. TRIM14 is a key regulator of the type I interferon response during Mycobacterium tuberculosis infection. *bioRxiv*.

Hong, D., J. Ding, O. Li, Q. He, M. Ke, M. Zhu, L. Liu, W. Bin Ou, Y. He, and Y. Wu. 2018. Human-induced pluripotent stem cell-derived macrophages and their immunological function in response to tuberculosis infection. *Stem Cell Res. Ther.* 9:1–14. doi:10.1186/s13287-018-0800-x.

Horwitz, M.A., and F.R. Maxfield. 1984. Legionella pneumophila inhibits acidification of its phagosome in human monocytes. *J. Cell Biol.* 99:1936–1943. doi:10.1083/jcb.99.6.1936.

Houben, D., C. Demangel, J. van Ingen, J. Perez, L. Baldeón, A.M. Abdallah, L. Caleechurn, D. Bottai, M. van Zon, K. de Punder, T. van der Laan, A. Kant, R. Bossers-de Vries, P. Willemsen, W. Bitter, D. van Soolingen, R. Brosch, N. van der Wel, and P.J. Peters. 2012. ESX-1-mediated translocation to the cytosol controls virulence of mycobacteria. *Cell. Microbiol.* 14:1287–1298. doi:10.1111/j.1462-5822.2012.01799.x.

Hu, D., J. Wu, W. Wang, M. Mu, R. Zhao, X. Xu, Z. Chen, J. Xiao, F. Hu, Y. Yang, and R. Zhang. 2015. Autophagy regulation revealed by SapM-induced block of autophagosome-lysosome fusion via binding RAB7. *Biochem. Biophys. Res. Commun.* 461:401–407. doi:10.1016/j.bbrc.2015.04.051.

Huang, J., V. Canadien, G.Y. Lam, B.E. Steinberg, M.C. Dinauer, M.A.O. Magalhaes, M. Glogauer, S. Grinstein, and J.H. Brumell. 2009. Activation of antibacterial autophagy by NADPH oxidases. *Proc. Natl. Acad. Sci.* 106:6226–6231. doi:10.1073/pnas.0811045106.

Hubber, A., T. Kubori, C. Coban, T. Matsuzawa, M. Ogawa, T. Kawabata, T. Yoshimori, and H. Nagai. 2017. Bacterial secretion system skews the fate of Legionella-containing vacuoles towards LC3-associated phagocytosis. *Sci. Rep.* 7:1–17. doi:10.1038/srep44795.

Huett, A., R.J. Heath, J. Begun, S.O. Sassi, L.A. Baxt, J.M. Vyas, M.B. Goldberg, and R.J. Xavier. 2012. The LRR and RING Domain Protein LRSAM1 Is an E3 Ligase Crucial for Ubiquitin-Dependent Autophagy of Intracellular Salmonella Typhimurium. *Cell Host Microbe*. 12:778–790. doi:10.1016/j.chom.2012.10.019.

Hunn, J.P., C.G. Feng, A. Sher, and J.C. Howard. 2011. The immunity-related GTPases in mammals: a fast-evolving cell-autonomous resistance system against intracellular pathogens. *Mamm. Genome*. 22:43–54. doi:10.1007/s00335-010-9293-3.

Ilic, D., and C. Ogilvie. 2017. Concise Review : Human Embryonic Stem Cells — What Have We Done ? What Are We Doing ? Where Are We Going ? *Stem Cells*. 35:17–25.

Iliopoulos, A., K. Psathakis, S. Aslanidis, L. Skagias, and P.P. Sfikakis. 2006. Tuberculosis and granuloma formation in patients receiving anti-TNF therapy. *Int. J. Tuberc. Lung Dis.* 10:588–590.

Inoue, J., E.W. Krueger, J. Chen, H. Cao, M. Ninomiya, and M.A. McNiven. 2015. HBV secretion is regulated through the activation of endocytic and autophagic compartments mediated by Rab7 stimulation. *J. Cell Sci.* 128:1696–706. doi:10.1242/jcs.158097.

Itakura, E., C. Kishi-Itakura, and N. Mizushima. 2012. The hairpin-type tail-anchored SNARE syntaxin 17 targets to autophagosomes for fusion with endosomes/lysosomes. *Cell*. 151:1256–1269. doi:10.1016/j.cell.2012.11.001.

Ito, C., Y. Saito, T. Nozawa, S. Fujii, T. Sawa, H. Inoue, T. Matsunaga, S. Khan, S. Akashi, R. Hashimoto, C. Aikawa, E. Takahashi, H. Sagara, M. Komatsu, K. Tanaka, T. Akaike, I. Nakagawa, and H. Arimoto. 2013. Endogenous nitrated nucleotide is a key mediator of autophagy and innate defense against bacteria. *Mol. Cell*. 52:794–804. doi:10.1016/j.molcel.2013.10.024.

Jayaswal, S., M.A. Kamal, R. Dua, S. Gupta, T. Majumdar, G. Das, D. Kumar, and K.V.S. Rao. 2010. Identification of host-dependent survival factors for

intracellular Mycobacterium tuberculosis through an siRNA screen. *PLoS Pathog.* 6:1–15. doi:10.1371/journal.ppat.1000839.

Ji, D.X., L.H. Yamashiro, K.J. Chen, N. Mukaida, I. Kramnik, K.H. Darwin, and R.E. Vance. 2019. Type I interferon-driven susceptibility to Mycobacterium tuberculosis is mediated by IL-1Ra. *Nat. Microbiol.* 4:2128–2135. doi:10.1038/s41564-019-0578-3.

Jia, J., Y.P. Abudu, A. Claude-Taupin, Y. Gu, S. Kumar, S.W. Choi, R. Peters, M.H. Mudd, L. Allers, M. Salemi, B. Phinney, T. Johansen, and V. Deretic. 2018. Galectins Control mTOR in Response to Endomembrane Damage. *Mol. Cell*. 70:120-135.e8. doi:10.1016/j.molcel.2018.03.009.

Jia, J., B. Bissa, L. Brecht, L. Allers, S.W. Choi, Y. Gu, M. Zbinden, M.R. Burge, G. Timmins, K. Hallows, C. Behrends, and V. Deretic. 2020a. AMPK, a Regulator of Metabolism and Autophagy, Is Activated by Lysosomal Damage via a Novel Galectin-Directed Ubiquitin Signal Transduction System. *Mol. Cell*. 77:951-969.e9. doi:10.1016/j.molcel.2019.12.028.

Jia, J., A. Claude-Taupin, Y. Gu, S.W. Choi, R. Peters, B. Bissa, M.H. Mudd, L. Allers, S. Pallikkuth, K.A. Lidke, M. Salemi, B. Phinney, M. Mari, F. Reggiori, and V. Deretic. 2020b. Galectin-3 Coordinates a Cellular System for Lysosomal Repair and Removal. *Dev. Cell*. 52. doi:10.1016/j.devcel.2019.10.025.

Jiang, Y., S.A. Cowley, U. Siler, D. Melguizo, K. Tilgner, C. Browne, A. Dewilton, S. Przyborski, G. Saretzki, W.S. James, R.A. Seger, J. Reichenbach, M. Lako, and L. Armstrong. 2012. Derivation and functional analysis of patient-specific induced pluripotent stem cells as an in vitro model of chronic granulomatous disease. *Stem Cells*. 30:599–611. doi:10.1002/stem.1053.

Jimenez, A.J., P. Maiuri, J. Lafaurie-Janvore, S. Divoux, M. Piel, and F. Perez. 2014. ESCRT machinery is required for plasma membrane repair. *Science (80-.).* 343. doi:10.1126/science.1247136.

Johnson, J.R., T. Parry, T. Repasy, K. Geiger, E. Verschueren, J.M. Budzik, D. Jimenez-Morales, B.W. Newton, E. Powell, L. Cocoy, D.A. Portnoy, N.J. Krogan, and J.S. Cox. 2020. Comparative analysis of macrophage post-translational modifications during intracellular bacterial pathogen infection. *bioRxiv*.

De Jonge, M.I., G. Pehau-Arnaudet, M.M. Fretz, F. Romain, D. Bottai, P. Brodin, N. Honoré, G. Marchal, W. Jiskoot, P. England, S.T. Cole, and R. Brosch. 2007. ESAT-6 from Mycobacterium tuberculosis dissociates from its putative chaperone CFP-10 under acidic conditions and exhibits membrane-lysing activity. *J. Bacteriol.* 189:6028–6034. doi:10.1128/JB.00469-07.

Kabeya, Y., N. Mizushima, T. Ueno, A. Yamamoto, T. Kirisako, T. Noda, E. Kominami, Y. Ohsumi, and T. Yoshimori. 2000. LC3, a mammalian homolog of yeast Apg8p, is localized in autophagosome membranes after processing. *EMBO J.* 19:5720–5728. doi:10.1093/emboj/cdg454.

Kabeya, Y., N. Mizushima, A. Yamamoto, S. Oshitani-Okamoto, Y. Ohsumi, and T. Yoshimori. 2004. LC3, GABARAP and GATE16 localize to autophagosomal membrane depending on form-II formation. *J. Cell Sci.* 117:2805–2812. doi:10.1242/jcs.01131\r117/13/2805 [pii].

Kageyama, S., H. Omori, T. Saitoh, T. Sone, J.L. Guan, S. Akira, F. Imamoto, T. Noda, and T. Yoshimori. 2011. The LC3 recruitment mechanism is separate from Atg9L1-dependent membrane formation in the autophagic response against Salmonella. *Mol. Biol. Cell*. 22:2290–2300. doi:10.1091/mbc.E10-11-0893.

Kambal, A., G. Mitchell, W. Cary, W. Gruenloh, Y. Jung, S. Kalomoiris, C. Nacey, J. McGee, M. Lindsey, B. Fury, G. Bauer, J.A. Nolta, and J.S. Anderson. 2011. Generation of HIV-1 resistant and functional macrophages from hematopoietic stem cell-derived induced pluripotent stem cells. *Mol. Ther.* 19:584–593. doi:10.1038/mt.2010.269.

Kamijo, R., H. Harada, T. Matsuyama, M. Bosland, J. Gerecitano, D. Shapiro, J. Le, S.I. Koh, T. Kimura, S.J. Green, T.W. Mak, T. Taniguchi, and J. Vilček. 1994. Requirement for transcription factor IRF-1 in NO synthase induction in macrophages. *Science (80-.).* 263:1612–1615. doi:10.1126/science.7510419.

Kaplan, G., F.A. Post, A.L. Moreira, H. Wainwright, B. Kreiswirth, M. Tanverdi, B. Mathema, S. V Ramaswamy, G. Walther, L.M. Steyn, C.E. Barry, and L. Bekker. 2003. Mycobacterium tuberculosis Growth at the Cavity Surface: a Microenvironment with Failed Immunity. *Infect. Immun.* 71:7099–7108. doi:10.1128/IAI.71.12.7099–7108.2003.

Katzmann, D.J., M. Babst, and S.D. Emr. 2001. Ubiquitin-dependent sorting into the multivesicular body pathway requires the function of a conserved endosomal protein sorting complex, ESCRT-I. *Cell*. 106:145–155. doi:10.1016/S0092-8674(01)00434-2.

Kauffman, K.J., S. Yu, J. Jin, B. Mugo, N. Nguyen, A. O'Brien, S. Nag, A.H. Lystad, and T.J. Melia. 2018. Delipidation of mammalian Atg8-family proteins by each of the four ATG4 proteases. *Autophagy*. 14:992–1010. doi:10.1080/15548627.2018.1437341.

Killick, K.E., C. Ní Cheallaigh, C. O'Farrelly, K. Hokamp, D.E. Machugh, and J. Harris. 2013. Receptor-mediated recognition of mycobacterial pathogens. *Cell. Microbiol.* 15:1484–1495. doi:10.1111/cmi.12161.

Kim, B.-H., A.R. Shenoy, P. Kumar, R. Das, S. Tiwari, and J.D. MacMicking. 2011a. A Family of IFN-gamma-Inducible 65-kD GTPases Protects Against Bacterial Infection. *Science (80-.).* 332:717–721. doi:10.1126/science.1201711.

Kim, H.J., Q. Zhong, Z.H. Sheng, T. Yoshimori, C. Liang, and J.U. Jung. 2012a. Beclin-1-interacting autophagy protein Atg14L targets the SNARE-associated protein Snapin to coordinate endocytic trafficking. *J. Cell Sci.* 125:4740–4750. doi:10.1242/jcs.100339.

Kim, J., V.M. Dalton, K.P. Eggerton, S. V. Scott, and D.J. Klionsky. 1999. Apg7p/Cvt2p is required for the cytoplasm-to-vacuole targeting, macroautophagy, and peroxisome degradation pathways. *Mol. Biol. Cell*. 10:1337–1351. doi:10.1091/mbc.10.5.1337.

Kim, J., B.-K. Koo, and J.A. Knoblich. 2020. Human organoids: model systems for human biology and medicine. *Nat. Rev. Mol. Cell Biol.* 21:571–584. doi:10.1038/s41580-020-0259-3.

Kim, J., M. Kundu, B. Viollet, and K.L. Guan. 2011b. AMPK and mTOR regulate autophagy through direct phosphorylation of Ulk1. *Nat. Cell Biol.* 13:132–141. doi:10.1038/ncb2152.

Kim, J.J., H.M. Lee, D.M. Shin, W. Kim, J.M. Yuk, H.S. Jin, S.H. Lee, G.H. Cha, J.M. Kim, Z.W. Lee, S.J. Shin, H. Yoo, Y.K. Park, J.B. Park, J. Chung, T. Yoshimori, and E.K. Jo. 2012b. Host cell autophagy activated by antibiotics is required for their effective antimycobacterial drug action. *Cell Host Microbe*. 11:457–468. doi:10.1016/j.chom.2012.03.008.

Kim, J.K., H.M. Lee, K.S. Park, D.M. Shin, T.S. Kim, Y.S. Kim, H.W. Suh, S.Y. Kim, I.S. Kim, J.M. Kim, J.W. Son, K.M. Sohn, S.S. Jung, C. Chung, S.B. Han, C.S. Yang, and E.K. Jo. 2017. MIR144* inhibits antimicrobial responses against Mycobacterium tuberculosis in human monocytes and macrophages by targeting the autophagy protein DRAM2. *Autophagy*. 13:423–441. doi:10.1080/15548627.2016.1241922.

Kim, J.K., J.-M. Yuk, S.Y. Kim, T.S. Kim, H.S. Jin, C.-S. Yang, and E.-K. Jo. 2015. MicroRNA-125a Inhibits Autophagy Activation and Antimicrobial Responses during Mycobacterial Infection. *J. Immunol.* 194:5355–5365. doi:10.4049/jimmunol.1402557.

Kimmey, J.M., J.P. Huynh, L.A. Weiss, S. Park, A. Kambal, J. Debnath, H.W. Virgin, and C.L. Stallings. 2015. Unique role for ATG5 in neutrophil-mediated immunopathology during M. tuberculosis infection. *Nature*. 528:565–9. doi:10.1038/nature16451.

Kimura, S., T. Noda, and T. Yoshimori. 2007. Dissection of the autophagosome maturation process by a novel reporter protein, tandem fluorescent-tagged LC3. *Autophagy*. 3:452–460. doi:10.4161/auto.4451.

Klionsky, D.J., K. Abdelmohsen, A. Abe, M.J. Abedin, H. Abeliovich, A.A. Arozena, H. Adachi, C.M. Adams, P.D. Adams, K. Adeli, P.J. Adhihetty, S.G. Adler, G. Agam, R. Agarwal, M.K. Aghi, M. Agnello, P. Agostinis, P. V. Aguilar, J. Aguirre-Ghiso, E.M. Airoldi, S. Ait-Si-Ali, T. Akematsu, E.T. Akporiaye, M. Al-Rubeai, G.M. Albaiceta, C. Albanese, D. Albani, M.L. Albert, J. Aldudo, H. Algül, M. Alirezaei, I. Alloza, A. Almasan, M. Almonte-Beceril, E.S. Alnemri, C. Alonso, N. Altan-Bonnet, D.C. Altieri, S. Alvarez, L. Alvarez-Erviti, S. Alves, G. Amadoro, A. Amano, C. Amantini, S. Ambrosio, I. Amelio, A.O. Amer, M. Amessou, A. Amon, Z. An, F.A. Anania, S.U. Andersen, U.P. Andley, C.K. Andreadi, N. Andrieu-Abadie, A. Anel, D.K. Ann, S. Anoopkumar-Dukie, M. Antonioli, H. Aoki,

N. Apostolova, S. Aquila, K. Aquilano, K. Araki, E. Arama, A. Aranda, J. Araya, A. Arcaro, E. Arias, H. Arimoto, A.R. Ariosa, J.L. Armstrong, T. Arnould, I. Arsov, K. Asanuma, V. Askanas, E. Asselin, R. Atarashi, S.S. Atherton, J.D. Atkin, L.D. Attardi, P. Auberger, G. Auburger, L. Aurelian, R. Autelli, L. Avagliano, M.L. Avantaggiati, L. Avrahami, N. Azad, S. Awale, T. Bachetti, J.M. Backer, D.H. Bae, J.S. Bae, O.N. Bae, S.H. Bae, E.H. Baehrecke, S.H. Baek, et al. 2016. Guidelines for the use and interpretation of assays for monitoring autophagy (3rd edition). *Autophagy*. 12:1–222. doi:10.1080/15548627.2015.1100356.

Klionsky, D.J., and E.L. Eskelinen. 2014. The vacuole versus the lysosome: When size matters. *Autophagy*. 10:185–187. doi:10.4161/auto.27367.

Knodler, L.A., B.A. Vallance, J. Celli, S. Winfree, B. Hansen, M. Montero, and O. Steele-Mortimer. 2010. Dissemination of invasive Salmonella via bacterial-induced extrusion of mucosal epithelia. *Proc. Natl. Acad. Sci. U. S. A.* 107:17733–17738. doi:10.1073/pnas.1006098107.

Koerver, L., C. Papadopoulos, B. Liu, B. Kravic, G. Rota, L. Brecht, T. Veenendaal, M. Polajnar, A. Bluemke, M. Ehrmann, J. Klumperman, M. Jäättelä, C. Behrends, and H. Meyer. 2019. The ubiquitin-conjugating enzyme UBE2QL1 coordinates lysophagy in response to endolysosomal damage. *EMBO Rep.* 20:1–17. doi:10.15252/embr.201948014.

Komander, D., and M. Rape. 2012. The ubiquitin code. *Annu. Rev. Biochem.* 81:203–229. doi:10.1146/annurev-biochem-060310-170328.

Konno, H., K. Konno, and G.N. Barber. 2013. XCyclic dinucleotides trigger ULK1 (ATG1) phosphorylation of STING to prevent sustained innate immune signaling. *Cell*. 155:688. doi:10.1016/j.cell.2013.09.049.

Köster, S., S. Upadhay, P. Changra, K. Papavinasasundaram, G. Yang, A. Hassan, S.J. Grigsby, E. Mittal, H.S. Park, V. Jones, F. Hsu, M. Jackson, C.M. Sassetti, and J.A. Philips. 2017. Mycobacterium tuberculosis is protected from NADPH oxidase and LC3-associated phagocytosis by the LCP protein CpsA. *Proc. Natl. Acad. Sci.* 114:E8711–E8720. doi:10.1073/pnas.1718266114.

Kramnik, I., and G. Beamer. 2016. Mouse models of human TB pathology: roles in the analysis of necrosis and the development of host-directed therapies. *Semin. Immunopathol.* 38:221–237. doi:10.1007/s00281-015-0538-9.

Kreibich, S., M. Emmenlauer, J. Fredlund, P. Rämö, C. Münz, C. Dehio, J. Enninga, and W.D. Hardt. 2015. Autophagy proteins promote repair of endosomal membranes damaged by the Salmonella type three secretion system 1. *Cell Host Microbe*. 18:527–537. doi:10.1016/j.chom.2015.10.015.

Kremer, J.R., D.N. Mastronarde, and J.R. McIntosh. 1996. Computer visualization of three-dimensional image data using IMOD. *J. Struct. Biol.* 116:71–76. doi:10.1006/jsbi.1996.0013.

Kumar, D., L. Nath, M.A. Kamal, A. Varshney, A. Jain, S. Singh, and K.V.S. Rao. 2010. Genome-wide Analysis of the Host Intracellular Network that Regulates

Survival of Mycobacterium tuberculosis. *Cell*. 140:731–743. doi:10.1016/j.cell.2010.02.012.

Kumar, S., A. Jain, F. Farzam, J. Jia, Y. Gu, S.W. Choi, M.H. Mudd, A. Claude-Taupin, M.J. Wester, K.A. Lidke, T.E. Rusten, and V. Deretic. 2018. Mechanism of Stx17 recruitment to autophagosomes via IRGM and mammalian Atg8 proteins. *J. Cell Biol.* 217:997–1013. doi:10.1083/jcb.201708039.

Kumar, V.A., R. Goyal, R. Bansal, N. Singh, R.R. Sevalkar, A. Kumar, and D. Sarkar. 2016. Espr-dependent ESAT-6 protein secretion of Mycobacterium tuberculosis requires the presence of virulence regulator phoP. *J. Biol. Chem.* 291:19018–19030. doi:10.1074/jbc.M116.746289.

van de Laar, L., W. Saelens, S. De Prijck, L. Martens, C.L. Scott, G. Van Isterdael, E. Hoffmann, R. Beyaert, Y. Saeys, B.N. Lambrecht, and M. Guilliams. 2016. Yolk Sac Macrophages, Fetal Liver, and Adult Monocytes Can Colonize an Empty Niche and Develop into Functional Tissue-Resident Macrophages. *Immunity*. 44:755–768. doi:10.1016/j.immuni.2016.02.017.

Lacey, D.C., A. Achuthan, A.J. Fleetwood, H. Dinh, J. Roiniotis, G.M. Scholz, M.W. Chang, S.K. Beckman, A.D. Cook, and J.A. Hamilton. 2012. Defining GM-CSF–and Macrophage-CSF–Dependent Macrophage Responses by In Vitro Models. *J. Immunol.* 188:5752–5765. doi:10.4049/jimmunol.1103426.

Lachmann, N., C. Happle, M. Ackermann, D. Lüttge, M. Wetzke, S. Merkert, M. Hetzel, G. Kensah, M. Jara-Avaca, A. Mucci, J. Skuljec, A.M. Dittrich, N. Pfaff, S. Brennig, A. Schambach, D. Steinemann, G. Göhring, T. Cantz, U. Martin, N. Schwerk, G. Hansen, and T. Moritz. 2014. Gene correction of human induced pluripotent stem cells repairs the cellular phenotype in pulmonary alveolar proteinosis. *Am. J. Respir. Crit. Care Med.* 189:167–182. doi:10.1164/rccm.201306-1012OC.

Lam, G.Y., M. Cemma, A.M. Muise, D.E. Higgins, and J.H. Brumell. 2013. Host and bacterial factors that regulate LC3 recruitment to Listeria monocytogenes during the early stages of macrophage infection. *Autophagy*. 9:985–995. doi:10.4161/auto.24406.

Lamb, C.A., H.C. Dooley, and S.A. Tooze. 2013. Endocytosis and autophagy: Shared machinery for degradation. *BioEssays*. 35:34–45. doi:10.1002/bies.201200130.

Lang, J., Y. Cheng, A. Rolfe, C. Hammack, D. Vera, K. Kyle, J. Wang, T.B. Meissner, Y. Ren, C. Cowan, and H. Tang. 2018. An hPSC-Derived Tissue-Resident Macrophage Model Reveals Differential Responses of Macrophages to ZIKV and DENV Infection. *Stem Cell Reports*. 11:348–362. doi:10.1016/j.stemcr.2018.06.006.

Lassen, K.G., P. Kuballa, K.L. Conway, K.K. Patel, C.E. Becker, J.M. Peloquin, E.J. Villablanca, J.M. Norman, T.-C. Liu, R.J. Heath, M.L. Becker, L. Fagbami, H. Horn, J. Mercer, O.H. Yilmaz, J.D. Jaffe, A.F. Shamji, A.K. Bhan, S.A. Carr, M.J.

Daly, H.W. Virgin, S.L. Schreiber, T.S. Stappenbeck, and R.J. Xavier. 2014. Atg16L1 T300A variant decreases selective autophagy resulting in altered cytokine signaling and decreased antibacterial defense. *Proc. Natl. Acad. Sci.* 111:7741–7746. doi:10.1073/pnas.1407001111.

Lazarevic, V., D. Nolt, and J.L. Flynn. 2005. Long-Term Control of Mycobacterium tuberculosis Infection Is Mediated by Dynamic Immune Responses. *J. Immunol.* 175:1107–1117. doi:10.4049/jimmunol.175.2.1107.

Leake, E.S., Q.N. Myrvik, and M.J. Wright. 1984. Phagosomal membranes of Mycobacterium bovis BCG-immune alveolar macrophages are resistant to disruption by Mycobacterium tuberculosis H37Rv. *Infect. Immun.* 45:443–446.

Lee, C.Z.W., T. Kozaki, and F. Ginhoux. 2018. Studying tissue macrophages in vitro: are iPSC-derived cells the answer? *Nat. Rev. Immunol.* 18:716–725. doi:10.1038/s41577-018-0054-y.

Lee, G., C.N. Ramirez, H. Kim, N. Zeltner, B. Liu, C. Radu, B. Bhinder, Y.J. Kim, I. Choi, H. Mukherjee-Clavin, B Djaballah, and L. Studer. 2012. Identification of Compounds that Rescue IKBKAP Expression in Familial Dysautonomia-iPS Cells. *Nat Biotechnol.* 30:1244–1248. doi:10.1038/nbt.2435.Identification.

Lee, H., R. Flynn, I. Sharma, E. Haberman, P.J. Carling, F.J. Nicholls, M. Stegmann, J. Vowles, W. Haenseler, R. Wade-Martins, W.S. James, and S.A. Cowley. 2020. LRRK2 Is Recruited to Phagosomes and Co-recruits RAB8 and RAB10 in Human Pluripotent Stem Cell-Derived Macrophages. *Stem Cell Reports*. 14:940–955. doi:10.1016/j.stemcr.2020.04.001.

Lee, I.H., L. Cao, R. Mostoslavsky, D.B. Lombard, J. Liu, N.E. Bruns, M. Tsokos, F.W. Alt, and T. Finkel. 2008. A role for the NAD-dependent deacetylase Sirt1 in the regulation of autophagy. *Proc. Natl. Acad. Sci.* 105:3374–3379. doi:10.1073/pnas.0712145105.

Leemans, J.C., N.P. Juffermans, S. Florquin, N. van Rooijen, M.J. Vervoordeldonk, A. Verbon, S.J.H. van Deventer, and T. van der Poll. 2001. Depletion of Alveolar Macrophages Exerts Protective Effects in Pulmonary Tuberculosis in Mice. *J. Immunol.* 166:4604–4611. doi:10.4049/jimmunol.166.7.4604.

Lerner, T.R., S. Borel, D.J. Greenwood, U. Repnik, M.R.G. Russell, S. Herbst, M.L. Jones, L.M. Collinson, G. Griffiths, and M.G. Gutierrez. 2017. Mycobacterium tuberculosis replicates within necrotic human macrophages. *J. Cell Biol.* 216:583–594. doi:10.1083/jcb.201603040.

Lerner, T.R., S. Borel, and M.G. Gutierrez. 2015. The innate immune response in human tuberculosis. *Cell. Microbiol.* 17:1277–1285. doi:10.1111/cmi.12480.

Lerner, T.R., C.D.S. Carvalho-Wodarz, U. Repnik, M.R.G. Russell, S. Borel, C.R. DIedrich, M. Rohde, H. Wainwright, L.M. Collinson, R.J. Wilkinson, G. Griffiths, and M.G. Gutierrez. 2016. Lymphatic endothelial cells are a replicative niche for Mycobacterium tuberculosis. *J. Clin. Invest.* 126:1093–1108. doi:10.1172/JCI83379.

Lerner, T.R., C.J. Queval, A. Fearns, U. Repnik, G. Griffiths, and M.G. Gutierrez. 2018. Phthiocerol dimycocerosates promote access to the cytosol and intracellular burden of Mycobacterium tuberculosis in lymphatic endothelial cells. *BMC Biol.* 16:1. doi:10.1186/s12915-017-0471-6.

Lerner, T.R., C.J. Queval, R.P. Lai, M.R.G. Russell, A. Fearns, D.J. Greenwood, L. Collinson, R.J. Wilkinson, and M.G. Gutierrez. 2020. Mycobacterium tuberculosis cords in the cytosol of live lymphatic endothelial cells to evade host immune surveillance. *JCI Insight*. doi:10.1172/jci.insight.136937.

Levine, B., and V. Deretic. 2007. Unveiling the roles of autophagy in innate and adaptive immunity. *Nat. Rev. Immunol.* 7:767–777. doi:10.1038/nri2161.

Levitte, S., K.N. Adams, R.D. Berg, C.L. Cosma, K.B. Urdahl, and L. Ramakrishnan. 2016. Mycobacterial Acid Tolerance Enables Phagolysosomal Survival and Establishment of Tuberculous Infection In Vivo. *Cell Host Microbe*. 20:250–258. doi:10.1016/j.chom.2016.07.007.

Lewis, K.N., R. Liao, K.M. Guinn, M.J. Hickey, S. Smith, M.A. Behr, and D.R. Sherman. 2003. Deletion of RD1 from Mycobacterium tuberculosis Mimics Bacille Calmette-Guérin Attenuation. *J. Infect. Dis.* 187:117–123. doi:10.1086/345862.

Li, Y. yuan, T. Wang, S. Gao, G. mei Xu, H. Niu, R. Huang, and S. yan Wu. 2016. Salmonella plasmid virulence gene spvB enhances bacterial virulence by inhibiting autophagy in a zebrafish infection model. *Fish Shellfish Immunol.* 49:252–259. doi:10.1016/j.fsi.2015.12.033.

Liang, Q., G.J. Seo, Y.J. Choi, M.J. Kwak, J. Ge, M.A. Rodgers, M. Shi, B.J. Leslie, K.P. Hopfner, T. Ha, B.H. Oh, and J.U. Jung. 2014. Crosstalk between the cGAS DNA sensor and beclin-1 autophagy protein shapes innate antimicrobial immune responses. *Cell Host Microbe*. 15:228–238. doi:10.1016/j.chom.2014.01.009.

Lienard, J., E. Movert, C. Valfridsson, E. Sturegård, and F. Carlsson. 2016. ESX-1 exploits type I IFN-signalling to promote a regulatory macrophage phenotype refractory to IFNγ-mediated autophagy and growth restriction of intracellular mycobacteria. *Cell. Microbiol.* 18:1471–1485. doi:10.1111/cmi.12594.

Lin, J., Y. Hu, S. Nunez, A.S. Foulkes, B. Cieply, C. Xue, M. Gerelus, W. Li, H. Zhang, D.J. Rader, K. Musunuru, M. Li, and M.P. Reilly. 2016. Transcriptome-Wide Analysis Reveals Modulation of Human Macrophage Inflammatory Phenotype Through Alternative Splicing. *Arterioscler. Thromb. Vasc. Biol.* 36:1434–1447. doi:10.1161/ATVBAHA.116.307573.

Lin, Y., J. Gong, M. Zhang, W. Xue, and P.F. Barnes. 1998. Production of monocyte chemoattractant protein 1 in tuberculosis patients. *Infect. Immun.* 66:2319–2322. doi:10.1128/iai.66.5.2319-2322.1998.

López-Jiménez, A.T., E. Cardenal-Muñoz, F. Leuba, L. Gerstenmaier, C. Barisch, M. Hagedorn, J.S. King, and T. Soldati. 2018. The ESCRT and autophagy

machineries cooperate to repair ESX-1-dependent damage at the Mycobacterium-containing vacuole but have opposite impact on containing the infection. *PLoS Pathog.* 14:1–29. doi:10.1371/journal.ppat.1007501.

López de Armentia, M.M., M.C. Gauron, and M.I. Colombo. 2017. Staphylococcus aureus Alpha-Toxin Induces the Formation of Dynamic Tubules Labeled with LC3 within Host Cells in a Rab7 and Rab1b-Dependent Manner. *Front. Cell. Infect. Microbiol.* 7:1–17. doi:10.3389/fcimb.2017.00431.

Losier, T.T., M. Akuma, O.C. McKee-Muir, N.D. LeBlond, Y. Suk, R.M. Alsaadi, Z. Guo, R. Reshke, S. Sad, F.-X. Campbell-Valois, D.J. Gibbings, M.D. Fullerton, and R.C. Russell. 2019. AMPK Promotes Xenophagy through Priming of Autophagic Kinases upon Detection of Bacterial Outer Membrane Vesicles. *Cell Rep.* 26:2150-2165.e5. doi:10.1016/j.celrep.2019.01.062.

Lowe, D.M., P.S. Redford, R.J. Wilkinson, A. O'Garra, and A.R. Martineau. 2012. Neutrophils in tuberculosis: Friend or foe? *Trends Immunol.* 33:14–25. doi:10.1016/j.it.2011.10.003.

Lugo-Villarino, G., C. Cougoule, E. Meunier, Y. Rombouts, C. Vérollet, and L. Balboa. 2019. Editorial: The mononuclear phagocyte system in infectious disease. *Front. Immunol.* 10. doi:10.3389/fimmu.2019.01443.

Ma, J., C. Becker, C.A. Lowell, and D.M. Underhill. 2012. Dectin-1-triggered recruitment of light chain 3 protein to phagosomes facilitates major histocompatibility complex class II presentation of fungal-derived antigens. *J. Biol. Chem.* 287:34149–34156. doi:10.1074/jbc.M112.382812.

Machiels, B., M. Dourcy, X. Xiao, J. Javaux, C. Mesnil, C. Sabatel, D. Desmecht, F. Lallemand, P. Martinive, H. Hammad, M. Guilliams, B. Dewals, A. Vanderplasschen, B.N. Lambrecht, F. Bureau, and L. Gillet. 2017. A gammaherpesvirus provides protection against allergic asthma by inducing the replacement of resident alveolar macrophages with regulatory monocytes. *Nat. Immunol.* 18:1310–1320. doi:10.1038/ni.3857.

Macian, F. 2019. Autophagy in T Cell Function and Aging. *Front. Cell Dev. Biol.* 7:1–9. doi:10.3389/fcell.2019.00213.

Maeda, S., C. Otomo, and T. Otomo. 2019. The autophagic membrane tether ATG2A transfers lipids between membranes. *Elife*. 8:1–24. doi:10.7554/eLife.45777.

Maeda, S., H. Yamamoto, L.N. Kinch, C.M. Garza, S. Takahashi, C. Otomo, N. V. Grishin, S. Forli, N. Mizushima, and T. Otomo. 2020. Structure, lipid scrambling activity and role in autophagosome formation of ATG9A. *Nat. Struct. Mol. Biol.* doi:10.1038/s41594-020-00520-2.

Maejima, I., A. Takahashi, H. Omori, T. Kimura, Y. Takabatake, T. Saitoh, A. Yamamoto, M. Hamasaki, T. Noda, Y. Isaka, and T. Yoshimori. 2013. Autophagy sequesters damaged lysosomes to control lysosomal biogenesis and kidney injury. *EMBO J.* 32:2336–2347. doi:10.1038/emboj.2013.171.

Majlessi, L., P. Brodin, R. Brosch, M.-J. Rojas, H. Khun, M. Huerre, S.T. Cole, and C. Leclerc. 2005. Influence of ESAT-6 Secretion System 1 (RD1) of Mycobacterium tuberculosis on the Interaction between Mycobacteria and the Host Immune System . *J. Immunol.* 174:3570–3579. doi:10.4049/jimmunol.174.6.3570.

Malik-Kale, P., S. Winfree, and O. Steele-Mortimer. 2012. The bimodal lifestyle of intracellular Salmonella in epithelial cells: Replication in the cytosol obscures defects in vacuolar replication. *PLoS One*. 7:1–10. doi:10.1371/journal.pone.0038732.

Manzanillo, P.S., J.S. Ayres, R.O. Watson, A.C. Collins, C.S. Rae, D.S. Schneider, K. Nakamura, M.U. Shiloh, and J.S. Cox. 2013. PARKIN ubiquitin ligase mediates resistance to intracellular pathogens. *Nature*. 501:512–516. doi:10.1038/nature12566.

Marrink, S.J., A.H. de Vries, and D.P. Tieleman. 2009. Lipids on the move: Simulations of membrane pores, domains, stalks and curves. *Biochim. Biophys. Acta - Biomembr.* 1788:149–168. doi:10.1016/j.bbamem.2008.10.006.

Martin, L.J., J. Gupta, S.S.S.K. Jyothula, M. Kovacic, J.M. Myers, T.L. Patterson, M.B. Ericksen, H. He, A.M. Gibson, T.M. Baye, S. Amirisetty, A.M. Tsoras, Y. Sha, N.T. Eissa, and G.K.K. Hershey. 2012. Functional variant in the autophagy-related 5 gene promotor is associated with childhood asthma. *PLoS One*. 7. doi:10.1371/journal.pone.0033454.

Martinez, J., J. Almendinger, A. Oberst, R. Ness, C.P. Dillon, P. Fitzgerald, M.O. Hengartner, and D.R. Green. 2011. Microtubule-associates protein 1 light chain 3 alpha (LC3) -associated phagocytosis is required for the efficient clearance of dead cells. *Proc. Natl. Acad. Sci.* 108:17396–17401. doi:10.1073/pnas.1113421108/-/DCSupplemental.www.pnas.org/cgi/doi/10.1073/pnas.1113421108.

Martinez, J., L.D. Cunha, S. Park, M. Yang, Q. Lu, R. Orchard, Q.Z. Li, M. Yan, L. Janke, C. Guy, A. Linkermann, H.W. Virgin, and D.R. Green. 2016. Noncanonical autophagy inhibits the autoinflammatory, lupus-like response to dying cells. *Nature*. 533:115–119. doi:10.1038/nature17950.

Martinez, J., R.K.S. Malireddi, Q. Lu, L.D. Cunha, S. Pelletier, S. Gingras, R. Orchard, J.-L. Guan, H. Tan, J. Peng, T.-D. Kanneganti, H.W. Virgin, and D.R. Green. 2015. Molecular characterization of LC3-associated phagocytosis reveals distinct roles for Rubicon, NOX2 and autophagy proteins. *Nat. Cell Biol.* 17:893–906. doi:10.1038/ncb3192.

Matoba, K., T. Kotani, A. Tsutsumi, T. Tsuji, T. Mori, D. Noshiro, Y. Sugita, N. Nomura, S. Iwata, Y. Ohsumi, T. Fujimoto, H. Nakatogawa, M. Kikkawa, and N.N. Noda. 2020. Atg9 is a lipid scramblase that mediates autophagosomal membrane expansion. *Nat. Struct. Mol. Biol.* doi:10.1038/s41594-020-00518-w.

Matsui, T., P. Jiang, S. Nakano, Y. Sakamaki, H. Yamamoto, and N. Mizushima.

2018. Autophagosomal YKT6 is required for fusion with lysosomes independently of syntaxin 17. *J. Cell Biol.* 217:2633–2645. doi:10.1083/jcb.201712058.

Matsunaga, K., T. Saitoh, K. Tabata, H. Omori, T. Satoh, N. Kurotori, I. Maejima, K. Shirahama-Noda, T. Ichimura, T. Isobe, S. Akira, T. Noda, and T. Yoshimori. 2009. Two Beclin 1-binding proteins, Atg14L and Rubicon, reciprocally regulate autophagy at different stages. *Nat. Cell Biol.* 11:385–96. doi:10.1038/ncb1846.

Matsuzawa-Ishimoto, Y., S. Hwang, and K. Cadwell. 2018. Autophagy and Inflammation. *Annu. Rev. Immunol.* 36:73–101. doi:10.1146/annurev-immunol-042617-053253.

Mattila, J.T., O.O. Ojo, D. Kepka-Lenhart, S. Marino, J.H. Kim, S.Y. Eum, L.E. Via, C.E. Barry, E. Klein, D.E. Kirschner, S.M. Morris, P.L. Lin, and J.L. Flynn. 2013. Microenvironments in Tuberculous Granulomas Are Delineated by Distinct Populations of Macrophage Subsets and Expression of Nitric Oxide Synthase and Arginase Isoforms. *J. Immunol.* 191:773–784. doi:10.4049/jimmunol.1300113.

McDonough, K.A., Y. Kress, and B.R. Bloom. 1993. The interaction of Mycobacterium tuberculosis with macrophages: a study of phagolysosome fusion. *Infect. Immun.* 2:232–235. doi: .

McEwan, D.G., D. Popovic, A. Gubas, S. Terawaki, H. Suzuki, D. Stadel, F.P. Coxon, D. MirandadeStegmann, S. Bhogaraju, K. Maddi, A. Kirchof, E. Gatti, M.H. Helfrich, S. Wakatsuki, C. Behrends, P. Pierre, and I. Dikic. 2015. PLEKHM1 regulates autophagosome-lysosome fusion through HOPS complex and LC3/GABARAP proteins. *Mol. Cell*. 57:39–54. doi:10.1016/j.molcel.2014.11.006.

Mcgourty, K., T.L. Thurston, S.A. Matthews, L. Pinaud, L.J. Mota, and D.W. Holden. 2012. Salmonella Inhibits Retrograde Trafficking of Mannose-6-Phosphate. *Science (80-.).* 338:963–967.

McNally, K.E., and P.J. Cullen. 2018. Endosomal Retrieval of Cargo: Retromer Is Not Alone. *Trends Cell Biol.* 28:807–822. doi:10.1016/j.tcb.2018.06.005.

Mehra, A., A. Zahra, V. Thompson, N. Sirisaengtaksin, A. Wells, M. Porto, S. Köster, K. Penberthy, Y. Kubota, A. Dricot, D. Rogan, M. Vidal, D.E. Hill, A.J. Bean, and J.A. Philips. 2013. Mycobacterium tuberculosis Type VII Secreted Effector EsxH Targets Host ESCRT to Impair Trafficking. *PLoS Pathog.* 9. doi:10.1371/journal.ppat.1003734.

Mellouk, N., A. Weiner, N. Aulner, C. Schmitt, M. Elbaum, S.L. Shorte, A. Danckaert, and J. Enninga. 2014. Shigella subverts the host recycling compartment to rupture its vacuole. *Cell Host Microbe*. 16:517–530. doi:10.1016/j.chom.2014.09.005.

Méresse, S., O. Steele-Mortimer, B.B. Finlay, and J.P. Gorvel. 1999. The rab7 GTPase controls the maturation of Salmonella typhimurium-containing vacuoles

in HeLa cells. *EMBO J.* 18:4394–4403. doi:10.1093/emboj/18.16.4394.

Mestas, J., and C.C.W. Hughes. 2004. Of Mice and Not Men: Differences between Mouse and Human Immunology. *J. Immunol.* 172:2731–2738. doi:10.4049/jimmunol.172.5.2731.

Minowa-Nozawa, A., T. Nozawa, K. Okamoto-Furuta, H. Kohda, and I. Nakagawa. 2017. Rab35 GTPase recruits NDP52 to autophagy targets. *EMBO J.* 36:2790–2807. doi:10.15252/embj.201796463.

Misharin, A. V., L. Morales-Nebreda, P.A. Reyfman, C.M. Cuda, J.M. Walter, A.C. McQuattie-Pimentel, C.I. Chen, K.R. Anekalla, N. Joshi, K.J.N. Williams, H. Abdala-Valencia, T.J. Yacoub, M. Chi, S. Chiu, F.J. Gonzalez-Gonzalez, K. Gates, A.P. Lam, T.T. Nicholson, P.J. Homan, S. Soberanes, S. Dominguez, V.K. Morgan, R. Saber, A. Shaffer, M. Hinchcliff, S.A. Marshall, A. Bharat, S. Berdnikovs, S.M. Bhorade, E.T. Bartom, R.I. Morimoto, W.E. Balch, J.I. Sznajder, N.S. Chandel, G.M. Mutlu, M. Jain, C.J. Gottardi, B.D. Singer, K.M. Ridge, N. Bagheri, A. Shilatifard, G.R.S. Budinger, and H. Perlman. 2017. Monocyte-derived alveolar macrophages drive lung fibrosis and persist in the lung over the life span. *J. Exp. Med.* 214:2387–2404. doi:10.1084/jem.20162152.

Mitchell, G., M.I. Cheng, C. Chen, B.N. Nguyen, A.T. Whiteley, S. Kianian, J.S. Cox, D.R. Green, K.L. McDonald, and D.A. Portnoy. 2017. Listeria monocytogenes triggers noncanonical autophagy upon phagocytosis, but avoids subsequent growth-restricting xenophagy. *Proc. Natl. Acad. Sci. U. S. A.* 115:E210–E217. doi:10.1073/pnas.1716055115.

Mitchell, G., L. Ge, Q. Huang, C. Chen, S. Kianian, M.F. Roberts, R. Schekman, and D.A. Portnoy. 2015. Avoidance of autophagy mediated by PlcA or ActA is required for listeria monocytogenes growth in macrophages. *Infect. Immun.* 83:2175–2184. doi:10.1128/IAI.00110-15.

Mittal, E., M.L. Skowyra, G. Uwase, E. Tinaztepe, A. Mehra, S. Koster, P.I. Hanson, and J.A. Philips. 2018. Mycobacterium tuberculosis Typi VII Secretion System Effectors Differentially Imapct the ESCRT Endomembrane Damage Response. *MBio*. 9:1–21. doi:10.1128.mBio.01865-18.

Molmeret, M., M. Santic', R. Asare, R.A. Carabeo, and Y.A. Kwaik. 2007. Rapid escape of the dot/icm mutants of Legionella pneumophila into the cytosol of mammalian and protozoan cells. *Infect. Immun.* 75:3290–3304. doi:10.1128/IAI.00292-07.

Moreau, K., S. Lacas-Gervais, N. Fujita, F. Sebbane, T. Yoshimori, M. Simonet, and F. Lafont. 2010. Autophagosomes can support Yersinia pseudotuberculosis replication in macrophages. *Cell. Microbiol.* 12:1108–1123. doi:10.1111/j.1462-5822.2010.01456.x.

Moreira-Teixeira, L., K. Mayer-Barber, A. Sher, and A. O'Garra. 2018. Type I interferons in tuberculosis: Foe and occasionally friend. *J. Exp. Med.* 215:1273–

1285. doi:10.1084/jem.20180325.

Mostowy, S., M. Bonazzi, M.A. Hamon, T.N. Tham, A. Mallet, M. Lelek, E. Gouin, C. Demangel, R. Brosch, C. Zimmer, A. Sartori, M. Kinoshita, M. Lecuit, and P. Cossart. 2010. Entrapment of intracytosolic bacteria by septin cage-like structures. *Cell Host Microbe*. 8:433–444. doi:10.1016/j.chom.2010.10.009.

Mucci, A., E. Lopez-Rodriguez, M. Hetzel, S. Liu, T. Suzuki, C. Happle, M. Ackermann, H. Kempf, R. Hillje, J. Kunkiel, E. Janosz, S. Brennig, S. Glage, J.P. Bankstahl, S. Dettmer, T. Rodt, G. Gohring, B. Trapnell, G. Hansen, C. Trapnell, L. Knudsen, N. Lachmann, and T. Moritz. 2018. iPSC-Derived Macrophages Effectively Treat Pulmonary Alveolar Proteinosis in Csf2rb-Deficient Mice. *Stem Cell Reports*. 11:696–710. doi:10.1016/j.stemcr.2018.07.006.

von Muhlinen, N., M. Akutsu, B.J. Ravenhill, Á. Foeglein, S. Bloor, T.J. Rutherford, S.M. V Freund, D. Komander, and F. Randow. 2012. LC3C, Bound Selectively by a Noncanonical LIR Motif in NDP52, Is Required for Antibacterial Autophagy. *Mol. Cell*. 48:329–342. doi:10.1016/j.molcel.2012.08.024.

Mukhopadhyay, S., E. Heinz, I. Porreca, K. Alasoo, A. Yeung, H. Yang, T. Schwerd, J.L. Forbester, C. Hale, C.A. Agu, Y.H. Choi, J. Rodrigues, M. Capitani, L. Jostins-Dean, D.C. Thomas, S. Travis, D. Gaffney, W.C. Skarnes, N. Thomson, H.H. Uhlig, G. Dougan, and F. Powrie. 2020. Loss of IL-10 signaling in macrophages limits bacterial killing driven by prostaglandin E2. *J. Exp. Med.* 217:1–19. doi:10.1084/jem.20180649.

Muller, I., S.P. Cobbold, H. Waldmann, and S.H.E. Kaufmann. 1987. Impaired resistance to Mycobacterium tuberculosis infection after selective in vivo depletion of L3T4+ and Lyt-2+ T cells. *Infect. Immun.* 55:2037–2041. doi:10.1128/iai.55.9.2037-2041.1987.

Murphy, K.C., S.J. Nelson, S. Nambi, K. Papavinasasundaram, C.E. Baer, and C.M. Sassetti. 2018. ORBIT: a New Paradigm for Genetic Engineering of Mycobacterial Chromosomes. *MBio*. 9:1–20. doi:10.1128/mBio.01467-18.

Murthy, A., Y. Li, I. Peng, M. Reichelt, A.K. Katakam, R. Noubade, M. Roose-Girma, J. Devoss, L. Diehl, R.R. Graham, and M. Van Lookeren Campagne. 2014. A Crohn's disease variant in Atg16l1 enhances its degradation by caspase 3. *Nature*. 506:456–462. doi:10.1038/nature13044.

Nakagawa, I., A. Amano, N. Mizushima, A. Yamamoto, H. Yamaguchi, T. Kamimoto, A. Nara, J. Funao, M. Nakata, K. Tsuda, S. Hamada, and T. Yoshimori. 2004. Autophagy Defends Cells Against Invading Group A Streptococcus. *Science (80-.).* 306:1037–1040. doi:10.1126/science.1103966.

Nakahira, K., J.A. Haspel, V.A.K. Rathinam, S.J. Lee, T. Dolinay, H.C. Lam, J.A. Englert, M. Rabinovitch, M. Cernadas, H.P. Kim, K.A. Fitzgerald, S.W. Ryter, and A.M.K. Choi. 2011. Autophagy proteins regulate innate immune responses by inhibiting the release of mitochondrial DNA mediated by the NALP3

inflammasome. *Nat. Immunol.* 12:222–230. doi:10.1038/ni.1980.

Nakatogawa, H., Y. Ichimura, and Y. Ohsumi. 2007. Atg8, a ubiquitin-like protein required for autophagosome formation, mediates membrane tethering and hemifusion. *Cell*. 130:165–78. doi:10.1016/j.cell.2007.05.021.

Napolitano, G., and A. Ballabio. 2016. TFEB at a glance. *J. Cell Sci.* 129:2475–2481. doi:10.1242/jcs.146365.

Narendra, D.P., L.A. Kane, D.N. Hauser, I.M. Fearnley, and R.J. Youle. 2010. p62/SQSTM1 is required for Parkin-induced mitochondrial clustering but not mitophagy; VDAC1 is dispensable for both. *Autophagy*. 6:1090–1106. doi:10.4161/auto.6.8.13426.

Nathan, B.Y.C.F., H.W. Murray, I.E. Wiebe, and B.Y. Rubin. 1983. Identification of Interferon-γ as the Lymphokine that Activates Human Macrophage Oxidative Metabolism and Antimicrobial Activity. *J. Exp. Med.* 158:670–689.

Nedjic, J., M. Aichinger, J. Emmerich, N. Mizushima, and L. Klein. 2008. Autophagy in thymic epithelium shapes the T-cell repertoire and is essential for tolerance. *Nature*. 455:396–400. doi:10.1038/nature07208.

Neehus, A.L., J. Lam, K. Haake, S. Merkert, N. Schmidt, A. Mucci, M. Ackermann, M. Schubert, C. Happle, M.P. Kühnel, P. Blank, F. Philipp, R. Goethe, D. Jonigk, U. Martin, U. Kalinke, U. Baumann, A. Schambach, J. Roesler, and N. Lachmann. 2018. Impaired IFNγ-Signaling and Mycobacterial Clearance in IFNγR1-Deficient Human iPSC-Derived Macrophages. *Stem Cell Reports*. 10:7–16. doi:10.1016/j.stemcr.2017.11.011.

Nenasheva, T., T. Gerasimova, Y. Serdyuk, E. Grigor'eva, G. Kosmiadi, A. Nikolaev, E. Dashinimaev, and I. Lyadova. 2020. Macrophages Derived From Human Induced Pluripotent Stem Cells Are Low-Activated "Naïve-Like" Cells Capable of Restricting Mycobacteria Growth. *Front. Immunol.* 11:1–15. doi:10.3389/fimmu.2020.01016.

Nguyen, T.N., B.S. Padman, J. Usher, V. Oorschot, G. Ramm, and M. Lazarou. 2016. Atg8 family LC3/GABARAP proteins are crucial for autophagosome – lysosome fusion but not autophagosome formation during PINK1 / Parkin mitophagy and starvation. *J. Cell Biol.* 215:1–18. doi:10.1083/jcb.201607039.

Niu, H., Q. Xiong, A. Yamamoto, M. Hayashi-Nishino, and Y. Rikihisa. 2012. Autophagosomes induced by a bacterial Beclin 1 binding protein facilitate obligatory intracellular infection. *Proc. Natl. Acad. Sci.* 109:20800–20807. doi:10.1073/pnas.1218674109.

Niu, H., M. Yamaguchi, and Y. Rikihisa. 2008. Subversion of cellular autophagy by Anaplasma phagocytophilum. *Cell. Microbiol.* 10:593–605. doi:10.1111/j.1462-5822.2007.01068.x.

Noad, J., A. Von Der Malsburg, C. Pathe, M.A. Michel, D. Komander, and F. Randow. 2017. LUBAC-synthesized linear ubiquitin chains restrict cytosol-

invading bacteria by activating autophagy and NF-κB. *Nat. Microbiol.* 2:1–10. doi:10.1038/nmicrobiol.2017.63.

Nozawa, T., S. Sano, A. Minowa-Nozawa, H. Toh, S. Nakajima, K. Murase, C. Aikawa, and I. Nakagawa. 2020. TBC1D9 regulates TBK1 activation through Ca2+ signaling in selective autophagy. *Nat. Commun.* 11:1–16. doi:10.1038/s41467-020-14533-4.

Nunes, P., N. Demaurex, and M.C. Dinauer. 2013. Regulation of the NADPH Oxidase and Associated Ion Fluxes During Phagocytosis. *Traffic*. 14:1118–1131. doi:10.1111/tra.12115.

O'Garra, A., P.S. Redford, F.W. McNab, C.I. Bloom, R.J. Wilkinson, and M.P.R. Berry. 2013. The Immune Response in Tuberculosis. 31. 475–527 pp.

O'Leary, S.M., M.M. Coleman, W.M. Chew, C. Morrow, A.M. McLaughlin, L.E. Gleeson, M.P. O'Sullivan, and J. Keane. 2014. Cigarette smoking impairs human pulmonary immunity to mycobacterium tuberculosis. *Am. J. Respir. Crit. Care Med.* 190:1430–1436. doi:10.1164/rccm.201407-1385OC.

Odero, M.D., N.J. Zeleznik-Le, V. Chinwalla, and J.D. Rowley. 2000. Cytogenetic and molecular analysis of the acute monocytic leukemia cell line THP-1 with an MLL-AF9 translocation. *Genes, Chromosom. Cancer*. 29:333–338. doi:10.1002/1098-2264(2000)9999:9999<::AID-GCC1040>3.0.CO:2;2-Z.

Ogawa, M., T. Yoshimori, T. Suzuki, H. Sagara, N. Mizushima, and C. Sasakawa. 2005. Escape of Intracellular Shigella from Autophagy. *Science (80-.).* 307:727–731. doi:10.1126/science.1106036.

Ohnstad, A.E., J.M. Delgado, B.J. North, I. Nasa, A.N. Kettenbach, S.W. Schultz, and C.J. Shoemaker. 2020. Receptor-mediated clustering of FIP200 bypasses the role of LC3 lipidation in autophagy. *EMBO J.* e104948. doi:10.15252/embj.2020104948.

Olmos, Y., L. Hodgson, J. Mantell, P. Verkade, and J.G. Carlton. 2015. ESCRT-III controls nuclear envelope reformation. *Nature*. 522:236–239. doi:10.1038/nature14503.

Olsvik, H.L., T. Lamark, K. Takagi, K.B. Larsen, G. Evjen, A. Øvervatn, T. Mizushima, and X.T. Johansen. 2015. FYCO1 contains a C-terminally extended, LC3A/B-preferring LC3-interacting region (LIR) motif required for efficient maturation of autophagosomes during basal autophagy. *J. Biol. Chem.* 290:29361–29374. doi:10.1074/jbc.M115.686915.

Onwueme, K.C., C.J. Vos, J. Zurita, J.A. Ferreras, and L.E.N. Quadri. 2005. The dimycocerosate ester polyketide virulence factors of mycobacteria. *Prog. Lipid Res.* 44:259–302. doi:10.1016/j.plipres.2005.07.001.

Orme, I.M., P. Andersen, and W.H. Boom. 1993. T Cell Response to Mycobacterium tuberculosis. *J. Infect. Dis.* 167:1481–1497.

Orme, I.M., and F.M. Collins. 1984. Adoptive protection of the Mycobacterium

tuberculosis-infected lung. *Cell. Immunol.* 84:113–120. doi:10.1016/0008-8749(84)90082-0.

Osawa, T., T. Kotani, T. Kawaoka, E. Hirata, K. Suzuki, H. Nakatogawa, Y. Ohsumi, and N.N. Noda. 2019. Atg2 mediates direct lipid transfer between membranes for autophagosome formation. *Nat. Struct. Mol. Biol.* 26:281–288. doi:10.1038/s41594-019-0203-4.

Osman, M.M., A.J. Pagán, J.K. Shanahan, and L. Ramakrishnan. 2020. Mycobacterium marinum phthiocerol dimycocerosates enhance macrophage phagosomal permeabilization and membrane damage. *PLoS One*. 15:e0233252. doi:10.1371/journal.pone.0233252.

Ouimet, M., S. Koster, E. Sakowski, B. Ramkhelawon, C. van Solingen, S. Oldebeken, D. Karunakaran, C. Portal-Celhay, F.J. Sheedy, T.D. Ray, K. Cecchini, P.D. Zamore, K.J. Rayner, Y.L. Marcel, J.A. Philips, and K.J. Moore. 2016. Mycobacterium tuberculosis induces the miR-33 locus to reprogram autophagy and host lipid metabolism. *Nat. Immunol.* 17:1–8. doi:10.1038/ni.3434.

Pakos-Zebrucka, K., I. Koryga, K. Mnich, M. Ljujic, A. Samali, and A.M. Gorman. 2016. The integrated stress response. *EMBO Rep.* 17:1374–1395. doi:10.15252/embr.201642195.

Pandey, A.K., and C.M. Sassetti. 2008. Mycobacterial persistence requires the utilization of host cholesterol. *Proc. Natl. Acad. Sci. U. S. A.* 105:4376–4380. doi:10.1073/pnas.0711159105.

Panicker, L.M., D. Miller, T.S. Park, B. Patel, J.L. Azevedo, O. Awad, M.A. Masood, T.D. Veenstra, E. Goldin, B.K. Stubblefield, N. Tayebi, S.K. Polumuri, S.N. Vogel, E. Sidransky, E.T. Zambidis, and R.A. Feldman. 2012. Induced pluripotent stem cell model recapitulates pathologic hallmarks of Gaucher disease. *Proc. Natl. Acad. Sci.* 109:18054–18059. doi:10.1073/pnas.1207889109.

Di Paolo, N.C., S. Shafiani, T. Day, T. Papayannopoulou, D.W. Russell, Y. Iwakura, D. Sherman, K. Urdahl, and D.M. Shayakhmetov. 2015. Interdependence between Interleukin-1 and Tumor Necrosis Factor Regulates TNF-Dependent Control of Mycobacterium tuberculosis Infection. *Immunity*. 43:1125–1136. doi:10.1016/j.immuni.2015.11.016.

Papadopoulos, C., B. Kravic, and H. Meyer. 2020. Repair or Lysophagy: Dealing with Damaged Lysosomes. *J. Mol. Biol.* 432:231–239. doi:10.1016/j.jmb.2019.08.010.

Papp, A.C., A.K. Azad, M. Pietrzak, A. Williams, S.K. Handelman, R.P. Igo, C.M. Stein, K. Hartmann, L.S. Schlesinger, and W. Sadee. 2018. AmpliSeq transcriptome analysis of human alveolar and monocyte-derived macrophages over time in response to Mycobacterium tuberculosis infection. *PLoS One*. 13:1–22. doi:10.1371/journal.pone.0198221.

Park, J.M., C.H. Jung, M. Seo, N.M. Otto, D. Grunwald, K.H. Kim, B. Moriarity, Y.M. Kim, C. Starker, R.S. Nho, D. Voytas, and D.H. Kim. 2016. The ULK1 complex mediates MTORC1 signaling to the autophagy initiation machinery via binding and phosphorylating ATG14. *Autophagy*. 12:547–564. doi:10.1080/15548627.2016.1140293.

Paul-Gilloteaux, P., X. Heiligenstein, M. Belle, M.C. Domart, B. Larijani, L. Collinson, G. Raposo, and J. Salamero. 2017. EC-CLEM: Flexible multidimensional registration software for correlative microscopies. *Nat. Methods*. 14:102–103. doi:10.1038/nmeth.4170.

Paz, I., M. Sachse, N. Dupont, J. Mounier, C. Cederfur, J. Enninga, H. Leffler, F. Poirier, M.C. Prevost, F. Lafont, and P. Sansonetti. 2010. Galectin-3, a marker for vacuole lysis by invasive pathogens. *Cell. Microbiol.* 12:530–544. doi:10.1111/j.1462-5822.2009.01415.x.

Perrin, A.J., X. Jiang, C.L. Birmingham, N.S.. So, and J.H. Brumell. 2004. Recognition of Bacteria in the Cytosol of Mammalian Cells by the Ubiquitin System. *Curr. Biol.* 14:806–811. doi:10.1016/j.cub.2004.04.033.

Peyron, P., J. Vaubourgeix, Y. Poquet, F. Levillain, C. Botanch, F. Bardou, M. Daffé, J.F. Emile, B. Marchou, P.J. Cardona, C. De Chastellier, and F. Altare. 2008. Foamy macrophages from tuberculous patients' granulomas constitute a nutrient-rich reservoir for M. tuberculosis persistence. *PLoS Pathog.* 4:1–14. doi:10.1371/journal.ppat.1000204.

Piccini, A., S. Carta, S. Tassi, D. Lasiglié, G. Fossati, and A. Rubartelli. 2008. ATP is released by monocytes stimulated with pathogen-sensing receptor ligands and induces IL-1β and IL-18 secretion in an autocrine way. *Proc. Natl. Acad. Sci.* 105:8067–8072. doi:10.1073/pnas.0709684105.

Pietzsch, T., S. Saalfeld, S. Preibisch, and P. Tomancak. 2015. BigDataViewer: Visualization and processing for large image data sets. *Nat. Methods*. 12:481–483. doi:10.1038/nmeth.3392.

Pilli, M., J. Arko-Mensah, M. Ponpuak, E. Roberts, S. Master, M.A. Mandell, N. Dupont, W. Ornatowski, S. Jiang, S.B. Bradfute, J.A. Bruun, T.E. Hansen, T. Johansen, and V. Deretic. 2012. TBK-1 Promotes Autophagy-Mediated Antimicrobial Defense by Controlling Autophagosome Maturation. *Immunity*. 37:223–234. doi:10.1016/j.immuni.2012.04.015.

Pisu, D., L. Huang, J.K. Grenier, and D.G. Russell. 2020. Dual RNA-Seq of Mtb-Infected Macrophages In Vivo Reveals Ontologically Distinct Host-Pathogen Interactions. *Cell Rep.* 30:335-350.e4. doi:10.1016/j.celrep.2019.12.033.

Pizarro-Cerdá, J., E. Moreno, V. Sanguedolce, J.L. Mege, and J.P. Gorvel. 1998. Virulent Brucella abortus prevents lysosome fusion and is distributed within autophagosome-like compartments. *Infect. Immun.* 66:2387–2392. doi:10.1128/iai.66.5.2387-2392.1998.

Polajnar, M., M.S. Dietz, M. Heilemann, and C. Behrends. 2017. Expanding the host

cell ubiquitylation machinery targeting cytosolic Salmonella. *EMBO Rep.* 18:1572–1585. doi:10.15252/embr.201643851.

Ponpuak, M., A.S. Davis, E.A. Roberts, M.A. Delgado, C. Dinkins, Z. Zhao, H.W.V. Iv, G.B. Kyei, T. Johansen, I. Vergne, and V. Deretic. 2010. Delivery of Cytosolic Components by Autophagic Adapter Protein p62 Endows Autophagosomes with Unique Anti-Microbial Properties. *Immunity*. 32:329–341. doi:10.1016/j.immuni.2010.02.009.

Portal-Celhay, C., J.M. Tufariello, S. Srivastava, A. Zahra, P.S. Grace, A. Mehra, H.S. Park, J.D. Ernst, W.R. Jacobs, and J.A. Philips. 2016. Mycobacterium tuberculosis EsxH inhibits ESCRT-dependent CD4+ T-cell activation. *Nat. Microbiol.* 2. doi:10.1038/nmicrobiol.2016.232.Mycobacterium.

Poweleit, N., N. Czudnochowski, R. Nakagawa, D. Trinidad, K.C. Murphy, C. Sassetti, and O.S. Rosenberg. 2019. The structure of the endogenous ESX-3 secretion system. *Elife*. 8:1–20. doi:10.7554/eLife.52983.

Pujol, C., K.A. Klein, G.A. Romanov, L.E. Palmer, C. Cirota, Z. Zhao, and J.B. Bliska. 2009. Yersinia pestis can reside in autophagosomes and avoid xenophagy in murine macrophages by preventing vacuole acidification. *Infect. Immun.* 77:2251–2261. doi:10.1128/IAI.00068-09.

Pym, A.S., P. Brodin, R. Brosch, M. Huerre, and S.T. Cole. 2002. Loss of RD1 contributed to the attenuation of the live tuberculosis vaccines Mycobacterium bovis BCG and Mycobacterium microti. *Mol. Microbiol.* 46:709–17.

Queval, C.J., R. Brosch, and R. Simeone. 2017. The macrophage: A disputed fortress in the battle against Mycobacterium tuberculosis. *Front. Microbiol.* 8:1–11. doi:10.3389/fmicb.2017.02284.

Quigley, J., V.K. Hughitt, C.A. Velikovsky, R.A. Mariuzza, N.M. El-Sayed, and V. Briken. 2017. The cell wall lipid PDIM contributes to phagosomal escape and host cell exit of Mycobacterium tuberculosis. *MBio*. 8:1–12. doi:10.1128/mBio.00148-17.

Rabadi, S.M., B.C. Sanchez, M. Varanat, Z. Ma, S. V. Catlett, J.A. Melendez, M. Malik, and C.S. Bakshi. 2016. Antioxidant defenses of Francisella tularensis modulate macrophage function and production of proinflammatory cytokines. *J. Biol. Chem.* 291:5009–5021. doi:10.1074/jbc.M115.681478.

Rabinovitch, M. 1995. Professional and non-professional phagocytes: an introduction. *Trends Cell Biol.* 5:85–87. doi:10.1016/S0962-8924(00)88955-2.

Radtke, A.L., K.L. Anderson, M.J. Davis, M.J. DiMagno, J.A. Swanson, and M.X. O'Riordan. 2011. Listeria monocytogenes exploits cystic fibrosis transmembrane conductance regulator (CFTR) to escape the phagosome. *Proc. Natl. Acad. Sci. U. S. A.* 108:1633–1638. doi:10.1073/pnas.1013262108.

Radulovic, M., K.O. Schink, E.M. Wenzel, V. Nähse, A. Bongiovanni, F. Lafont, and H. Stenmark. 2018. ESCRT -mediated lysosome repair precedes lysophagy

and promotes cell survival . *EMBO J.* 37:1–15. doi:10.15252/embj.201899753.

Raffy, S., and J. Teissié. 1999. Control of lipid membrane stability by cholesterol content. *Biophys. J.* 76:2072–2080. doi:10.1016/S0006-3495(99)77363-7.

Ramos, P.S., L.A. Criswell, K.L. Moser, M.E. Comeau, A.H. Williams, N.M. Pajewski, S.A. Chung, R.R. Graham, R. Zidovetzki, J.A. Kelly, K.M. Kaufman, C.O. Jacob, T.J. Vyse, B.P. Tsao, R.P. Kimberly, P.M. Gaffney, M.E. Alarcón-Riquelme, J.B. Harley, and C.D. Langefeld. 2011. A comprehensive analysis of shared loci between systemic lupus erythematosus (SLE) and sixteen autoimmune diseases reveals limited genetic overlap. *PLoS Genet.* 7. doi:10.1371/journal.pgen.1002406.

Randall, P.J., N.J. Hsu, V. Quesniaux, B. Ryffel, and M. Jacobs. 2015. Mycobacterium tuberculosis infection of the “non-classical immune cell.” *Immunol. Cell Biol.* 93:789–795. doi:10.1038/icb.2015.43.

Randow, F., and C. Münz. 2012. Autophagy in the regulation of pathogen replication and adaptive immunity. *Trends Immunol.* 33:475–487. doi:10.1016/j.it.2012.06.003.

Ravenhill, B.J., K.B. Boyle, N. von Muhlinen, C.J. Ellison, G.R. Masson, E.G. Otten, A. Foeglein, R. Williams, and F. Randow. 2019. The Cargo Receptor NDP52 Initiates Selective Autophagy by Recruiting the ULK Complex to Cytosol-Invading Bacteria. *Mol. Cell*. 0:1–10. doi:10.1016/j.molcel.2019.01.041.

Reddy, A., E. V Caler, N.W. Andrews, and N. Haven. 2001. Plasma Membrane Repair Is Mediated by Ca2+-Regulated Exocytosis of Lysosomes. *Cell*. 106:157–169.

Repnik, U., M.B. Distefano, M.T. Speth, M.Y.W. Ng, C. Prodiga, B. Hoflack, J. Gruenberg, and G. Griffiths. 2017. L-leucyl-L-leucine methyl ester does not release cysteine cathepsins to the cytosol but inactivates them in transiently permeabilized lysosomes. *J. Cell Sci.* 130:3124–3140. doi:10.1242/jcs.204529.

Rhee, H.W., P. Zou, N.D. Udeshi, J.D. Martell, V.K. Mootha, S.A. Carr, and A.Y. Ting. 2013. Proteomic mapping of mitochondria in living cells via spatially restricted enzymatic tagging. *Science (80-.).* 339:1328–1331. doi:10.1126/science.1230593.

Rich, E.A., M. Torres, E. Sada, C.K. Finegan, B.D. Hamilton, and Z. Toossi. 1997. Mycobacterium tuberculosis (MTB)-stimulated production of nitric oxide by human alveolar macrophages and relationship of nitric oxide production to growth inhibition of MTB. *Tuber. Lung Dis.* 78:247–255. doi:10.1016/S0962-8479(97)90005-8.

Richter, B., D.A. Sliter, L. Herhaus, A. Stolz, C. Wang, P. Beli, G. Zaffagnini, P. Wild, S. Martens, S.A. Wagner, R.J. Youle, and I. Dikic. 2016. Phosphorylation of OPTN by TBK1 enhances its binding to Ub chains and promotes selective autophagy of damaged mitochondria. *Proc. Natl. Acad. Sci.* 113:4039–4044. doi:10.1073/pnas.1523926113.

Rockett, K.A., R. Brookes, I. Udalova, V. Vidal, A.V.S. Hill, and D. Kwiatkowski. 1998. 1,25-Dihydroxyvitamin D3 induces nitric oxide synthase and suppresses growth of Mycobacterium tuberculosis in a human macrophage-like cell line. *Infect. Immun.* 66:5314–5321. doi:10.1128/iai.66.11.5314-5321.1998.

Roczniak-Ferguson, A., C.S. Petit, F. Froehlich, S. Qian, J. Ky, B. Angarola, T.C. Walther, and S.M. Ferguson. 2012. The transcription factor TFEB links mTORC1 signaling to transcriptional control of lysosome homeostasis. *Sci. Signal.* 5. doi:10.1126/scisignal.2002790.

Roder, J., P. Felgner, and M. Hensel. 2020. Comprehensive single cell analyses of the nutritional environment of intracellular Salmonella enterica. *bioRxiv*.

Rogov, V. V, A. Stolz, A.C. Ravichandran, D.O. Rios-Szwed, H. Suzuki, A. Kniss, F. Löhr, S. Wakatsuki, V. Dötsch, I. Dikic, R.C. Dobson, and D.G. McEwan. 2017. Structural and functional analysis of the GABARAP interaction motif (GIM). *EMBO Rep.* 18:1382–1396. doi:10.15252/embr.201643587.

Rojko, N., and G. Anderluh. 2015. How Lipid Membranes Affect Pore Forming Toxin Activity. *Acc. Chem. Res.* 48:3073–3079. doi:10.1021/acs.accounts.5b00403.

Rolando, M., P. Escoll, T. Nora, J. Botti, V. Boitez, C. Bedia, C. Daniels, G. Abraham, P.J. Stogios, T. Skarina, C. Christophe, D. Dervins-Ravault, C. Cazalet, H. Hilbi, T.W.T. Rupasinghe, D. Tull, M.J. McConville, S.Y. Ong, E.L. Hartland, P. Codogno, T. Levade, T. Naderer, A. Savchenko, and C. Buchrieser. 2016. Legionella pneumophila S1P-lyase targets host sphingolipid metabolism and restrains autophagy. *Proc. Natl. Acad. Sci.* 113:1901–1906. doi:10.1073/pnas.1522067113.

Romagnoli, A., M.P. Etna, E. Giacomini, M. Pardini, M.E. Remoli, M. Corazzari, L. Falasca, D. Goletti, V. Gafa, R. Simeone, G. Delogu, M. Piacentini, R. Brosch, G.M. Fimia, and E.M. Coccia. 2012. ESX-1 dependent impairment of autophagic flux by Mycobacterium tuberculosis in human dendritic cells. *Autophagy*. 8:1357–1370. doi:10.4161/auto.20881.

Romao, S., N. Gasser, A.C. Becker, B. Guhl, M. Bajagic, D. Vanoaica, U. Ziegler, J. Roesler, J. Dengjel, J. Reichenbach, and C. Münz. 2013. Autophagy proteins stabilize pathogen-containing phagosomes for prolonged MHC II antigen processing. *J. Cell Biol.* 203:757–766. doi:10.1083/jcb.201308173.

Rook, G.A., J. Steele, M. Ainsworth, and B.R. Champion. 1986. Activation of macrophages to inhibit proliferation of Mycobacterium tuberculosis: comparison of the effects of recombinant gamma-interferon on human monocytes and murine peritoneal macrophages. *Immunology*. 59:333–8.

Roshick, C., H. Wood, H.D. Caldwell, and G. McClarty. 2006. Comparison of gamma interferon-mediated antichlamydial defense mechanisms in human and mouse cells. *Infect. Immun.* 74:225–238. doi:10.1128/IAI.74.1.225-238.2006.

Rossi, G., A. Manfrin, and M.P. Lutolf. 2018. Progress and potential in organoid research. *Nat. Rev. Genet.* 19:671–687. doi:10.1038/s41576-018-0051-9.

Roy, C.R., K.H. Berger, and R.R. Isberg. 1998. Legionella pneumophila DotA protein is required for early phagosome trafficking decisions that occur within minutes of bacterial uptake. *Mol. Microbiol.* 28:663–674. doi:10.1046/j.1365-2958.1998.00841.x.

Roy, D., D.R. Liston, V.J. Idone, A. Di, D.J. Nelson, C. Pujol, J.B. Bliska, S. Chakrabarti, and N.W. Andrews. 2004. A process for controlling intracellular bacterial infections induced by membrane injury. *Science (80-.).* 304:1515–1518. doi:10.1126/science.1098371.

Runwal, G., E. Stamatakou, F.H. Siddiqi, C. Puri, Y. Zhu, and D.C. Rubinsztein. 2019. LC3-positive structures are prominent in autophagy-deficient cells. *Sci. Rep.* 9:1–14. doi:10.1038/s41598-019-46657-z.

Russell, D.G., P. Cardona, M. Kim, S. Allain, and F. Altare. 2009. Foamy macrophages and the progression of the human tuberculosis granuloma. *Nat. Immunol.* 10:943–948. doi:10.1038/ni.1781.

Russell, R.C., Y. Tian, H. Yuan, H.W. Park, Y.-Y. Chang, J. Kim, H. Kim, T.P. Neufeld, A. Dillin, and K.-L. Guan. 2013. ULK1 induces autophagy by phosphorylating Beclin-1 and activating VPS34 lipid kinase. *Nat. Cell Biol.* 15:741–50. doi:10.1038/ncb2757.

Ryndak, M., S. Wang, and I. Smith. 2008. PhoP, a key player in Mycobacterium tuberculosis virulence. *Trends Microbiol.* 16:528–534. doi:10.1016/j.tim.2008.08.006.

Sadek, M.I., E. Sada, Z. Toossi, S.K. Schwander, and E.A. Rich. 1998. Chemokines induced by infection of mononuclear phagocytes with mycobacteria and present in lung alveoli during active pulmonary tuberculosis. *Am. J. Respir. Cell Mol. Biol.* 19:513–521. doi:10.1165/ajrcmb.19.3.2815.

Saini, N.K., A. Baena, T.W. Ng, M.M. Venkataswamy, S.C. Kennedy, S. Kunnath-Velayudhan, L.J. Carreño, J. Xu, J. Chan, M.H. Larsen, W.R. Jacobs, and S.A. Porcelli. 2016. Suppression of autophagy and antigen presentation by Mycobacterium tuberculosis PE-PGRS47. *Nat. Microbiol.* 1:1–12. doi:10.1038/nmicrobiol.2016.133.

Saitoh, T., N. Fujita, M.H. Jang, S. Uematsu, B.G. Yang, T. Satoh, H. Omori, T. Noda, N. Yamamoto, M. Komatsu, K. Tanaka, T. Kawai, T. Tsujimura, O. Takeuchi, T. Yoshimori, and S. Akira. 2008. Loss of the autophagy protein Atg16L1 enhances endotoxin-induced IL-1β production. *Nature*. 456:264–268. doi:10.1038/nature07383.

Sakowski, E.T., S. Koster, C. Portal Celhay, H.S. Park, E. Shrestha, S.E. Hetzenecker, K. Maurer, K. Cadwell, and J.A. Philips. 2015. Ubiquilin 1 Promotes IFNγ Induced Xenophagy of Mycobacterium tuberculosis. *PLoS Pathog.* 11:1–18. doi:10.1371/journal.ppat.1005076.

Sanjuan, M.A., C.P. Dillon, S.W.G. Tait, S. Moshiach, F. Dorsey, S. Connell, M. Komatsu, K. Tanaka, J.L. Cleveland, S. Withoff, and D.R. Green. 2007. Toll-like

receptor signalling in macrophages links the autophagy pathway to phagocytosis. *Nature*. 450:1253–7. doi:10.1038/nature06421.

Santos, J.C., D. Boucher, L.K. Schneider, B. Demarco, M. Dilucca, K. Shkarina, R. Heilig, K.W. Chen, R.Y.H. Lim, and P. Broz. 2020. Human GBP1 binds LPS to initiate assembly of a caspase-4 activating platform on cytosolic bacteria. *Nat. Commun.* 11. doi:10.1038/s41467-020-16889-z.

Sarraf, S.A., H. V Shah, G. Kanfer, A.M. Pickrell, L.A. Holtzclaw, M.E. Ward, and R.J. Youle. 2020. Loss of TAX1BP1-Directed Autophagy Results in Protein Aggregate Accumulation in the Brain. *Mol. Cell*. 1–17. doi:10.1016/j.molcel.2020.10.041.

Scheffer, L.L., S.C. handra Sreetama, N. Sharma, S. Medikayala, K.J. Brown, A. Defour, and J.K. Jaiswal. 2014. Mechanism of Ca^{2+}-triggered ESCRT assembly and regulation of cell membrane repair. *Nat. Commun.* 5:5646. doi:10.1038/ncomms6646.

Scherr, N., P. Müller, D. Perisa, B. Combaluzier, P. Jenö, and J. Pieters. 2009. Survival of pathogenic mycobacteria in macrophages is mediated through autophosphorylation of protein kinase G. *J. Bacteriol.* 191:4546–4554. doi:10.1128/JB.00245-09.

Schnaith, A., H. Kashkar, S.A. Leggio, K. Addicks, M. Krönke, and O. Krut. 2007. Staphylococcus aureus Subvert Autophagy for Induction of Caspase-independent Host Cell Death. *J. Biol. Chem.* 282:2695–2706. doi:10.1074/jbc.M609784200.

Schnettger, L. 2016. The role of the small GTPase Rab20 in Mycobacterium tuberculosis phagosome biology. University College London. 1–124 pp.

Schnettger, L., and M.G. Gutierrez. 2017. Quantitative Spatiotemporal Analysis of Phagosome Maturation in Live Cells. *In* Phagocytosis and Phagosomes: Methods and Protocols. R. Botelho, editor. Springer New York, New York, NY. 169–184.

Schnettger, L., A. Rodgers, U. Repnik, R.P. Lai, G. Pei, M. Verdoes, R.J. Wilkinson, D.B. Young, and M.G. Gutierrez. 2017. A Rab20-Dependent Membrane Trafficking Pathway Controls M. tuberculosis Replication by Regulating Phagosome Spaciousness and Integrity. *Cell Host Microbe*. 21:619-628.e5. doi:10.1016/j.chom.2017.04.004.

Schnupf, P., and D.A. Portnoy. 2007. Listeriolysin O: a phagosome-specific lysin. *Microbes Infect.* 9:1176–1187. doi:10.1016/j.micinf.2007.05.005.

Schroder, K., K.M. Irvine, M.S. Taylor, N.J. Bokil, K.A. Le Cao, K.A. Masterman, L.I. Labzin, C.A. Semple, R. Kapetanovic, L. Fairbairn, A. Akalin, G.J. Faulkner, J.K. Baillie, M. Gongora, C.O. Daub, H. Kawaji, G.J. McLachlan, N. Goldman, S.M. Grimmond, P. Carninci, H. Suzuki, Y. Hayashizaki, B. Lenhard, D.A. Hume, and M.J. Sweet. 2012. Conservation and divergence in Toll-like receptor 4-regulated gene expression in primary human versus mouse macrophages. *Proc. Natl.*

Acad. Sci. 109. doi:10.1073/pnas.1110156109.

Schulz, D., Y. Severin, V.R.T. Zanotelli, and B. Bodenmiller. 2019. In-Depth Characterization of Monocyte-Derived Macrophages using a Mass Cytometry-Based Phagocytosis Assay. *Sci. Rep.* 9:1–12. doi:10.1038/s41598-018-38127-9.

Schuster, C., K.D. Gerold, K. Schober, L. Probst, K. Boerner, M.J. Kim, A. Ruckdeschel, T. Serwold, and S. Kissler. 2015. The Autoimmunity-Associated Gene CLEC16A Modulates Thymic Epithelial Cell Autophagy and Alters T Cell Selection. *Immunity*. 42:942–952. doi:10.1016/j.immuni.2015.04.011.

Scianimanico, S., M. Desrosiers, J.F. Dermine, S. Méresse, A. Descoteaux, and M. Desjardins. 1999. Impaired recruitment of the small GTPase rab7 correlates with the inhibition of phagosome maturation by Leishmania donovani promastigotes. *Cell. Microbiol.* 1:19–32. doi:10.1046/j.1462-5822.1999.00002.x.

Scudellari, M. 2016. A Decade of iPS Cells. *Nature*. 534:310–312.

Seimon, T.A., M.J. Kim, A. Blumenthal, J. Koo, S. Ehrt, H. Wainwright, L.G. Bekker, G. Kaplan, C. Nathan, I. Tabas, and D.G. Russell. 2010. Induction of ER stress in macrophages of tuberculosis granulomas. *PLoS One*. 5:1–12. doi:10.1371/journal.pone.0012772.

Selwyn, P.A., D. Hartel, V.A. Lewis, E.E. Schoenbaum, S.H. Vermund, R.S. Klein, A.T. Walker, and G.H. Friedland. 1989. A Prospective of the Risk of Tuberculosis Among Intravenous Drug Users with Human Immunodeficiency Virus Infection. *N. Engl. J. Med.* 320:545–550.

Senju, S., M. Haruta, K. Matsumura, Y. Matsunaga, S. Fukushima, T. Ikeda, K. Takamatsu, A. Irie, and Y. Nishimura. 2011. Generation of dendritic cells and macrophages from human induced pluripotent stem cells aiming at cell therapy. *Gene Ther.* 18:874–883. doi:10.1038/gt.2011.22.

Seto, S., K. Tsujimura, T. Horii, and Y. Koide. 2013. Autophagy adaptor protein p62/SQSTM1 and autophagy-related gene Atg5 mediate autophagosome formation in response to Mycobacterium tuberculosis infection in dendritic cells. *PLoS One*. 8:1–13. doi:10.1371/journal.pone.0086017.

Seto, S., K. Tsujimura, and Y. Koide. 2012. Coronin-1a inhibits autophagosome formation around Mycobacterium tuberculosis-containing phagosomes and assists mycobacterial survival in macrophages. *Cell. Microbiol.* 14:710–727. doi:10.1111/j.1462-5822.2012.01754.x.

Settembre, C., C. Di Malta, V.A. Polito, M.G. Arencibia, F. Vetrini, S. Erdin, S.U. Erdin, T. Huynh, D. Medina, P. Colella, M. Sardiello, D.C. Rubinsztein, and A. Ballabio. 2011. TFEB links autophagy to lysosomal biogenesis. *Science (80-.).* 332:1429–1433. doi:10.1126/science.1204592.

Settembre, C., R. Zoncu, D.L. Medina, F. Vetrini, S. Erdin, S. Erdin, T. Huynh, M.

Ferron, G. Karsenty, M.C. Vellard, V. Facchinetti, D.M. Sabatini, and A. Ballabio. 2012. A lysosome-to-nucleus signalling mechanism senses and regulates the lysosome via mTOR and TFEB. *EMBO J.* 31:1095–1108. doi:10.1038/emboj.2012.32.

Shahnazari, S., W.L. Yen, C.L. Birmingham, J. Shiu, A. Namolovan, Y.T. Zheng, K. Nakayama, D.J. Klionsky, and J.H. Brumell. 2010. A diacylglycerol-dependent signaling pathway contributes to regulation of antibacterial autophagy. *Cell Host Microbe*. 8:137–146. doi:10.1016/j.chom.2010.07.002.

Sharma, R., V. Khristov, A. Rising, B.S. Jha, R. Dejene, N. Hotaling, Y. Li, J. Stoddard, C. Stankewicz, Q. Wan, C. Zhang, M.M. Campos, K.J. Miyagishima, D. McGaughey, R. Villasmil, M. Mattapallil, B. Stanzel, H. Qian, W. Wong, L. Chase, S. Charles, T. McGill, S. Miller, A. Maminishkis, J. Amaral, and K. Bharti. 2019. Clinical-grade stem cell–derived retinal pigment epithelium patch rescues retinal degeneration in rodents and pigs. *Sci. Transl. Med.* 11:eaat5580. doi:10.1126/scitranslmed.aat5580.

Shi, C., and E.G. Pamer. 2011. Monocyte recruitment during infection and inflammation. *Nat. Rev. Immunol.* 11:762–774. doi:10.1038/nri3070.

Shi, C.S., K. Shenderov, N.N. Huang, J. Kabat, M. Abu-Asab, K.A. Fitzgerald, A. Sher, and J.H. Kehrl. 2012. Activation of autophagy by inflammatory signals limits IL-1β production by targeting ubiquitinated inflammasomes for destruction. *Nat. Immunol.* 13:255–263. doi:10.1038/ni.2215.

Shibata, Y., Z. Zsengeller, K. Otake, N. Palaniyar, and B.C. Trapnell. 2001. Alveolar macrophage deficiency in osteopetrotic mice deficient in macrophage colony-stimulating factor is spontaneously corrected with age and associated with matrix metalloproteinase expression and emphysema. *Blood*. 98:2845–2852. doi:10.1182/blood.V98.9.2845.

Shin, D.M., B.Y. Jeon, H.M. Lee, H.S. Jin, J.M. Yuk, C.H. Song, S.H. Lee, Z.W. Lee, S.N. Cho, J.M. Kim, R.L. Friedman, and E.K. Jo. 2010. Mycobacterium tuberculosis eis regulates autophagy, inflammation, and cell death through redox-dependent signaling. *PLoS Pathog.* 6. doi:10.1371/journal.ppat.1001230.

Shpilka, T., H. Weidberg, S. Pietrokovski, and Z. Elazar. 2011. Atg8: An autophagy-related ubiquitin-like protein family. *Genome Biol.* 12. doi:10.1186/gb-2011-12-7-226.

Shrestha, N., W. Bahnan, D.J. Wiley, G. Barber, K.A. Fields, and K. Schesser. 2012. Eukaryotic Initiation Factor 2 (eIF2) signaling regulates proinflammatory cytokine expression and bacterial invasion. *J. Biol. Chem.* 287:28738–28744. doi:10.1074/jbc.M112.375915.

Silva, M.T., and M. Correia-Neves. 2012. Neutrophils and macrophages: The main partners of phagocyte cell systems. *Front. Immunol.* 3:2008–2013. doi:10.3389/fimmu.2012.00174.

Silver, R.F., J. Walrath, H. Lee, B.A. Jacobson, H. Horton, M.R. Bowman, K. Nocka,

and J.P. Sypek. 2009. Human alveolar macrophage gene responses to mycobacterium tuberculosis strains H37Ra and H37Rv. *Am. J. Respir. Cell Mol. Biol.* 40:491–504. doi:10.1165/rcmb.2008-0219OC.

Simeone, R., A. Bobard, J. Lippmann, W. Bitter, L. Majlessi, R. Brosch, and J. Enninga. 2012. Phagosomal rupture by Mycobacterium tuberculosis results in toxicity and host cell death. *PLoS Pathog.* 8. doi:10.1371/journal.ppat.1002507.

Simeone, R., F. Sayes, O. Song, M.I. Gröschel, P. Brodin, R. Brosch, and L. Majlessi. 2015. Cytosolic Access of Mycobacterium tuberculosis: Critical Impact of Phagosomal Acidification Control and Demonstration of Occurrence In Vivo. *PLoS Pathog.* 11:1–24. doi:10.1371/journal.ppat.1004650.

Singh, R., A. Jamieson, and P. Cresswell. 2008. GILT is a critical host factor for Listeria monocytogenes infection. *Nature*. 455:1244–1247. doi:10.1038/nature07344.

Singh, S.B., A.S. Davis, G.A. Taylor, and V. Deretic. 2006. Human IRGM induces autophagy to eliminate intracellular mycobacteria. *Science (80-.).* 313:1438–1441. doi:10.1126/science.1129577.

Singhania, A., R. Verma, C.M. Graham, J. Lee, T. Tran, M. Richardson, P. Lecine, P. Leissner, M.P.R. Berry, R.J. Wilkinson, K. Kaiser, M. Rodrigue, G. Woltmann, P. Haldar, and A. O'Garra. 2018. A modular transcriptional signature identifies phenotypic heterogeneity of human tuberculosis infection. *Nat. Commun.* 9. doi:10.1038/s41467-018-04579-w.

Sivangala Thandi, R., R.K. Radhakrishnan, D. Tripathi, P. Paidipally, A.K. Azad, L.S. Schlesinger, B. Samten, S. Mulik, and R. Vankayalapati. 2020. Ornithine-A urea cycle metabolite enhances autophagy and controls Mycobacterium tuberculosis infection. *Nat. Commun.* 11:1–15. doi:10.1038/s41467-020-17310-5.

Skowyra, M.L., P.H. Schlesinger, T. V. Naismith, and P.I. Hanson. 2018. Triggered recruitment of ESCRT machinery promotes endolysosomal repair. *Science (80-.).* 360. doi:10.1126/science.aar5078.

Slobodkin, M.R., and Z. Elazar. 2013. The Atg8 family: multifunctional ubiquitin-like key regulators of autophagy. *Essays Biochem.* 55:51–64. doi:10.1042/bse0550051.

Small, J.L., A.J. O'Donoghue, E.C. Boritsch, O. V Tsodikov, G.M. Knudsen, O. Vandal, C.S. Craik, and S. Ehrt. 2013. Substrate specificity of MarP, a periplasmic protease required for resistance to acid and oxidative stress in Mycobacterium tuberculosis. *J. Biol. Chem.* 288:12489–12499. doi:10.1074/jbc.M113.456541.

Smith, G.A., H. Marquis, S. Jones, N.C. Johnston, D.A. Portnoy, and H. Goldfine. 1995. The two distinct phospholipases C of Listeria monocytogenes have overlapping roles in escape from a vacuole and cell-to-cell spread. *Infect. Immun.* 63:4231–4237. doi:10.1128/iai.63.11.4231-4237.1995.

Sola-Landa, A., J. Pizarro-Cerdá, M.J. Grilló, E. Moreno, I. Moriyón, J.M. Blasco, J.P. Gorvel, and I. López-Goñi. 1998. A two-component regulatory system playing a critical role in plant pathogens and endosymbionts is present in Brucella abortus and controls cell invasion and virulence. *Mol. Microbiol.* 29:125–138. doi:10.1046/j.1365-2958.1998.00913.x.

Solans, L., N. Aguiló, S. Samper, A. Pawlik, W. Frigui, C. Martín, R. Brosch, and J. Gonzalo-Asensio. 2014. A Specific polymorphism in Mycobacterium tuberculosis H37Rv causes differential ESAT-6 expression and identifies whiB6 as a novel ESX-1 component. *Infect. Immun.* 82:3446–3456. doi:10.1128/IAI.01824-14.

Sou, Y.S., I. Tanida, M. Komatsu, T. Ueno, and E. Kominami. 2006. Phosphatidylserine in addition to phosphatidylethanolamine is an in vitro target of the mammalian Atg8 modifiers, LC3, GABARAP, and GATE-16. *J. Biol. Chem.* 281:3017–3024. doi:10.1074/jbc.M505888200.

Stanley, S.A., J.E. Johndrow, P. Manzanillo, and J.S. Cox. 2007. The Type I IFN Response to Infection with Mycobacterium tuberculosis Requires ESX-1-Mediated Secretion and Contributes to Pathogenesis. *J. Immunol.* 178:3143–3152. doi:10.4049/jimmunol.178.5.3143.

Steele-Mortimer, O., S. Méresse, J.P. Gorvel, B.H. Toh, and B.B. Finlay. 1999. Biogenesis of Salmonella typhimurium-containing vacuoles in epithelial cells involves interactions with the early endocytic pathway. *Cell. Microbiol.* 1:33–49. doi:10.1046/j.1462-5822.1999.00003.x.

Stévenin, V., Y.Y. Chang, Y. Le Toquin, M. Duchateau, Q.G. Gianetto, C.H. Luk, A. Salles, V. Sohst, M. Matondo, N. Reiling, and J. Enninga. 2019. Dynamic Growth and Shrinkage of the Salmonella-Containing Vacuole Determines the Intracellular Pathogen Niche. *Cell Rep.* 29:3958-3973.e7. doi:10.1016/j.celrep.2019.11.049.

Stoddard-Bennett, T., and R.R. Pera. 2019. Treatment of Parkinson's Disease through Personalized Medicine and Induced Pluripotent Stem Cells. *Cells*. 8:26. doi:10.3390/cells8010026.

Sturgill-Koszycki, S., P.H. Schlesinger, P. Chakraborty, P.L. Haddix, H.L. Collins, A.K. Fok, R.D. Allen, S.L. Gluck, J. Heuser, and D.G. Russell. 1994. Lack of acidification in Mycobacterium phagosomes produced by exclusion of the vesicular proton-ATPase. *Science (80-.).* 263:678–681. doi:10.1126/science.8303277.

Sugawara, I., H. Yamada, S. Hua, and S. Mizuno. 2001. Role of interleukin (IL)-1 type 1 receptor in mycobacterial infection. *Microbiol. Immunol.* 45:743–750. doi:10.1111/j.1348-0421.2001.tb01310.x.

Sun, J., A.-E. Deghmane, H. Soualhine, T. Hong, C. Bucci, A. Solodkin, and Z. Hmama. 2007. Mycobacterium bovis BCG disrupts the interaction of Rab7 with RILP contributing to inhibition of phagosome maturation. *J. Leukoc. Biol.*

82:1437–1445. doi:10.1189/jlb.0507289.

Sun, J., X. Wang, A. Lau, T.Y.A. Liao, C. Bucci, and Z. Hmama. 2010. Mycobacterial nucleoside diphosphate kinase blocks phagosome maturation in murine raw 264.7 macrophages. *PLoS One*. 5:1–12. doi:10.1371/journal.pone.0008769.

Sundström, C., and K. Nilsson. 1976. Establishment and characterization of a human histiocytic lymphoma cell line (U-937). *Int. J. Cancer*. 17:565–577. doi:10.1002/ijc.2910170504.

T'Jonck, W., M. Guilliams, and J. Bonnardel. 2018. Niche signals and transcription factors involved in tissue-resident macrophage development. *Cell. Immunol.* 330:43–53. doi:10.1016/j.cellimm.2018.02.005.

Tabata, K., K. Matsunaga, A. Sakane, T. Sasaki, T. Noda, and T. Yoshimori. 2010. Rubicon and PLEKHM1 Negatively Regulate the Endocytic/Autophagic Pathway via a Novel Rab7-binding Domain. *Mol. Biol. Cell*. 21:4162–4172. doi:10.1091/mbc.E10–06–0495.

Takada, S., N. Kambe, Y. Kawasaki, A. Niwa, F. Honda-Ozaki, K. Kobayashi, M. Osawa, A. Nagahashi, K. Semi, A. Hotta, I. Asaka, Y. Yamada, R. Nishikomori, T. Heike, H. Matsue, T. Nakahata, and M.K. Saito. 2018. Pluripotent stem cell models of Blau syndrome reveal an IFN-γ–dependent inflammatory response in macrophages. *J. Allergy Clin. Immunol.* 141:339-349.e11. doi:10.1016/j.jaci.2017.04.013.

Takahashi, K., and S. Yamanaka. 2006. Induction of Pluripotent Stem Cells from Mouse Embryonic and Adult Fibroblast Cultures by Defined Factors. *Cell*. 126:663–676. doi:10.1016/j.cell.2006.07.024.

Takahashi, Y., H. He, Z. Tang, T. Hattori, Y. Liu, M.M. Young, J.M. Serfass, L. Chen, M. Gebru, C. Chen, C.A. Wills, J.M. Atkinson, H. Chen, T. Abraham, and H.G. Wang. 2018. An autophagy assay reveals the ESCRT-III component CHMP2A as a regulator of phagophore closure. *Nat. Commun.* 9. doi:10.1038/s41467-018-05254-w.

Takata, K., T. Kozaki, C.Z.W. Lee, M.S. Thion, M. Otsuka, S. Lim, K.H. Utami, K. Fidan, D.S. Park, B. Malleret, S. Chakarov, P. See, D. Low, G. Low, M. Garcia-Miralles, R. Zeng, J. Zhang, C.C. Goh, A. Gul, S. Hubert, B. Lee, J. Chen, I. Low, N.B. Shadan, J. Lum, T.S. Wei, E. Mok, S. Kawanishi, Y. Kitamura, A. Larbi, M. Poidinger, L. Renia, L.G. Ng, Y. Wolf, S. Jung, T. Önder, E. Newell, T. Huber, E. Ashihara, S. Garel, M.A. Pouladi, and F. Ginhoux. 2017. Induced-Pluripotent-Stem-Cell-Derived Primitive Macrophages Provide a Platform for Modeling Tissue-Resident Macrophage Differentiation and Function. *Immunity*. 47:183-198.e6. doi:10.1016/j.immuni.2017.06.017.

Tam, J.M., M.K. Mansour, N.S. Khan, M. Seward, S. Puranam, A. Tanne, A. Sokolovska, C.E. Becker, M. Acharya, M.A. Baird, A.M.K. Choi, M.W. Davidson, B.H. Segal, A. Lacy-Hulbert, L.M. Stuart, R.J. Xavier, and J.M. Vyas. 2014. Dectin-1-dependent LC3 recruitment to phagosomes enhances fungicidal

activity in macrophages. *J. Infect. Dis.* 210:1844–1854. doi:10.1093/infdis/jiu290.

Tanaka, T., K. Takahashi, M. Yamane, S. Tomida, S. Nakamura, K. Oshima, A. Niwa, R. Nishikomori, N. Kambe, H. Hara, M. Mitsuyama, N. Morone, J.E. Heuser, T. Yamamoto, A. Watanabe, A. Sato-Otsubo, S. Ogawa, I. Asaka, T. Heike, S. Yamanaka, T. Nakahata, and M.K. Saito. 2012. Induced pluripotent stem cells from CINCA syndrome patients as a model for dissecting somatic mosaicism and drug discovery. *Blood*. 120:1299–1308. doi:10.1182/blood-2012-03-417881.

Tang, Z., Y. Takahashi, H. He, T. Hattori, C. Chen, X. Liang, H. Chen, M.M. Young, and H.G. Wang. 2019. TOM40 Targets Atg2 to Mitochondria-Associated ER Membranes for Phagophore Expansion. *Cell Rep.* 28:1744-1757.e5. doi:10.1016/j.celrep.2019.07.036.

Tanida, I., N. Mizushima, M. Kiyooka, M. Ohsumi, T. Ueno, Y. Ohsumi, and E. Kominami. 1999. Apg7p/Cvt2p: A novel protein-activating enzyme essential for autophagy. *Mol. Biol. Cell*. 10:1367–1379. doi:10.1091/mbc.10.5.1367.

Tarique, A.A., J. Logan, E. Thomas, P.G. Holt, P.D. Sly, and E. Fantino. 2015. Phenotypic,functional,and plasticity features of classical and alternatively activated human macrophages. *Am. J. Respir. Cell Mol. Biol.* 53:676–688. doi:10.1165/rcmb.2015-0012OC.

Tascon, R.E., E. Stavropoulos, K. V. Lukacs, and M.J. Colston. 1998. Protection against Mycobacterium tuberculosis infection by CD8+ T cells requires the production of gamma interferon. *Infect. Immun.* 66:830–834. doi:10.1128/iai.66.2.830-834.1998.

Thacker, A.V. V, N. Dhar, K. Sharma, and R. Barrile. 2020. A lung-on-chip model reveals an essential role for alveolar epithelial cells in controlling bacterial growth during early tuberculosis Affiliations : School of Life Sciences , Swiss Federal Institute of Technology Lausanne (EPFL), Emulate Inc , Boston ,. *Elife*.

Thuong, N.T.T., S.J. Dunstan, T.T.H. Chau, V. Thorsson, C.P. Simmons, N.T.H. Quyen, G.E. Thwaites, N.T.N. Lan, M. Hibberd, Y.Y. Teo, M. Seielstad, A. Aderem, J.J. Farrar, and T.R. Hawn. 2008. Identification of tuberculosis susceptibility genes with human macrophage gene expression profiles. *PLoS Pathog.* 4:1–13. doi:10.1371/journal.ppat.1000229.

Thurston, T.L.M., K.B. Boyle, M. Allen, B.J. Ravenhill, M. Karpiyevich, S. Bloor, A. Kaul, J. Noad, A. Foeglein, S.A. Matthews, D. Komander, M. Bycroft, and F. Randow. 2016. Recruitment of TBK 1 to cytosol-invading Salmonella induces WIPI 2 -dependent antibacterial autophagy. *EMBO J.* 35:1–14. doi:10.15252/embj.201694491.

Thurston, T.L.M., G. Ryzhakov, S. Bloor, N. von Muhlinen, and F. Randow. 2009. The TBK1 adaptor and autophagy receptor NDP52 restricts the proliferation of ubiquitin-coated bacteria. *Nat. Immunol.* 10:1215–1221. doi:10.1038/ni.1800.

Thurston, T.L.M., M.P. Wandel, N. von Muhlinen, Á. Foeglein, and F. Randow. 2012. Galectin 8 targets damaged vesicles for autophagy to defend cells against bacterial invasion. *Nature*. 482:414–418. doi:10.1038/nature10744.

Tian, T., J. Woodworth, M. Sköld, and S.M. Behar. 2005. In Vivo Depletion of CD11c + Cells Delays the CD4 + T Cell Response to Mycobacterium tuberculosis and Exacerbates the Outcome of Infection . *J. Immunol.* 175:3268–3272. doi:10.4049/jimmunol.175.5.3268.

Tilney, L.G., and D.A. Portnoy. 1989. Actin filaments and the growth, movement, and spread of the intracellular bacterial parasite, Listeria monocytogenes. *J. Cell Biol.* 109:1597–1608. doi:10.1083/jcb.109.4.1597.

Ting, L.M., A.C. Kim, A. Cattamanchi, and J.D. Ernst. 1999. Mycobacterium tuberculosis inhibits IFN-gamma transcriptional responses without inhibiting activation of STAT1. *J. Immunol.* 163:3898–906.

De Tito, S., J.H. Hervás, A.R. van Vliet, and S.A. Tooze. 2020. The Golgi as an Assembly Line to the Autophagosome. *Trends Biochem. Sci.* 45:484–496. doi:10.1016/j.tibs.2020.03.010.

Tooze, S.A., A. Abada, and Z. Elazar. 2014. Endocytosis and autophagy: Exploitation or cooperation? *Cold Spring Harb. Perspect. Biol.* 6:1–16. doi:10.1101/cshperspect.a018358.

Travassos, L.H., L.A.M. Carneiro, M. Ramjeet, S. Hussey, Y.-G. Kim, J.G. Magalhães, L. Yuan, F. Soares, E. Chea, L. Le Bourhis, I.G. Boneca, A. Allaoui, N.L. Jones, G. Nuñez, S.E. Girardin, and D.J. Philpott. 2010. Nod1 and Nod2 direct autophagy by recruiting ATG16L1 to the plasma membrane at the site of bacterial entry. *Nat. Immunol.* 11:55–62. doi:10.1038/ni.1823.

Tsang, T.K., E.A. Bushong, D. Boassa, J. Hu, B. Romoli, S. Phan, D. Dulcis, C.-Y. Su, and M.H. Ellisman. 2018. High-quality ultrastructural preservation using cryofixation for 3D electron microscopy of genetically labeled tissues. *Elife*. 7:1–23. doi:10.7554/eLife.35524.

Tsuboyama, A.K., I. Koyama, and Y. Sakamaki. 2016. The ATG conjugation systems are important for degradation of the inner autophagosomal membrane. *Science (80-.).* 354:1036–1041. doi:10.1126/science.aaf6136.

Tsuchiya, S., M. Yamabe, Y. Yamaguchi, Y. Kobayashi, T. Konno, and K. Tada. 1980. Establishment and characterization of a human acute monocytic leukemia cell line (THP-1). *Int. J. Cancer*. 26:171–176. doi:10.1002/ijc.2910260208.

Tumbarello, D.A., P.T. Manna, M. Allen, M. Bycroft, S.D. Arden, J. Kendrick-Jones, and F. Buss. 2015. The Autophagy Receptor TAX1BP1 and the Molecular Motor Myosin VI Are Required for Clearance of Salmonella Typhimurium by Autophagy. *PLoS Pathog.* 11:1–26. doi:10.1371/journal.ppat.1005174.

Turco, E., M. Witt, C. Abert, T. Bock-Bierbaum, M.-Y. Su, R. Trapannone, M. Sztacho, A. Danieli, X. Shi, G. Zaffagnini, A. Gamper, M. Schuschnig, D.

Fracchiolla, D. Bernklau, J. Romanov, M. Hartl, J.H. Hurley, O. Daumke, and S. Martens. 2019. FIP200 Claw Domain Binding to p62 Promotes Autophagosome Formation at Ubiquitin Condensates. *Mol. Cell*. 0:1–17. doi:10.1016/j.molcel.2019.01.035.

Upadhyay, S., and J.A. Philips. 2019. LC3-associated phagocytosis: host defense and microbial response. *Curr. Opin. Immunol.* 60:81–90. doi:10.1016/j.coi.2019.04.012.

Van Der Vaart, M., C.J. Korbee, G.E.M. Lamers, A.C. Tengeler, R. Hosseini, M.C. Haks, T.H.M. Ottenhoff, H.P. Spaink, and A.H. Meijer. 2014. The DNA damage-regulated autophagy modulator DRAM1 links mycobacterial recognition via TLP-MYD88 to authophagic defense. *Cell Host Microbe*. 15:753–767. doi:10.1016/j.chom.2014.05.005.

Valverde, D.P., S. Yu, V. Boggavarapu, N. Kumar, J.A. Lees, T. Walz, K.M. Reinisch, and T.J. Melia. 2019. ATG2 transports lipids to promote autophagosome biogenesis. *J. Cell Biol.* 218:1787–1798. doi:10.1083/jcb.201811139.

Vandal, O.H., L.M. Pierini, D. Schnappinger, C.F. Nathan, and S. Ehrt. 2008. A membrane protein preserves intrabacterial pH in intraphagosomal Mycobacterium tuberculosis. *Nat. Med.* 14:849–854. doi:10.1038/nm.1795.

Vargas, J.N.S., C. Wang, E. Bunker, L. Hao, D. Maric, G. Schiavo, F. Randow, and R.J. Youle. 2019. Spatiotemporal Control of ULK1 Activation by NDP52 and TBK1 during Selective Autophagy. *Mol. Cell*. 0:1–16. doi:10.1016/j.molcel.2019.02.010.

Vaughan-Jackson, A., S. Stodolak, K.H. Ebrahimi, C. Browne, P.K. Reardon, E. Pires, J. Gilbert-Jaramillo, S.A. Cowley, and W.S. James. 2020. Differentiation of Human induced Pluripotent Stem Cells to Authentic Macrophages using Fully Defined, Serum Free, Open Source Media. *bioRxiv*.

Velychko, S., K. Adachi, K.P. Kim, Y. Hou, C.M. MacCarthy, G. Wu, and H.R. Schöler. 2019. Excluding Oct4 from Yamanaka Cocktail Unleashes the Developmental Potential of iPSCs. *Cell Stem Cell*. 25:737-753.e4. doi:10.1016/j.stem.2019.10.002.

Vergne, I., J. Chua, and V. Deretic. 2003. Tuberculosis toxin blocking phagosome maturation inhibits a novel Ca 2+/calmodulin-PI3K hVPS34 cascade. *J. Exp. Med.* 198:653–659. doi:10.1084/jem.20030527.

Vergne, I., J. Chua, H.-H. Lee, M. Lucas, J. Belisle, and V. Deretic. 2005. Mechanism of phagolysosome biogenesis block by viable Mycobacterium tuberculosis. *Proc. Natl. Acad. Sci.* 102:4033–4038. doi:10.1073/pnas.0409716102.

Via, L.E., D. Deretic, R.J. Ulmer, N.S. Hibler, L.A. Huber, and V. Deretic. 1997. Arrest of Mycobacterial Phagosome Maturation Is Caused by a Block in Vesicle Fusion between Stages Controlled by rab5 and rab7. *J. Biol. Chem.* 272:13326–13331. doi:10.1074/jbc.272.20.13326.

Volkman, H.E., H. Clay, D. Beery, J.C.W. Chang, D.R. Sherman, and L. Ramakrishnan. 2004. Tuberculous granuloma formation is enhanced by a Mycobacterium virulence determinant. *PLoS Biol.* 2. doi:10.1371/journal.pbio.0020367.

Walburger, A., A. Koul, G. Ferrari, L. Nguyen, C. Prescianotto-Baschong, K. Huygen, B. Klebl, C. Thompson, G. Bacher, and J. Pieters. 2004. Protein kinase G from pathogenic mycobacteria promotes survival within macrophages. *Science (80-.).* 304:1800–1804. doi:10.1126/science.1099384.

Wan, J., E. Weiss, S. Ben Mkaddem, M. Mabire, P.-M. Choinier, O. Picq, T. Thibault-Sogorb, P. Hegde, D. Pishvaie, M. Bens, L. Broer, H. Gilgenkrantz, R. Moreau, L. Saveanu, P. Codogno, R.C. Monteiro, and S. Lotersztajn. 2020. LC3-associated phagocytosis protects against inflammation and liver fibrosis via immunoreceptor inhibitory signaling. *Sci. Transl. Med.* 12:eaaw8523. doi:10.1126/scitranslmed.aaw8523.

Wandel, M.P., B. Kim, E. Park, K.B. Boyle, K. Nayak, B. Lagrange, A. Herod, T. Henry, M. Zilbauer, J. Rohde, J.D. MacMicking, and F. Randow. 2020. Guanylate-binding proteins convert cytosolic bacteria into caspase-4 signaling platforms. *Nat. Immunol.* 21:880–891. doi:10.1038/s41590-020-0697-2.

Wandel, M.P., C. Pathe, E.I. Werner, C.J. Ellison, K.B. Boyle, A. von der Malsburg, J. Rohde, and F. Randow. 2017. GBPs Inhibit Motility of Shigella flexneri but Are Targeted for Degradation by the Bacterial Ubiquitin Ligase IpaH9.8. *Cell Host Microbe*. 22:507-518.e5. doi:10.1016/j.chom.2017.09.007.

Wang, Z., G. Miao, X. Xue, X. Guo, C. Yuan, Z. Wang, G. Zhang, Y. Chen, D. Feng, J. Hu, and H. Zhang. 2016. The Vici Syndrome Protein EPG5 Is a Rab7 Effector that Determines the Fusion Specificity of Autophagosomes with Late Endosomes/Lysosomes. *Mol. Cell*. 63:781–795. doi:10.1016/j.molcel.2016.08.021.

Watson, R.O., S.L. Bell, D.A. MacDuff, J.M. Kimmey, E.J. Diner, J. Olivas, R.E. Vance, C.L. Stallings, H.W. Virgin, and J.S. Cox. 2015. The Cytosolic Sensor cGAS Detects Mycobacterium tuberculosis DNA to Induce Type I Interferons and Activate Autophagy. *Cell Host Microbe*. 17:811–819. doi:10.1016/j.chom.2015.05.004.

Watson, R.O., P.S. Manzanillo, and J.S. Cox. 2012. Extracellular M. tuberculosis DNA targets bacteria for autophagy by activating the host DNA-sensing pathway. *Cell*. 150:803–815. doi:10.1016/j.cell.2012.06.040.

Weidberg, H., E. Shvets, T. Shpilka, F. Shimron, V. Shinder, and Z. Elazar. 2010. LC3 and GATE-16/GABARAP subfamilies are both essential yet act differently in autophagosome biogenesis. *EMBO J.* 29:1792–1802. doi:10.1038/emboj.2010.74.

Weiner, A., and J. Enninga. 2019. The Pathogen–Host Interface in Three Dimensions: Correlative FIB/SEM Applications. *Trends Microbiol.* 27:426–439.

doi:10.1016/j.tim.2018.11.011.

Weiner, A., N. Mellouk, N. Lopez-Montero, Y.Y. Chang, C. Souque, C. Schmitt, and J. Enninga. 2016. Macropinosomes are Key Players in Early Shigella Invasion and Vacuolar Escape in Epithelial Cells. *PLoS Pathog.* 12:1–24. doi:10.1371/journal.ppat.1005602.

van der Wel, N., D. Hava, D. Houben, D. Fluitsma, M. Van Zon, J. Pierson, M. Brenner, and P.J. Peters. 2007. M . tuberculosis and M . leprae Translocate from the Phagolysosome to the Cytosol in Myeloid Cells. *Cell*. 129:1287–1298. doi:10.1016/j.cell.2007.05.059.

Westman, J., G.F.W. Walpole, L. Kasper, B.Y. Xue, O. Elshafee, B. Hube, S. Grinstein, J. Westman, G.F.W. Walpole, L. Kasper, B.Y. Xue, O. Elshafee, and B. Hube. 2020. Lysosome Fusion Maintains Phagosome Integrity during Fungal Infection Article Lysosome Fusion Maintains Phagosome Integrity during Fungal Infection. *Cell Host Microbe*. 28:1–15. doi:10.1016/j.chom.2020.09.004.

Wild, P., H. Farhan, D.G. McEwan, S. Wagner, V. V. Rogov, N.R. Brady, B. Richter, J. Korac, O. Waidmann, C. Choudhary, V. Dotsch, D. Bumann, and I. Dikic. 2011. Phosphorylation of the Autophagy Receptor Optineurin Restricts Salmonella Growth. *Science (80-.).* 333:228–233. doi:10.1126/science.1205405.

van Wilgenburg, B., C. Browne, J. Vowles, and S.A. Cowley. 2013. Efficient, Long Term Production of Monocyte-Derived Macrophages from Human Pluripotent Stem Cells under Partly-Defined and Fully-Defined Conditions. *PLoS One*. 8:1–18. doi:10.1371/journal.pone.0071098.

Winchell, C.G., J.G. Graham, R.C. Kurten, and D.E. Voth. 2014. Coxiella burnetii type IV secretion-dependent recruitment of macrophage autophagosomes. *Infect. Immun.* 82:2229–2238. doi:10.1128/IAI.01236-13.

Wong, D., H. Bach, J. Sun, Z. Hmama, and Y. Av-Gay. 2011. Mycobacterium tuberculosis protein tyrosine phosphatase (PtpA) excludes host vacuolar-H +-ATPase to inhibit phagosome acidification. *Proc. Natl. Acad. Sci.* 108:19371–19376. doi:10.1073/pnas.1109201108.

World Health Organisation. 2020. Global Tuberculosis Report 2020.

Xu, W., X. Zhao, M.R. Daha, and C. van Kooten. 2013. Reversible differentiation of pro- and anti-inflammatory macrophages. *Mol. Immunol.* 53:179–186. doi:10.1016/j.molimm.2012.07.005.

Xu, Y., P. Zhou, S. Cheng, Q. Lu, K. Nowak, A.-K. Hopp, L. Li, X. Shi, Z. Zhou, W. Gao, D. Li, H. He, X. Liu, J. Ding, M.O. Hottiger, and F. Shao. 2019. A Bacterial Effector Reveals the V-ATPase-ATG16L1 Axis that Initiates Xenophagy. *Cell*. 178:552–566. doi:10.1016/j.cell.2019.06.007.

Yamaji, A., Y. Sekizawa, K. Emoto, H. Sakuraba, K. Inoue, H. Kobayashi, and M. Umeda. 1998. Lysenin, a novel sphingomyelin-specific binding protein. *J. Biol.*

Chem. 273:5300–5306. doi:10.1074/jbc.273.9.5300.

Yamamoto, H., S. Kakuta, T.M. Watanabe, A. Kitamura, T. Sekito, C. Kondo-Kakuta, R. Ichikawa, M. Kinjo, and Y. Ohsumi. 2012. Atg9 vesicles are an important membrane source during early steps of autophagosome formation. *J. Cell Biol.* 198:219–233. doi:10.1083/jcb.201202061.

Yang, C.S., J.J. Kim, H.M. Lee, H.S. Jin, S.H. Lee, J.H. Park, S.J. Kim, J.M. Kim, Y.M. Han, M.S. Lee, G.R. Kweon, M. Shong, and E.K. Jo. 2014. The AMPK-PPARGC1A pathway is required for antimicrobial host defense through activation of autophagy. *Autophagy*. 10:785–802. doi:10.4161/auto.28072.

Yang, C.S., J.S. Lee, M. Rodgers, C.K. Min, J.Y. Lee, H.J. Kim, K.H. Lee, C.J. Kim, B. Oh, E. Zandi, Z. Yue, I. Kramnik, C. Liang, and J.U. Jung. 2012. Autophagy protein rubicon mediates phagocytic NADPH oxidase activation in response to microbial infection or TLR stimulation. *Cell Host Microbe*. 11:264–276. doi:10.1016/j.chom.2012.01.018.

Yang, W., H. Tang, Y. Zhang, X. Tang, J. Zhang, L. Sun, J. Yang, Y. Cui, L. Zhang, N. Hirankarn, H. Cheng, H.F. Pan, J. Gao, T.L. Lee, Y. Sheng, C.S. Lau, Y. Li, T.M. Chan, X. Yin, D. Ying, Q. Lu, A.M.H. Leung, X. Zuo, X. Chen, K.L. Tong, F. Zhou, Q. Diao, N.K.C. Tse, H. Xie, C.C. Mok, F. Hao, S.N. Wong, B. Shi, K.W. Lee, Y. Hui, M.H.K. Ho, B. Liang, P.P.W. Lee, H. Cui, Q. Guo, B.H.Y. Chung, X. Pu, Q. Liu, X. Zhang, C. Zhang, C.Y. Chong, H. Fang, R.W.S. Wong, Y. Sun, M.Y. Mok, X.P. Li, Y. Avihingsanon, Z. Zhai, P. Rianthavorn, T. Deekajorndej, K. Suphapeetiporn, F. Gao, V. Shotelersuk, X. Kang, S.K.Y. Ying, L. Zhang, W.H.S. Wong, D. Zhu, S.K.S. Fung, F. Zeng, W.M. Lai, C.M. Wong, I.O.L. Ng, M.M. Garcia-Barceló, S.S. Cherny, N. Shen, P.K.H. Tam, P.C. Sham, D.Q. Ye, S. Yang, X. Zhang, and Y.L. Lau. 2013. Meta-analysis followed by replication identifies loci in or near CDKN1B, TET3, CD80, DRAM1, and ARID5B as associated with systemic lupus erythematosus in Asians. *Am. J. Hum. Genet.* 92:41–51. doi:10.1016/j.ajhg.2012.11.018.

Yang, Z., and D.J. Klionsky. 2009. An Overview of the Molecular Mechanism of Autophagy. *In* Current Topics in Microbiology and Immunology. 1–32.

Yeung, A.T.Y., C. Hale, A.H. Lee, E.E. Gill, W. Bushell, D. Parry-Smith, D. Goulding, D. Pickard, T. Roumeliotis, J. Choudhary, N. Thomson, W.C. Skarnes, G. Dougan, and R.E.W. Hancock. 2017. Exploiting induced pluripotent stem cell-derived macrophages to unravel host factors influencing Chlamydia trachomatis pathogenesis. *Nat. Commun.* 8:1–12. doi:10.1038/ncomms15013.

Yoshikawa, Y., M. Ogawa, T. Hain, M. Yoshida, M. Fukumatsu, M. Kim, H. Mimuro, I. Nakagawa, T. Yanagawa, T. Ishii, A. Kakizuka, E. Sztul, T. Chakraborty, and C. Sasakawa. 2009. Listeria monocytogenes ActA-mediated escape from autophagic recognition. *Nat. Cell Biol.* 11:1233–1240. doi:10.1038/ncb1967.

Yousefi, S., R. Perozzo, I. Schmid, A. Ziemiecki, T. Schaffner, L. Scapozza, T. Brunner, and H.U. Simon. 2006. Calpain-mediated cleavage of Atg5 switches autophagy to apoptosis. *Nat. Cell Biol.* 8:1124–1132. doi:10.1038/ncb1482.

Yu, L., C.K. McPhee, L. Zheng, G.A. Mardones, Y. Rong, J. Peng, N. Mi, Y. Zhao, Z. Liu, F. Wan, D.W. Hailey, V. Oorschot, J. Klumperman, E.H. Baehrecke, and M.J. Lenardo. 2010. Termination of autophagy and reformation of lysosomes regulated by mTOR. *Nature*. 465:942–946. doi:10.1038/nature09076.

Zachari, M., S.R. Gudmundsson, Z. Li, M. Manifava, R. Shah, M. Smith, J. Stronge, E. Karanasios, C. Piunti, C. Kishi-Itakura, H. Vihinen, E. Jokitalo, J.L. Guan, F. Buss, A.M. Smith, S.A. Walker, E.L. Eskelinen, and N.T. Ktistakis. 2019. Selective Autophagy of Mitochondria on a Ubiquitin-Endoplasmic-Reticulum Platform. *Dev. Cell*. 50:627-643.e5. doi:10.1016/j.devcel.2019.06.016.

Zhang, H., and M.P. Reilly. 2017. Human induced pluripotent stem cell-derived macrophages for unraveling human macrophage biology. *Arterioscler. Thromb. Vasc. Biol.* 37:2000–2006. doi:10.1161/ATVBAHA.117.309195.

Zhang, H., C. Xue, R. Shah, K. Bermingham, C.C. Hinkle, W. Li, A. Rodrigues, J. Tabita-Martinez, J.S. Millar, M. Cuchel, E.E. Pashos, Y. Liu, R. Yan, W. Yang, S.J. Gosai, D. Vandorn, S.T. Chou, B.D. Gregory, E.E. Morrisey, M. Li, D.J. Rader, and M.P. Reilly. 2015. Functional Analysis and Transcriptomic Profiling of iPSC-Derived Macrophages and Their Application in Modeling Mendelian Disease. *Circ. Res.* 117:17–28. doi:10.1161/CIRCRESAHA.117.305860.

Zhang, L., X. Jiang, D. Pfau, Y. Ling, and C.F. Nathan. 2020a. Type I interferon signaling mediates Mycobacterium tuberculosis–induced macrophage death. *J. Exp. Med.* 218. doi:10.1084/jem.20200887.

Zhang, R., M. Varela, G. Forn-Cuní, V. Torraca, M. van der Vaart, and A.H. Meijer. 2020b. Deficiency in the autophagy modulator Dram1 exacerbates pyroptotic cell death of Mycobacteria-infected macrophages. *Cell Death Dis.* 11. doi:10.1038/s41419-020-2477-1.

Zhang, R., M. Varela, W. Vallentgoed, G. Forn-Cuni, M. van der Vaart, and A.H. Meijer. 2019. The selective autophagy receptors Optineurin and p62 are both required for zebrafish host resistance to mycobacterial infection. *PLOS Pathog.* 15. doi:10.1371/journal.ppat.1007329.

Zhang, X., L. Wang, B. Lak, J. Li, E. Jokitalo, and Y. Wang. 2018. GRASP55 Senses Glucose Deprivation through O-GlcNAcylation to Promote Autophagosome-Lysosome Fusion. *Dev. Cell*. 45:245-261.e6. doi:10.1016/j.devcel.2018.03.023.

Zhao, Y.G., and H. Zhang. 2019. Autophagosome maturation: An epic journey from the ER to lysosomes. *J. Cell Biol.* 218:757–770. doi:10.1083/jcb.201810099.

Zhao, Z., B. Fux, M. Goodwin, I.R. Dunay, D. Strong, B.C. Miller, K. Cadwell, M.A. Delgado, M. Ponpuak, K.G. Green, R.E. Schmidt, N. Mizushima, V. Deretic, L.D. Sibley, and H.W. Virgin. 2008. Autophagosome-Independent Essential Function for the Autophagy Protein Atg5 in Cellular Immunity to Intracellular Pathogens. *Cell Host Microbe*. 4:458–469. doi:10.1016/j.chom.2008.10.003.

Zhen, Y., H. Spangenberg, M.J. Munson, A. Brech, K.O. Schink, K.W. Tan, V. Sørensen, E.M. Wenzel, M. Radulovic, N. Engedal, A. Simonsen, C. Raiborg,

and H. Stenmark. 2020. ESCRT-mediated phagophore sealing during mitophagy. *Autophagy*. 16:826–841. doi:10.1080/15548627.2019.1639301.

Zheng, H., L. Lu, B. Wang, S. Pu, X. Zhang, G. Zhu, W. Shi, Z. Lu, H. Wang, S. Wang, G. Zhao, and Y. Zhang. 2008. Genetic basis of virulence attenuation revealed by comparative genomic analysis of Mycobacterium tuberculosis strain H37Ra versus H37Rv. *PLoS One*. 3. doi:10.1371/journal.pone.0002375.

Zheng, Y.T., S. Shahnazari, A. Brech, T. Lamark, T. Johansen, and J.H. Brumell. 2009. The adaptor protein p62/SQSTM1 targets invading bacteria to the autophagy pathway. *J. Immunol.* 183:5909–5916. doi:10.4049/jimmunol.0900441.

Zhou, F., Z. Wu, M. Zhao, R. Murtazina, J. Cai, A. Zhang, R. Li, D. Sun, W. Li, L. Zhao, Q. Li, J. Zhu, X. Cong, Y. Zhou, Z. Xie, V. Gyurkovska, L. Li, X. Huang, Y. Xue, L. Chen, H. Xu, H. Xu, Y. Liang, and N. Segev. 2019. Rab5-dependent autophagosome closure by ESCRT. *J. Cell Biol.* 218:1908–1927. doi:10.1083/jcb.201811173.

Zhou, R., A.S. Yazdi, P. Menu, and J. Tschopp. 2011. A role for mitochondria in NLRP3 inflammasome activation. *Nature*. 469:221–226. doi:10.1038/nature09663.